Understanding of Global Variations in Plant Hydraulic Traits and their Coordination with Photosynthesis

Submitted by Huiying Xu
to the University of Exeter as a thesis for the degree of
Doctor of Philosophy in Geography
April 2024

To be jointly awarded by the University of Exeter and Tsinghua University

I certify that all material in this thesis which is not my own work has been identified and that any material that has previously been submitted and approved for the award of a degree by this or any other University has been acknowledged.

Signature ……..

ABSTRACT

Terrestrial carbon and water cycling are predicted to undergo large changes over the coming decades due to anthropogenic climate change. These cycles are dependent on the plant hydraulic system, because of its close link with leaf photosynthesis, however these dependencies remain poorly understood. Plant hydraulic traits play a pivotal role in regulating transpiration, water supply, carbon uptake and ecosystem resilience, but how these traits control these ecosystem scale variables is yet to be properly quantified. This is, in part, because the controls on the spatial variations in hydraulic traits themselves remains poorly understood. Eco-evolutionary optimality (EEO) principles have been successfully applied to trait predictions globally, this makes it a promising approach to enhance our ability to predict global hydraulic trait distributions. Within this thesis I progress through a series of steps to develop and test a global hydraulic EEO model.

Close coupling of water loss and carbon uptake requires close coordination between hydraulic and photosynthetic traits. Therefore, firstly I develop a hydraulic trait model incorporating photosynthetic traits based on EEO principles. The model predicts that optimal carbon allocation to leaves and stems generates equilibrium between stem water supply and water demand for photosynthesis, allowing the prediction of the sapwood to leaf area ratio (v_H). This model is the first step in quantifying trait-trait and trait-climate relationships in a model that incorporates hydraulic traits. In the second chapter, I use empirical data from 18 sites along an elevation gradient in the Gongga Mountains in China to reveal a trait coordination network with v_H at its nexus. This trait network connects hydraulic, photosynthetic, and resource acquisition strategies. v_H exhibits a positive correlation with carboxylation capacity, is negatively related to hydraulic efficiency, aligning well with my model predictions. The comparisons between observed and predicted photosynthetic traits suggest the plants are well acclimated to short-term midday climate conditions, supporting them having a water supply-demand balance, as predicted by the model. Finally, I develop this analysis at a global scale using global hydraulic trait databases to evaluate the model and to show that plants in cold, dry, and high-irradiance environments have low hydraulic efficiency and exhibit high v_H, consistent with predicted patterns. The EEO-based hydraulic trait model explains 56% of variation in v_H on a global scale with only one

parameter. These findings provide insights to predict how plants adjust coordinated traits to adapt to climate change.

The hydraulic trait model developed in this thesis offers an alternative way to offer significant improvements to the carbon allocation scheme in dynamic vegetation models, without the use of many additional parameters, which increase model uncertainty. Consequently, this modelling approach offers the opportunity to considerably enhance future capacity to predict vegetation responses to climate change, particularly extreme conditions, such as drought.

Acknowledgements

As a dual degree candidate at Tsinghua University and University of Exeter, I am filled with deep gratitude for the individuals and institutions that have supported me throughout this remarkable PhD journey. I am extremely grateful to my kind supervisors Prof. Lucy Rowland, Dr. Han Wang, Prof. Colin Prentice, Prof. Sandy Harrison and Prof. Stephen Sitch for mentoring and guiding me over the last five years. Their insights and feedback are invaluable to my PhD research. My one-year experience at University of Exeter would be impossible without the funding of China Scholarship Council, which was essential for the completion of my PhD research.

My study at University of Exeter under the supervision of Lucy really enhanced my scientific acumen, broadened my horizons, teaching me how to tackle meaningful scientific questions. Lucy's assistance began even before my arrival in Exeter, by providing me with accommodation options and, upon my arrival, introducing me to the city and its best hot chocolate. Her warm welcome and consistent support throughout the year were incredibly reassuring. From establishing the initial research plan to the biweekly meetings that directed my next steps, Lucy played a pivotal role in my PhD. She also facilitated a month-long collaboration with Prof. Maurizio Mencuccini at CREAF, which was crucial to my dissertation's final chapter. In my final year of PhD, Lucy encouraged me to contemplate my career path and postdoctoral opportunities, which I found immensely beneficial.

I cannot thank Dr. Han Wang enough for leading me into world of science and encouraging me to apply for this joint-program. I still vividly recalled the summer camp when I met Han for the first time. Her enthusiasm and kindness inspired me deeply. She taught me how to code in R hand by hand and explained the plant physiology behind the equations patiently when I first started my PhD at Tsinghua. Han guided me to explore my interests and offered support to learn hydraulic trait measurement techniques from another lab, which laid foundation to my PhD research. With the tremendous help from Han, I managed to attend my first conference, present my first work and publish my first paper.

I am also immensely thankful to my family, friends and colleagues who stand by my side and support me always. I owe a debt of gratitude to Dr. Tianyang Lei for being there during late-night talks, to Dr. Paulo Bittencourt and Dr. Pengcheng

He for sharing their hydraulic knowledge, to Dr. Shengchao Qiao and Dr. Shen Tan for coding assistance, and to Dr. Anggi Hapsari, Mateus, and Arne for their companionship and joy in Exeter.

My sincere appreciation extends to all who assisted with data collection for my thesis. This thesis would not have been possible without the collective support and encouragement of everyone mentioned above, as well as many others who have contributed in various ways. To all of you, I extend my deepest thanks.

List of Contents

ABSTRACT **2**
ACKNOWLEDGEMENTS **4**
LIST OF CONTENTS **6**
LIST OF FIGURES AND TABLES **9**
ABBREVIATIONS **11**
CHAPTER 1 INTRODUCTION **14**
1.1 Climate change and terrestrial carbon cycle 14
1.2 Plant hydraulics and carbon cycling 15
1.3 The introduction of plant hydraulics to vegetation modelling 17
1.4 Plant hydraulic system 20
1.4.1 Hydraulic trait correlation 23
1.4.2 Coordination of hydraulic and non-hydraulic traits 26
1.4.3 Hydraulic trait variation with climate 28
1.5 Existing application of eco-evolutionary optimality principles in ecology 31
1.6 Applying EEO principles to hydraulic trait modelling 32
1.7 Outline of thesis 34
CHAPTER 2 COORDINATION OF PLANT HYDRAULIC AND PHOTOSYNTHETIC TRAITS: CONFRONTING OPTIMALITY THEORY WITH FIELD MEASUREMENTS **38**
2.1 Abstract 39
2.2 Introduction 40
2.3 Theory 43
2.4 Data and Methods 46
2.4.1 Trait data 46
2.4.2 Climate data 50
2.4.3 Data analysis 50
2.5 Results 52
2.6 Discussion 59
CHAPTER 3 PREDICTABILITY OF LEAF TRAITS WITH CLIMATE AND ELEVATION: A CASE STUDY IN GONGGA MOUNTAIN, CHINA **65**
3.1 Abstract 66
3.2 Introduction 66
3.3 Methods 70

3.3.1 Study sites 70
3.3.2 Sample collection and analysis 71
3.3.3 Climate data 75
3.3.4 Trait data analysis 77
3.3.5 Trait prediction 77
3.3.5.1 The model for χ 78
3.3.5.2 The model for V_{cmax25} 79
3.3.5.3 A new model for M_a 80
3.3.5.4 A simple model for N_{area} 83
3.3.5.5 Estimating the contribution of individual predictor variables 84
3.3.5.6 Uncertainty of the model predictions 85
3.3.6 Model evaluation 85
3.4 Results 86
3.4.1 Traits variation related to climate 86
3.4.2 Observed and predicted trait variation with elevation 87
3.4.3 Contribution of climate and elevation to trait variations 93
3.5 Discussion 95
3.6 Implications for terrestrial ecosystem models 101
CHAPTER 4 GLOBAL VARIATION IN THE RATIO OF SAPWOOD TO LEAF AREA EXPLAINED BY OPTIMALITY PRINCIPLES 103
4.1 Abstract 103
4.2 Introduction 104
4.3 Theory 107
4.4 Methods 110
4.4.1 Theory based on eco-evolutionary optimality 110
4.4.2 Datasets 112
4.4.3 Statistical analysis 114
4.5 Results 116
4.5.1 Correlations between hydraulic traits 116
4.5.2 v_H variation along climate gradient 118
4.5.3 Prediction of hydraulic traits 119
4.6 Discussion 120
CHAPTER 5 SUMMARY AND OUTLOOK 127
5.1 Conclusions 127
5.2 Limitations and outlook 128

APPENDICES **136**
Appendix 1 – Other publications 136
Appendix 2 – Supplementary material to Chapter 2 137
Appendix 3 – Supplementary material to Chapter 3 141
Appendix 4 – Supplementary material to Chapter 4 155
BIBLIOGRAPHY **165**

List of Figures and Tables

Figure 1.1 The schematic of trait variations along climate gradients (a) and trait trade-offs (b). 19
Figure 1.2 The published papers containing the term “plant hydraulic trait” during the last two decades 20
Figure 1.3 The water transport process and key hydraulic traits 22
Figure 1.4 Hypothesized hydraulic traits trade-offs. 26
Figure 1.5 A trait network summarized from the literature. 28
Figure 1.6 The roadmap of objectives and aims. The green part represents data analysis and yellow part represents model development and validation. 35
Figure 2.1 Variance partitioning (%) for each trait. 53
Figure 2.2 Path analysis of hydraulic and photosynthetic traits for all species (a), separately deciduous (b) and evergreen species (c). 55
Figure 2.3 The modelled contribution of different predictors to v_H variation at 11 sites sampled along an elevational gradient in the Gongga Mountains, China. 57
Figure 2.4 Comparison between site-mean observed and predicted ratios of sapwood to leaf area (v_H). 59
Figure 3.1 The study area. 71
Figure 3.2 Climate-related trait dimensions from redundancy analysis (RDA).. 87
Figure 3.3 The observed and predicted values of traits along the altitudinal gradient. 89
Figure 3.4 The distribution of predicted trait values in a climate space defined by elevation and a moisture index (α_p) using Generalized Additive Models. 90
Figure 3.5 Site-mean values of traits 92
Figure 3.6 Partial residual plots showing leaf nitrogen content per unit area (N_{area}) as a function of leaf mass per area (M_a) and the maximum capacity of carboxylation standardized to 25 ˚C (V_{cmax25}) with N-fixer as an interaction term. 93
Figure 3.7 The modelled contributions of individual climate variables for each trait at each site. 94
Figure 4.1 The sensitivities of theoretical model to climate and hydraulic traits. 109
Figure 4.2 Partial residual plots from the multiple linear regression of $\log_e$-transformed the ratio of sapwood to leaf area (v_H) against different predictors at site level using Dataset1. 117
Figure 4.3 Partial residual plots from the multiple linear regression of $\log_e$-

transformed the ratio of sapwood to leaf area (v_H) against different predictors at species level using Dataset1. 118
Figure 4.4 Comparison between site-mean observed and predicted ratios of sapwood to leaf area (v_H) using Dataset1. 120
Figure 5.1 The trait coordination network across three sites in tropical rainforests in China. 130
Figure 5.2 The locations of plots I have with available traits and species abundance data (a) and distributions of LMA in Ghana (b) and Brazil (c). 133
Figure 5.3 The comparisons of v_H distribution at different climate zones in Dataset1. 134
Table 3.1 Parameters and abbreviations frequently used in the text. 72
Table 3.2 The comparison between R^2 of statistical models (multiple linear regressions of the site-mean trait values against the driving climate data) and optimality models..... 91

Abbreviations

A	Carbon assimilation rate
A_a	Daily carbon assimilation rate per unit leaf area
b	The potential age when leaves can no longer photosynthesize and assimilate CO_2
c	A constant proportional to the unit carbon cost for the maintenance of electron transport capacity
C	Parameter in the hydraulic trait model
CC	A constant representing the construction carbon cost per unit leaf mass carbon
c_a	Ambient CO_2 partial pressure
c_i	Leaf internal CO_2 partial pressure
CO_2	Carbon dioxide
CV	Coefficient of variation
D	Vapour pressure deficit
D_0	Mean vapour pressure deficit during the growing season
D_{max}	Monthly mean maximum vapour pressure deficit
DGVMs	Dynamic global vegetation models
E	Transpiration rate
EEO	Eco-evolutionary optimality
f	The ratio of growing season length to the number of days in the year
GAMs	Generalized Additive Models
g_s	Stomatal conductance
h	Path length of water transport, roughly equivalent to plant height
I_{abs}	Photosynthetically active radiation
k	Scaling factor from mol C^{-1} to g biomass
K	The effective Michaelis-Menten coefficient of Rubisco
K_c	The Michaelis-Menten coefficients of Rubisco for carboxylation (Pa)
K_S	Sapwood-specific hydraulic conductivity
K_{S25}	Sapwood-specific hydraulic conductivity at standard 25 ˚C
LES	Leaf economic spectrum
LL	Leaf longevity
LMA, M_a	Leaf mass per area, note that M_a is used in Chapter 3
MAP	Mean annual precipitation

N_{area}	Leaf nitrogen content per area (g m^{-2})
$N_{rubisco}$	Nitrogen content in Rubisco enzymes
$N_{structure}$	Nitrogen content in leaf structure
p	Probability value
P_{atm}	Atmospheric pressure (Pa)
PCA	Principal component analysis
PFT	Plant functional type
P50	Xylem water potential at which 50% loss of conductivity
Q_{10}	Temperature sensitivity of hydraulic conductivity
r	Coefficient of correlation
R_0	Mean photosynthetically active radiation during the growing season
R_{LAI}	Mean leaf area index weighted photosynthetically active radiation during the growing season
RDA	Redundancy analysis
RMSE, rmse	The Root Mean Square Error
r^2	Coefficient of determination
T	Temperature
T_g	Mean temperature during the growing season (˚C)
T_{dJ}	Mean daytime temperature of July (˚C)
T_{max}	Monthly mean maximum temperature (˚C)
u	Unit conversion coefficient from μmol to mol
V_{cmax}	The maximum capacity of carboxylation
V_{cmax25}	The maximum capacity of carboxylation at 25 ˚C
v_H	Sapwood to leaf area ratio (unitless)
WES	Wood economic spectrum
WD	Wood density
α_p	Ratio of potential to actual evapotranspiration
β	The ratio at 25 ˚C of the unit costs of maintaining carboxylation and transpiration capacities (estimated as 146)
$\delta^{13}C$	Leaf stable carbon isotope ratio
$\Delta\Psi_{max}$	Maximum water potential difference between soil and leaf
Δ	Carbon isotopic discrimination
Γ^*	The photorespiratory compensation point
φ_0	The intrinsic quantum efficiency of photosynthesis
η	Viscosity of water relative to its value at 25 ˚C

Ψ_{min}	Minimum leaf water potential
Ψ_{soil}	Soil water potential
Ψ_{tlp}	Leaf water potential at turgor loss point
χ	The ratio of leaf-internal to ambient CO_2 partial pressures

CHAPTER 1 Introduction

1.1 Vegetation, climate change and the terrestrial carbon cycle

Vegetation plays a central role in controlling the terrestrial carbon cycle, through key processes such as photosynthesis, respiration and mortality, it also stores ~28% of global carbon sink (Friedlingstein et al., 2023; Le Quéré et al., 2018). Anthropogenic climate change is predicted to have profound effects on global climate, including rising global temperatures and shifts in precipitation patterns, causing considerable alterations to the global carbon cycle (IPCC, 2023). These changes in global carbon cycling will be largely mediated by vegetation as changes in climate alter the capacity of vegetation to absorb CO_2 from the atmosphere (Dusenge et al., 2019; Frank et al., 2015) and are likely to increase vegetation mortality (Allen et al., 2010; McDowell et al., 2022). These changes in vegetation function and mortality will have a positive feedback on climate change, as they have the potential to rapidly increase the amount of CO_2 in the atmosphere, accelerating climate change (Richardson et al., 2013). We must understand and predict the interactions between terrestrial vegetation and global climate in order to predict how climate change will impact our planet, as these predictions are central to enabling climate adaptation and mitigation to take place.

The changes predicted to occur as a consequence of anthropogenic climate change can alter the terrestrial carbon cycle in various ways. Some of these changes may lead to increasing CO_2 uptake by vegetation, for example rising temperatures can increases growing season length, leading to vegetation greening (Fu et al., 2015; Piao et al., 2019; Zhu et al., 2023), furthermore CO_2 fertilisation is predicted to increase terrestrial carbon uptake (Schimel et al., 2015; Wang et al., 2020b). However, these phenomenon can create complex

feedbacks in the climate system including increased evapotranspiration and irradiance absorption, which may for example accelerate soil dryness and extreme heat events (Wu et al., 2024; Yang et al., 2023). The impacts of extreme heat and drought that will occur across the globe as climate change occurs (Tripathy et al., 2023) are however predicted to have a far greater negative impact on terrestrial CO_2 storage, than any positive effects (Xu et al., 2019). Drought and heatwave events increase plant vulnerability to disturbances (i.e. pests and diseases), downregulate photosynthesis and even causing widespread tree mortality (Hammond, 2020; Li et al., 2023; Trugman et al., 2021; Yan et al., 2024). However, the feedbacks between the carbon stored in vegetation and the atmosphere, under climate changes are hugely complex and high uncertainty remains concerning exactly how climate change will influence vegetation functioning globally (Bonan, 2008; Seddon et al., 2016; Zhu et al., 2016).

1.2 Plant hydraulics and global carbon cycling

Increasing drought frequency and intensity around the globe as a consequence of climate change (Cook et al., 2018; Lehner et al., 2017) makes understanding plant water relations essential to predicting changes in plant carbon source, sink dynamics. Processes such as stomatal opening, plant growth and in many instances mortality are governed by the stress the plants vascular system is subject to (Hoeber et al., 2014; Rowland et al., 2021; Sperry et al., 2017; Torres-Ruiz et al., 2024; Venturas et al., 2020). In particular, water loss and carbon uptake via stomata inextricably link water and carbon cycling within plants (Brodribb, 2009). This means that a plants hydraulic traits are critical to explaining the changes in water and carbon fluxes which occur in response to periods of drought (Anderegg et al., 2018; Jiménez‐Rodríguez et al., 2024). Limited soil water availability and greater leaf-to-air vapour pressure

deficit reduces stomatal conductance, limiting water loss and hydraulic damage, but simultaneously reducing photosynthesis and growth (Grossiord et al., 2020; Sperry et al., 2016; Wang et al., 2019b). Plant hydraulics not only affect carbon assimilation and plant growth, but also plant mortality and recruitment under water limited conditions, which can have long-term effects on carbon storage within an ecosystem (Song et al., 2023).

Plant hydraulic theory has emerged as a key set of principles which allow us to better understand how plant water transport and mortality risk are altered under increasing atmospheric and soil dryness (Choat et al., 2018; Hammond et al., 2019; McDowell et al., 2022). Critically, the plant wants to avoid hydraulic failure, which triggers death under severe drought conditions (Rowland et al., 2015; Trugman et al., 2021). The risk of hydraulic failure is principally driven by the vulnerability of the xylem to embolism, the formation of air bubbles, which block water flow in the vessels (Hacke et al., 2001b; Tyree and Sperry, 1989; Venturas et al., 2017). However, there are many other traits which are also key to understanding a plants capacity to function during drought. For example, leaf turgor loss point, the capacity for leaf cells to maintain turgor during drought stress is key to understanding the limit of leaf function and can be used to predict drought-induced tree mortality risk (Álvarez-Cansino et al., 2022; Choat et al., 2018; Pivovaroff et al., 2021). Furthermore, the hydraulic status of the plant can also indirectly impact a plants susceptibility to damage and mortality. Hydraulic stress within a plant can increase the susceptibility of plants to fire and pathogens (Ruffault et al., 2023; Torres-Ruiz et al., 2024). Currently, however, at a global scale we understand much less about the processes involved in plant water transport, particularly under drought, than we do about many other areas of plant functioning. This means that currently there we have a limited capacity to accurately predict the feedback from changes in plant water status on carbon cycling as the climate changes.

1.3 The introduction of plant hydraulics to vegetation modelling

Dynamic global vegetation models (DGVMs) were developed to simulate vegetation processes to improve the predictions of the feedback between the land and the atmosphere in global climate models. Most models focus on the effects of climate variables on vegetation processes related to carbon cycling, such as photosynthesis and plant carbon allocation, mostly using empirical functions (Clark et al., 2011; Fatichi et al., 2019; Krinner et al., 2005; Lawrence et al., 2019; Quillet et al., 2010). However, different models predict diverging magnitudes of land carbon sink, especially under future climate conditions (Bugmann et al., 2019; Friedlingstein et al., 2023). A substantial part of this uncertainty comes from the use of static parameter/trait values for plant functional types (PFTs) and empirical functions used to simulate the climate effect on plant physiological processes (Bonan and Doney, 2018; Cui et al., 2019; O'Sullivan et al., 2022). For example, photosynthetic capacity at a standard temperature, a key parameter in calculations of photosynthetic rate and leaf respiration, is treated as one value for all trees in broadleaf evergreen tropical forest, which neglects large inter- and intra-specific variations in photosynthetic capacity and its acclimation to key variables like temperature (Yan et al., 2023). In most models the downregulation of photosynthesis under water-limited condition is estimated using empirical function related to soil moisture (Martín Belda et al., 2022; Stocker et al., 2018). This approach neglects the underlying adjustment of plant hydraulic process that couples with photosynthesis when soil water availability drops. The static PFTs and simplification of certain plant physiological processes can reduce the complexity of DGVMs, which is necessary when there is limited data available for parameterization and the underlying mechanisms remain unclear (Box, 1996). However, recently many attempts have been made to develop next-generation trait-based DGVMs with more complex processes and parameterization

(Berzaghi et al., 2020; Pavlick et al., 2013; Prentice et al., 2015; Scheiter et al., 2013).

An increasing number of studies have been carried out regarding the prediction of trait variation with climate (Butler et al., 2017; Dong et al., 2023), facilitating the implementation of more complex plant physiological processes into DGVMs, such as mechanistic plant hydraulic process (Christoffersen et al., 2016; Hickler et al., 2006; Kennedy et al., 2019; Li et al., 2021). The hydraulic process in most DGVMs is adopted from the main structure of soil-plant plant water transport model based on Darcy's law (Sperry et al., 1998; Sperry and Love, 2015). The water transport model calculates plant water flow under water potential gradient, using the principle of changing hydraulic conductivity along flow path through a plant. Although this can greatly improve model capability to predict plant responses under drought conditions (Eller et al., 2020; Venturas et al., 2018; Xie et al., 2023; Xu et al., 2016; Yan and Dickinson, 2014), the incorporation of hydraulic process brings extra parameters, which in turn increases uncertainty of DGVMs (Cui et al., 2019; Kennedy et al., 2019; Oberpriller et al., 2022; Song and Zeng, 2014; Zaehle et al., 2005). Hydraulic parameters are hard to constrain relative to photosynthesis parameters, due to greater limitations in field observations, which can hinder model evaluation at large spatial scales. How changes in environmental conditions expected as a consequence of climate change control global patterns of hydraulic trait variation remain a challenge to understand, but an essential piece of information to improve plant hydraulic trait representation in DGVMs.

1.4 Plant trait variation

Plant traits, including hydraulic traits are known to vary along environmental gradients in response to changes in climate and soil conditions and variations in the species composition of a community (Moran et al., 2016; Wang et al., 2023;

Wright et al., 2017). The observed trait-climate relationships at large spatial scales result from environment filtering and long-term adaptation of plants to their environmental niche, often through evolutionary processes. However, trait relationships are more complex than a direct relationship with climate, as trait trade-offs mean a climate related adaptation in one trait is likely to necessitate a change in one or more of the plants other traits. For example if a plant allocates more resource in one aspect of function, for example growing tall, it must inevitably reduce investment in another aspect of its function in order to increase fitness under the current habitat (Figure 1.1) (Chave et al., 2009; Diaz et al., 2016; Reich and Cornelissen, 2014). The “leaf economic spectrum (LES)” proposes a suite of plant trait trade-offs which are coordinated with one another (Wright et al., 2004b). LES states that plants with high leaf mass per area (LMA) have longer leaf life spans, the cost of which is lower low nitrogen content and carbon assimilation rates. This strategy within LES is known as a conservative resource-use strategy, where traits associated with survival and resistance are prioritised over those associated with rapid resource acquisition and growth.

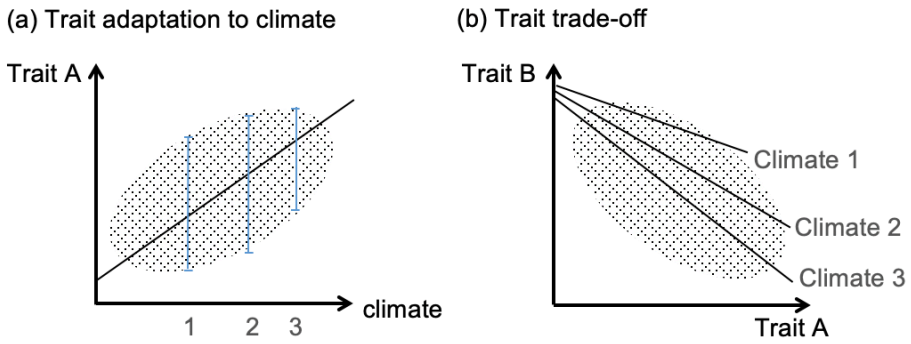

Figure 1.1 The schematic of trait variations along climate gradients (a) and trait trade-offs (b). (a) Variation of Trait A (black dots) across different climate conditions, with the range of variation under each condition illustrated by blue bars. (b) Trait A is related to Trait B (black lines), which is potentially affected by climate conditions.

Relative to traits related to photosynthesis and the LES, the global study of plant hydraulic traits is far more recent. For example, although more than 3000 papers have been published in hydraulic traits in the last two decades, over half of them have been published within the last five years (Figure 1.2). Given this, many gaps in our knowledge still exist regarding the major global controls on plant hydraulic trait variation. More data and more combined model, data analyses are urgently needed to understand the theoretical mechanisms behind plant hydraulic trait variations in response to climate variables and the traits trade-offs they generate. This will provide the foundations to fully incorporate plant hydraulics into DGVMs.

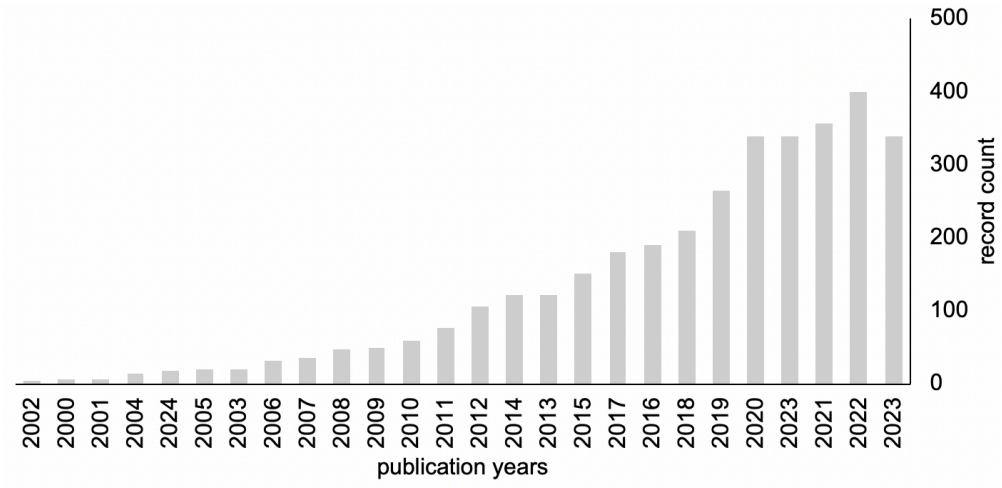

Figure 1.2 The published papers containing the term “plant hydraulic trait” during the last two decades.

1.5 Plant hydraulic system

The process of water movement in plants is governed by a series of physiological mechanisms, where water is absorbed by the roots, transported via the xylem to the leaves, and ultimately transpired into the atmosphere through stomatal openings (Figure 1.3). Soil water potential determines the soil water limitation for a plant and the level to which a plant needs to reduce its own water potential below in order to extract water from the soil. Cohesion-Tension

theory demonstrates that water potential difference between leaf and soil ($\Delta\Psi_{max}$) drives continuous water flow from root to leaf surface (Bohm, 1893; Dixon and Joly, 1894). This process drives transpiration, enabling stomata to open and photosynthesis to occur within the plant.

Several key hydraulic traits regulate this water transport process, including the vulnerability of the xylem to embolism and the sapwood-specific hydraulic conductivity (K_S). K_S is defined as the efficiency of water movement through the xylem, the water flow rate on mass basis per unit conducting area (sapwood) combined with the hydraulic gradient (water potential difference per unit length in the direction of water flow) (Reid et al., 2005). K_S is likely to be determined to a large degree by xylem vessel properties (Yang et al., 2019a; Zanne et al., 2010), meaning it is connected to the wood density (WD) of the xylem, an integrative trait which linked to both mechanical support and hydraulic transport. The sapwood to leaf area ratio (Huber Value, v_H) is also another key integrative hydraulic trait reflecting the balance between water supply through xylem and water demand by the leaves. As soil water potential (Ψ_{soil}) drops or atmospheric demand from the leaves increases driven by high VPD, leaf water potential can reduce sufficiently to drive turgor loss, making leaf water potential at turgor loss point (Ψ_{tlp}) another key trait determining drought tolerance (Brodribb et al., 2003). If soil water keeps being depleted and/or VPD keeps rising, embolism occurs in the xylem and the continuous water flow breaks, leading to the loss of conductivity. The xylem water potential at which 50% loss of conductivity occurs (P50) is a key parameter used to determine plants vulnerability to embolism (Choat et al., 2018).

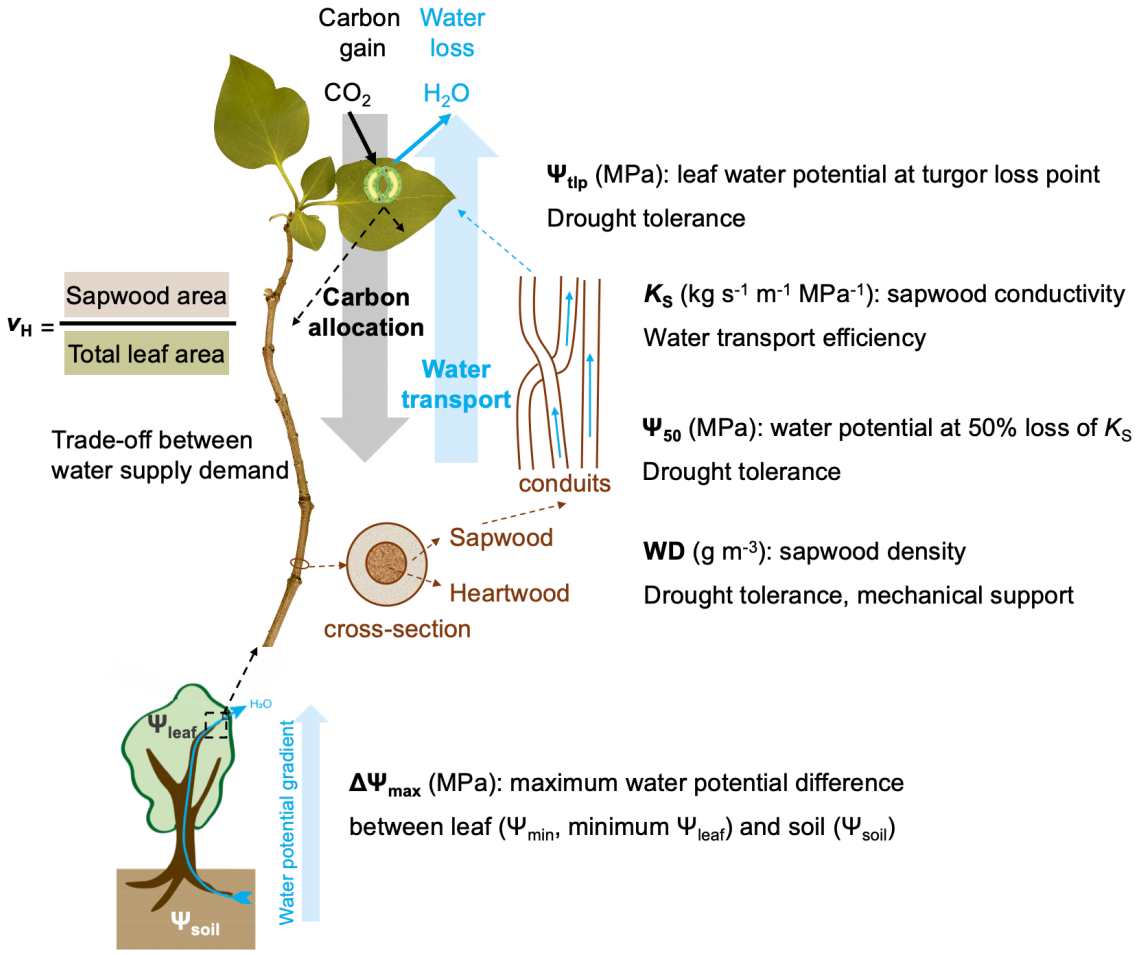

Figure 1.3 The water transport process and key hydraulic traits. v_H is the ratio of sapwood area to total leaf area supported by the branch, representing balance between water supply and demand. K_S is sapwood-specific hydraulic conductivity, a measure of xylem water transport efficiency. Ψ_{soil} and Ψ_{leaf} are soil and water potential, respectively. The difference between Ψ_{soil} and minimum Ψ_{leaf} is $\Delta\Psi_{max}$. Ψ_{tlp} is leaf water potential at turgor loss point and P50 is xylem water potential at 50% loss of K_S, which reflects drought resistance at leaf and stem levels respectively. Sapwood density (WD) is related to drought resistance and mechanical support.

1.5.1 Hydraulic trait correlation

The creation of LES and a corresponding wood economic spectrum (WES) (Chave et al., 2009) has accelerated the investigation of traits trade-offs of other plant functions over the last decade. WES is centred on trade-offs related to WD and its associations with different functions of wood, including water transport, as well as mechanical resistance and nutrient allocation (Chave et al., 2009; Reich and Cornelissen, 2014). Dense wood necessitates less vessel lumen area and small conduit diameters, which limits water transport capacity (Fan et al., 2012; Hoeber et al., 2014). This leads to a negative relationship between wood density and hydraulic efficiency (Janssen et al., 2020), as water flow rate is related to fourth power of conduit diameter based on the Hagen-Poiseuille equation (Hagen, 1839). However, narrower vessels associated with denser wood often enhances xylem safety through enhanced cavitation resistance (i.e. low Ψ_{50}) at the expense of water transport efficiency (Hacke and Sperry, 2001). Numerous studies have investigated these presumed WES traits trade-offs, but often there are contrasting findings (Fan et al., 2012; Poorter et al., 2010; Sperry et al., 2008). For example, Ocheltree et al. (2016) demonstrate the trade-off between hydraulic efficiency and safety exists in C_4 grass, while van der Sande et al. (2019) finds it in trees, but not lianas in tropical moist forest. The safety efficiency trade-off is also found to be weak or absent across sites and species on a global scale, possibly due to large sensitivities to climate and seasonality (Gleason et al., 2016; Liu et al., 2021). Measurement limitations of hydraulic traits could also contribute to these discrepancies. The trade-offs is theorised to exist at a tissue level across the plant, however hydraulic traits are often measured in one specific piece of xylem in a branch (Blackman et al., 2010; Franklin et al., 2023; Hacke and Sperry, 2001; Meinzer et al., 2010). What's more, xylem vulnerability and conductance are not the only traits that determined whole plant safety and efficiency and therefore the trade-off is likely

to be more complex than the traits contained within WES (Oliveira et al., 2021; Rowland et al., 2023). In fact WES, although it encompasses hydraulic and anatomical traits related to the xylem, is more focused on resource allocation strategies at stem level for optimizing growth and survival (Choat et al., 2008; Venturas et al., 2017), meaning it can't fully capture plant hydraulic trait trade-offs.

For hydraulic traits new theories surrounding trait trade-offs are being created in relation to the huber value (v_H), linking leaf water demand and stem water supply, to tissue resource allocation and the equilibrium between water supply and loss (Mencuccini et al., 2019b; Trugman et al., 2019a) (Figure 1-3). A limit exists regarding the total leaf area that can be supported by a given amount of sapwood, constrained by its capacity to supply water. Plants balance this by either increasing sapwood investment to meet higher water demands or shedding leaves to reduce water loss, thereby tightly coupling v_H with other hydraulic traits. Plants with high hydraulic conductivity can allocate more carbon to leaf area to maintain sufficient water supply, despite small sapwood area. The xylem hydraulic efficiency (K_S) has been widely observed to scale with v_H (Liu et al., 2019; Mencuccini et al., 2019b; Pivovaroff et al., 2014; Rosas et al., 2019). Additionally, an evolutionary correlation between K_S and v_H suggests they are co-adapted in relation to environmental stress, highlighting their importance for plant survival (Sanchez‐Martinez et al., 2020). This trade-off leads to indirect associations between v_H with WD (Limousin et al., 2010; Mencuccini et al., 2019b; Preston et al., 2006) and hydraulic safety (Markesteijn et al., 2011), however this is not detected across all ecosystems (Rosas et al., 2019), for example it is absent in moist tropical forests (De Guzman et al., 2021).

Alongside v_H, Ψ_{tlp} is another trait that is likely to underpin plant hydraulic strategy, as it is inherently linked to stomatal behaviour, vulnerability to xylem

cavitation, and resource allocation (Álvarez-Cansino et al., 2022; Bartlett et al., 2012b; Rodriguez-Dominguez et al., 2016). Bartlett et al. (2012b) illustrate that osmotic potential at full turgor, rather than bulk modulus of elasticity, predominantly determines Ψ_{tlp}, meaning osmotic adjustments and their associated changes in water potential will determine which traits link to Ψ_{tlp}. Ψ_{tlp} is therefore found to be coupled with stem-level hydraulic traits (i.e. P50) and WD in some studies (De Guzman et al., 2021; Fu et al., 2012; Ocheltree et al., 2016; Santiago et al., 2018; Zhu et al., 2018), indicating a coordinated response to drought resistance across different plant organs is likely to exist (Pivovaroff et al., 2018). However, like the v_H associations, these trade-offs are not consistent across ecosystems. Ψ_{tlp} is not significantly associated with WD in tropical rainforest (Maréchaux et al., 2015), nor is Ψ_{tlp} consistently associated with hydraulic efficiency across all species (Rosas et al., 2019). Given this a high degree of uncertainty remains concerning the interaction between leaf- and stem-level hydraulic traits.

Overall, plants with low WD generally exhibit high water transport efficiency (K_S) to compensate for evaporation demand and support low v_H. This acquisitive strategy potentially allows plants to grow faster, but at the cost of reduced tolerance to environmental stress like drought (low Ψ_{tlp}, Ψ_{50}). In contrast, plants with low K_S and high WD tend to have high v_H, achieved either through smaller leaf areas (reducing evaporation demand) or larger sapwood areas (increasing water supply). This conservative strategy prioritizes greater safety under dry conditions, balancing the trade-offs between growth and drought resistance (Figure 1.4). However, these hydraulic traits trade-offs still remain uncertain, mostly due to limited data availability.

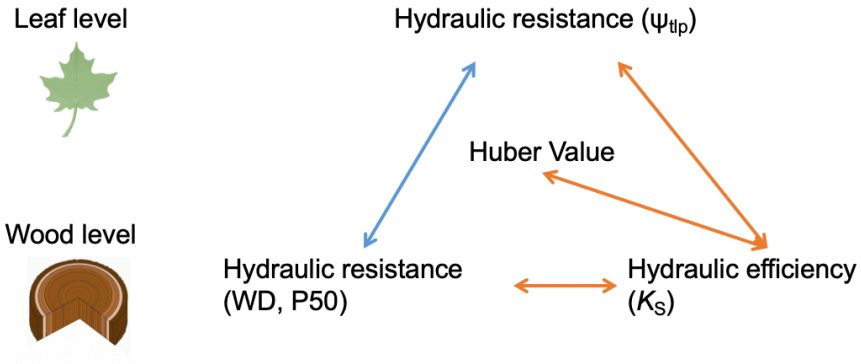

Figure 1.4 Hypothesized hydraulic traits trade-offs. Blue line represents positive correlations and orange lines represent negative correlations.

1.5.2 Coordination of hydraulic and non-hydraulic traits

Traits relating to different plant physiological processes are often well integrated to regulate whole plants behaviour under the local climate conditions the plant evolved within (Fontana et al., 2021; Pigliucci, 2003). Plant water transport processes are linked with other physiological processes, such as photosynthesis and resource allocation, leading to the coordination between hydraulic traits and non-hydraulic traits. In theory, plant hydraulic and photosynthetic traits should be coordinated due to them both influencing leaf gas exchange via stomata (Sperry, 2000; Sperry et al., 2016). At the leaf level, stomatal behaviour, influenced by leaf turgor, modulates water loss in response to changes in soil water potential. This is supported by correlations between Ψ_{tlp} and several traits including leaf water potential at 50% of stomatal closure, minimum water potential and leaf stable carbon isotope ratios ($\delta^{13}C$, reflective of leaf internal CO_2 concentration) (Brodribb et al., 2003; De Guzman et al., 2021; Jin et al., 2023; Rosas et al., 2019). At the stem level, sapwood hydraulic conductivity, which controls water supply for transpiration affects stomatal behaviour and, consequently, leaf internal CO_2 concentration (c_i). Thus, hydraulic conductivity theoretically imposes indirect effect on photosynthetic capacity, which are linked with c_i, and photosynthetic assimilation rate (A).

While many studies identify a negative correlation between hydraulic conductivity and $\delta^{13}C$, this pattern is not universally observed across all species (Ambrose et al., 2009; Ávila‐Lovera et al., 2020; Hoeber et al., 2014; Rosas et al., 2019). However, very few studies have investigated the relationships between hydraulic traits and photosynthetic capacity (Brodribb and Feild, 2000; Meinzer et al., 2008). Limited paired dataset including both hydraulic and photosynthetic traits currently hinders our capacity to comprehensively understand how these trait networks coordinate.

A growing number of studies have investigated the relationships between LES and hydraulic traits, however the coordination with hydraulic traits remains unclear. Leaf mass per area (LMA), reflects the construction cost of a leaf, when allocating a fixed amount of carbon to leaf development, therefore plants can either increase total leaf area by producing thinner leaves (low LMA) or decrease leaf area by developing thicker leaves (high LMA). This links LMA directly to transpiration and water demand via its impact on the v_H (Mencuccini et al 2019b). This leads to the interaction between LMA and hydraulic traits, K_S in particular (Fu et al., 2012; Guan et al., 2023; Mencuccini et al., 2019b; Yang et al., 2019a). Furthermore, some studies show that LMA is significantly related to vessel diameter and WD, but independently of K_S (Méndez-Alonzo et al., 2012; Zhang et al., 2020). In addition to hydraulic efficiency, it has been reported that the trade-off between LMA and leaf life span correlate with drought tolerance (Nadal et al., 2023; Savi et al., 2017; Zhu et al., 2018), but the underlying mechanism for this remains unclear. One plausible explanation is that the more resources invested in strengthening cell structures (i.e. bulk modulus of elasticity) enhance stress tolerance through adjustment of osmotic potential (Bartlett et al., 2012b; Iqbal et al., 2020).

In summary, plants with high resource-acquisition strategy (greater assimilation rates and low LMA and leaf longevity), tend to have high hydraulic

efficiency to facilitate greater water supply (Figure 1.5). As the leaves of acquisitive plants tend to have short-life spans, it is less efficient to invest carbon into drought tolerance strategies, for example high Ψ_{tlp}. The opposite is true for longer-lived conservative plants. The coordination between hydraulic and non-hydraulic traits has however, yet to be clearly placed within a unified theoretical framework, mostly due to the lack of sufficient data.

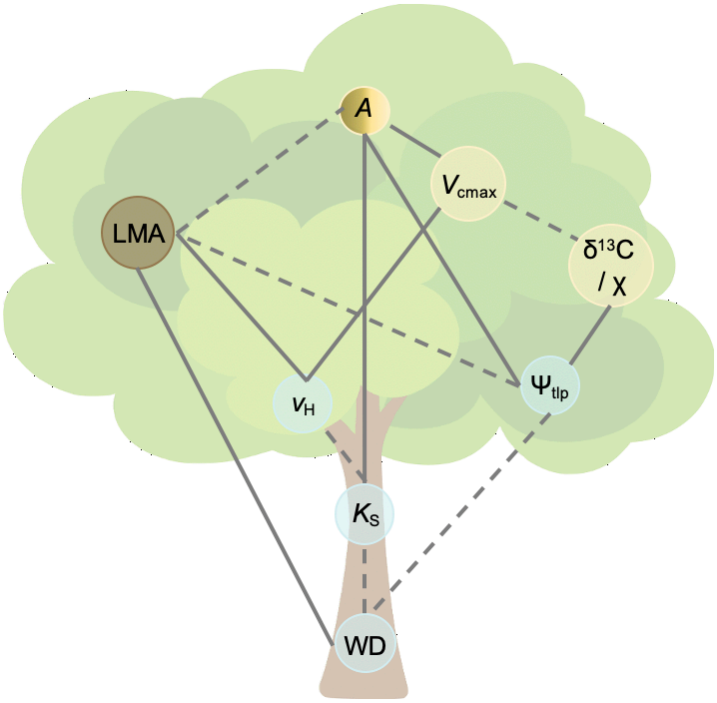

Figure 1.5 A trait network summarized from the literature. The blue, brown and yellow circles represent hydraulic, LES and photosynthetic traits respectively. The solid and dashed lines indicate positive and negative relationships respectively.

1.5.3 Hydraulic trait variation with climate

Plant traits variations are affected by diverse climate variables, the significance of which varies across different timescales. Evolution drives trait variations over long timescale through several mechanisms, such as natural selection, mutation and gene flow. These evolutionary processes lead to convergence of traits within lineages, indicating that closely related species tend

to have similar traits values (Guillemot et al., 2022; Sanchez‐Martinez et al., 2020). The selective pressure of environment is also a critical factor that shapes spatial pattern of traits through local adaptation and species turnover occurring over multiple generations (Anderegg, 2023; Meng et al., 2015; Xu et al., 2023). Moreover, changes in environment during short-time periods can also induce trait responses which are not related to genetic changes, known as plasticity (Bartlett et al., 2014; Liu et al., 2022; Valladares et al., 2007). Trait variation is a complex outcome of these underlying processes, reflecting both evolutionary history, community change and plasticity.

At large spatial scales or long timescales, hydraulic traits show large variations across environmental gradients. Large interspecific hydraulic traits variations are mainly explained by phylogeny and taxonomy (Rosas et al., 2019; Sanchez‐Martinez et al., 2020). This indicates the variations in hydraulic traits along climate gradient is mainly mediated by species turnover. For example, hydraulic efficiency is high in tropical rainforest to support high water demand/transpiration and protect leaves from high temperatures (Doughty et al., 2023; Guan et al., 2023; He et al., 2020; Jin et al., 2023; Zhu and Zhao, 2022). Conversely, drought tolerance both at leaf and stem levels increases towards arid environments to increase plants fitness and survival in the face of greater water stress (Kunert et al., 2021; Rosas et al., 2019; Zhu et al., 2018). In addition, plants in these dry environments have small total leaf area (high v_H) to reduce total transpiration and/or water demand (Anderegg et al., 2021; Togashi et al., 2015; Towers et al., 2023; Trugman et al., 2019b). Most studies intuitively focus on the effect of moisture on hydraulic traits variations, but seldom examine the effects of other climate variables. A recent review by Grunwald et al. (2024) emphasizes the importance of light on leaf hydraulics, as light drives photosynthesis which determines the demand on the hydraulic system. These robust trait-environment relationships suggest that hydraulic

traits are pivotal in determining the evolutionary selection of plants for a given environment.

On short timescale, plants may be able to adjust some hydraulic traits plastically in response to fluctuating climate. Ψ_{tlp} being mainly controlled by osmotic potential at full turgor enables it to change more easily with elevated drought stress (Bartlett et al., 2012b). Ψ_{tlp} can decline following drought via osmotic adjustment, which is far less costly than changed in wood structure (Bartlett et al., 2014; Choat et al., 2007). However, the plasticity of Ψ_{tlp} is constrained within a narrow range (Limousin et al., 2022), only adjusting 16% of its average value across species (Bartlett et al., 2014). This indicates the limited power of Ψ_{tlp} to mitigate the impact of severe drought. Some species shed leaves to decrease transpiration under drought (Nadal-Sala et al., 2021), as they fail to adjust hydraulic efficiency and safety (i.e. P50) within a short period due to the dependence of this trait on wood anatomy (Bittencourt et al., 2020; Limousin et al., 2010; Limousin et al., 2022). Leaf shedding (change in v_H) is therefore a more common and efficient strategy for plants to regulate water demand and avoid xylem cavitation under drought over short time periods (Nadal-Sala et al., 2021; Trugman et al., 2019b; Wolfe et al., 2016). Nevertheless, McBranch et al. (2019) observe no change in v_H under drought and warming treatments. Therefore, it is possible different species may adopt different strategies to cope with unfavourable climate conditions. The capacity of hydraulic traits to be plastic is however very poorly understood and for the majority of hydraulic traits there is limited evidence to support large plastic changes being possible and the evidence that does exist shows key hydraulic traits, like P50 and $K_{S,}$ have inconsistent directional adjustments to drought stress (Bucci et al., 2012; Martinez-Vilalta et al., 2009; Rowland et al., 2023).

1.6 Existing application of eco-evolutionary optimality principles in ecology

Recent progress in the application of eco-evolutionary optimality (EEO) principles allows us to test predictions about trait coordination and can also provide strong explanations for observed responses of traits to environment (Franklin et al., 2020; Harrison et al., 2021). EEO principles propose that through evolutionary processes (including selection for plasticity, as well as environmental filtering of plant lineages) plants adapt to the environmental conditions under which they live. Photosynthetic traits are predicted to emerge from trade-offs between competing requirements, such as the need to balance CO_2 uptake with water loss. Analyses of $\delta^{13}C$ data have shown quantitative agreement between observed and theoretically predicted environmental responses of the ratio of leaf internal to ambient CO_2 (χ) based on least-cost hypothesis (Lavergne et al., 2020a; Prentice et al., 2014a; Wang et al., 2017b). The coordination hypothesis states that optimal maximum capacity of carboxylation (V_{cmax}) is determined by local climate conditions, leading to the capacity to predict V_{cmax} variation globally (Peng et al., 2021; Smith et al., 2019). This challenges previous assumption that photosynthetic capacity is driven by nitrogen content invested to support metabolic processes (Walker et al., 2014). However, the simulation of photosynthetic traits using long-term climate data as inputs (Dong et al., 2023), overlooks the plasticity of photosynthetic traits in response to short-term climate changes. With growing attention on hydraulic traits, water transport has been coupled into current EEO photosynthesis models to improve prediction of stomatal conductance under water-limited condition (Joshi et al., 2022; Sperry and Love, 2015).

Other than key photosynthetic traits, EEO has also been applied to simulate the variations in leaf nitrogen per area (N_{area}) (Dong et al., 2022) and leaf mass per area (LMA) (Wang et al., 2023). The need to allocate nitrogen to structural

and metabolic processes allows us to predict N_{area}. This EEO-based hypothesis has been shown to accurately capture observed temporal and spatial patterns of leaf nitrogen variation (Dong et al., 2022). Using the optimal leaf-longevity hypothesis (Kikuzawa, 1991), which states plants maximize the time-averaged net carbon gain of leaves taking into account construction costs (paid off over the leaf lifetime), an EEO model was also developed for LMA (Wang et al., 2023). This model reveals the mechanisms behind the trend of LMA with latitude (Wang et al., 2023). The successful applications of EEO principles to trait predictions confirm the feasibility of EEO principles to enhance the input of trait-based ecology into models. This enhances our understanding of how evolutionary processes shape plant traits, thereby reinforcing the integral role of EEO principles in ecological research and modelling.

1.7 Applying EEO principles to hydraulic trait modelling

Two types of models have been developed to explain the response of v_H variation to the environment based on EEO principles. Such models allow us to understand and quantify trait responses to climate in a simple way. One model type is based on the hypothesis that whole-tree transpiration rate should equal water flow rate through the stem, which was first proposed by Whitehead et al. (1984). Earlier in the 1980s, several studies have found that total leaf weight or area is proportional to the cross-sectional area of sapwood, and their slope – Huber value (v_H) – varies across species and sites (Waring et al., 1982; Whitehead et al., 1984). This confirms the pipe model theory that suggests a unit sapwood, or a pipe, supports a set amount of leaves (Lehnebach et al., 2018; Shinozaki et al., 1964). In order to examine the factors controlling this relationship, Whitehead et al. (1984) use Darcy's law and the Jarvis-Stewart modelling approach (Jarvis and McNaughton, 1986) to estimate the transpiration rate of a stem and of a forest stand respectively. They reported

that sapwood permeability plays a key role in controlling the relationship between leaf and sapwood area. However, this model used an empirical transpiration function to represent water demand driven by photosynthesis, as a more mechanistic approach had not been developed yet. This limits the model capacity of running at large scales or estimating climate effect on v_H variation from a mechanistic perspective.

The other type of EEO model which links v_H to plant hydraulic traits is based on the maximization of net carbon gain by optimal v_H, which incorporates physiological processes such as respiration and tissue turnover (Magnani et al., 2002; Trugman et al., 2019a; Westoby et al., 2012). In the model proposed by Westoby et al. (2012), carbon gain is leaf photosynthesis and the cost of this includes plant construction, investment and maintenance cost. The difference between carbon gain and total cost is maximized during a leaf's lifetime. Trugman et al. (2019a) create a different version of this model which hypothesizes that plants can maximize net primary productivity, photosynthesis minus only the maintenance cost (leaf, stem and root respiration). Although the maximization criteria differ between these two models, they produce similar predictions of how v_H responds to climate. Plants have lower v_H under elevated CO_2 and low atmospheric dryness. However, the effect of temperature is not directly deduced from the model. What's more, these two models emphasize different plant traits that affect the maximization process and in turn, optimal v_H. For example, Westoby et al. (2012) show that nitrogen concentration and wood density influence carbon cost and gain, while Trugman et al. (2019b) demonstrate the important role of K_S and V_{cmax}. These differences are concerning, as if placed within a DGVM, they could result in greater uncertainty or unconstrained parameters and maximization criteria which may conflict with other optimization processes.

Given the above contrasts in model results, it is critical to advance our understanding of hydraulic trait variation in relation to climate and other traits from both field observations and EEO principles. It is also equally important to investigate how key non-hydraulic traits vary along climate gradient to further disentangle indirect climate effects on hydraulic trait variation. A unified framework based on coordination of different physiological processes should be proposed to improve realism and reduce parameterization.

1.8 Outline of thesis

This thesis aims to develop a hydraulic trait model based on new EEO principles to explore how variations in hydraulic traits coordinate with non-hydraulic traits and climate variables. The thesis is divided into three chapters, first, a study across a 4000-m elevation transect in the Gongga Mountains, Sichuan Province, China, is presented. The large temperature and moisture gradients found here are used to measure traits at 18 sites along the elevation gradient, with traits grouped into those related to hydraulic processes (WD, K_S, v_H, Ψ_{tlp}), photosynthetic processes ($\delta^{13}C$, V_{cmax}) and leaf structure (LMA, N_{area}). This paired trait dataset is used to explore the coordination between different axes of traits. In the second research chapter this same dataset is used to test an EEO-based photosynthetic and hydraulic traits model. Finally in the third research chapter the model is evaluated at scale using global hydraulic trait datasets I compiled at species and individual levels, I examine the trait-environment relationships and compare with the EEO model predictions (Figure 1.6). The key questions my thesis aims to address are as follows:

(1) How do hydraulic, photosynthetic and LES traits coordinate with each other?

(2) What is the timeframe of climate variation that photosynthetic traits adjust to?

(3) How do hydraulic traits vary along climate gradients found at a global scale?

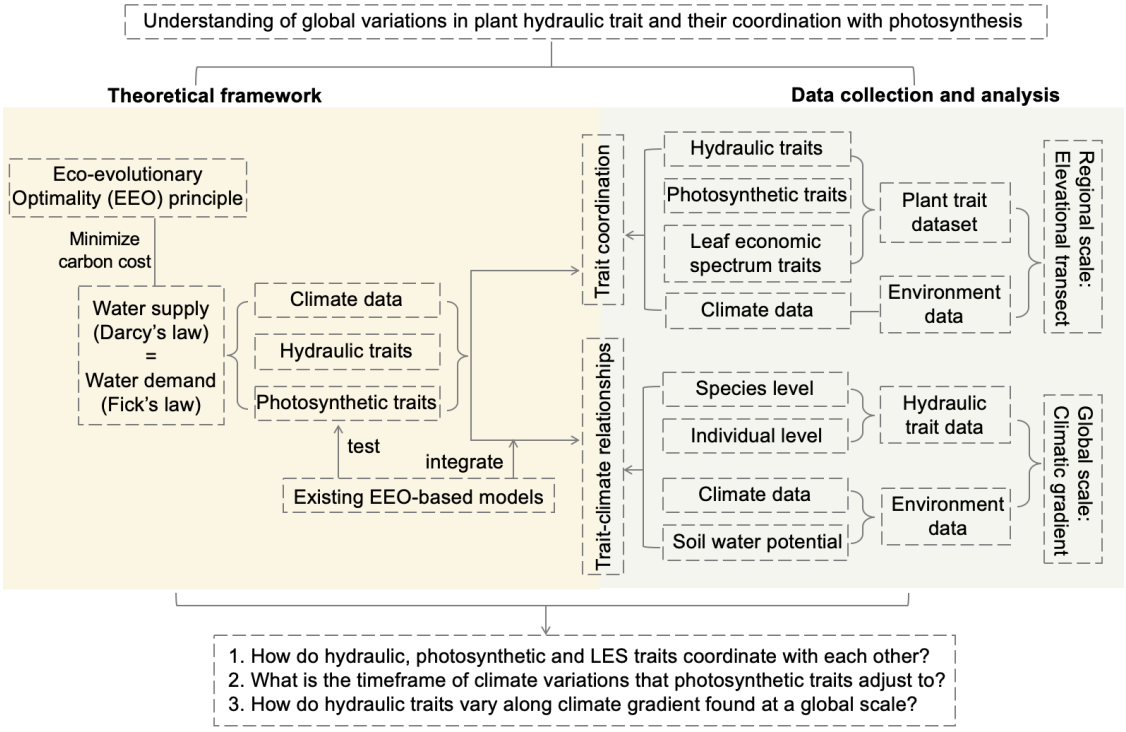

Figure 1.6 The roadmap of objectives and aims. The green part represents data analysis and yellow part represents model development and validation.

Chapter 1 briefly outlines the importance of hydraulic traits and the water transport process for understanding the feedback between the land and atmosphere under global climate change scenarios. The current state of knowledge related to relationships between hydraulic traits and non-hydraulic traits and climate variables are summarized. In particular, the theoretical principles of the links between hydraulic processes to photosynthesis processes are demonstrated. The value and application of recent EEO approaches to traits prediction are discussed alongside current theories linking hydraulic trait to the EEO prediction method. Critically this chapter outlines the key knowledge gaps this thesis contributes to.

Chapter 2 uses a supply-demand-balance hypothesis to develop a trait coordination model based on EEO principles and examines the coordination between hydraulic and non-hydraulic traits. Critically the contributions of different environmental factors in controlling trait variations are assessed and bivariate relationships between traits are examined. This enables me to build a trait coordination network to reveal the links between the different underlying physiological processes influencing trait trade-offs. Empirical relationships between the traits are then compared with model predictions and the hydraulic and photosynthetic traits are used to estimate v_H to validate model hypothesis at a regional scale. Chapter 2 therefore explains the complex coordination between hydraulic and non-hydraulic traits from both empirical and theoretical perspectives.

In Chapter 3, the capacity of a recently-developed EEO-based photosynthetic traits models (Smith et al., 2019; Wang et al., 2017b) is tested along an elevation gradient and the effects of climate variables on photosynthetic traits are disentangled. Different timeframes of climate data are used to detect the timescale of photosynthetic traits acclimation to climate. The climatic drivers of each photosynthetic trait are quantified. This chapter addresses the appropriate timeframes of climate variables for predictions of photosynthetic traits, which serves as a basis for incorporating the photosynthetic traits models into the hydraulic trait model.

In Chapter 4, the model from Chapter 2 is extended into a more advanced hydraulic trait model after incorporating the photosynthetic traits model from Chapter 3. The relationships between hydraulic traits and climate variables are examined using two global hydraulic traits datasets resolved at species and individual plant scale. The fitted sensitivities of v_H to climate variables are compared against model predictions. The hydraulic traits (K_S and v_H) variations are predicted using hydraulic trait model. The advanced hydraulic trait model

theoretically predicts the v_H variation with K_S, temperature, vapour pressure deficit and irradiance, which helps to determine how v_H changes under climate change.

Finally, in Chapter 5, the key findings of this thesis are summarised and the ongoing challenges are then discussed to provide guidance for future research.

CHAPTER 2 Coordination of plant hydraulic and photosynthetic traits: confronting optimality theory with field measurements

This chapter is **published** in New Phytologist.

Citation: Xu H, Wang H, Prentice IC, Harrison SP and Wright IJ (2021), Coordination of plant hydraulic and photosynthetic traits: confronting optimality theory with field measurements. New Phytologist, 232: 1286-1296. https://doi.org/10.1111/nph.17656

Author contribution: H.X. carried out the analyses and prepared the manuscript with contributions from all co-authors. H.W., S.P.H. and I.C.P. designed the fieldwork, collected samples and measured plant traits. I.C.P and I.J.W developed and extended the least-cost theory. All authors contributed to the interpretation of the results.

Acknowledgment and funding: We thank Yuechen Chu, Yingying Ji, Meng Li, Xinyu Liu, Giulia Mengoli, Yunke Peng, Shengchao Qiao, Yifan Su, Runxi Wang, Yuhui Wu, Shuxia Zhu and Wei Zheng for their assistance in collecting trait data in Gongga Mountain. We also thank Shen Tan for help with extraction of LAI data. This work was funded by National Science Foundation China (grant no. 31971495, 32022052, 91837312). Participation of I.C.P. and S.P.H has been supported by the High-End Foreign Expert program of the China State Administration of Foreign Expert Affairs at Tsinghua University (GDW20181100161, G20190001075, G20200001064). I.C.P. acknowledges support from the European Research Council (787203 REALM) under the European Union's Horizon 2020 research programme. S.P.H. is supported by

the European Research Council (694481 GC2.0) under the same programme. I.J.W. acknowledges support from the Australian Research Council (DP170103410). This work is a contribution to the LEMONTREE (Land Ecosystem Models based On New Theory, obseRvations and ExperimEnts) project, funded through the generosity of Eric and Wendy Schmidt by recommendation of the Schmidt Futures program.

2.1 Abstract

- Close coupling between water loss and carbon dioxide uptake requires coordination of plant hydraulics and photosynthesis. However, there is still limited information on the quantitative relationships between hydraulic and photosynthetic traits.
- We propose a basis for these relationships based on optimality theory, and test its predictions by analysis of measurements on 107 species from 11 sites, distributed along a nearly 3000-m elevation gradient.
- Hydraulic and leaf-economic traits were less plastic, and more closely associated with phylogeny, than photosynthetic traits. The two sets of traits are linked by the sapwood-to-leaf area ratio (Huber value, v_H). The observed coordination between v_H and sapwood hydraulic conductivity (K_S) and photosynthetic capacity (V_{cmax}) conformed to the proposed quantitative theory. Substantial hydraulic diversity was related to the trade-off between K_S and v_H. Leaf drought tolerance (inferred from turgor loss point, $-\Psi_{tlp}$) increased with wood density, but the trade-off between hydraulic efficiency (K_S) and $-\Psi_{tlp}$ was weak. Plant trait effects on v_H were dominated by variation in K_S, while effects of environment were dominated by variation in temperature.
- This research unifies hydraulics, photosynthesis and the leaf economics spectrum in a common theoretical framework, and suggests a route

towards the integration of photosynthesis and hydraulics in land-surface models.

2.2 Introduction

Water transport is essential for plant survival and growth. Hydraulic failure triggers death under severe drought (Rowland et al., 2015), and differences in hydraulic traits can be used to predict drought-induced tree mortality (Choat et al., 2018). Photosynthesis is constrained by hydraulics because water transported through the xylem must replenish water lost through stomata during CO_2 uptake (Brodribb, 2009). Empirical studies (Brodribb et al., 2007; Scoffoni et al., 2016; Zhu et al., 2018) and optimality arguments (Deans et al., 2020) support a tight coordination between hydraulic and photosynthetic traits. Nonetheless, quantitative understanding of their relationships remains incomplete (Mencuccini et al., 2019b). Embedding plant hydraulics in vegetation and land-surface models is desirable (Christoffersen et al., 2016; Mencuccini et al., 2019a), not least because an improved understanding of drought effects on photosynthesis and transpiration could remove a leading source of uncertainty in global models (De Kauwe et al., 2015). This situation provides a strong motivation for theoretical and empirical research on how whole-plant hydraulic traits are related to (better-studied) leaf photosynthetic traits.

The ratio of sapwood area to subtended leaf area (the Huber value, v_H) links whole-plant to leaf processes (Mencuccini et al., 2019b; Rosas et al., 2019). There is a limit to the amount of leaves that a given area of sapwood can support due to its limited capacity to supply water. The plant needs to invest more carbon in sapwood to meet increasing water loss, or to shed leaves to decrease water loss. Thus, v_H reflects not only the balance between water supply and loss, but also carbon allocation to stems versus leaves. Plants with low v_H tend to have low leaf mass-per-area (LMA) and low leaf stable carbon

isotope ratios ($\delta^{13}C$), implying a high ratio of leaf-internal to ambient CO_2 (χ); high maximum CO_2 assimilation rate (A_{sat}); high leaf water potential at the turgor loss point (Ψ_{tlp}, a negative quantity); and high sapwood-specific hydraulic conductivity (K_S) (Mencuccini et al., 2019b; Rosas et al., 2019; Zhu et al., 2018). High V_{cmax} and high LMA both require (all else equal) a high v_H, the former because high V_{cmax} is associated with high photosynthetic rate, stomatal conductance and transpiration, the latter because high-LMA leaves tend to be associated with low hydraulic conductance. There is considerable independent variation in V_{cmax} (expressed on an area basis) and LMA which implies that these are separate dimensions influencing v_H. Previous studies have also shown that hydraulic traits are influenced by environmental variables, particularly aridity (Gleason et al., 2013; Liu et al., 2019; Martinez-Vilalta et al., 2009; Togashi et al., 2015), in a coordinated way. Drought-adapted plants are characterized by reduced water supply through stems (low hydraulic efficiency, K_S; e.g. associated with narrow conduits) and/or reduced demand (high v_H), and increased leaf hydraulic safety (low Ψ_{tlp}). Photosynthetic and leaf-economic traits are also influenced by climate. χ increases with growth temperature, and decreases with vapour pressure deficit (D) and elevation (Prentice et al., 2014a; Wang et al., 2017b). Photosynthetic capacity (maximum Rubisco carboxylation rate, V_{cmax}) increases with light, and weakly with temperature and VPD (Smith et al., 2019). LMA increases with light and aridity, and decreases with temperature (Poorter et al., 2009; Wright et al., 2004b). Although these traits show strong trends with climate, phylogeny controls the variation of hydraulic traits to a large extent due to their dependence on conservative characteristics such as wood anatomy (Rosas et al., 2019), while photosynthesis-related traits regulated by biochemical processes show a high degree of plasticity (Dong et al., 2020).

Optimality theory allows testable predictions about trait-trait coordination and can also provide strong explanations for observed responses of traits to environment (Franklin et al., 2020). Among photosynthetic traits, analyses of $\delta^{13}C$ data have shown quantitative agreement between observed and theoretically predicted environmental responses of χ (Lavergne et al., 2020a; Prentice et al., 2014a; Wang et al., 2017b). Smith et al. (2019), similarly, used optimality theory to predict the observed environmental responses of V_{cmax} in a global data set. Sperry et al. (2017) integrated hydraulic traits with a photosynthesis model to predict stomatal conductance using optimality theory. Less attention has been paid to applying optimality theory to predict leaf-economic or hydraulic traits. Here we investigate the relationships among photosynthetic, leaf-economic and hydraulic traits, and between these traits and climate, using field data collected from 11 sites in the Gongga Mountain region of western China. We extend the optimality framework of Prentice et al. (2014a) and Wang et al. (2017b), which hypothesizes that plants minimize the total cost of maintaining the capacities for photosynthesis and water transport relative to photosynthesis rate, in order to make explicit quantitative predictions of these relationships. K_S and V_{cmax} are two key traits related to water transport and photosynthesis/water demand, respectively. Based on the requirement that water transport through xylem must equal water loss via stomata, our optimality model indicates a key role for v_H in achieving this requirement (Mencuccini et al., 2019b), and confirms a positive relationship between v_H and V_{cmax} but a negative one with K_S theoretically in a unified framework. Our model thus provides a new theoretical basis to understand the variations of v_H along environmental gradients.

To test the model, we measured photosynthetic and hydraulic traits on 107 species at 11 sites located in the Gongga Mountain region of Sichuan Province, China. This region (Figure S2.1) extends from 29° 22' to 29° 55' N and 101° 1'

to 102° 9' E and spans an elevation range from near sea level to 8000 m, creating a long gradient in growing-season temperature. Sites from the western side of Gongga Mountain also tend to be drier than sites at corresponding elevations on the eastern side. By sampling 11 sites over a range of nearly 3000 m in elevation, from both the western and eastern sides, we assembled a data set on woody plants encompassing a wide range of climates.

2.3 Theory

The theory of v_H variation extends the least-cost hypothesis of Prentice et al. (2014a). According to Fick's law and Darcy's law respectively (Fick, 1855; Whitehead, 1998), transpiration can be calculated from either water demand (Equation 2.1) or supply (Equation 2.2). The coordination of xylem water transport and stomatal water loss implies that plants should optimally allocate resources so that maximum water transport matches maximum photosynthesis, which leads to Equation 2.3.

$$E = \frac{1.6\, g_s D}{P_{atm}} \tag{2.1}$$

$$E = \frac{K_S \Delta\Psi v_H}{h} \tag{2.2}$$

$$\frac{1.6\, g_s D}{P_{atm}} = \frac{K_S \Delta\Psi_{max} v_H}{h} \tag{2.3}$$

where E is the transpiration rate (mol m^{-2} s^{-1}), g_s is stomatal conductance to CO_2 (mol m^{-2} s^{-1}), D is the vapour pressure deficit (Pa) and P_{atm} is the atmospheric pressure (Pa). Here h is the path length (m), roughly equivalent to plant height; K_S is the sapwood-specific hydraulic conductivity (mol m^{-1} s^{-1} Pa^{-1}); v_H is the ratio of sapwood to leaf area (m^2 m^{-2}); $\Delta\Psi$ is the difference between leaf and soil water potential and $\Delta\Psi_{max}$ is the maximum decrease in water potential from soil to leaves (Ψ_{min} and Ψ_{soil}, Pa).

From the diffusion equation and the photosynthesis model of Farquhar, von Caemmerer and Berry (Farquhar et al., 1980b), we can calculate g_s from V_{cmax}, χ and m_C:

$$g_s = \frac{A}{\left(\frac{c_a}{P_{atm}}\right)(1-\chi)} \tag{2.4}$$

$$A = m_C\, V_{cmax}\, u \tag{2.5}$$

$$m_C = \frac{\chi\, c_a - \Gamma^*}{\chi\, c_a + K} \tag{2.6}$$

where A is the assimilation (photosynthesis) rate (mol m^{-2} s^{-1}), c_a is the ambient partial pressure of CO_2 (Pa), χ is the ratio of leaf-internal to ambient CO_2 partial pressure (Pa Pa^{-1}), V_{cmax} is the maximum capacity of carboxylation (mol m^{-2} s^{-1}), Γ^* is the photorespiratory compensation point (Pa), and K is the effective Michaelis-Menten coefficient of Rubisco (Pa). The factor m_C reduces photosynthesis under natural conditions relative to V_{cmax}. Substituting g_s from Equations (2.4-2.6) into Equation 2.3 yields Equation 2.7, which represents our key optimality theory linking hydraulic and photosynthetic traits. It states that maximum rate of water transport through the xylem equals the maximum rate of water loss through the stomata.

$$\frac{K_S}{h}\Delta\Psi_{max} v_H = \frac{1.6D}{c_a} m_C \frac{V_{cmax}}{1-\chi} \tag{2.7}$$

Since V_{cmax} acclimates to the environment on a weekly to monthly timescale while K_S is determined by xylem structure and therefore less able to vary seasonally, we work with V_{cmax} at the mean daily maximum temperature in July ($V_{cmax,jt}$) and K_S at the mean daily maximum temperature during the growing season (defined as the period with daytime temperatures > 0 ˚C) ($K_{S,gt}$).

In practice, effects of K_S and h are not separable, because the tip-to-base widening of xylem elements implies a positive correlation between them that

greatly reduces the effect of path length on whole-stem conductance, so that the whole-stem conductance is similar to or only slightly lower than the conductance measured near the branch tip (Christoffersen et al., 2016; Mencuccini et al., 2019b; Olson et al., 2021). We assume $\Delta\Psi_{max}$ equal to $-\Psi_{tlp}$ ($\Psi_{soil} \approx 0$ under well-watered conditions) since Ψ_{tlp} is a proxy for Ψ_{min} (Hochberg et al., 2018). The uncertainty of the Ψ_{tlp} proxy has little impact on our results as it is not a principal predictor in our model (shown in Figure 2.4). Thus, to test Equation 2.7 we take $-\Psi_{tlp}$ as a surrogate for $\Delta\Psi_{max}$ (Hochberg et al., 2018) and subsume the effect of height in a composite constant (C), leading to the following relationship after Log_e transformation of Equation 2.7:

$$\begin{aligned}\text{Log}_\text{e}(v_\text{H}) = \text{Log}_\text{e}(D) + \text{Log}_\text{e}(m_\text{C}) + \text{Log}_\text{e}\left(V_\text{cmax,jt}\right) - \text{Log}_\text{e}\left(K_\text{S,gt}\right) - \\ \text{Log}_\text{e}\left(-\Psi_\text{tlp}\right) - \text{Log}_\text{e}(1-\chi) - \text{Log}_\text{e}(c_\text{a}) + C\end{aligned} \quad (2.8)$$

where *C* has a fitted value of 2.27 using all the species sampled (see Figure S2.4), which suggests an average "effective tree height" of 6 m.

Photosynthetic traits can be estimated from existing optimality models. The least-cost hypothesis states that plants minimize the combined unit costs (that is, costs per unit of carbon assimilated) of maintaining the capacities for carbon fixation and water transport (Prentice et al., 2014a). The coordination hypothesis states that light- and Rubisco-limited photosynthesis rates are approximately equal, in order to be able to utilize the available light while avoiding wasteful maintenance costs (Chen et al., 1993a). These two hypotheses have already been corroborated by many studies at regional or global scale (Lavergne et al., 2020b; Smith et al., 2019; Xu et al., 2021b). χ in Equation 2.8 can be estimated as follows, based on the least-cost hypothesis (Wang et al., 2017b):

$$\chi = \frac{\Gamma^*}{c_\text{a}} + \frac{\xi\left(1 - \frac{\Gamma^*}{c_\text{a}}\right)}{\xi + \sqrt{D}} \quad \text{where} \quad (2.9)$$

$$\xi = \sqrt{\frac{\beta(K+\Gamma^*)}{1.6\eta^*}} \quad (2.10)$$

where β is the ratio at 25 ˚C of the unit costs of maintaining carboxylation and transpiration capacities (146, based on a global compilation of leaf $\delta^{13}C$ measurements), η^* is the viscosity of water relative to its value at 25 ˚C, and ξ ($Pa^{1/2}$) is a stomatal sensitivity parameter that increases with temperature due to the temperature dependencies of K, Γ^* (increasing) and η^* (decreasing).

$V_{cmax,jt}$ can also be predicted from climate, based on the coordination hypothesis (Smith et al., 2019):

$$V_{cmax} \approx \varphi_0 I_{abs} \left(\frac{c_i+K}{c_i+2\Gamma^*}\right) \quad (2.11)$$

where ϕ_0 is the intrinsic quantum efficiency of photosynthesis (to which we assign the value 0.085 μmol C μmol^{-1} photon), I_{abs} is the photosynthetic photon flux density (PPFD) absorbed by leaves (mol m^{-2} s^{-1}), and c_i is the leaf-internal CO_2 partial pressure ($c_i = \chi c_a$) (Pa).

2.4 Data and Methods

2.4.1 Trait data

Trait data were measured at 11 sites in late July 2018 and August 2019, during the active growing season, in the Gongga Mountain region (29° 34' 16" – 29° 54' 52" N and 101° 59' 08" – 102° 9' 42" E, Fig. S1). We collected the data needed to allow the calculation of four leaf traits: leaf mass per area (LMA), leaf nitrogen per unit area (N_{area}), the maximum capacity of carboxylation (V_{cmax}), and the ratio of leaf-internal to ambient CO_2 partial pressure (χ). Hydraulic traits, specifically the ratio of sapwood to leaf area (Huber value, v_H), sapwood-specific hydraulic conductivity (K_S), wood density (WD) and leaf potential at turgor loss point (Ψ_{tlp}), were measured on all the woody broad-leaved species.

We sampled all the tree species and at least five shrub species at each site. All samples were taken from the top canopy layer receiving direct sunshine.

LMA was calculated from the measurements of leaf area and dry weight following standard protocols (Cornelissen et al., 2003a). Multiple leaves, or leaflets for compound leaves, were randomly selected and scanned using a Canon LiDE 220 Scanner. The dry weights of these leaves were measured after oven-drying at 75 ˚C for 48 h to constant weight. We calculated LMA as the ratio of dry mass to leaf area. Leaf nitrogen content was measured using an Isotope Ratio Mass Spectrometer (Thermo Fisher Scientific Inc., USA). N_{area} was calculated from LMA and leaf nitrogen content. The LMA value for a species at a given site was the average of three separate measurements made on leaves from multiple individuals, while N_{area} measurements were made on pooled samples of leaves from multiple individuals.

Carbon isotopic values ($\delta^{13}C$) were measured using an Isotope Ratio Mass Spectrometer (Thermo Fisher Scientific Inc., USA). Values were measured on pooled samples of leaves from multiple individuals. Estimates of χ were made using the method of Cornwell et al. (2018) to calculate isotopic discrimination (Δ) from $\delta^{13}C$ with a standard formula using the recommended values of *a'* and *b'* of 4.4 ‰ and 27 ‰, respectively (Cernusak et al., 2013; Farquhar et al., 1989):

$$\chi = \frac{\Delta - a'}{b' - a'} \tag{2.12}$$

Leaf gas-exchange measurements were made in the field using a portable infrared gas analyser (IRGA) system (LI-6400; Li-Cor Inc., Lincoln, NB, USA). Sunlit branches from the outer canopy were collected and re-cut under water immediately prior to measurement. In-situ measurements were taken with relative humidity and chamber block temperature similar to the ambient conditions, and a constant airflow rate (500 μmol s^{-1}). V_{cmax} at leaf temperature

($V_{cmax,lt}$) was calculated from the light-saturated rate of net CO_2 fixation at ambient CO_2, measured on one individual of each species, using the one-point method (De Kauwe et al., 2016b) and adjusted to a standard temperature of 25 ˚C (V_{cmax25}) and maximum temperature in July ($V_{cmax,jt}$) using the method of Bernacchi et al. (2001).

Branches with a diameter wider than 7 mm were sampled for hydraulic traits. We cut the branch as close to the bifurcation point as possible, in order to minimize any effect of the measurement location on the measured area. We measured the cross-sectional area of the xylem at both ends of the short piece recut from the bottom of the branch using digital calipers. Sapwood area was calculated as the average of these two measurements. All leaves attached to the branch were removed and dried at 70 ˚C for 72 hours before weighing. The total leaf area was obtained from dry mass and LMA. The ratio of sapwood area and leaf area was calculated as v_H. The v_H value of one species at each site was the average of three measurements made on branches from different individuals.

Five branches from at least three mature individuals of the same species at each site were collected, wrapped in moist towels and sealed in black plastic bags, and then immediately transported to the laboratory. All the samples were re-cut under water, put into water and sealed in black plastic bags to rehydrate overnight. K_S was measured using the method described in Sperry et al. (1988). Segments (10 - 15 cm length) were cut from the rehydrated branches and flushed using 20 mmol L^{-1} KCl solution for at least 30 minutes (to remove air from the vessels) until constant fluid dripped from the segment section. The segments were then placed under 0.005 MPa pressure to record the time (t) they took to transport a known water volume (W, m^3). Length (L, m), sapwood areas of both ends (S_1 and S_2, m^2) and temperature (T_m, ˚C) were recorded. Sapwood-specific hydraulic conductivity at measurement temperature ($K_{S,m}$, mol

m^{-1} s^{-1} MPa^{-1}) was calculated using Equation 2.13. This was transformed to K_S at mean maximum temperature during the growing season ($K_{S,gt}$) and standard temperature (K_{S25}) following Equations 2.14 and 2.15:

$$K_{\mathrm{S,m}} = \frac{W\ L\ \rho_{\mathrm{w}}}{0.005\ t\ (S_1 + S_2)/2} \frac{1000}{18} \tag{2.13}$$

$$K_{\mathrm{S,t}} = K_{\mathrm{S,m}} \frac{\eta_m}{\eta_{\mathrm{t}}} \tag{2.14}$$

$$\eta = 10^{-3} e^{\left(A + \frac{B}{C+T}\right)} \tag{2.15}$$

where η_m and η_t (Pa s) are the water viscosity at measurement temperature and transformed temperature (i.e. mean maximum daytime temperature during the growing season and standard temperature, 25 ˚C in this study), respectively, and ρ_w (kg m^{-3}) is the density of water. The parameter values adopted in Equation 2.15 were A = −3.719, B = 580 and C = −138 (Vogel, 1921).

A small part of each sapwood segment was used to measure wood density, the ratio of dry weight to volume of sapwood. After removal of bark and heartwood, the displacement method was used to measure the volume of sapwood and the dry weight of sapwood was obtained after drying at 70 ˚C for 72 hours to constant weight. Wood density was calculated as the ratio of dry weight to the volume of sapwood.

We applied the method described by Bartlett et al. (2012a) for the rapid determination of Ψ_{tlp}. After rehydration overnight, discs were sampled from mature, healthy leaves collected on each branch, avoiding major and minor veins and using a 6-mm-diameter punch. Leaf discs wrapped in foil were frozen in liquid nitrogen for at least 2 minutes and then punctured 20 times quickly with sharp-tipped tweezers. Five repeat experiments using leaves from multiple individuals were carried out for every species at each site. We measured osmotic potential (Ψ_{osm}) with a VAPRO 5600 vapor pressure osmometer (Wescor, Logan, UT, USA) and calculated Ψ_{tlp} (in MPa) as:

$$\Psi_{tlp} = 0.832\,\Psi_{osm} - 0.631 \quad (2.16)$$

2.4.2 Climate data

We derived climate variables at each of the 11 sampled sites using meteorological data (monthly maximum and minimum temperature, fraction of sunshine hours and water vapour pressure) from 17 weather stations in the Gongga region (http://data.cma.cn/data/cdcdetail/dataCode/SURF_CLI_CHN_MUL_MON.html) and the elevation-sensitive ANUSPLIN interpolation scheme (Hutchinson and Xu, 2004). The meteorological data were available from January 2017 to December 2019. The monthly data were converted to daily values by linear interpolation in order to calculate the bioclimatic variables mean maximum temperature during the growing-season (defined as the period with daytime temperature > 0 ˚C), growing-season mean PPFD, and vapour pressure deficit under maximum daytime temperature in July, using the Simple Process-Led Algorithms for Simulating Habitats (SPLASH) model (Davis et al., 2017a).

2.4.3 Data analysis

All statistical analyses were carried out in R3.1.3 (R Core Team 2015). To homogenize the variance, traits were $\log_e$-transformed and χ was logit-transformed; for Ψ_{tlp}, the absolute value ($-\Psi_{tlp}$) was $\log_e$-transformed. Trait variance partitioning was carried out using the *vegan* package (Oksanen et al., 2017) to quantify the amount of variation explained by different groups of factors. In this study, the groups are families (representing phylogenetic relatedness), life forms, climate and sites. Path analysis was used to characterize the trait coordination framework built on the idea that plastic traits are influenced by structural traits, using the *lavaan* package (Rosseel, 2012). The model was evaluated using the ratio of χ^2 and degree of freedom (χ^2/df)

and goodness-of-fit index (GFI). The χ^2/df of models using all species and only evergreen species were below 3, and the GFI of all three models were larger than 0.9 (Figure 2.2). Traits under standard conditions (V_{cmax25} and K_{S25}) were used in variance partitioning, path analysis and bivariate regressions to eliminate the effect of temperature, while trait values under growth conditions were used for theoretical prediction.

To examine the importance of each predictor in Equation 2.8 for the prediction of v_H, we evaluated the contributions of each variable in four steps as follows. We analysed the contributions to variation in v_H using two sets of predictors: (1) the traits and environmental variables in Equation 2.8 (D, K_S, Ψ_{tlp}, V_{cmax}, χ, c_a), with the contribution of the integrative predictor m_C included in the effects of χ and c_a; (2) the hydraulic traits (K_S, Ψ_{tlp}) and environmental predictors (D, temperature, radiation, elevation) that influence v_H indirectly through their influence on photosynthesis-related traits. First the baseline value of each predictor was defined as the median of its site-mean values across the 11 sites. These baseline values were used to generate baseline, a predicted value of $\text{Log}_e(v_H)$. Second, each predictor in turn was changed to its actual values at each site, while other predictors were kept at their baseline values. We used these inputs to calculate values of $\text{Log}_e(v_H)$ representing v_H variation across sites induced by this predictor alone. Third, the contribution of each predictor at each site was calculated as the difference between simulated $\text{Log}_e(v_H)$ values from the second and first steps (indicated as $\Delta\text{Log}_e(v_H)$ in Figure 2.4). Last, we calculated the improvement in R^2 of the relationships between predicted $\text{Log}_e(v_H)$ and contributions of each predictor across sites. R^2 improvements due to each variable were averaged over orderings among predictors, yielding the relative importance of each variable. This procedure was run using the *relaimpo* package (Groemping, 2006). The partial residual plots from the regression model of the second set of predictors were plotted using the

visreg package (Breheny and Burchett, 2017) to better understand the environmental effects on v_H variation.

To assess the predictive power of the model, we used Deming regression of site-mean predicted versus observed $Log_e(v_H)$ with its corresponding standard deviation (SD). The SD of predictions came from the observed variations of sapwood-specific hydraulic conductivity (K_S) and leaf water potential at turgor loss point (Ψ_{tlp}). Root mean square error (rmse) was estimated between the observed and predicted values both across sites and species. The Deming regression and rmse were calculated using the *deming* and *xxIRT* packages respectively.

2.5 Results

The measured traits can be ranked by phylogenetic influence, according to the fraction of variation explained by family alone in a variation partitioning analysis (Figure 2.1). The hydraulic traits wood density (WD) and sapwood-specific hydraulic conductivity at 25 ˚C (K_{S25}) were most influenced by phylogeny (49-52%); LMA, leaf nitrogen per unit area (N_{area}) and Ψ_{tlp} were intermediate (28-31%); photosynthetic traits (χ and V_{cmax} at 25˚C, V_{cmax25}) and v_H were least influenced by phylogeny (19-24%). These rankings are approximately mirrored by the percentages of variation explained by site factors and climate (Figure 2.1).

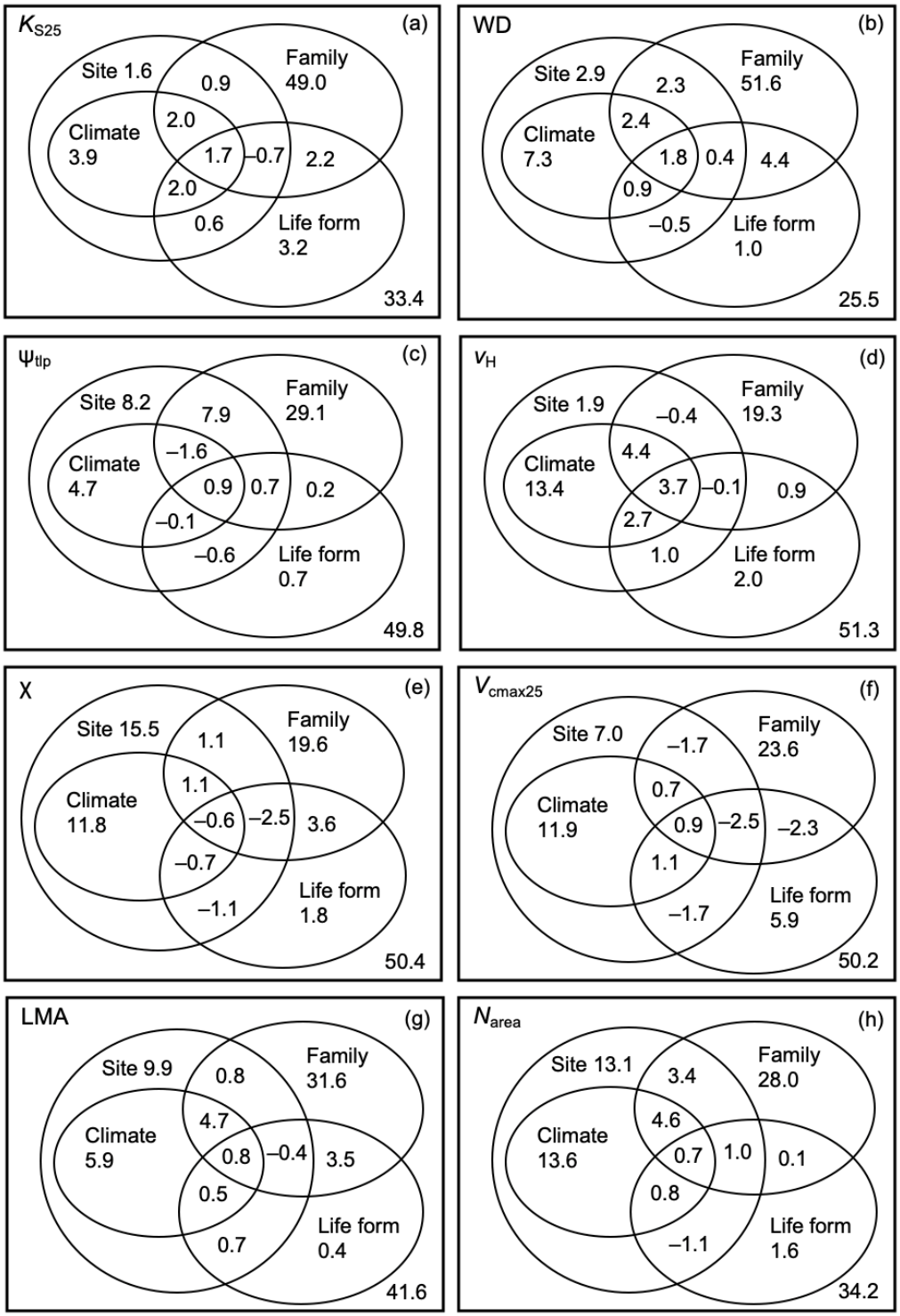

Figure 2.1 Variance partitioning (%) for each trait.

Path analysis (Figure 2.2) was used to test a framework for trait coordination, based on the hypothesis that the traits that are structurally dependent and more phylogenetically influenced impose a constraint on more

plastic traits, with v_H as the key trait linking the two sets of traits. Analyses conducted separately on evergreen and deciduous woody plants revealed several general patterns. First, v_H decreased with K_{S25}, but increased with V_{cmax25} (especially in evergreen plants) (Figure 2.2). K_{S25} was also lower, and v_H higher, in plants with high LMA. The leaf economics spectrum (from low to high LMA: Wright et al. (2004b)) thus also influenced v_H, both directly, and indirectly through K_{S25}. Second, WD was negatively related to K_{S25} (especially in deciduous plants), and positively related to $-\Psi_{tlp}$. Third, both LMA and $-\Psi_{tlp}$ negatively influenced χ. In other words, plants with low (more negative) turgor loss point and/or high LMA tend to operate with low χ, with low χ in turn being linked to higher V_{cmax} and therefore higher v_H. Fourth, N_{area} was found to depend jointly on LMA and V_{cmax25}, consistent with accumulating evidence – e.g. Dong et al. (2017b), Xu et al. (2021a) – for the dependence of N_{area} on leaf structure (with LMA as the dominant control, here as in other analyses), and a weaker relationship to V_{cmax25}. Together, through direct and indirect effects, these hypothesized causal pathways accounted for all of the significant bivariate relationship among traits (Figure 2.2; Table S2.1).

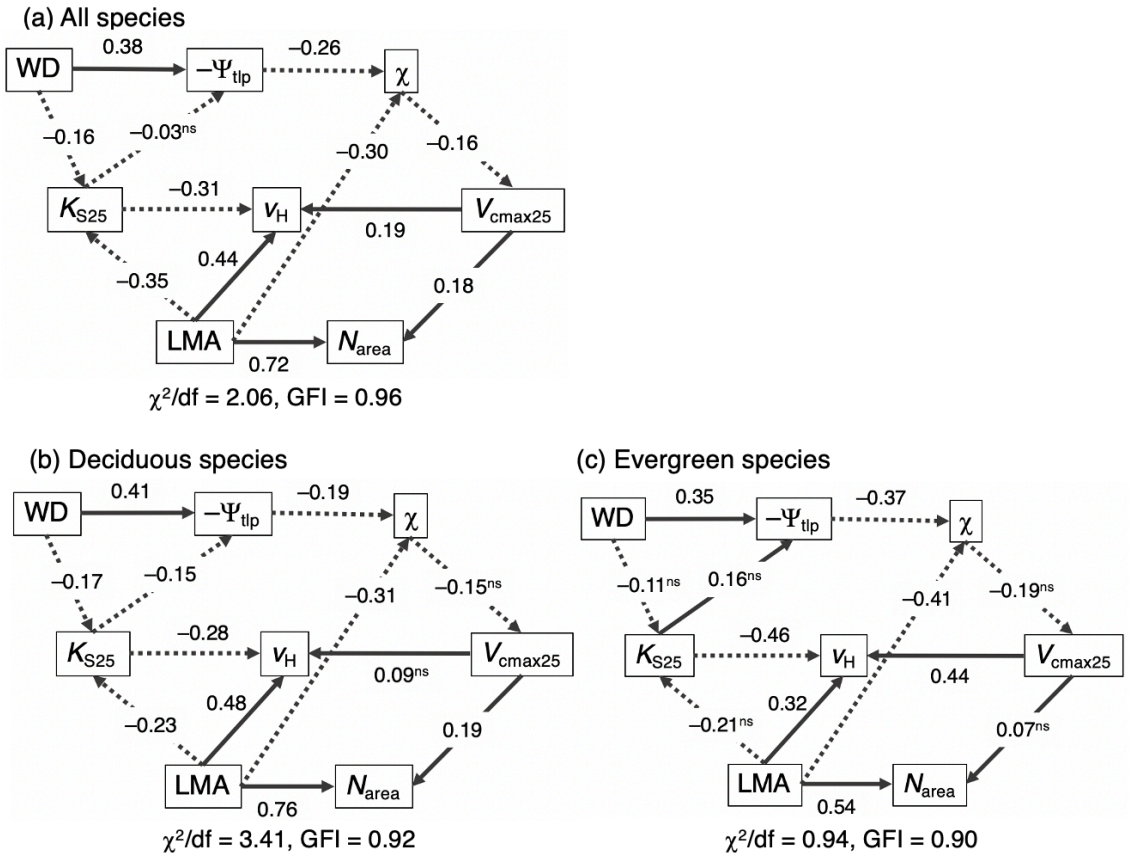

Figure 2.2 Path analysis of hydraulic and photosynthetic traits for all species (a), separately deciduous (b) and evergreen species (c). WD is wood density, K_{S25} is sapwood-specific hydraulic conductivity at 25 ˚C, Ψ_{tlp} is leaf water potential at turgor loss point, v_H is the ratio of sapwood to leaf area, LMA is leaf mass per area, χ is the ratio of leaf-internal to ambient CO_2 partial pressure, N_{area} is leaf nitrogen content per area, and V_{cmax25} is the maximum capacity of carboxylation at 25 ˚C. The arrows indicate the proposed links between traits. Solid lines indicate positive relationships, dotted lines negative relationships. Standard path coefficients are shown near the line (not significant: ns). The trait coordination structure was evaluated using the ratio of χ^2 and degree of freedom (χ^2/df) and goodness-of-fit index (GFI).

Our analyses (Figure 2.2, S2.2) indicated only a weak trade-off between leaf drought tolerance and xylem hydraulic efficiency. K_{S25} and $-\Psi_{tlp}$ were

negatively related for deciduous species, but this relationship was not significant for evergreen species, or across all species considered together.

The theoretical model, including just a single fitted parameter across all species (the intercept, reflecting the implicit effect of height), captured the essential trade-off between v_H and K_S. Both quantities v_H and K_S varied greatly among species (variance of Log_e-transformed variables = 0.4 and 0.73, respectively, averaged across the deciduous and evergreen species-sets; Table S1), allowing a wide variety of hydraulic strategies to coexist within communities. V_{cmax25} also varied widely among species (0.69), and more so than either χ (0.28) or Ψ_{tlp} (0.03) (Table S2.1). The model also predicted a tendency for plants with high V_{cmax} to have large v_H, and/or K_S, to allow a correspondingly high rate of water loss. This prediction was consistent with the partial residual plots based on the data (Figures 2.2 and S2.3). Relationships between A_{sat} and plant hydraulic traits found in many studies (Santiago et al., 2004; Zhu et al., 2018) were consistent with this prediction. Moreover, Equation 2.8 predicted environmental modulation of the relationship between v_H and other traits. Specifically, it predicted a positive impact of vapour pressure deficit (D) on v_H. As D increases, plants are thus expected to allocate relatively less carbon to leaves, and more to stems and roots, resulting in increasing v_H. Temperature was another essential climate variable affecting v_H variation through χ and m_C with contrasting effects (positive on χ, but negative on m_C). Partial residual plots showed a net negative effect of temperature on v_H (Figure S2.4a). However, elevation contributed little to v_H variation (Figure 2.3b).

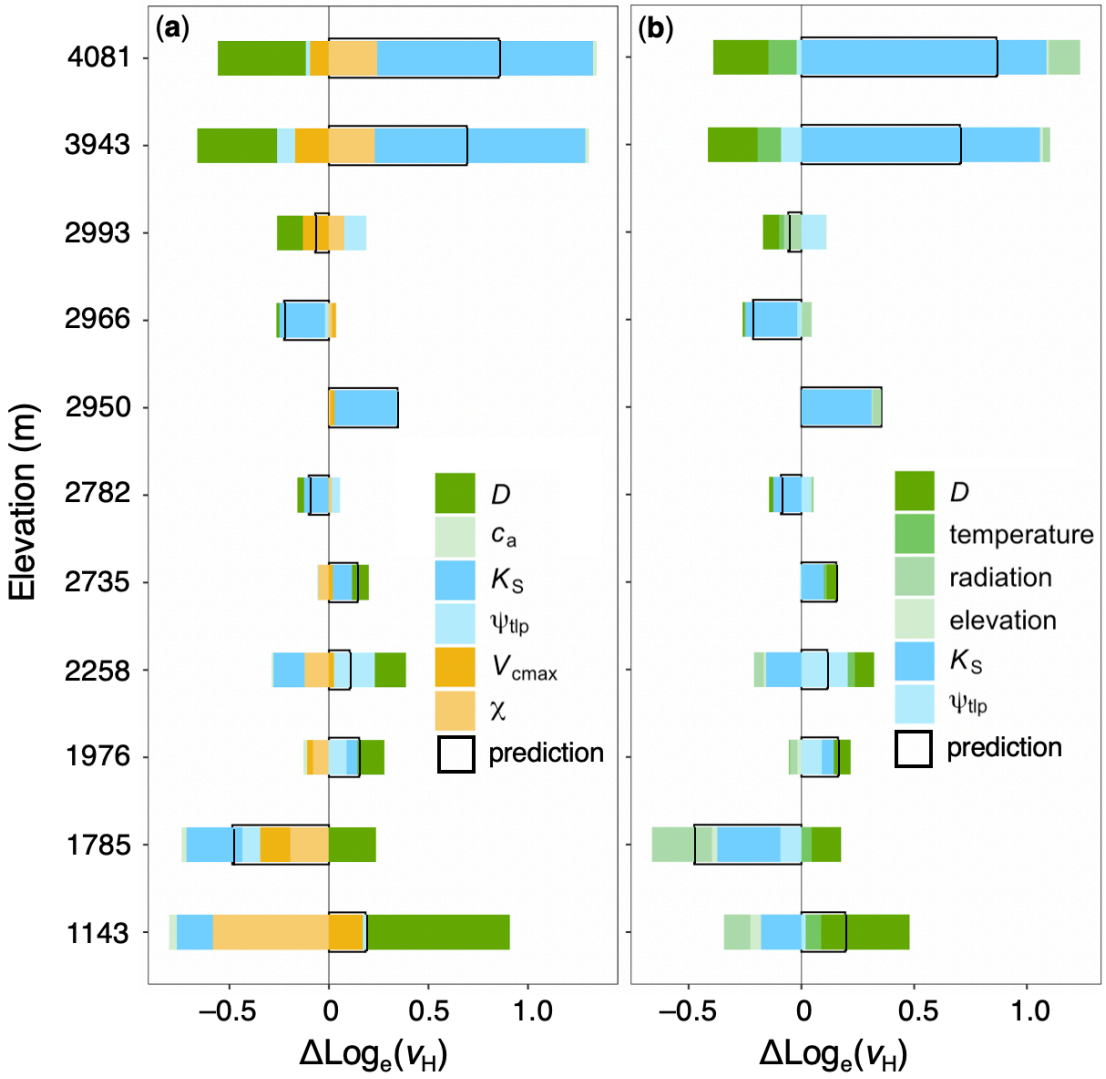

Figure 2.3 The modelled contribution of different predictors to v_H variation at 11 sites sampled along an elevational gradient in the Gongga Mountains, China. (a) The contribution of direct predictors from Equation 2.8. (b) The total contribution of environmental predictors through maximum capacity of carboxylation (V_{cmax}), the ratio of leaf-internal to ambient CO_2 partial pressure (χ) and c_a, along with hydraulic traits. In each panel, the vertical black line represents the baseline $Log_e(v_H)$ across sites (on which the data were centred, such that the *x*-axis represents the contribution of predictors: $\Delta Log_e(v_H)$). Transparent bars with black borders show the changes in predicted values compared to the baseline $Log_e(v_H)$. Environmental effects are shown in green; photosynthesis-related effects in orange; hydraulic trait effects – sapwood-

specific hydraulic conductivity (K_S) and leaf water potential at turgor loss point (Ψ_{tlp}) – are shown in blue.

Predicted v_H captured 90% of the observed variation in v_H across sites (Figure 2.4) and 20% across all species (Figure S2.4). These predictions (see Equation 2.8) were based on observed hydraulic traits and c_a, and on predicted optimal values of V_{cmax}, m_C and χ. Analysis of the modelled contribution of individual factors showed that K_S was the most important predictor of the variation in site-mean v_H along the elevation gradient (Figure 2.3). With high K_S, plants had large leaf area, leading to low v_H. Besides, χ played a crucial role in v_H variation, as well as being included in the effect of m_C. The improvement in R^2 contributions for the relationships of predicted $\text{Log}_e(v_H)$ to contributions due to different predictors was 0.59 for K_S, 0.14 for D, 0.10 for χ, 0.09 for c_a, and 0.06 for V_{cmax} and 0.03 for Ψ_{tlp} (Figure 2.3a); or in an alternative breakdown of controls, 0.42 for K_S, 0.21 for temperature, 0.17 for radiation, 0.10 for D, 0.06 for elevation and 0.03 for Ψ_{tlp} (Figure 2.3b).

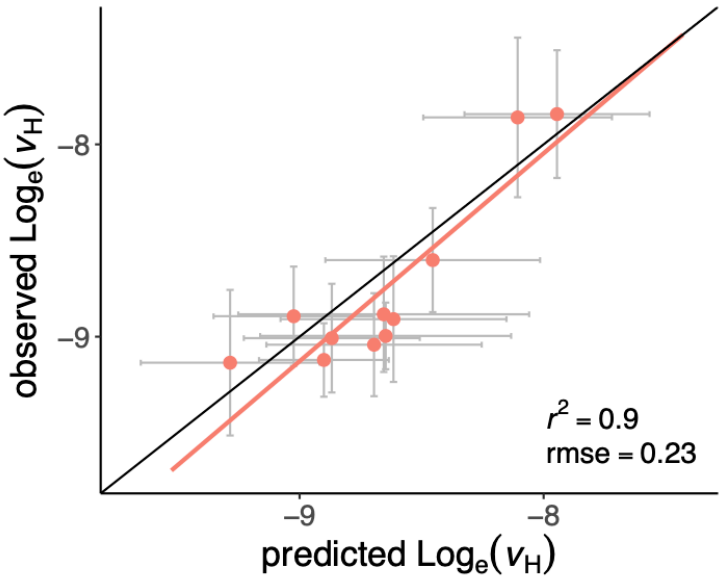

Figure 2.4 Comparison between site-mean observed and predicted ratios of sapwood to leaf area (v_H). The error bar on the *y*-axis is the standard deviation of observed Log$_e$(v_H) at each site; that on the *x*-axis is the standard deviation of predictions, considering observed variations of sapwood-specific hydraulic conductivity (K_S) and leaf water potential at turgor loss point (Ψ_{tlp}).

2.6 Discussion

The results of path analysis (Figure 2.2) and the success of the optimality model (Figure 2.4) are consistent with the proposed central role of v_H in coordinating hydraulic and photosynthetic traits (Rosas et al., 2019). The v_H variation mainly results from that in K_S and χ or temperature. Species deploying a larger total leaf area at a given sapwood area (lower v_H) tend to have higher K_S (Togashi et al., 2015). The relatively rapid acclimation of photosynthetic traits to the local environment (Smith and Dukes, 2017a) that leads to the indirect relationship between v_H and χ (Figure S2.2i) has been noted before (Martinez-Vilalta et al., 2009). However, the weak trade-off between Ψ_{tlp} and K_S in deciduous species and the apparent absence of these trade-offs in evergreen species implies that low hydraulic safety does not always accompany high K_S. Although the xylem tension at which 50% of the maximum conductivity is lost

(P_{50}) is the most commonly used index of hydraulic safety, we used Ψ_{tlp} for this purpose, noting that the two measures are significantly correlated (Joshi et al., 2020; Zhu et al., 2018). Globally, a weak trade-off between hydraulic safety and efficiency has been reported (Gleason et al., 2016), and new work suggests a tight trade-off between efficiency and safety may be a feature of climates with highly seasonal precipitation (Liu et al., 2021). That is, plants in environments with less seasonal precipitation need not have high hydraulic efficiency, which may be accompanied by unknown costs or risks.

The key role of v_H in mediating leaf physiology and hydraulics arises because of its relative plasticity. Variance partitioning (Figure 2.1) showed that WD and K_S are far more strongly linked to phylogeny than other traits. This is presumably because both are related to wood anatomy. K_S is proportional to the fourth power of mean xylem conduit diameter (according to the Hagen–Poiseuille equation: Tyree and Ewers (1991)), while WD is largely dependent on fibre wall and lumen fractions (Ziemińska et al., 2013). Thus, it might be expected that these traits would show a strong evolutionary convergence within lineages. By contrast, Ψ_{tlp} is known to change after drought through osmotic adjustment (Bartlett et al., 2014), implying a higher degree of plasticity consistent with the lower influence of family, and the higher influence of environmental factors, on this trait compared to other hydraulic traits (Figure 2.1). The correlation between v_H and V_{cmax} provides the bridge between two sets of plant traits, resulting in the observed relationship between A_{sat} and hydraulic traits (Deans et al., 2020; Zhu et al., 2018). With higher V_{cmax}, leaves can fix more carbon, and stomata open to allow this – entailing greater water loss. Since photosynthetic traits, particularly χ and V_{cmax}, respond to environmental conditions on timescales of weeks to months by regulating intrinsic biochemical characteristics (Cavanagh and Kubien, 2014b; Smith and Dukes, 2017a), plants can adjust v_H relatively quickly by shedding leaves to

balance water supply and demand (Choat et al., 2018), while potentially regulating K_S on a longer timescale. The acclimation timescales of different hydraulic traits lead to tight coordination with photosynthesis process. This coordination also avoids unnecessary carbon costs of hydraulic traits, and may help to ensure survival under unfavourable (drought) conditions. The prediction of v_H based on these essential trade-offs with observed hydraulic traits proves the intrinsic adjustment of hydraulic traits, implying that there is no need to try to predict hydraulic traits individually from climate alone. The key importance of this optimality model is to successfully predict and unite the trade-offs among traits in an optimality framework.

Wood density has been considered as a crucial trait in a “wood economics spectrum” linking water transport, mechanical support and tree mortality (Chave et al., 2009). Dense wood, found in many species from arid habitats, is generally associated with narrow conduits (Hacke and Sperry, 2001) that restrict hydraulic conductivity (Zanne et al., 2010) but also confers resistance to embolism (Anderegg et al., 2016), possibly owing to thicker conduit walls and smaller pores in the pit membranes (Hacke et al., 2001a; Pittermann et al., 2010). Wood xylem is the foundation for water transport; but leaves are often a major bottleneck for water flow, contributing 30% of whole-plant hydraulic resistance on average (Sack and Holbrook, 2006). Leaves with lower Ψ_{tlp} can keep their stomata open and continue photosynthesizing at more negative water potentials; on the other hand, this strategy may incur a greater carbon cost to maintain leaf turgor (Bartlett et al., 2012a; Deans et al., 2020; Sapes et al., 2021).

The tight relationships among LMA, v_H and K_S indicate biologically important interactions between carbon investment strategy and hydraulics. Leaves with low LMA tend to display a larger leaf area to fix carbon within a relatively short leaf life span. Meanwhile, high hydraulic conductivity at both leaf and stem

levels ensures that large amount of water can be transported to leaves for transpiration, in order to maintain open stomata and a high rate of CO_2 uptake (Joshi et al., 2020; Mencuccini et al., 2019b). This relationship between hydraulics and LMA may also be associated with physiological characteristics. Thicker leaves (high LMA) tend to have a longer diffusional pathways in the mesophyll, which increases water movement resistance outside leaf xylem and decreases hydraulic conductivity (Flexas et al., 2013). The relationships between WD and K_S, and between LMA and K_S, for evergreen species was non-significant, possibly due to the relatively small sample size. Nonetheless, the fitted coefficients had the same sign and were of similar magnitude to those found for deciduous species. The reason for the weak relationship between v_H and V_{cmax} for deciduous species is unclear; again, the sign of the relationship was the same as for evergreen species.

The theory predicts direct impacts of vapour pressure deficit (D), and indirect effects of temperature, elevation and radiation, on v_H mediated by photosynthetic traits. As D increases, plants shed leaves and allocate more carbon to the root in order to reduce transpiration and absorb more water, leading to increasing v_H to balance water supply and demand (Trugman et al., 2019b). High D also causes reductions in gross primary production, and tree mortality (Park Williams et al., 2012; Yuan et al., 2019). Other environmental variables, including temperature and elevation, mainly influence hydraulic traits through their coordination with photosynthetic traits, which has been less examined in the field. The theory predicts a small positive impact of elevation on v_H, consistent with the occurrence of small-leaved species at high elevations (Wright et al., 2017) and the observed negative relationship between leaf size and v_H (Mencuccini et al., 2019b). Temperature has multiple competing effects that can be hard to disentangle, but the optimality model predicts an overall negative effect on v_H. Under future scenarios where both D and temperature are

projected to increase (Grossiord et al., 2020), the optimality model offers a way to explore the potential v_H response as the net effect of several competing effects.

The prediction of site-mean v_H using optimality theory offers a promising approach to implement hydraulics into vegetation and land-surface models. Although hydraulic processes are incorporated into some vegetation models to constrain photosynthesis, parameterization of hydraulic traits such as v_H is required (Christoffersen et al., 2016; Eller et al., 2020). If the focus is on "typical" vegetation in a given climate, the relationship we have predicted (and demonstrated) that applies to site-mean v_H (Equation 2.8), with photosynthetic traits predicted by optimality theory, could provide a straightforward way to couple photosynthetic and hydraulic traits in models. The prediction is much stronger for site means than for individual species – not surprisingly because the micro-environmental conditions to which each species acclimates are not known; while most current model applications are concerned only with the aggregate properties of the community.

The Huber value also reflects carbon allocation to leaf and biomass, which further affects productivity. A fixed parameter is used to partition carbon into leaf and stem in many vegetation models (Trugman et al., 2019a). With the optimality model, the fixed parameter could be replaced by acclimated variation in v_H, leading to improved realism. However, there is considerable diversity in hydraulic traits (notably K_S) that is linked to LMA, which raises two practical issues if we are concerned with functional diversity: first, how to predict environmental influences on the leaf economics spectrum; second, how to deal with the large within-community variation in both LMA and K_S. Xu et al. (2021a) have demonstrated a method to predict optimal LMA for deciduous plants, and a different approach is applicable to evergreen plants (Wang et al., 2023). A way needs to be found to simultaneously estimate the *distribution* of values for

highly variable, non-plastic traits. A solution to this problem would be a major step forward for modelling the terrestrial carbon, water and nitrogen cycles.

CHAPTER 3 Predictability of leaf traits with climate and elevation: a case study in Gongga Mountain, China

This chapter is **published** in Tree Physiology.

Citation: Xu H, Wang H, Prentice IC, Harrison SP, Wang G and Sun X (2021), Predictability of leaf traits with climate and elevation: a case study in Gongga Mountain, China. Tree Physiology, 41: 1336–1352. https://doi.org/10.1093/treephys/tpab003

Author contribution: H.X. carried out the analyses and prepared the manuscript with contributions from all co-authors. H.W., S.P.H. and I.C.P. designed and carried out the fieldwork, and contributed to the analyses. H.W. and I.C.P developed the model of Ma. G.W. and X.S. provided climate data for the five sites.

Acknowledgment and funding: We also thank Zonghan Ma for his help with interpolation of climate data. This work is a contribution to the Imperial College initiative on Grand Challenges in Ecosystems and the Environment. National Natural Science Foundation of China (no. 91837312, 31971495); Tsinghua University Initiative Scientific Research Program (no. 2019Z07L01001). The High-End Foreign Expert program of the China State Administration of Foreign Expert Affairs at Tsinghua University (GDW20191100161); European Research Council (787203 REALM to I.C.P. under the European Union's Horizon 2020 research and innovation programme, 694481 to S.P.H.).

3.1 Abstract

Leaf mass per area (M_a), nitrogen content per unit leaf area (N_{area}), maximum carboxylation capacity (V_{cmax}) and the ratio of leaf-internal to ambient CO_2 partial pressure (χ) are important traits related to photosynthetic function, and show systematic variation along climatic and elevational gradients. Separating the effects of air pressure and climate along elevational gradients is challenging due to the covariation of elevation, pressure and climate. However, recently developed models based on optimality theory offer an independent way to predict leaf traits, and thus to separate the contributions of different controls. We apply optimality theory to predict variation in leaf traits across 18 sites in the Gongga Mountain region. We show that the models explain 59% of trait variability on average, without site- or region-specific calibration. Temperature, photosynthetically active radiation, vapour pressure deficit, soil moisture and growing-season length are all necessary to explain the observed patterns. The direct effect of air pressure is shown to have a relatively minor impact. These findings contribute to a growing body of research indicating that leaf-level traits vary with the physical environment in predictable ways, suggesting a promising direction for the improvement for terrestrial ecosystem models.

3.2 Introduction

A number of leaf traits are diagnostic of photosynthetic processes. The ratio of leaf-internal to external CO_2 (χ) reflects stomatal regulation of CO_2 uptake, which has to be balanced against water loss (Wang et al., 2017b). The maintenance of transpiration involves a carbon cost, in the form of respiration by living parenchyma cells, to maintain active water-transport tissues. V_{cmax25}, the maximum capacity of carboxylation at a standard temperature of 25 ˚C, is a measure of the control of photosynthesis by the amount of the enzyme (Rubisco) responsible for carbon fixation (Wang et al., 2020a). The

maintenance of photosynthetic capacity also incurs a substantial carbon cost, in the form of leaf respiration to support protein synthesis. Leaf mass per unit area (M_a) determines the total carbon cost of leaf construction (Wright et al., 2004a). Nitrogen is required both for metabolic processes and for leaf construction (Lambers and Poorter, 1992; Onoda et al., 2004). Leaf nitrogen content per unit area (N_{area}) thus provides a combined measure of metabolic and structural costs.

Empirical analyses of large trait data sets have shown that variation in each of these traits is related to climate, and indeed specific climate variables can be shown to influence individual processes (Meng et al., 2015; Ordoñez et al., 2009; Wright et al., 2005). V_{cmax25} is primarily determined by the amount of Rubisco, while the activity of Rubisco varies with leaf temperature (Devos et al., 2010; Rokka et al., 2010). Vapour pressure deficit represents the atmospheric moisture demand: it is the difference between the saturated vapour pressure of water (a function of temperature) and the actual vapour pressure, which depends on atmospheric pressure and moisture content. Vapour pressure deficit influences stomatal behaviour and thereby induces variation in χ (Wang et al., 2017b). The amount of light reaching the leaves influences M_a and N_{area} within the canopy (Peltoniemi et al., 2012; Werger and Hirose, 1991). Both also vary with latitude because this determines total incident radiation and day length (Forsythe et al., 1995). Analyses have shown that the variability in each of these traits is largely independent of variability in the others (Yang et al., 2019b).

Elevational transects provide examples of trait variability along environmental gradients (Asner and Martin, 2016; Asner et al., 2017; Jian et al., 2009; Pfennigwerth et al., 2017). Although this variability is partly related to changes in climate with elevation, the impact of changing elevation on air pressure is also thought to be significant (Gale, 1972; Terashima et al., 1995; Wang et al., 2017a; Wang et al., 2014). Reduction in air pressure at higher

elevations lowers the partial pressure of oxygen. All else equal, it also decreases the water vapour pressure, and increases the atmospheric transmissivity to solar radiation. The reduction in partial pressure of oxygen increases the affinity of Rubisco for CO_2, which reduces photorespiration. The effects of decreasing water vapour pressure and increasing transmissivity are often countered by decreasing temperature and increasing cloudiness. Nonetheless, their contribution (compared to the situation at constant elevation) is to increase the vapour pressure deficit – because atmospheric pressure automatically declines with elevation while the saturated vapour pressure does not – resulting in higher water transport costs and lower χ; and to increase absorbed light, resulting in increased V_{cmax25}, M_a and N_{area} (Wang et al., 2017a).

It is difficult to disentangle the effects of air pressure and climate along elevation gradients because of their covariation. Attempts to separate out climate and elevation empirically by comparing low-elevation sites at higher latitude with high-elevation sites at lower latitude (Körner et al., 1991) have distinguished the impacts of temperature from air pressure, but have not addressed specific climate influences. However, understanding the relative importance of air pressure effects on photosynthesis could be important in the face of projected climate changes, in particular given the apparent sensitivity of high-elevation sites to these changes (Settele et al., 2015; Stocker et al., 2013).

Recent progress in the application of optimality theory to predict trait variation (Dong et al., 2017a; Prentice et al., 2014b; Wang et al., 2017b) offers an alternative way to examine the impacts of climate and elevation on photosynthesis. Optimality theory is predicated on the idea that through evolutionary processes (including selection for plasticity, as well as environmental filtering of lineages) plants are adapted to the environmental conditions under which they live. The values of photosynthetic parameters are then predicted as the result of trade-offs between competing requirements, such

as the need to balance CO_2 uptake against water loss. The balance between maintaining carboxylation capacity and transpiration capacity can be described in terms of the least-cost hypothesis (Prentice et al., 2014b; Wright et al., 2003), which states that plants minimize the combined costs of maintaining these capacities. This hypothesis allows us to predict χ. The coordination hypothesis (Chen and Reynolds, 1997; Maire et al., 2012; Wang et al., 2017b) indicates that carbon gain is maximized through balancing light- and Rubisco-limitations on photosynthesis. This hypothesis allows us to predict V_{cmax25} (Smith et al., 2019). The need to allocate nitrogen to structural and metabolic processes allows us to predict N_{area} as a function of V_{cmax25} and M_a (Dong et al., 2017a). According to the optimal leaf-longevity hypothesis (Kikuzawa, 1991), plants maximize the time-averaged net carbon gain of leaves taking into account construction costs (amortized over the leaf lifetime) and the decline in photosynthetic capacity with increasing age. This hypothesis allows M_a to be predicted from leaf longevity. The leaf longevity of deciduous species is constrained by growing-season length; thus, M_a of deciduous species should be predictable from growing-season length.

In this study, we draw on these theoretical developments to predict trait variability in response to climate and elevation gradients in the Gongga Mountain region, China. We develop a new optimality model to predict M_a of deciduous species and a simplified optimality approach to predict N_{area}. These optimality models were developed independently of the observations used in this study and require no calibration. We show that these models capture observed variations in photosynthetic traits at sites in the Gongga Mountain region. We then use these models to quantify the relative contribution of different factors to the observed changes in trait values at these sites.

3.3 Methods

3.3.1 Study sites

We collected photosynthetic trait data from 18 sites in the Gongga Mountain region of Sichuan Province, China (Figure 3.1a,b). The study area extends from 29° 22' to 29° 55' N and 101° 1' to 102° 9' E. The sampled sites span an elevation gradient from 1143 to 4361 m, and as a result there is a considerable gradient in growing season temperature (Table S3.1). Sites from the western part of the Gongga Mountain region tend to be drier than sites at a corresponding elevation in the eastern part, and thus our data set also samples a large moisture gradient (Table S3.1). The vegetation at lower elevations is deciduous broad-leaved forest dominated by Betulaceae, Urticaceae, Caprifoliaceae and Rosaceae, and is replaced by evergreen needle-leaved forest and subsequently by deciduous shrubland dominated by Pinaceae and/or Rosaceae and Ericaceae (Table S3.2) with increasing elevation. Although evergreen woody species are present at all of the sites (Table S3.2), and trait measurements were made on these species, our subsequent analyses of photosynthetic traits focused entirely on the deciduous species because of the difficulty of obtaining reliable estimates of leaf age based on a single sampling of a site.

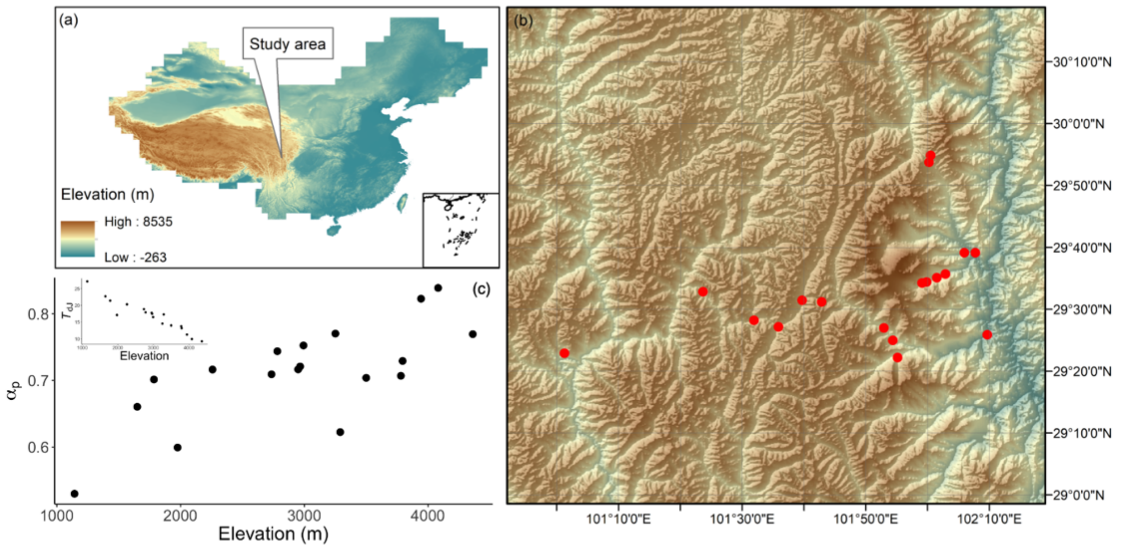

Figure 3.1 The study area. (a) the location of the Gongga Mountain region in China, (b) spatial distributions of the sampled sites in the Gongga mountain region, shown by red dots, (c) the daytime temperature in July (T_{dJ}) and the ratio of annul actual evapotranspiration to annual potential evapotranspiration (α_p) at the sampled sites. The background to plots (a) and (b) shows elevation.

3.3.2 Sample collection and analysis

Trait data were measured in late July 2018 and early August 2019 during the active growing season in the Gongga Mountain region. We used a stratified sampling strategy at each site, in order to sample the dominant species in each canopy stratum. In forest sites, we sampled a minimum of five tree, five shrub and five forb species at each site, and also sampled graminoids, lianas and climbers, and pteridophytes when present (Table S3.2). At the highest elevation sites (3794 m, 3943 m, 4081 m, 4361 m), where shrubs form the upper canopy, we only sampled shrubs and forbs (and at the highest site one pteridophyte) but again we sampled a minimum of five species in each category. All samples were taken from the outer canopy. Measurements were made on young but fully expanded leaves, attached to the cut branch.

Our analyses focus on four leaf traits: (1) leaf mass per unit area (M_a, g biomass m^{-2}), (2) the maximum capacity of carboxylation at 25 ˚C (V_{cmax25}, μmolC m^{-2} s^{-1}), (3) the ratio of leaf-internal to ambient CO_2 partial pressure (χ, unitless), and (4) leaf nitrogen content per unit area (N_{area}, g m^{-2}). (See Table 3.1 for definitions of parameters and other abbreviations frequently used in the text.) M_a was obtained from measurements of leaf area and dry weight following standard protocols (Cornelissen et al., 2003b). Leaf area was taken as the projected area of a leaf, or leaflet for compound leaves, using a Canon LiDE 220 Scanner and Matlab. Dry weight was obtained after air-drying for several days and then oven-drying at 75 ˚C for 48 h to constant weight. The M_a value of one species at each site was the average of three measurements made on leaves from multiple individuals. Leaf nitrogen content was measured using an Isotope Ratio Mass Spectrometer (Thermo Fisher Scientific Inc., USA). N_{area} was calculated from M_a and leaf nitrogen content. Leaf nitrogen content (for N_{area}) and stable carbon isotope ($\delta^{13}C$, for χ) measurements were made on pooled samples of leaves from multiple individuals.

Table 3.1 Parameters and abbreviations frequently used in the text.
The table provides information on the meaning and units of them.

Parameters and abbreviations	Unit	Description
χ	Pa Pa^{-1}	The ratio of leaf-internal to ambient CO_2 partial pressures
M_a	g biomass m^{-2}	Leaf mass per area
N_{area}	g m^{-2}	Leaf nitrogen content per area
V_{cmax}	μmolC m^{-2} s^{-1}	The maximum capacity of carboxylation

V_{cmax25}	μmolC m^{-2} s^{-1}	The maximum capacity of carboxylation at standard 25 ˚C
	molC m^{-2} day^{-1}	Used when calculating b in M_a section
T_g	˚C	Mean temperature during the growing season (mean daily temperature above a baseline of 0 ˚C)
D_0	kPa	Mean vapor pressure deficit during the growing season
R_0	μmol photon m^{-2} s^{-1}	Mean photosynthetically active radiation during the growing season
R_{LAI}	mol photon m^{-2} day^{-1}	Mean leaf area index weighted photosynthetically active radiation during the growing season
f	day day^{-1}	The ratio of growing season length to the number of days in the year
MAP	mm	Mean annual precipitation
α_p	mm mm^{-1}	The ratio of annual actual evapotranspiration to annual potential evapotranspiration
T_{dJ}	˚C	Mean daytime temperature of July
Γ^*	Pa	The photorespiratory compensation point
c_a	Pa	Ambient CO_2 partial pressure
c_i	Pa	Internal CO_2 partial pressure
β	unitless	The ratio at 25 ˚C of the unit costs of maintaining carboxylation and transpiration capacities (estimated as 146)
K	Pa	The effective Michaelis-Menten coefficient of Rubisco
K_c	Pa	The Michaelis-Menten coefficients of Rubisco for carboxylation
c	unitless	A constant proportional to the unit carbon cost for the maintenance of electron transport capacity (0.41)

LL	day	Leaf longevity
b	day	The potential age when leaves can no longer photosynthesize and assimilate CO_2
k	g biomass mol C^{-1}	Scaling factor
I_{abs}	mol photon m^{-2} day^{-1}	The photosynthetically active radiation absorbed by leaves
CC	gC gC^{-1}	A constant representing the construction carbon cost per unit leaf mass carbon
A_a	g biomass m^{-2} day^{-1}	Daily carbon assimilation rate per unit leaf area
φ_0	μmol C μmol^{-1} photon	The intrinsic quantum efficiency of photosynthesis
	mol C mol^{-1} photon	Used in Equation 3.12 of the M_a section
$N_{rubisco}$	g m^{-2}	Nitrogen content in Rubisco enzymes
$N_{structure}$	g m^{-2}	Nitrogen content in leaf structure

We used a portable infrared gas analyser (IRGA) system (LI-6400; Li-Cor Inc., Lincoln, NB, USA) to make the leaf gas-exchange measurements. Sunlit terminal branches from the upper canopy were collected and re-cut under water immediately prior to measurement. Measurements were made in the field with relative humidity and chamber block temperature close to that of the ambient air at the time of measurement, and a constant airflow rate (500 μmol s^{-1}). V_{cmax} was calculated from the light-saturated rate of net CO_2 fixation at ambient CO_2 using the one-point method (De Kauwe et al., 2016a) and adjusted to a standard temperature of 25 ˚C (V_{cmax25}) using the method of Bernacchi et al. (2003a). The V_{cmax} value of one species at each site was obtained from one individual only, due to the time-consuming nature of the measurement.

Carbon isotopic values ($\delta^{13}C$) were measured using an Isotope Ratio Mass Spectrometer (Thermo Fisher Scientific Inc., USA). Estimates of χ were made using the simplified method of Ubierna and Farquhar (2014) to calculate isotopic discrimination (Δ) from $\delta^{13}C$ considering discrimination during stomatal diffusion, carboxylation and photorespiration, thus following the relationship:

$$\chi = \frac{\Delta + \frac{f' \Gamma^*}{c_a} - a_s}{b' - a_s} \quad (3.1)$$

where a_s, b' and f' are the fractionations associated with diffusion in air (4.4 ‰), Rubisco carboxylation (30 ‰) and photorespiration (16 ‰), respectively. Γ^* is the photorespiratory compensation point, and c_a is ambient CO_2 partial pressure.

3.3.3 Climate data

In-situ climate data were only available for five (1785 m, 2782 m, 2993 m 3251 m and 3943 m) of the 18 sampled sites. We therefore estimated the climate at each site consistently by interpolation between a larger set of weather stations in the region (17 stations, Figure S3.1) for the period from January 2017 to December 2019 (http://data.cma.cn/data/cdcdetail/dataCode/SURF_CLI_CHN_MUL_MON.html) to create seasonal climatologies of monthly maximum and minimum temperature, fraction of sunshine hours, water vapor pressure and precipitation. These 17 stations range in elevation from 422 m to 3951 m. We then used the elevationally-sensitive ANUSPLIN interpolation scheme (Hutchinson and Xu, 2004) to provide estimates of these meteorological variables at each of the sites. The monthly estimates at each site were converted to daily values by linear interpolation in order to calculate the bioclimatic variables required as inputs to our models, specifically growing-season mean daytime temperature (T_g), growing-season mean vapour pressure deficit (D_0) and growing-season

mean photosynthetically active radiation (R_0), where the growing season was defined as the period when the daily temperature is above 0 ˚C. We also calculated the ratio of growing-season length to the number of days in the year (f), and the leaf-area-index weighted R_0 (R_{LAI}) to represent the effect of light interception by different layers in the canopy (Dong et al., 2017a). The average leaf area index during July and August (i.e. the months the trait data were collected) in 2018 and 2019 was derived from the MODIS leaf area index product (MCD15A3H: https://modis.gsfc.nasa.gov/). An annual moisture index (α_p, an estimate of the ratio of annual actual evapotranspiration to annual potential evapotranspiration) was calculated from the monthly temperature, precipitation and fraction of sunshine hours at each site using the Simple Process-Led Algorithms for Simulating Habitats (SPLASH) model (Davis et al., 2017b). Given the large difference between daytime and night-time temperature at high elevations, we also calculated the mean daytime temperature of July (T_{dJ}) by approximating the daily temperature cycle with a sine curve:

$$T_{\mathrm{dJ}} = T_{\mathrm{mx}} \left\{ \frac{1}{2} + \frac{(1-x^2)^{\frac{1}{2}}}{2\cos^{-1} x} \right\} + T_{\mathrm{mn}} \left\{ \frac{1}{2} - \frac{(1-x^2)^{\frac{1}{2}}}{2\cos^{-1} x} \right\} \quad (3.2)$$

where T_{max} is the mean daily maximum air temperature, T_{min} is the mean daily minimum air temperature, and $x = -\tan\varphi \tan\delta$, where φ is site latitude and δ is the average solar declination in July.

Comparison of the interpolated bioclimate variables with values calculated using in-situ data at the five sites where such data are available (Figure S3.2) suggests that the ANUSPLIN interpolation provides robust estimates of the patterns of variation in climate across sites although, except for July temperature, the absolute values differ.

3.3.4 Trait data analysis

Analyses of the trait data focused on the predominant deciduous component of each community. We used redundancy analysis (RDA: Legendre and Legendre (2012)) to determine the main patterns of trait variation using species average values from each site, assess how much of this variation is explained by environmental factors, and determine the correlations between traits and environment. RDA was performed using the *vegan* package in R (Oksanen et al., 2017). In order to compare the trait variability within and across sites, we calculated the coefficient of variation (CV: Lovie (2005)), a standardised measure of the dispersion of a frequency distribution, for the data set as a whole and at each site, for each of the traits independently.

We used Generalized Additive Models (GAMs) to analyse trait variability with α_p and elevation. GAMs (Hastie and Tibshirani, 1990) allow flexible relationships between response and predictor variables to be fitted to the data, avoiding the need to assume the form of the function in advance. Convex hulls were used to exclude areas of the fitted surface that were not well constrained by observations. GAMs were fitted using the *mgcv* package (Wood, 2001) and α-convex hull was produced using *alphahull* package in R (Rodríguez Casal and Pateiro López, 2010).

3.3.5 Trait prediction

We used existing optimality-based models of χ and V_{cmax25} and new models of M_a and N_{area} to predict the distribution of traits with climate and elevation across the sites. We used growing-season length as a proxy for the leaf longevity of deciduous plants. Specific photosynthetic traits adjust to environmental conditions over different timeframes (Jiang et al., 2020; Xu and Baldocchi, 2003), so we tried two alternative measures of temperature (T_g and

T_{dJ}) as predictors. The models for χ and V_{cmax25} apply for both deciduous and evergreen species.

3.3.5.1 The model for χ

This model is based on the assumption of evolutionary optimality in the trade-off between the costs of transpiration and carbon gain. The least-cost hypothesis predicts that plants minimize the total costs of photosynthesis, i.e. the requirement to maintain capacities for both carboxylation and transpiration (Prentice et al., 2014b; Wright et al., 2003). Using the standard photosynthesis model due to Farquhar et al. (1980a), Wang et al. (2017b) showed that χ could be predicted by:

$$\chi = \frac{\Gamma^*}{c_a} + \frac{\xi\left(1-\frac{\Gamma^*}{c_a}\right)}{\xi+\sqrt{D_0}} \tag{3.3}$$

where

$$\xi = \sqrt{\frac{\beta(K+\Gamma^*)}{1.6\eta}} \tag{3.4}$$

and

$$K = K_c\left(1+\frac{P_o}{K_o}\right) \tag{3.5}$$

Here Γ^* is the photorespiratory compensation point, and c_a is ambient CO_2 partial pressure. η is the viscosity of water relative to its value at 25 ˚C. β is the ratio at 25 ˚C of the unit costs of maintaining carboxylation and transpiration capacities. Based on a global compilation of leaf ^{13}C measurements, Wang et al. (2017b) estimated β = 146. K is the effective Michaelis-Menten coefficient of Rubisco. K_c and K_o are the temperature-dependent Michaelis–Menten coefficients for carboxylation and oxygenation, with reference values at 25 ˚C of 39.97 Pa and 27.48 kPa, respectively (Bernacchi et al., 2001). P_o is the ambient partial pressure of O_2. The composite variable ξ determines the sensitivity of χ

to D_0. This dependence is influenced by temperature (via Γ^*, K and η) and O_2 pressure (via K), according to Equations. 3.4 and 3.5.

3.3.5.2 The model for V_{cmax25}

The coordination hypothesis states that plants coordinate light-limited and Rubisco-limited photosynthesis rates so as to be equal under average daytime conditions (Chen et al., 1993b). This coordination ensures that the use of absorbed light is maximized, without incurring additional maintenance costs for V_{cmax}. V_{cmax} acclimated to growth temperature can be predicted from the universal model of carbon uptake proposed by Wang et al. (2017b):

$$V_{cmax} = \varphi_0 R_0 \left(\frac{c_i + K}{c_i + 2\Gamma^*}\right)\sqrt{1-\left(\frac{c}{m}\right)^{\frac{2}{3}}} \tag{3.6}$$

$$m = \left(\frac{c_i - \Gamma^*}{c_i + 2\Gamma^*}\right) \tag{3.7}$$

where φ_0 is the intrinsic quantum efficiency of photosynthesis (0.085 μmol C μmol^{-1} photon), and c_i is the leaf-internal CO_2 partial pressure, which is the product of observed χ and c_a. c is a constant proportional to the unit carbon cost for the maintenance of electron transport capacity (a value of 0.41 was estimated from an independent global dataset on photosynthetic capacities). m represents the effect of subsaturating CO_2 on the light-limited rate of photosynthesis.

The kinetic response of Rubisco to temperature allows V_{cmax25} to be estimated from V_{cmax} at growth temperature (T_g), by the following relationship:

$$V_{cmax} = V_{cmax25} f_v \tag{3.8}$$

$$f_v = e^{H_a\left(\frac{T_g - 298.15}{298.15 T_g R}\right)} \times \frac{\left[1+e^{\frac{(298.15\Delta S - H_d)}{298.15R}}\right]}{\left[1+e^{\frac{(T_g\Delta S - H_d)}{T_g R}}\right]} \tag{3.9}$$

where H_a is the activation energy (71513 J mol^{-1}), R is the universal gas constant (8.314 J mol^{-1} K^{-1}), H_d is the deactivation energy (200000 J mol^{-1}), and ΔS is an entropy term (J mol^{-1} K^{-1}) calculated using a linear relationship with T_g with a slope of 1.07 J mol^{-1} K^{-2} and intercept of 668.39 J mol^{-1} K^{-1} (Kattge and Knorr, 2007).

3.3.5.3 A new model for M_a

M_a contributes to determining how much leaf area can be displayed for a given amount of carbon allocated to above-ground tissues (Cui et al., 2019). There is a universal trade-off between M_a and leaf longevity (LL) across growth forms, plant functional types and biomes, known as the 'leaf economics spectrum' (Wright et al., 2004a). The spectrum runs from a 'fast' to a 'slow' economic strategy. Plants adopting a fast economic strategy have rapid returns on investment (low M_a) and short longevity (low LL), while plants adopting the slow strategy have high M_a and high LL.

Here we propose a novel model for M_a, which combines three optimality-based predictions. We start from the model proposed by Kikuzawa (1991). By assuming that the average net carbon gain by a leaf during its lifetime is maximized, this model provides an optimality-based prediction of the trade-off between M_a and LL:

$$LL = \sqrt{\frac{2b*CC*M_a}{A_a}} \tag{3.10}$$

Here b (day) is the potential age at which leaves can no longer photosynthesize, CC (gC gC^{-1}) is the construction cost per unit mass of leaf carbon, and A_a (g biomass m^{-2} day^{-1}) is the daily carbon assimilation rate per unit leaf area. M_a can be written as a function of LL, b and A_a from Equation 3.10. Consequently, understanding the environmental responses of these three traits is the key to predicting M_a.

Second, Xu et al. (2017) showed that b is approximately proportional to M_a and inversely proportional to V_{cmax25}:

$$b = \frac{u\, M_a}{k\, V_{cmax25}} \tag{3.11}$$

Here $u \approx 8889$ (dimensionless), estimated from a meta-analysis of data on 49 species across temperate and tropical biomes (Xu et al., 2017), and k is a scaling factor (30 g biomass mol C^{-1}).

Third, the coordination hypothesis allows optimal values of V_{cmax} to be predicted, by equating the Rubisco-limited assimilation rate with the electron-transport limited rate under typical daytime conditions that include temperature, vapour pressure deficit, ambient CO_2 and the photosynthetically active radiation absorbed by leaves (I_{abs}). The model has the mathematical form of a "light use efficiency model": that is, modelled total photosynthesis over any period is proportional to the total light absorbed during that period, consistent with classical studies on crop growth (Wang et al., 2017b). For this derivation, we made the simplifying assumption that the maximum rate of electron transport (J_{max}) is large enough that the square-root term in Equation 3.6 can be neglected. We substituted Equations 3.8 and 3.9 into 3.11 to predict b from M_a and V_{cmax}, which is then predictable from φ_0, I_{abs}, c_i, Γ^* and K. In this way we obtained a theoretical prediction of M_a:

$$M_a = \varphi_0\, I_{abs}\, \mathrm{LL}\, k \sqrt{\frac{(c_i - \Gamma^*)(c_i + K)}{(2uCCf_v)\left(c_i + 2\Gamma^*\right)^2}} \tag{3.12}$$

In addition to the implied proportionality of M_a with both absorbed light and leaf longevity, Equation 3.12 indicates the existence of a composite temperature effect due to the temperature dependencies of χ, Γ^*, K and f_v. In order to separate these dependencies, estimate the net effect of temperature more easily and account for the moisture effect detected in the China Plant Trait Database (Wang et al., 2018), we obtained the partial derivative of ln (M_a) in

Equation 3.12 with respect to temperature (T_g), and evaluated the result under standard environmental conditions. This predicts a decline in ln (M_a), for a given LL and I_{abs}, of ≈ 3% per degree increase in growth temperature (T_g). In addition, all the constants (φ_0, *u, k*, CC and reference values of f_v, K, c_i, and Γ^* at 25 ˚C) are combined into a single parameter C_1, to reduce the complexity of the model. A linearized equation for predicted M_a can then be derived as:

$$\ln(M_a) = \ln(I_{abs}) - 0.03\ T_g + \ln(LL) + \ln(C_1) \quad (3.13)$$

where C_1 is a free parameter. For deciduous species, there is an additional constraint on LL by growing-season length in Equation 3.13, thus we obtained the equation for deciduous species:

$$\ln(M_a) = \ln(I_{abs}) - 0.03\ T_g + \ln(f) + \ln(C_2) \quad (3.14)$$

where f is the ratio of growing season length to the number of days in the year. Thus, information on the number of days in a year is considered in the free parameter (ln (C_2) = ln (C_1) + ln (365)), resulting in changing C_1 to C_2. C_1 and C_2 are unknown *a priori* but could be estimated from observations.

Although not included in this theoretical derivation, a strong negative effect of increasing moisture availability on M_a has been reported (Meng et al., 2015). We used the ratio of actual to potential evapotranspiration (α_p) as an index of moisture availability in order to estimate this effect from the data. Thus, parameter C_2 is further replaced by C_3 to denote the parameter difference in Equations 3.14 and 3.15 after the moisture effect is included.

We used an independent data set of ln (M_a) for 621 deciduous species from the China Plant Trait Database (Wang et al., 2018) to estimate the parameter C_3. Using R_{LAI} to represent the averaged light absorbed by leaves, we regressed the observations of ln (M_a) against ln (R_{LAI}), T_g, ln (f) and ln (α_p) and obtained an estimate of ln (C_3) of 1.70. The predictors in this analysis explained 53% of the variation in M_a, and the fitted slopes of R_{LAI}, T_g and ln (f) were

quantitatively consistent with their theoretical values as given in Equation 3.14. Thus, the final model for M_a was:

$$\ln(M_a) = 1.22\ln(R_{LAI}) + 0.78\ln(f) - 0.06\ T_g - 0.60\ln(\alpha_p) + 1.70 \quad (3.15)$$

3.3.5.4 A simple model for N_{area}

N_{area} represents the sum of nitrogen in both metabolic and structural components of a leaf. Dong et al. (2017a) proposed a model to predict N_{area} from M_a and V_{cmax25} by assuming (based on previously published analyses) that (1) V_{cmax25} is proportional to nitrogen in Rubisco, and (2) non-photosynthetic nitrogen is almost proportional to M_a. The model of Dong et al. (2017a) is as follows:

$$N_{area} = 9.5N_{rubisco} + N_{structure} \quad (3.16)$$

$$N_{structure} = 10^{-2.67} M_a^{\ 0.99} \quad (3.17)$$

and

$$N_{rubisco} = 0.003135V_{cmax25} \quad (3.18)$$

The coefficient of $N_{rubisco}$ in Equation 3.16 reflects the allocation of total metabolic nitrogen to Rubisco, which however varies among species. We used the observed M_a and V_{cmax25} in this study to estimate $N_{structure}$ and $N_{rubisco}$ in Equations 3.17 and 3.18, then fitted a regression of metabolic nitrogen (estimated as the difference between N_{area} and $N_{structure}$) against $N_{rubisco}$ to estimate this coefficient for the deciduous species from the Gongga sites. We obtained a value for the coefficient of $N_{rubisco}$ of 7.2, which is within the predicted range given in Dong et al. (2017a).

However, there is considerable uncertainty in Equation 3.18, which describes the maximal catalytic turnover rate of Rubisco at 25 ˚C (Harrison et al., 2009; von Caemmerer et al., 1994), as well as in Equations 3.16 and 3.17. To simplify the calculations and avoid these uncertainties, we adopted an

alternative method to estimate N_{area} directly by regression as a linear combination of all observed M_a and V_{cmax25} (without intercept) in this study, yielding a simpler model that applies to non-nitrogen-fixing plants:

$$N_{area} = 0.02M_a + 0.003V_{cmax25} \quad (3.19)$$

We used this simple model to predict N_{area} first from observed – and then from predicted – V_{cmax25} and M_a. In this way, we could first test whether N_{area} is indeed predictable from V_{cmax25} and M_a in our data set, and then test whether N_{area} is predictable from climate data alone. In order to examine the impact of nitrogen fixation on this relationship, we also included "N-fixer" as a factor in this linear model. Partial residuals from the regression model for N_{area} were plotted using the *visreg* package (Breheny and Burchett, 2013).

3.3.5.5 Estimating the contribution of individual predictor variables

The contribution of each predictor variable to trait variation was calculated in three steps. At step 1, we created a baseline by averaging the values of each predictor variable across the 18 sites to create a data set for an "average" site. We used this average site data to calculate baseline trait values. At step 2, we changed one predictor variable at a time to the actual value at that site, keeping all the other variables constant at the average site value. We then calculated trait values using these new inputs. At step 3, the contribution of each predictor variable was calculated as the difference between the traits simulated at step 2 and the baseline value of the traits from step 1. This procedure allowed us to separate out the individual influences of changes in air pressure with elevation, T_{dJ} and D_0 on χ, the influence of changes in air pressure with elevation, T_{dJ} and R_0 on V_{cmax25}, as well as the impact of χ itself on V_{cmax25}. It also allowed us to separate the effects of T_g and R_{LAI} on M_a, and the effects of leaf longevity (indexed by growing season length, *gsl*) and moisture (indexed by the ratio of annual actual evapotranspiration to annual potential evapotranspiration) on M_a.

3.3.5.6 Uncertainty of the model predictions

The uncertainty of trait prediction can come from two sources: parameter values and input data. To evaluate the parameter uncertainty, we calculated the uncertainty of each parameter separately and combined them using the standard error propagation formula:

$$u^2(y) = \sum_i (\partial m/\partial n_i)^2 u^2(n_i) \quad (3.20)$$

where $u(y)$ is the standard uncertainty of the trait, $\partial m/\partial n_i$ is the sensitivity to variable n_i (obtained by differentiating the individual equations), and $u(n_i)$ is the standard uncertainty of n_i. The uncertainty of predicted M_a and N_{area} values arises from the uncertainties in coefficients fitted by regression and additional observed M_a and V_{cmax25} for N_{area}. The uncertainty of χ and V_{cmax25} arises from the values of the various ecophysiological quantities in the prediction equations and additional observed χ for V_{cmax25}, which show some degree of variation among species.

3.3.6 Model evaluation

We evaluated model performance by comparing the observed mean trait value at each site with predictions of each trait, using r and root mean square error (RMSE) between observed and predicted values across the sites. We compared the R^2 explained by the optimality models and statistical models. To test whether the optimality-based models can capture the climate variability, we also fitted multiple linear regressions of the site-mean trait values against the driving climate data, which serves as a statistical benchmark. All statistics were performed in R3.1.3 (R Core Team 2015).

3.4 Results

3.4.1 Traits variation related to climate

The four climate variables together accounted for 22.2 % of trait variation as shown in the RDA. The first axis explained 22.9 % of the variability in the observations. On this axis, variability was negatively related with temperature and positively related with R_0 (Figure 3.2). The second axis reflected gradients in moisture (α_p and vapour pressure deficit). Variability in χ was shown to be controlled by moisture, although with a small influence from temperature. V_{cmax25} varied positively with radiation, and negatively with temperature and moisture, in the opposite direction from χ. Temperature had a small positive influence on M_a but moisture had a negative impact, reflecting the fact that leaves were thicker in hotter and drier environments. N_{area} was mainly controlled by radiation and moisture, and covaried with M_a and V_{cmax25}.

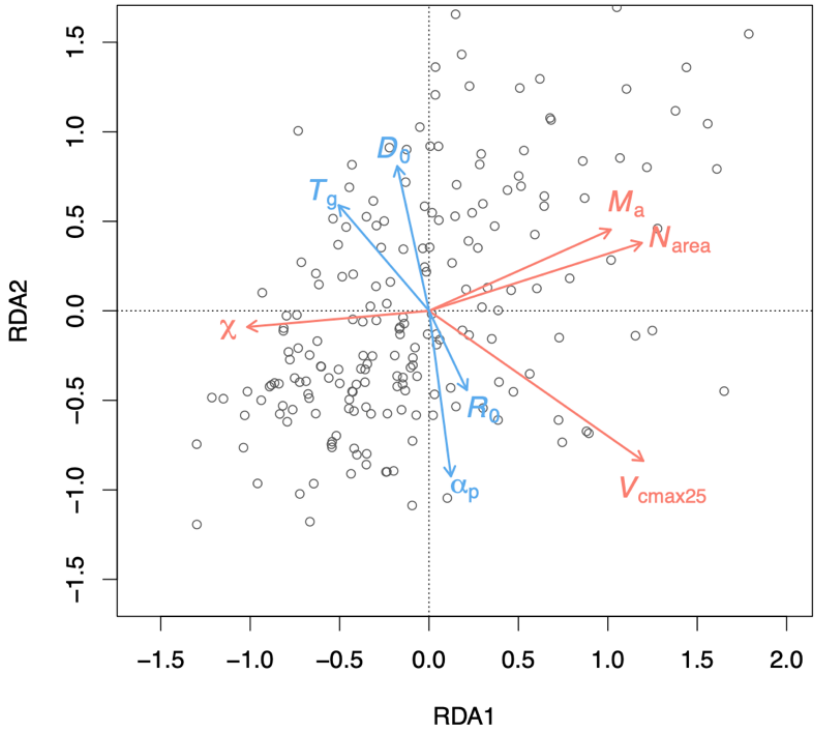

Figure 3.2 Climate-related trait dimensions from redundancy analysis (RDA). The climate variables (shown by blue arrows) are mean temperature during the growing season, defined as days above a baseline of 0 ˚C (T_g), mean vapour pressure deficit (D_0), mean photosynthetically active radiation (R_0), and a moisture index (α_p) defined as the ratio of annual actual evapotranspiration to annual potential evapotranspiration. The traits (shown by red arrows) are leaf mass per area (M_a), leaf nitrogen content per area (N_{area}), the maximum capacity of carboxylation standardized to 25 ˚C (V_{cmax25}) and the ratio of leaf-internal to ambient CO_2 partial pressures (χ). The grey circles are species average values from each site.

3.4.2 Observed and predicted trait variation with elevation

All observed traits showed non-linear relationships with elevation (Figure 3.3). Trait distributions in climate space also showed non-linear relationships. (Figure 3.4). These non-linear relationships arose because although temperature (as measured by either T_g or T_{dJ}) decreased monotonically with

elevation, the moisture-related variables in the Gongga Mountain region had non-linear relationships with elevation (Figure 3.1c): the lowest and uppermost sites had lower mean annual precipitation (MAP) and α_p than the sites at intermediate elevations (Table S3.1). The combination of these different trends in individual climate variables led to a complex pattern of trait variability. M_a and N_{area} were large under dry conditions and high elevation. V_{cmax25} increased along elevation and moisture gradients. χ was lower under dry conditions and low elevation. Nevertheless, M_a, V_{cmax25}, N_{area} tended to increase overall with elevation, while χ showed an overall decrease with elevation. There was no trend in the CV of any of the traits with elevation (Figure S3.3). Within-site CV values were larger than across-site CV values at nearly half of the sites for M_a, χ and N_{area}, while most of the within-site CV values were smaller than across-site CV values for V_{cmax25}. However, within-site variability differed between the traits. V_{cmax25} was the most, and χ the least, variable trait.

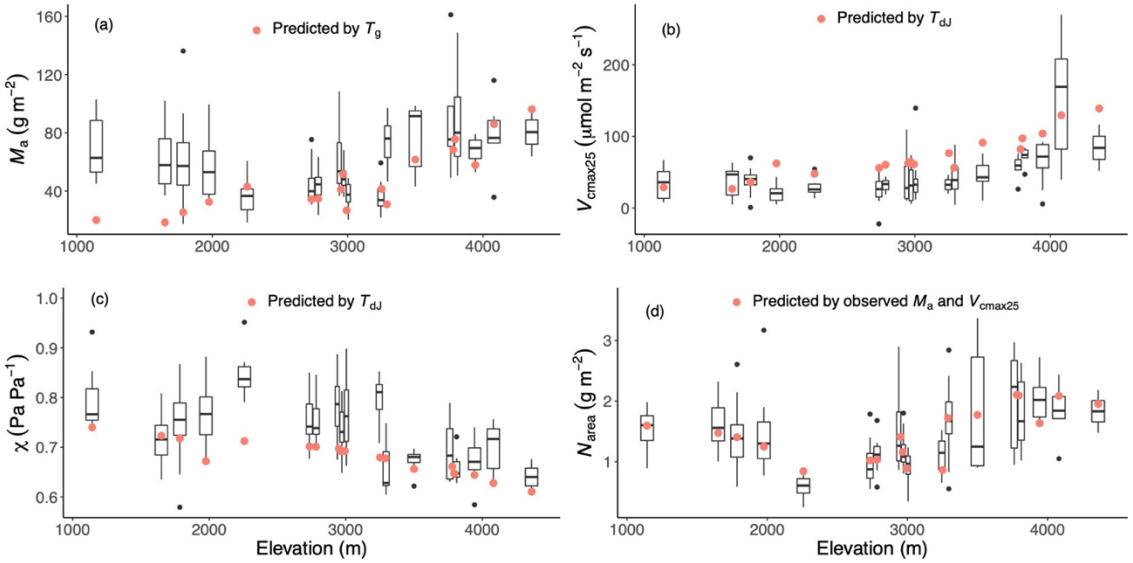

Figure 3.3 The observed and predicted values of traits along the altitudinal gradient. The traits are leaf mass per area (M_a), leaf nitrogen content per unit area (N_{area}), the maximum capacity of carboxylation standardized to 25 ˚C (V_{cmax25}) and the ratio of leaf-internal to ambient CO_2 partial pressure (χ). Only the observed trait values of deciduous plants are shown in black with box plots. The best versions of each predicted trait are shown in red dots: predicted M_a using mean temperature during the growing season, defined as days above a baseline of 0 ˚C (T_g), predicted V_{cmax25} and χ driven by daily temperature in July (T_{dJ}), predicted N_{area} using observed M_a and V_{cmax25}.

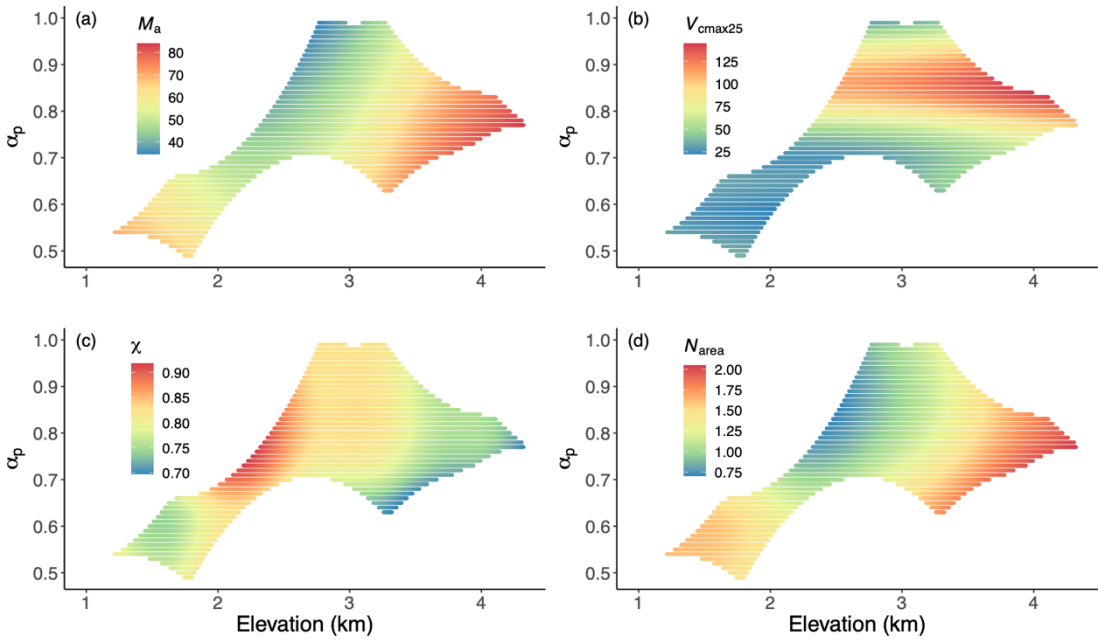

Figure 3.4 The distribution of predicted trait values in a climate space defined by elevation and a moisture index (α_p) using Generalized Additive Models. The traits are leaf mass per area (M_a), leaf nitrogen content per unit area (N_{area}), the maximum capacity of carboxylation standardized to 25 ˚C (V_{cmax25}) and the ratio of leaf-internal to ambient CO_2 partial pressure (χ). Trait values are indicated by the colour scale.

The models captured the overall patterns of variability of the four traits between sites, with most of predicted values falling within the range of the observed values. The observed and predicted site-mean values followed the 1:1 line (Figure 3.5) and the average of the *r* values for the four traits was 0.75. Mean RMSE values showed that differences between observations and predictions accounted for close to 30% of the mean trait values. The R^2 values produced by the optimality models were generally higher, except for M_a due to its underestimation at low elevation (Table 3.2). The models also captured χ and V_{cmax25} variations for evergreen species, with *r* values of 0.68 and 0.67 respectively (Figure S3.4). However, predicted M_a using T_{dJ}, χ using T_g and predicted N_{area} using $N_{structure}$ and $N_{rubisco}$ were underestimated, and V_{cmax25} using T_g was overestimated (Figure S3.5). Using T_{dJ} instead of T_g improved the

predictions of V_{cmax25} and χ, but degraded the prediction for M_a (Figure 3.5, S3.6). The predicted χ values using T_{dJ} were better than those using T_g, and the best-fit model could predict values across sites with r = 0.71 and RMSE = 0.06 despite the bias, with median values of χ underpredicted at most sites (Figure 3.3). The uncertainties of predicted V_{cmax25} and N_{area} were much narrower than the observed ranges. All parameters in the N_{area} models contributed almost equally to the uncertainty, while the parameter c was the major source of uncertainty for V_{cmax25}. The large uncertainty of M_a and χ mainly resulted from the intercept and the parameter β, respectively (Figure S3.7).

Table 3.2 The comparison between R^2 of statistical models (multiple linear regressions of the site-mean trait values against the driving climate data) and optimality models. For M_a, V_{cmax25} and χ, 'T_g' in brackets represents the predicted traits using mean temperature during growing season, 'T_{dJ}' represents the predicted traits using daytime temperature in July. For N_{area}, 'M_a + V_{cmax25}' represents the predicted N_{area} using observed M_a and V_{cmax25}' in Equation 3.19.

Traits	Statistical model	Optimality model
M_a (T_g)	0.55	0.33
V_{cmax25} (T_{dJ})	0.45	0.60
χ (T_{dJ})	0.49	0.51
N_{area} (M_a + V_{cmax25})	0.65	0.84

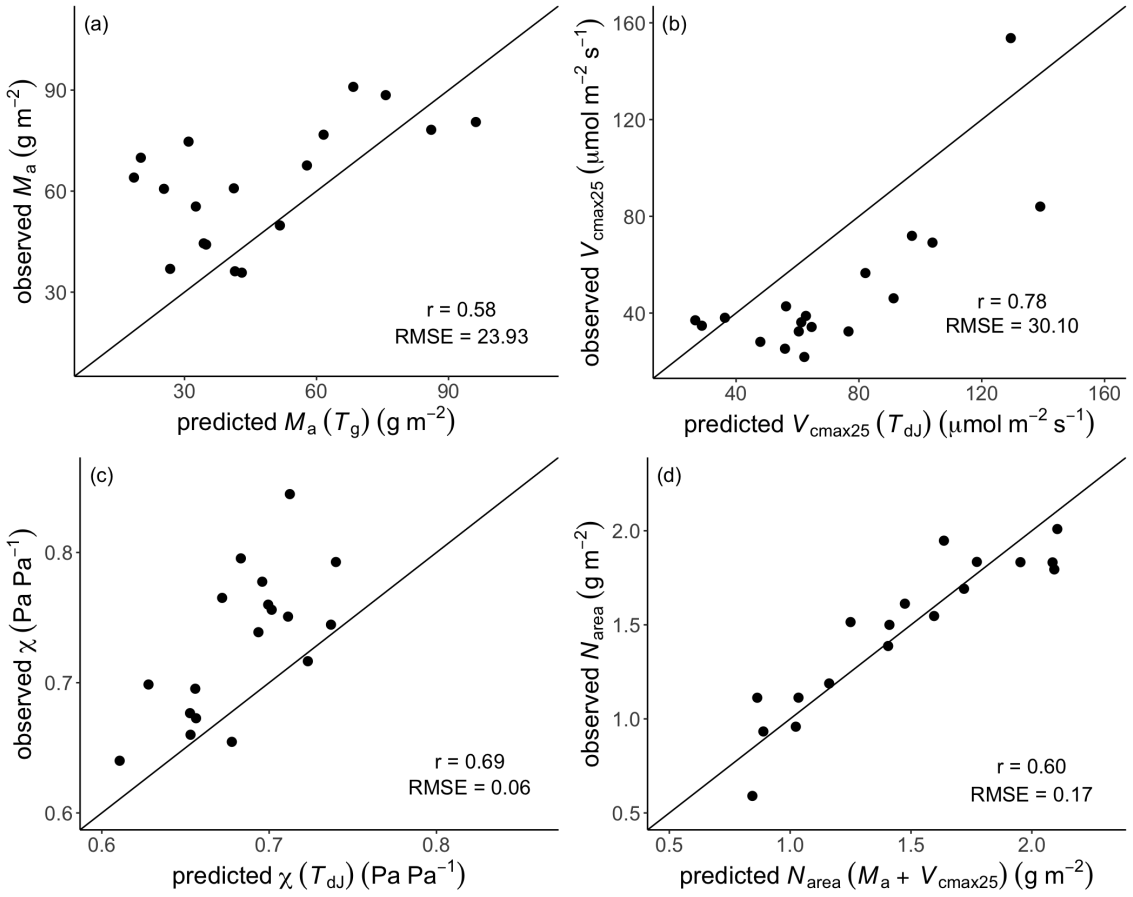

Figure 3.5 Site-mean values of traits. The traits are leaf mass per area (M_a), leaf nitrogen content per unit area (N_{area}), the maximum capacity of carboxylation standardized to 25 ˚C (V_{cmax25}) and the ratio of leaf-internal to ambient CO_2 partial pressure (χ). Observations are site-mean values and predictions are the best versions of different driven data at each site: predicted M_a using mean temperature during the growing season (T_g), predicted V_{cmax25} and χ driven by daily temperature in July (T_{dJ}), and predicted N_{area} using observed M_a and V_{cmax25}. The solid line is the 1:1 line.

N_{area} was shown to be strongly correlated with both M_a and V_{cmax25} (Figure 3.6, S3.8). However, there was a significant effect of including nitrogen fixation ("N-fixer") as a factor. At any given M_a or V_{cmax25}, N_{area} was slightly higher in N-fixing species. The prediction of N_{area} directly from M_a and V_{cmax25} with our simple method (Equation 3.19) was marginally closer to the data than the prediction from M_a and V_{cmax25} via $N_{structure}$ and $N_{rubisco}$ (Figure S3.5). The

predicted site-mean N_{area} with our new method but from predicted M_a and V_{cmax25} was also not significantly different from observed N_{area} (p = 0.08). These "fully predicted" N_{area} values were within the range of observations at most sites, but underestimated at low elevation due to the underestimation of predicted M_a (Figure S3.5).

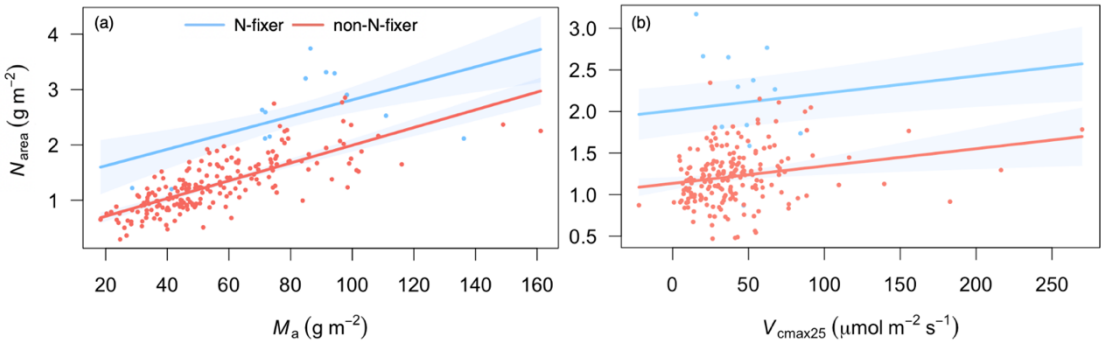

Figure 3.6 Partial residual plots showing leaf nitrogen content per unit area (N_{area}) as a function of leaf mass per area (M_a) and the maximum capacity of carboxylation standardized to 25 ˚C (V_{cmax25}) with N-fixer as an interaction term. (a) N_{area} as a function of M_a, (b) N_{area} as a function of V_{cmax25}. Blue, nitrogen-fixing plants (N-fixer); red, non-nitrogen-fixing plants (non-N-fixer).

3.4.3 Contribution of climate and elevation to trait variations

Vapour pressure deficit and temperature were shown to be the most important factors influencing the variation in χ between sites at different elevations in the Gongga Mountain region, but with opposing effects. Elevation made little contribution to the variation of χ. V_{cmax25} was influenced most by temperature and radiation, but elevation also had a small impact on V_{cmax25}. The effects of all the predictors were important for M_a (Figure 3.7).

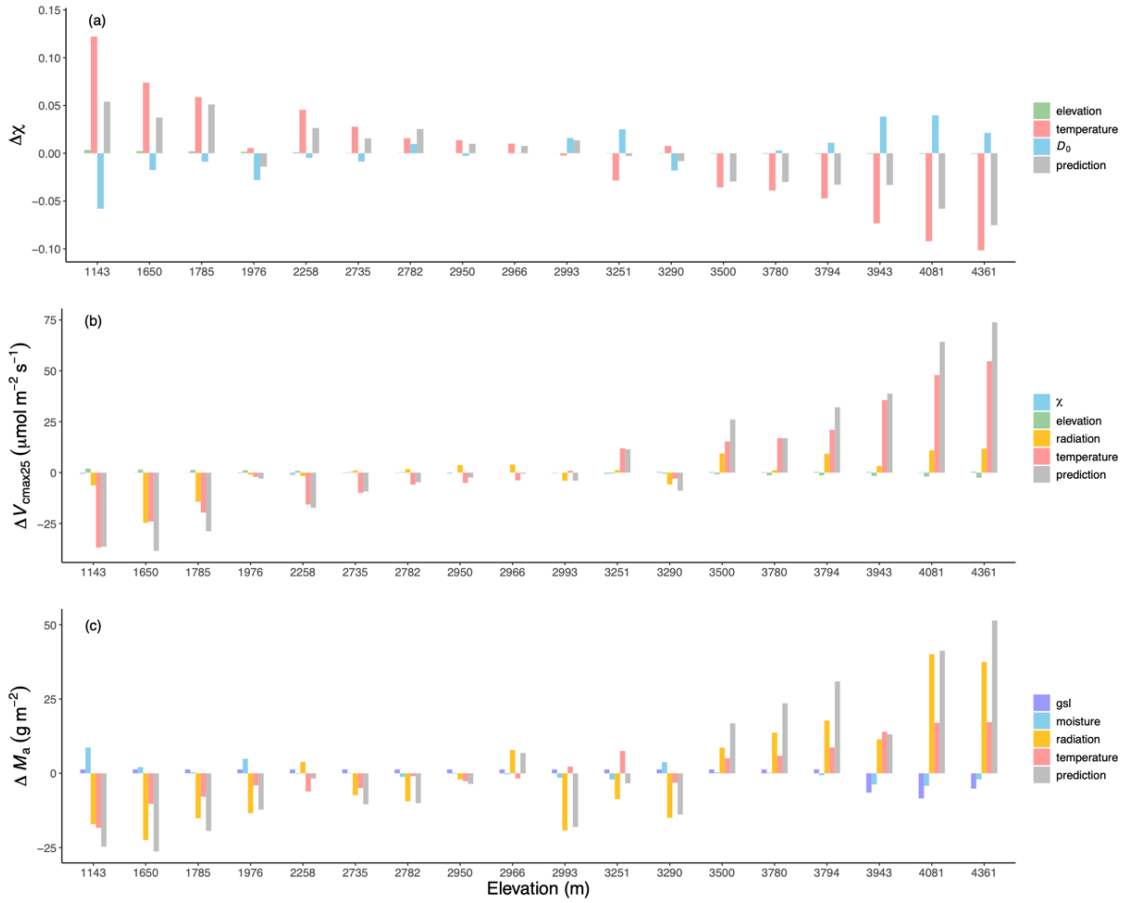

Figure 3.7 The modelled contributions of individual climate variables for each trait at each site. The traits are the ratio of leaf-internal to ambient CO_2 partial pressures (χ), the maximum capacity of carboxylation standardized to 25 ˚C (V_{cmax25}) and leaf mass per area (M_a). The grey bars show the changes in predicted trait values compared to the reference level driven by site-mean environment. The green bars show the elevation effect on χ and V_{cmax25} due to the changes in air pressure. The red bars show the effects of average daytime temperature in July on χ and V_{cmax25}, and the effect of growing season mean temperature on M_a, respectively. The blue bars show the effect of vapour pressure deficit (D_0) on χ, and then the effect of χ on V_{cmax25}. The yellow bars show the effect of growing season mean radiation on V_{cmax25}, and the effect of leaf area index weighted growing season mean radiation on M_a, respectively. The effects of leaf longevity (indexed by growing season length, gsl) and moisture

(indexed by the ratio of annual actual evapotranspiration to annual potential evapotranspiration) on M_a are shown in purple and blue.

3.5 Discussion

Optimality models have shown skill in predicting the trait variations along the elevation gradient in the Gongga Mountain region, without site- or region-specific calibration of parameters. The *r* of optimality models was generally higher than statistical models (Table 3.2). The *r* of the optimal M_a model was 0.73 when four predictions at low elevation were excluded. This finding suggests that the optimality models considering the underlying mechanisms are better than the statistical models, and supports the general validity of these models. The new model for M_a – calibrated using an independent set of measurements – correctly predicted patterns in the community-mean M_a of deciduous plants at the Gongga Mountain sites. When the coefficients of I_{abs}, f, T_g and α_p were calibrated with the sampled data, the values obtained were 0.99, 0.52, –0.03 and –0.75, not significantly different from the values obtained using the China Plant Trait Database but closer to the values for I_{abs} and T_g deduced from the theory. We did not apply the new model to evergreen species, because we had no information about their leaf longevity. Leaf longevity is strongly related to M_a (Kikuzawa, 1991; Reich et al., 1997; Wright et al., 2004a; Wright and Westoby, 2002). According to the leaf economics spectrum, the leaf longevity and M_a of deciduous plants are smaller than those of evergreen plants (Wright et al., 2004a). However, leaf longevity cannot be reliably estimated in the field without monitoring over a long period (Cornelissen et al., 2003b). If such data were available, it would be possible to extend the M_a model to evergreen species.

We have developed a simplified approach to predict N_{area}. This approach produced results close to those obtained using the two-step approach put

forward by Dong et al. (2017a). The agreement between predictions using the two methods suggests that the hypothesis underpinning both, namely that N_{area} can be predicted as the sum of a photosynthetic component related to V_{cmax25} and a non-photosynthetic component proportional to M_a (Evans, 1989; Lambers and Poorter, 1992; Onoda et al., 2004), is reasonable. However, our simpler approach does not require explicit specification of the relative allocation to metabolic and structural components and, by removing the intermediate steps, reduces the uncertainties and improves the predictions. We have shown that M_a and V_{cmax25} are predictable from climate, and that fully predicted N_{area} values lie within the range of observations at most sites (Figure S3.5). This interpretation differs from some previous studies in which leaf N availability, implicitly assumed to be related to soil N availability, is used to predict V_{cmax25} (Luo et al., 2004). There is evidence that soil nutrients, particularly phosphorus (P) rather than N, can influence N_{area} and V_{cmax25} (Gvozdevaite et al., 2018; He et al., 2014). However, there is growing evidence (a) that LMA exerts a major control on N_{area} (Dong et al., 2017a), and (b) that climate variables are the dominant drivers of V_{cmax}. Smith et al. (2019) found that climate variables accounted for about two-thirds of global variation in V_{cmax}; soil fertility indices about one-third. Liang et al. (2020), in a meta-analysis of soil N enhancement experiments, showed a 2-4 times greater effect on leaf area and biomass (i.e. whole-plant carbon allocation responses) than on leaf-level N_{area} and V_{cmax}. In other words, consistent with optimality theory, plants react to nutrient deficiency more by reducing leaf area, and increasing below-ground carbon investment, than by developing suboptimal leaves. Thus, a key implication of our results is that leaf nitrogen content can be predicted from climate alone. No global analysis of N_{area} is yet available, but the consistency of results for Australia (Dong et al., 2017a), Peru (Peng et al., 2020) and this study strongly supports the idea. Moreover, further work should focus on improving M_a prediction, since fully predicted N_{area}

is underestimated at low elevation due to the underestimation of M_a. We have also shown that R_0 is positively related to N_{area} – consistent with widespread observations that leaf nitrogen is higher at the top of the canopy (Chen et al., 1993b; Hirose and Werger, 1987) and the optimality hypothesis that nitrogen is unequally allocated within the canopy so as to maximize photosynthesis at each canopy level (Peltoniemi et al., 2012; Werger and Hirose, 1991).

Our analyses provide insights into the timescales on which leaf trait acclimation and adaptation operate. Since optimality models implicitly consider acclimation and adaptation in physiological processes, the use of climate inputs at the appropriate timescale – which resulted in better predictions – might provide insight on the corresponding adaptation/acclimation timescale of a trait. We showed that T_g was a better predictor than T_{dJ} for M_a, suggesting that M_a adapts to the whole-growing-season environment. The adaptation of M_a to long-term temperature is consistent with the fact that deciduous leaves are built at the beginning of the growing season with one-time carbon investment from the previous year, and maximize average carbon gain per day, and in turn net carbon gain during the whole growing season (Kikuzawa, 1991). However, although predictions of V_{cmax25} have commonly been made using long-term temperature inputs such as T_g (Smith et al., 2019; Wang et al., 2017a), our results show this can lead to a mis-estimation of V_{cmax25}. Using T_{dJ} (i.e. daytime during the month the plants were sampled) gives a better prediction, suggesting that V_{cmax25} adapts to environmental conditions during the previous few weeks. Several studies have shown that photosynthetic traits can acclimate quickly to temperature changes (Smith and Dukes, 2017b; Smith et al., 2017a), by regulating intrinsic biochemical characteristics, such as Rubisco content or catalytic turnover rate (Cavanagh and Kubien, 2014a). Our model-data comparison also suggests that χ acclimates to T_{dJ} rather than T_g. The least-cost hypothesis underlying the model of χ considers the total cost of maintaining

plant carboxylation and transpiration. Both metabolic processes function mainly in the daytime and can be adjusted rapidly. Therefore, the regulation of χ is also expected to acclimate to daytime temperature at a weekly to monthly scale, consistent with our finding that χ is better predicted using T_{dJ} than T_g. χ is highly plastic compared to M_a (Dong et al., 2017a), and seasonal variations in χ for deciduous species have been observed in many studies (Chen and Chen, 2007; Ma et al., 2010; McKown et al., 2013); however, the correlation of leaf phenology with seasonal changes in the growth environment of deciduous leaves indicates a need to disentangle their effects in the future. Given that different processes have different time-scales for acclimation/adaptation, model inputs should be selected to reflect this.

We have focused on predicting community-mean trait values. Although between-site variation is larger than within-site variation for all traits, nevertheless there is considerable variability at each site. This variability presumably reflects the within-canopy heterogeneity in bioclimate and in particular in radiation. There are large differences in photosynthetic traits between sunlit and shaded leaves, and it has also been shown that sunflecks contribute greatly to the photosynthesis of shaded leaves. Our model for M_a is sensitive to radiation inputs. By using R_{LAI} to estimate the average light level absorbed by leaves within the canopy to drive the M_a model, we were able to obtain relatively good predictions of the community-mean values except at the lowest sites, which may be attributable to disturbance – since many people live at lower elevations in this region. This approach would be insufficient to model within-canopy variability. However, site-based radiation measurements could be used in order to test whether this optimality-based model could predict within-site variation given appropriate inputs. The within-canopy heterogeneity of other bioclimatic factors may also be important in the choice of appropriate model

inputs (Blonder et al., 2018) and for testing the applicability of optimality-based models to explain within-site variability.

The comparison between observed and simulated traits allows us to identify mechanisms that are missing from the current optimality framework. For example, our analysis emphasizes the importance of soil moisture constraints. RDA showed that V_{cmax25} was positively associated with soil moisture, indexed by α_p. We found significant relationships between α_p and the residuals of predicted χ and V_{cmax25}. Some hydraulic traits, including the ratio of leaf-to-sapwood area and specific-sapwood hydraulic conductance, also showed significant correlations with photosynthetic traits (Figure S3.9), suggesting co-ordination between photosynthesis and water transport. Many studies have shown a strong coordination between hydraulic and photosynthetic traits across species (Brodribb, 2009; Scoffoni et al., 2016; Zhu et al., 2018), especially when hydraulic structure plays a crucial role in limiting photosynthesis process under water stress (Tyree and Sperry, 1989). Lin et al. (2015) analysed a large global dataset and found a positive relationship between wood density and carbon cost per unit water use. We have detected a significant positive effect of wood density on V_{cmax25}. Further empirical analysis on the coordination between photosynthetic and hydraulic traits over a larger environmental gradient is required. The coordination of photosynthesis and hydraulic traits has already been considered in models to predict stomatal response (Sperry et al., 2017) and vegetation response to drought (Eller et al., 2018a), and shown to produce improved predictions under water-limited conditions. Our results underline the need to consider aspects of water limitation, in addition to the stomatal response to vapour pressure deficit, in order to predict key plant traits.

Empirical analyses have shown that leaf longevity is positively related to potential evapotranspiration and vapour pressure deficit (Wright et al., 2004a). In our model to predict M_a, the effect of α_p was based on an empirical analysis

of an independent global trait dataset, because there is currently no theory to explain the impact of moisture on optimal leaf longevity. Using local data to calibrate the parameters for the theoretical model of M_a showed that the estimated effect of α_p is stronger than that indicated by the China Plant Trait Database. RMSE of predictions using the two different sets of calibrated parameters showed larger differences in the lowest values, where the soil moisture constraint is more severe. Given that the effects of other climate variables on M_a are well captured by the model, it would be worthwhile to try to identify and incorporate the mechanism of moisture impact on optimal leaf longevity.

The large functional diversity within sites may result from species attributes, biotic factors or microenvironment (Pappas et al., 2016; Violle et al., 2014). The model uncertainty analysis may provide a new way to estimate the functional diversity. Uncertainty analysis showed that the parameters β and *c*, representing unit costs for the maintenance of carboxylation, electron transport and transpiration, are the main contributors to uncertainty in χ and V_{cmax25}, respectively (Figure S3.7). Empirical analysis has shown substantial interspecific variation in β, but the current model of χ uses a single value of β for all species (Wang et al., 2017b). Using a single value estimated from published values of photosynthetic capacity (Kattge and Knorr, 2007; Wang et al., 2017b) for the parameter *c* in the model of V_{cmax25}, similarly, cannot fully represent its variation among species. Predictions using average values of β and *c* estimated from published data could cause mismatches with observed values, such as the predicted χ being lower than median observed value at many sites (Figure 3.3). At the same time, parameter uncertainty due to species variation also represents functional diversity in the community, which could in principle be considered in ecosystem models by specifying a realistic range of values for

each parameter. Meanwhile, modelling functional diversity still needs further work both in theory and application.

3.6 Implications for terrestrial ecosystem models

Optimality theory relies on the concept that natural selection requires plants to acclimate or adapt to prevailing environmental conditions. The development of optimality-based models therefore focuses on identifying the trade-offs between competing requirements. We have shown that optimality-based models for four key traits related to photosynthesis, M_a, N_{area}, V_{cmax} and χ, predict community-level variability with elevation and climate in the Gongga region, with no need for site- or regional-scale calibration. This finding adds to the growing number of studies showing that patterns of variation in these traits along climate gradients are predictable (Meng et al., 2015; Wang et al., 2017a).

Optimality-based models could be beneficially incorporated into vegetation or land-surface models since they provide a natural way of accounting for trait variability within plant functional types (PFTs), or across vegetation types, as a function of environmental gradients. The prediction of continuous trait variation with environment would obviate the need to specify parameter values separately for different PFTs (Kim et al., 2018; Kucharik et al., 2000; Sitch et al., 2003) or to account for within-PFT variability probabilistically (see e.g. Kelley et al., 2014). Moving from PFT-based parameters to optimality-based formulations would have the desirable effect of reducing the number of parameters that have to be specified. Moreover, models should improve in realism if parameter values are allowed to adjust to changing environmental conditions.

However, some issues need to be addressed before implementing optimality-based trait models into vegetation models. First, the timescales of acclimation and adaptation differ between traits. Thus, it is important to ensure that the variability of a given trait is predicted using the appropriate climate

information, for example daytime temperature over a week or month (rather than a climatological growing-season average) in the case of V_{cmax25}. Second, although soil moisture can limit photosynthesis, we lack theoretical understanding of the coordination between plant photosynthesis and hydraulics required to account for this constraint within the current optimality-based modelling framework. Third, the current framework does not account for within-site trait variability, and thus does not account for functional diversity within communities. Nevertheless, our study suggests a promising way forward to improve both the robustness (with fewer parameters) and realism (considering the acclimation and adaptation of traits) of terrestrial ecosystem models through the prediction of continuous trait variation along environmental gradients.

CHAPTER 4 Global variation in the ratio of sapwood to leaf area explained by optimality principles

This chapter is **preprinted** in bioRxiv.

Citation: Xu H, Wang H, Prentice IC, Harrison SP, Rowland L, Mencuccini M, Sanchez-Martinez P, He P, Wright IJ, Sitch S and Ye Q (2023), Global variation in the ratio of sapwood to leaf area explained by optimality principles. bioRxiv, https://doi.org/10.1101/2024.02.24.581904

Author contribution: H.X., H.W., I.C.P., S.P.H., L.R., and M.M. designed the study. H.X., H.W. and I.C.P. developed the theory. M.M. and P.S. compiled hydraulic trait dataset and extracted climate data (Dataset1). P.H. and Q.Y. compiled hydraulic trait dataset (Dataset2). H.X. performed the analysis and wrote the first draft of the manuscript; all authors contributed to the final draft.

4.1 Abstract

The sapwood area supporting a given leaf area (v_H) reflects a coordinated coupling between carbon uptake, water transport and loss at a whole plant level. Worldwide variation in v_H reflects diverse plants strategies adapt to prevailing environments and impacts the evolution of global carbon and water cycles. The fact that such variation has not been convincingly explained hinders its representation in Earth System Models. Here we hypothesize that optimal v_H tends to mediate between plant hydraulics and leaf photosynthesis so that leaf water loss matches water supply. By compiling and testing against two extensive datasets, we show that our hypothesis explains nearly 60% of v_H variation responding to light, vapour pressure deficit, temperature, and sapwood

conductance in a quantitively predictable manner. Sapwood conductance or warming-enhanced hydraulic efficiency reduces the demand on sapwood area for a given total leaf area and, whereas brightening and air dryness enhance photosynthetic capacities consequently increasing the demand. This knowledge can enrich Earth System Models where carbon allocation and water hydraulics play key roles in predicting future climate-carbon feedback.

4.2 Introduction

Continued atmospheric warming and drying worldwide (Fang et al., 2022) severely impacts terrestrial carbon and water cycling, which influences the global energy balance and climate system (Friedlingstein et al., 2023; Le Quéré et al., 2018). These processes are mediated by complex and coordinated plant physiological processes, leading to variations in plant traits in response to climate. Leaf photosynthesis and transpiration are closely linked, as stomata simultaneously control water loss and CO_2 uptake (Brodribb, 2009). This results in the coordination between leaf-level photosynthetic traits and whole-plant hydraulic traits (Rosas et al., 2019; Xu et al., 2021c), regulated by resource allocation to different plant organs (i.e. ratio of sapwood to leaf area). Plants adjust these traits at different timescales altering their performance and fitness in response to climate. For example, photosynthesis-related traits can be changed on relatively short timescale (Smith and Dukes, 2017a; Smith et al., 2017b), while hydraulic traits related to wood/leaf anatomy require much longer timescale to adapt (Bittencourt et al., 2020; Blackman et al., 2010; Limousin et al., 2022; Meinzer et al., 2010). Thus, spatial pattern of hydraulic traits variation might be achieved through species turnover, which affects species distribution especially in arid areas (Cosme et al., 2017; Trugman et al., 2020). It is urgent to investigate how plant hydraulic traits adapt to climate in order to improve our understanding of carbon and water cycling under global climate change.

Diverse plant eco-physiological traits and allocation strategies are shaped by the surrounding environments, reflecting various adaptation strategies evolved through natural selection. Eco-evolutionary optimality principles (EEO) offer an alternative perspective to examine the effect of climate on plant traits based on the idea that plants adapt to their surrounding environment through evolutionary processes (Franklin et al., 2020; Harrison et al., 2021). It has been successfully applied to explain optimal trait behaviour in response to climate, such as maximum capacity of carboxylation (V_{cmax}), ratio of leaf-internal to ambient CO_2 partial pressure (χ) and leaf mass per area (Smith et al., 2019; Wang et al., 2017b; Wang et al., 2023). However, previous applications of EEO mainly focus on leaf-level traits related to plant carbon cycling. Few studies consider the interactions between physiological processes across different organs due to the complex nature of trait coordination networks (Diaz et al., 2016). Whole-plant hydraulic traits may be the bridge that connects traits across different organs. Xylem hydraulic conductivity (K_S) has long been observed to be related to wood density and scale with the ratio of sapwood to leaf area (v_H) to maintain sufficient water supply (Janssen et al., 2020; Mencuccini et al., 2019b). Leaf water potential at turgor loss point (Ψ_{tlp}) coordinated with drought resistance traits at stem level (i.e. wood density) (Fu et al., 2012) indicates these traits also relate to photosynthesis and stomatal behaviour (Bartlett et al., 2016; Jin et al., 2023). Hence, hydraulic, photosynthetic and allocation traits are tightly coupled at the whole-plant level, but these relationships remain poorly understood at this scale (Diaz et al., 2016). Recent study shows that v_H sits at the centre of trait coordination network and mediates multiple processes in the coupling of plant water-carbon cycle (Xu et al., 2021c). Whether or not its variation and its trade-off with other hydraulic traits could be explicitly explained by a unified framework of optimal regulation on the carbon-water coupling hasn’t yet been tested globally.

The lack of understanding on the variation in v_H and other key hydraulic processes with climate is likely partially responsible for the ongoing uncertainties in how process-based models as a tool of simulating the future earth system show large uncertainties in their predictions on future climate-carbon feedbacks, especially under drought and heatwave events (Bonan and Doney, 2018). Current representation of carbon allocation is either derived from empirical relationships involving response to environment without considering its coordination with other physiological processes or the use of many tuneable plant functional types parameters (Trugman et al., 2019a). A realistic, efficient and unified model of v_H that can be directly implemented in process-based models may therefore be able to improve land-surface models (LSMs), without the need for increased model uncertainty from the use of many additional uncertain parameters.

Here based on EEO concepts, we propose a universal parsimonious theory to explain the variation in v_H as a trade-off with hydraulic traits regulated by environment in order to coordinate photosynthesis, transpiration and hydraulics at whole-plant level. In other words, how the water demand by transpiration for supporting canopy photosynthesis equals the water supply from trunk water transport. We evaluate the role of environmental variables (irradiance, temperature, vapour pressure deficit and CO_2) in controlling the water demand-supply balance and consequently how they shape the variation in v_H and its trade-off with hydraulic traits. We test our theory using two global hydraulic traits datasets collected at species and individual-at-site levels. We show that our theory predicts v_H variation at global scale. This model can be incorporated into LSMs as flexible plant allocation and hydraulic schemes to improve the prediction of land carbon and water cycling under future climate.

4.3 Theory

Based on EEO, we hypothesize that maximum plant water transport through the xylem matches maximum water demand required to maintain photosynthesis, considering resources are optimally allocated (Whitehead et al., 1984). In other words, the water uptake from soil driven by the maximum water potential difference between soil and leaf ($\Delta\Psi_{max}$) is transported through root and sapwood to the leaf evaporating surface for transpiration through stomata so that CO_2 from atmosphere is absorbed to sustain optimal photosynthetic capacity.

The canopy water demand is determined by canopy total leaf area and transpiration rate per leaf area. The latter is regulated by stomata, and predictable from EEO-based least-cost and coordination hypotheses via the coupling between photosynthesis and transpiration using Fick's law (Fick, 1855). The carbon assimilation is co-limited by carboxylation and electron transport processes, based on the theory that light- and Rubisco-limited photosynthetic rates are equal in order to optimally utilize light without additional carbon costs (Wang et al., 2017b). The leaf internal CO_2 level for carboxylation is controlled by stomatal conductance and an optimal ratio of leaf-internal to ambient CO_2 (χ) is achieved by minimizing unit carbon cost of photosynthesis and transpiration over a timescale of weeks to months (Lavergne et al., 2020a; Prentice et al., 2014a; Wang et al., 2017b). Both these traits determine the maximum water demand for leaf gas exchange and optimal photosynthesis. Furthermore, combing with the classic biochemical model of photosynthesis (Farquhar et al., 1980a) and Fick's law, the leaf level transpiration demand can be predicted as a function of irradiance, temperature, vapour pressure deficit (D) and CO_2. The tree water supply is controlled by hydraulic properties, including compensation effect of maximum hydraulic efficiency and a driving force of $\Delta\Psi_{max}$. The maximum hydraulic efficiency is influenced by structure of

hydraulic systems (i.e. pit membrane, conduit diameter), and temperature, which controls water viscosity (Vogel, 1921) and cell membrane permeability. All else being equal, plants with higher hydraulic efficiency (due to enhanced K_S or warming-reduced water viscosity and cell membrane permeability) can transport more water through a given stem, which could increase total leaf area. We assumed that (1) this match between water supply and demand often occurs around noon where stomatal conductance and transpiration reach their peak; (2) the optimal v_H is achieved at multiple-year timescale under environmental selection. Although photosynthetic traits optimize at weekly to monthly timescale, the hydraulic properties, especially maximum hydraulic efficiency, have limited plasticity. v_H is the intermediate trait to coordinate both sets of traits in respond to the surrounding environment and optimized to meet the balance as a result of coordinated physiological processes (Xu et al., 2021c). At site level, the optimal v_H is achieved through plasticity and species turnover over years.

These processes eventually lead to an optimal v_H balancing between the hydraulic efficiency in trunks and the water demand from canopy as predicted by irradiance, maximum temperature and vapour pressure deficit:

$$\mathrm{Log_e}(v_H) = 0.6\mathrm{Log_e}(D_{max}) + \mathrm{Log_e}(I_{abs}) - 0.03T_{max} - \mathrm{Log_e}(K_S) - \mathrm{Log_e}(\Delta\Psi_{max}) + C_1 \quad (4.1)$$

Here C_1 is the parameter containing information about photosynthetic traits values under standard climate condition and plant height. The model predicted that v_H was positively related to D_{max} and irradiance, negatively to air temperature and CO_2, and its negative correlations with K_S and $\Delta\Psi_{max}$ (Figure 4.1, S4.1). The sensitivities of maximum vapour pressure deficit (D_{max}) and air temperature (T_{max}), mean irradiance (I_{abs}) during growing season to v_H variation after log-transformed were 0.6, 1 and –0.03 theoretically derived from our model, which implied that high v_H was expected in dry and cold areas, with high

irradiance. A detailed model description is presented in Methods, and derivation of the theoretical prediction is presented in Appendix 4.1.

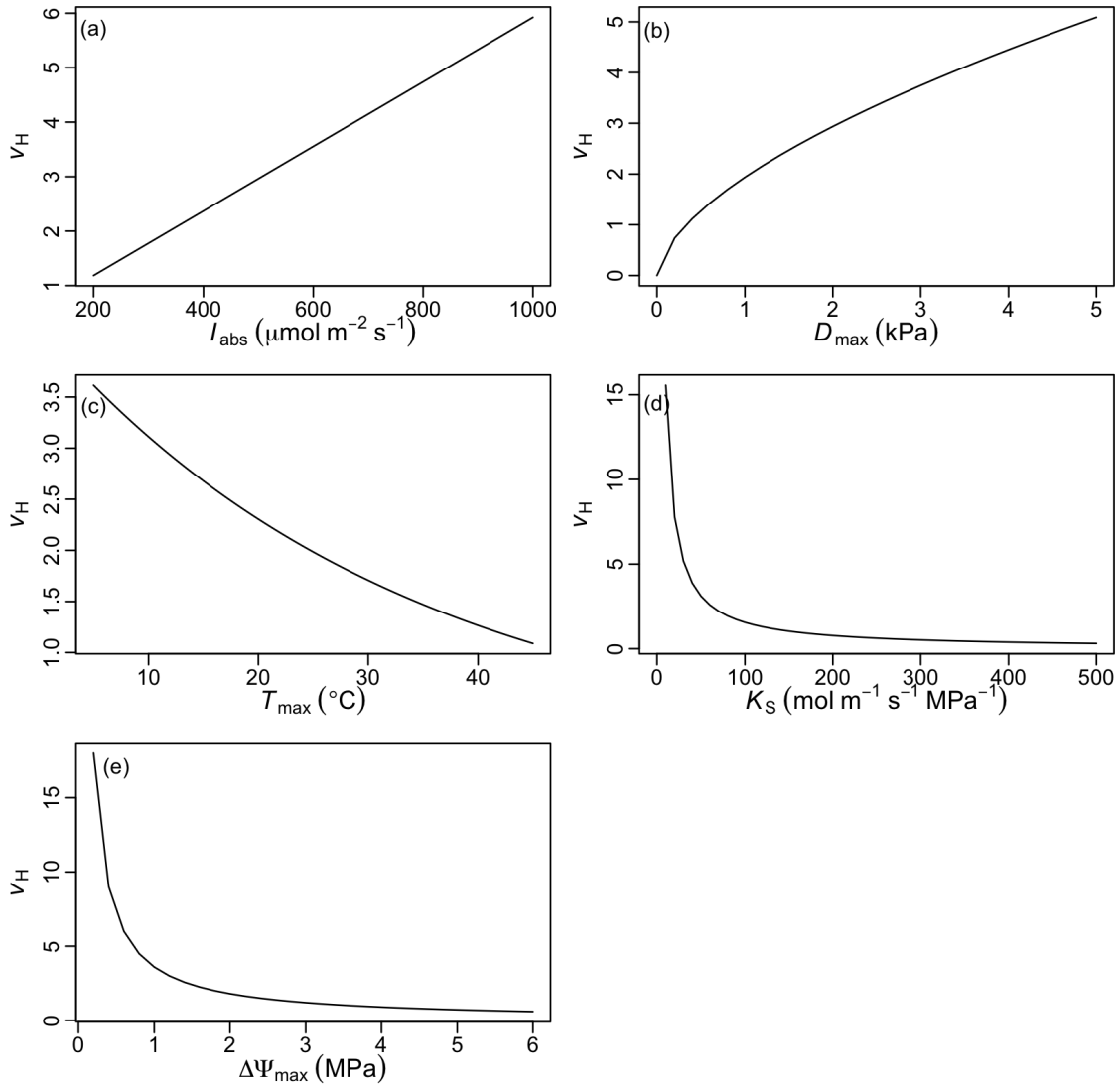

Figure 4.1 The sensitivities of theoretical model to climate and hydraulic traits. Sensitivity of the theoretical ratio of sapwood to leaf area (v_H, 10^{-4}) to irradiance (I_{abs}, panel a), vapour pressure deficit (D, panel b), temperature (T, panel c), hydraulic conductivity (K_S, panel d) and water potential difference between soil and leaf ($\Delta\Psi_{max}$, panel e). Sensitivity analyses were done while keeping all other climate variables at median levels across species: T = 25.5 °C, D = 1.5 kPa.

Our new theoretical hypothesis therefore, for the first time, explicitly incorporates the known functional coordination between hydraulic traits (i.e. the correlations between v_H and K_S, $\Delta\Psi_{max}$) in a parsimonious and analytical way, and quantitatively predicts the impacts of climates on this coordination network in terms of both the directions and sensitivities of those responses.

4.4 Methods

4.4.1 Theory based on eco-evolutionary optimality

The model of v_H variation builds on the hypothesis proposed by Whitehead et al. (1984) and Xu et al. (2021c), which predicts that maximum plant water transport should match maximum photosynthesis with resources optimally allocated. This implies that water loss through stomata should match water transport through xylem, which can be estimated using Fick's and Darcy's law respectively. The use of water storage and xylem water refilling are not considered in our model as they often occur during abrupt extreme events and night.

$$\frac{1.6\ g_s D}{P_{atm}} = \frac{K_S \Delta\Psi_{max} v_H}{h} \tag{4.2}$$

where g_s is stomatal conductance to CO_2 (mol m^{-2} s^{-1}), D is the vapour pressure deficit (Pa) and P_{atm} is the atmospheric pressure (Pa). On the right-hand side of the equation, v_H is the ratio of sapwood to leaf area (m^2 m^{-2}); K_S is the maximum sapwood-specific hydraulic conductivity (mol m^{-1} s^{-1} MPa^{-1}); $\Delta\Psi_{max}$ is the maximum difference between leaf and soil water potential (Ψ_{min} and Ψ_{soil}, MPa); h is the path length, approximately equal to tree height (m).

We can calculate g_s from the diffusion equation and the photosynthesis model (Farquhar et al., 1980b):

$$g_{\mathrm{s}} = \frac{A}{\left(\frac{c_{\mathrm{a}}}{P_{\mathrm{atm}}}\right)(1-\chi)} \tag{4.3}$$

$$A = m_{\mathrm{C}}\, V_{cmax}\, u \tag{4.4}$$

$$m_{\mathrm{C}} = \frac{\chi\, c_{\mathrm{a}} - \Gamma^{*}}{\chi\, c_{\mathrm{a}} + K} \tag{4.5}$$

where A is the assimilation (photosynthesis) rate (mol m^{-2} s^{-1}), c_a is the ambient partial pressure of CO_2 (Pa), χ is the ratio of leaf-internal to ambient CO_2 partial pressure (Pa Pa^{-1}), V_{cmax} is the maximum capacity of carboxylation (mol m^{-2} s^{-1}), Γ^* is the photorespiratory compensation point (Pa), and K is the effective Michaelis-Menten coefficient of Rubisco (Pa), u is the unit conversion from μmol to mol.

By replacing g_s from Equations 4.3-4.5 in Equation 4.2 and rearranging after $\mathrm{Log_e}$ transformation, we derive the following Equation 4.6 that describes the coordination between hydraulic and photosynthetic traits:

$$\begin{aligned}\mathrm{Log_e}(v_{\mathrm{H}}) = \mathrm{Log_e}(D) + \mathrm{Log_e}(m_{\mathrm{C}}) + \mathrm{Log_e}(V_{\mathrm{cmax}}) - \mathrm{Log_e}(K_{\mathrm{S}}) - \\ \mathrm{Log_e}(\Delta\Psi_{\mathrm{max}}) - \mathrm{Log_e}(1-\chi) - \mathrm{Log_e}(c_{\mathrm{a}}) + \mathrm{Log_e}(1.6h)\end{aligned} \tag{4.6}$$

We can estimate photosynthetic traits (χ, V_{cmax}) using existing models based on EEO. The least-cost hypothesis states that plants minimize the unit cost of both photosynthesis and transpiration (Prentice et al., 2014a; Wang et al., 2017b), leading to the prediction of χ (Equation 4.7).

$$\chi = \frac{\Gamma^{*}}{c_{\mathrm{a}}} + \frac{\xi\left(1 - \frac{\Gamma^{*}}{c_{\mathrm{a}}}\right)}{\xi + \sqrt{D}} \tag{4.7}$$

$$\xi = \sqrt{\frac{\beta(K + \Gamma^{*})}{1.6\eta^{*}}} \tag{4.8}$$

where β is a dimensionless constant (146, based on a global compilation of leaf $\delta^{13}C$ measurements), and η^* is the viscosity of water relative to its value at 25 ˚C.

The coordination hypothesis states that light- and Rubisco-limited photosynthesis rates should match to optimally utilize light without extra maintenance costs (Smith et al., 2019), leading to the prediction of V_{cmax} (Equation 4.9).

$$V_{cmax} \approx \varphi_0 I_{abs} \left(\frac{c_i + K}{c_i + 2\Gamma^*} \right) \quad (4.9)$$

where ϕ_0 (μmol C μmol^{-1} photon) is the intrinsic quantum efficiency of photosynthesis calculated by temperature-dependence relationship (Bernacchi et al., 2003b), I_{abs} is the photosynthetic photon flux density absorbed by leaves (μmol m^{-2} s^{-1}).

Since photosynthetic traits can be estimated from climate variables alone, the relationship between v_H and its drivers can be represented in Equation 4.10. Thus, the sensitivities of climate variables can be derived from the photosynthesis optimality models (see detailed steps in Appendix 4.1), which results in the simple form of our theoretical model for v_H (Equation 4.1).

$$\text{Log}_e(v_H) = f(D, T_{max}, I_{abs}) - \text{Log}_e(K_S) - \text{Log}_e(\Delta\Psi_{max}) + C_1 \quad (4.10)$$

4.4.2 Datasets

The global species-averaged dataset (Dataset1) for 1727 species was an updated version of HydraTRY (Mencuccini et al., 2019b; Sanchez‐Martinez et al., 2020). It includes 1624 angiosperms and 103 gymnosperms, 332 deciduous and 694 evergreen species with remaining species unknown. Species names and taxonomy (angiosperm and gymnosperm) were checked against the Plant List using *plantlist* package in R (Zhang et al., 2019). The information of leaf habit was matched with original publications and online reports. The dataset contained the branch-based ratio of sapwood to leaf area (v_H, m^2 m^{-2}, dimensionless), maximum sapwood-specific hydraulic conductivity (K_S, mol m^{-1} s^{-1} MPa^{-1}) and Ψ_{tlp} (MPa). The traits values were averaged if multiple samples

for one species occurred, in order to achieve maximum number of species with all traits values available at the same time.

Monthly climate data for Dataset1 from year 1970 to 2000 was extracted from Worldclim interpolated from weather stations (Fick and Hijmans, 2017), including maximum temperature, mean temperature, vapour pressure, solar radiation and precipitation. Monthly maximum vapour pressure deficit (D_{max}) was calculated using maximum temperature and vapour pressure. Monthly volumetric soil water content ($m^3\ m^{-3}$) of the ECMWF Integrated Forecasting System for 7-100cm depth from 1981-2019 (https://cds.climate.copernicus.eu/#!/home), soil texture, soil organic carbon content were extracted from SoilGrids (https://soilgrids.org/) to generate soil water potential (Ψ_{soil}) using *medfate* R package (Saxton and Rawls, 2006). Monthly aridity index (AI, the ratio of precipitation to evapotranspiration) was obtained from Global Aridity and PET Database (https://cgiarcsi.community/data/global-aridity-and-pet-database/) to determine growing season for plants. We defined the growing season as the months when mean temperature was above 0˚C and aridity index was above 0.1 and limited our study data to these periods, as in temperate ecosystems at periods below these values our study species will either be leafless or not photosynthesising. Maximum temperature (T_{max}), vapour pressure deficit (D_{max}), mean photosynthetically active radiation (I_{abs}) and Ψ_{soil} during growing season were calculated. The maximum difference between leaf and soil water potential ($\Delta\Psi_{max}$) was estimated using Ψ_{tlp} and soil water potential during growing season. The climate data for each species were calculated as the mean value of the per pixel value across its spatial extent within the observational data.

The global dataset (Dataset2) of 1612 individual samples (1247 species) was compiled from published literatures for validation of our results without aggregating into species level. Most of K_S data came from He et al. (2020) and

corresponding v_H values for each record have been implemented from the original publications. We added more K_S and v_H data from 2017-2021 by conducting searches on Web of Science, Google Scholar, and China National Knowledge Infrastructure (http://www.cnki.net) using the keywords “leaf area to sapwood area ratio”, “Huber value”, and “hydraulic traits”. To minimize the errors from ontogenesis and our methodology, we excluded the data that failed to meet the following criteria: (a) wild plants that were growing in natural ecosystems without experiments; (b) measurements which were made on adult plants or saplings; (c) v_H measured which were made on terminal stem or branch segments at the top of the canopy; (d) v_H estimates presented as the mean value for each species at the same site when the data was available for more than one individual. Because the corresponding Ψ_{tlp} data was limited, we did not include it in Dataset2. Monthly climate data from year 2011 to 2020 was extracted from CRU (https://crudata.uea.ac.uk/cru/data/hrg/, Harris et al. 2020) for each site, including maximum temperature, vapour pressure, cloud cover and precipitation. We calculated growing-season T_{max}, D_{max} and I_{abs} using Simple Process-Led Algorithms for Simulating Habitats (SPLASH) model (Davis et al., 2017a).

4.4.3 Statistical analysis

We used Dataset1 at species level to test our EEO-based hypothesis by investigating how v_H changed along environmental gradient and comparing with model predictions. Principal components analysis (PCA) was conducted to analyse climate covariance and reduce three climate variables (temperature, irradiance and D) to two axes. The first axis of Principal Component Analysis (PCA) explained 74.6% of climate variation, which was dominated by maximum vapour pressure deficit (D_{max}) and temperature (T_{max}) during growing season (Figure S4.4). The second axis (accounting for 20% of variation) largely

reflected variation in site irradiance during growing season (I_{abs}). In order to find the clear pattern of v_H variation in climate space, species with available three hydraulic traits values were divided into 48 climate zones/sites according to the loadings of first and second PC axes to investigate trait variation at site level (Figure S4.4a). The relationships between v_H and its driving factors were analysed at species and site levels.

To examine the relationships between v_H and its driving factors in a linear format, the multiple linear regression was carried between v_H and K_S, T_{max}, D_{max}, I_{abs} and $\Delta\Psi_{max}$ at species and site level using Dataset1 after trait values were natural log-transformed. Due to data absence of one or more trait for some species, sites with only one species were excluded from the multiple linear regression. The regression was repeated without $\Delta\Psi_{max}$ due to its insignificant effect on v_H variation and large uncertainty. Due to the unknown information about path length for water transport, the intercept (C_2 = –9.59) in Equation 4.11 was fitted for v_H prediction at site level when the coefficients of other factors were kept as theoretical values. C_2 was the only parameter in our EEO-based model and contained the information about path length, photosynthetic traits values at standard conditions and unit conversion. The sensitivity plots of v_H to its driving factors were drawn when one factor changed at a time while others were kept as median of their observed values. To quantify the contribution of different factors in v_H prediction, the r^2 of observed and predicted v_H with one factor added each time was calculated.

$$\mathrm{Log_e}(v_H) = f(D, T_{max}, I_{abs}) - \mathrm{Log_e}(K_S) - \mathrm{Log_e}(\Delta\Psi_{max}) + C_1 \quad (4.11)$$

The multiple linear regression between v_H and K_S, T_{max}, D_{max}, I_{abs} was conducted repeatedly using Dataset2 at site level for validation.

To assess the trade-off between v_H and K_S among different leaf phenologies (evergreen and deciduous), their bivariate relationship was examined using standardised major axis (SMA) regression and the slopes were tested if

different from theoretical values (–1) or not using *smatr* package (Warton et al., 2012). To show the opposite effects of temperature and vapour pressure deficit on v_H variation clearly, we estimated v_H value in continuous climate space (temperature and vapour pressure deficit) using theoretical sensitivities of *D* temperature, while kept K_S and I_{abs} as median values.

4.5 Results

4.5.1 Correlations between hydraulic traits

We observed that greater K_S was associated with lower v_H and this trade-off was consistent across species and sites from the multiple linear regressions including climate variables (Figure 4.2, 4.3). In multiple linear regressions including K_S and climate variables, the correlation between v_H and K_S was tighter at site level than species level. K_S was the most important driver of v_H, explaining 46% of its variation at site level. The fitted K_S – v_H slopes (either at species or site level) were flatter than that predicted from theory (–1) (Figure 4.2a, 3a). The fitted site-level slope was closer to theoretical prediction than that at species level. Analyses across a comprehensive sample of biomes and climate gradients (Figure S4.2) showed that deciduous and evergreen species had similar mean value of v_H (2×10^{-4} and 1.6×10^{-4}, respectively), but evergreen species had significantly lower K_S value than deciduous species (1.15 and 1.93 kg m^{-1} MPa^{-1} s^{-1}, respectively, Figure S4.3). In order to assess the variation in this trade-off among leaf phenology types, standard major axis (SMA) regressions were carried out for evergreen and deciduous species separately. However, the evergreen and deciduous species behaved the same and the slopes of their relationship were steeper than that from multiple linear regression expected by, and not significantly different from, the theoretical value (–1) (Figure S4.5). Though few gymnosperms were included, the relationship

between v_H and K_S was similar among angiosperms and gymnosperms (Figure 4.3a). An insignificant relationship between v_H and $\Delta\Psi_{max}$ was found at species and site level when $\Delta\Psi_{max}$ was added into multiple linear regression (Figure S4.6e), which might be masked by the strong negative relationship between K_S and $\Delta\Psi_{max}$ (Figure S4.7a). The relationship between v_H and $\Delta\Psi_{max}$ could be indirect through the covariation with K_S, which might be hard to examine empirically. The insignificant effect of $\Delta\Psi_{max}$ may also attribute to the uncertainty in gridded soil water potential data (Figure S4.7b).

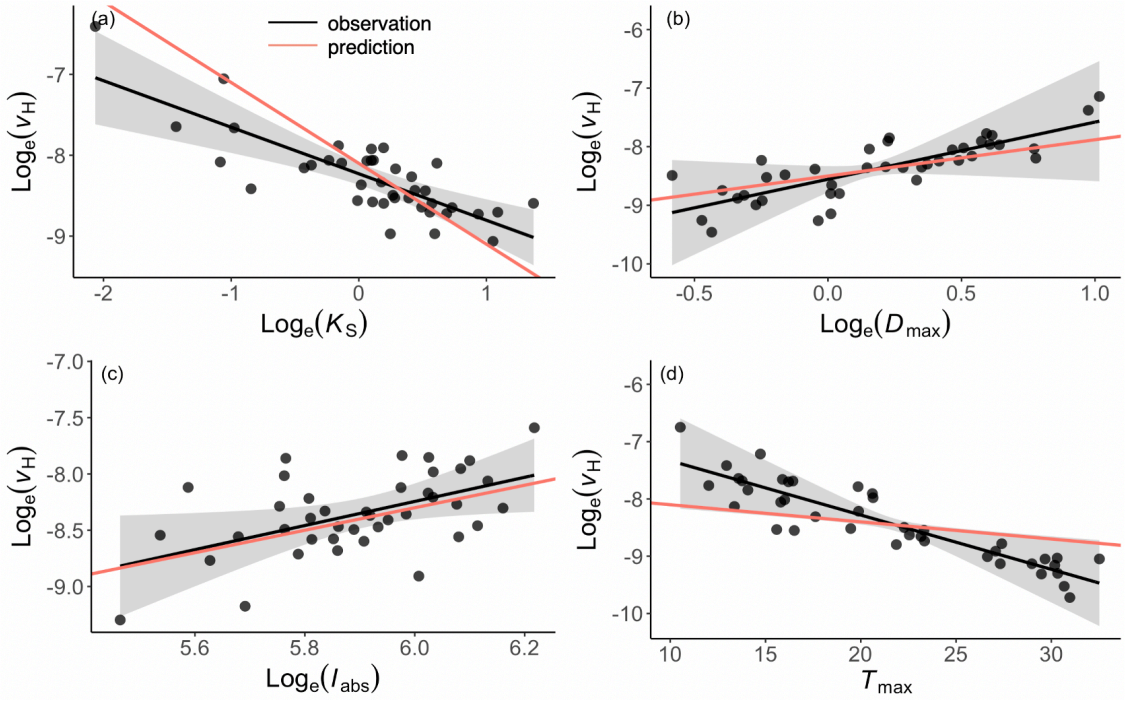

Figure 4.2 Partial residual plots from the multiple linear regression of log$_e$-transformed the ratio of sapwood to leaf area (v_H) against different predictors at site level using Dataset1. The predictors are shown in (a) sapwood-specific hydraulic conductivity (K_S), (b) maximum vapour pressure deficit (D_{max}), (c) mean irradiance (I_{abs}), (d) maximum temperature (T_{max}) during growing season. Black lines are the fitted across all sites and the gray shadings are the 95% confidence intervals around the fitted lines. The red lines are theoretical sensitivities in Equation 4.1.

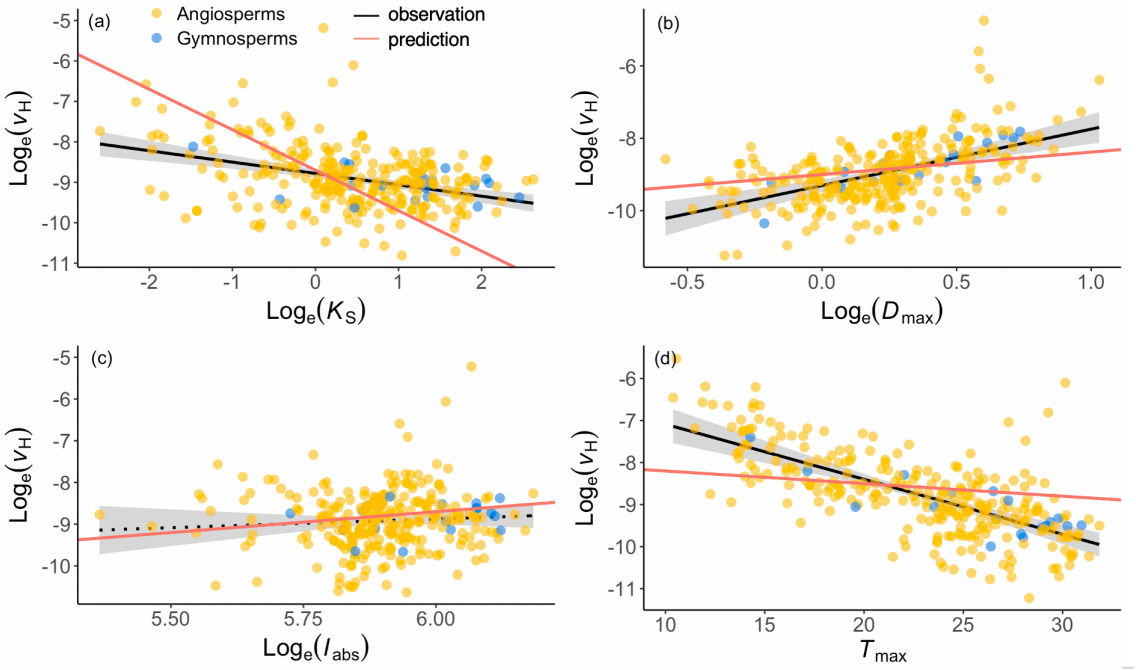

Figure 4.3 Partial residual plots from the multiple linear regression of $\log_e$-transformed the ratio of sapwood to leaf area (v_H) against different predictors at species level using Dataset1. The predictors are shown in (a) sapwood-specific hydraulic conductivity (K_S), (b) maximum vapour pressure deficit (D_{max}), (c) mean irradiance (I_{abs}), (d) maximum temperature (T_{max}) during growing season. Black lines are the fitted across all sites and the gray shadings are the 95% confidence intervals around the fitted lines. The black solid lines are significant (p<0.05) and the dotted lines are insignificant (p>0.05). The red lines are theoretical sensitivities in Equation 4.1.

4.5.2 v_H variation along climate gradient

Across both species and site levels, we found that plants tended to have larger sapwood area and/or lower total leaf area as vapour pressure deficit and irradiance increased, and temperature dropped after consideration of traits correlation. The observed climatic effects on v_H variation were similar whether using species-averaged dataset (Dataset1) or individual-at-site dataset (Dataset2) (Figure 4.3, S4.8). In Dataset1, the significant effects of temperature

and D_{max} on v_H variation were stronger at site level than species level, but the effect of light was only significant at site level (Figure 4.2, 4.3, S4.6). The multiple linear regressions showed that these climatic effects together led to 23% more of v_H variation explained at site level (Figure 4.3). The observed directions of climatic effects were consistent with EEO-based predictions and their predicted magnitudes fell into the confidence interval of slopes fitted at site level (Figure 4.3b-d, S4.8b-d). The site-level observed effects of D_{max} and irradiance were close to theoretical sensitivities in species-averaged dataset (Dataset1, Figure 4.3b, c). The observed effect of temperature in Dataset2 was smaller than that in species-averaged dataset and matched well with theoretical prediction (Figure S4.8d).

4.5.3 Prediction of hydraulic traits

The EEO-based model captured 56% of v_H variation using theoretical sensitivities of K_S, irradiance, D_{max} and temperature, a fitted parameter (Equation 4.11, Figure 4.4a). The 46% of v_H variation was contributed from K_S, followed by 6% from light, 4% from D_{max} and only 1% from temperature (Figure S4.9). Substituting K_S with v_H in Equation 4.12 could also lead to 66% of K_S variation predicted across sites (Figure 4.4b).

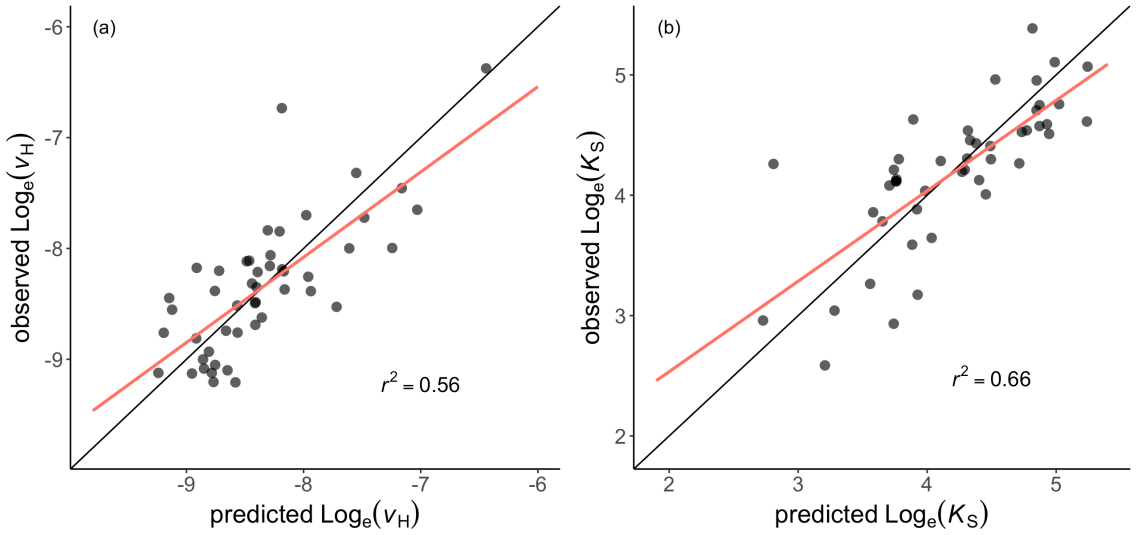

Figure 4.4 Comparison between site-mean observed and predicted ratios of sapwood to leaf area (v_H) using Dataset1. (a) v_H is predicted using observed sapwood-specific hydraulic conductivity (K_S) and climate variables with theoretical sensitivities of predictors and a fitted intercept. (b) K_S is predicted using observed v_H and the same climate variables.

4.6 Discussion

The comparison between observations and predictions by our theoretical model confirms the hypothesis that plants allocate resources optimally to balance the water supply through stem and water demand via leaf to maintain CO_2 capture and photosynthesis, without wasting additional carbon. The climate effects on v_H and global patterns of v_H were examined for the first time by extending the model proposed by Whitehead et al. (1984) further and incorporating recently developed EEO-based models for photosynthetic traits. The EEO-based theory, using a simple equation with only one fitted parameter to represent the coordination of hydraulic and photosynthetic processes, clearly describes the correlations between traits, quantifies the sensitivities of driving factors of v_H variation and largely captures its observed variation along climate gradients at a global scale. Hydraulic efficiency has a significant and large

impact on v_H values globally and certain climate variables also affects v_H indirectly through coordination with photosynthetic traits (Mencuccini et al., 2019b). It is crucial to understand trait integration to reveal mechanism behind complex trait-climate relationships (Anderegg, 2023).

v_H is directly associated with plant transpiration and regulates water cycling from soil to atmosphere. The sensitivity of v_H to climate is important for us to understand how water cycling at plant level will be influenced by climate change. The estimated sensitivity of v_H to climate will therefore help us elucidate the response of plant water cycling under climate change. In addition to the widely acknowledged positive effect of vapour pressure deficit (D), the theory predicts a negative temperature and positive irradiance effects on v_H, which is consistent with the observation that plants with higher v_H value are observed at dry and cold area with high light availability at two hydraulic datasets. Globally increasing vapour pressure deficit poses a dominant impact on leaf water potential regulated by stomata to control the water demand or leaf gas exchange (Fang et al., 2022; Turner et al., 1984; Yuan et al., 2019). The induced changes in stomatal conductance alter CO_2 uptake and photosynthetic process, leading to the shift in water demand and v_H. Other studies also find higher v_H value at sites with low soil water availability (Rosas et al., 2019). On the one hand, soil water availability is related to soil water potential and alters $\Delta\Psi_{max}$. This may further influence whole-plant trait – carbon allocation between belowground and aboveground (more carbon invested in roots when soil water availability is low) (Rowland et al., 2023). However, temperature covaries with atmospheric dryness, making it hard to disentangle their effects (Fu et al., 2022).

It is difficult to separate the effects of D and temperature due to their collinearity even with divergent results from warming experiments (McBranch et al., 2019; Way et al., 2013). The EEO-based model provides an alternative

approach to disentangle their effects theoretically and reveals the opposite impacts of D and temperature on v_H, which emphasizes the importance of quantifying their sensitivities to predict plant allocation strategy under future scenarios when both temperature and D are projected to increase (Grossiord et al., 2020). The total temperature effect is the sum of its effect on photosynthetic trait and hydraulic efficiency. The response of photosynthetic traits to temperature has been widely studied. As temperature increases, photosynthetic capacity increases and the ratio of leaf internal to external CO_2 becomes larger, leading to higher stomatal conductance and water demand. At the same time, hydraulic efficiency increases due to low water viscosity and high permeability in the symplastic pathway that is rarely studied and poorly understood. Here we employed a rather conservative temperature dependency of hydraulic efficiency (Cochard et al., 2000; Matzner and Comstock, 2001). This indicates that theoretical temperature sensitivity on v_H may be greater if less conservative temperature sensitivity was applied. The results highlight the need to study the instantaneous temperature response of hydraulic efficiency in the future, due to its important role in constraining photosynthesis process and water transport, especially under global warming. The EEO-based model offers a way to explore the potential v_H response as the net effect of competing effects.

The impact of irradiance is often overlooked in previous hydraulic traits-climate analysis, however hydraulic processes are tightly coupled with photosynthetic process (Brodribb et al., 2002), leading to the crucial role of light in influencing hydraulic traits. The observation and prediction from our EEO-based model both find plants need more sapwood area to support the same leaf area when irradiation is high. More water is required to maintain high assimilation rate under high irradiation in order to utilize light optimally at the whole-plant level. Plants may have greater leaf vein length per unit area to match increased water supply through xylem (Sack et al., 2013). The integration

of hydraulic and photosynthetic processes can help us better comprehend plant strategy from a more synthetic perspective. Our EEO-based theory predicts that plants support more leaves without allocating extra carbon to sapwood under higher CO_2, probably due to increasing water use efficiency which is observed in FACE experiments (De Kauwe et al., 2013). We do not examine the empirical CO_2 effect here since hydraulic data along a CO_2 gradient or under elevated CO_2 treatment is unavailable, however our theoretical prediction of its negative effect matches the direction found in other studies (Trugman et al., 2019b; Westoby et al., 2012).

The hypothesis for v_H variation is tested spatially at species and site level, indicating that the model works well on a longer timescale (multiple years) that is likely to involve evolutionary processes, such as plant genetic adaptation and species turnover. Theoretically, photosynthetic traits in our model acclimate to climate on a monthly timescale, while the plasticity of hydraulic traits is poorly known (Rowland et al., 2023). We presume that part of v_H variation can be mediated by climate effects via photosynthetic traits within a month, while another part requires a longer time period when hydraulic efficiency is altered in response to climate change (Niccoli et al., 2023). The shortest time frame for v_H to reach its optimal value to reconcile different timescales from water supply and demand still needs further verification. Previous studies show that plants can increase v_H to cope with drought event by shedding leaves to prevent water loss or hydraulic failure during a rather short time period (Carnicer et al., 2011; Choat et al., 2018; Trugman et al., 2018). During drought, photosynthetic traits can be adjusted quickly to alter water demand (Mengoli et al., 2022), but maximum hydraulic conductivity is not achieved and water storage within stem may be released, leading to disequilibrium between water demand and supply through xylem. More efforts are required to implement instantaneous hydraulic

processes and test the model at a temporal scale to improve drought phenology scheme in DGVMs (Martín Belda et al., 2022).

Other than external climate effects, plant internal trait coordination also plays an important role in adjusting plant performance. The robust trade-off between v_H and K_S across site and species has long been recognized as compensation effect, indicating its essential role in maintaining plant fitness. It is consistent with the prediction of our model that the relationship between v_H and K_S should be negative and modified by climate and other traits. Hydraulic efficiency is fundamental for v_H due to its direct constrains on water supply within plants. When more leaves are produced, plants either increase conducting area or efficiency to maintain water supply when assimilation rate and stomatal control remain constant. This compensation effect guarantees the balance between water supply though xylem and water demand from leaf to avoid wasted carbon investment or protect xylem from excessive tension. The importance of this compensation effect also manifests in their evolutionary correlation at species level, which means v_H and K_S cooperatively adapt to the changing environment over long timescale (Sanchez‐Martinez et al., 2020). This implies that the trade-off between v_H and K_S in our model shows plasticity to some extent and can still maintain under future climate conditions. Such key trade-off could be used to constrain species properties in individual-based vegetation models (Berzaghi et al., 2020).

The EEO-based model predicts a negative relationship between v_H and $\Delta\Psi_{max}$, nonetheless, this correlation might be partially affected by the significant relationship between $\Delta\Psi_{max}$ and K_S on a global scale and uncertainty in gridded product of soil water potential (Ψ_{soil}) (Hengl et al., 2017). The effect of $\Delta\Psi_{max}$ is the combination of Ψ_{soil} and leaf water potential at turgor loss point (Ψ_{tlp}), which is directly related to stomatal behaviour. Leaf turgor has shown to be the dominant contributor to changes in stomatal conductance, and Ψ_{tlp} well

represents the point when stomata fully close and carbon assimilation stops (Bartlett et al., 2016; Cochard et al., 2002; Knipfer et al., 2020; Mantova et al., 2023; Rodriguez-Dominguez et al., 2016). Soil water potential influences the water potential from soil to stem to regulate stomatal conductance and affect carbon assimilation (Rodriguez-Dominguez and Brodribb, 2020). Due to unclear mechanism, most models apply an empirical function to downregulate productivity using soil water availability (De Kauwe et al., 2013; Stocker et al., 2020). However, different stomatal conductance schemes show large variation in its response to soil water potential (Sabot et al., 2022). Some DGVMs including plant hydraulics employ another important hydraulic trait (P50, water potential at 50% loss of hydraulic conductivity) to represent the species' response to drought via its relationship with hydraulic conductivity (Christoffersen et al., 2016; Eller et al., 2018b). Whereas, Brodribb et al. (2003) finds no correlation between P50 and stomatal closure point across species. Previous studies demonstrate stomata closure occurs before P50 or xylem cavitation (Bartlett et al., 2016; Martin-StPaul et al., 2017). The direct incorporation of Ψ_{tlp} effect into this model increases its realism and robustness of stomatal behaviour under drought event.

Current DGVMs adopt fixed or flexible carbon allocation to leaf and stem mostly based on PFTs parameters or empirical relationships in response to environment (Berzaghi et al., 2020; Trugman et al., 2019a), leading to the uncertainty of land carbon sink (O'Sullivan et al., 2022; Sitch et al., 2008). v_H represents carbon allocation between leaf and stem, which has been observed to vary with climate. The allocation to leaf and stem directly influences the amount of low-turnover-rate carbon stored in stem and quick-turnover-rate carbon invested in leaves for productivity and transpiration, which in turn, affects land carbon and water cycling (Trugman et al., 2019a; Yang et al., 2021). Under future climate warming scenario, increasing CO_2 and temperature

can alleviate part of positive effect of D on v_H, resulting in more leaves supported for a given stem. This attributes to the co-acclimation of trait relationships in response to climate. The rate of change in climate variables along with their sensitivities of v_H together determine the carbon allocation and influence land-atmosphere feedback under continuous climate change (Anderegg et al., 2019). Our EEO-based model for v_H provides a new route of flexible carbon allocation representation in DGVMs to generate more realistic model output (Deckmyn et al., 2006; Magnani et al., 2000; Trugman et al., 2019a).

Compared to other models the EEO-based model is validated spatially on a longer timescale and considers coordinated physiological processes to achieve parsimonious solution using a single parameter. This hydraulic trait model avoids the dependency of complicated processes that requires simplifications and parameters, which is beneficial for improvement of PFTs scheme in DGVMs without jeopardizing original model structure and increasing process complexity. Inclusion of such a parsimonious scheme in DGVMs will lead to improved representation of plant responses to future climate change, with projected increases in temperature, D, regional drought, and extreme events, and thus in turn a critical for improved future climate prediction.

CHAPTER 5 Summary and Outlook

5.1 Conclusions

This thesis aims to understand how hydraulic traits vary in relation to non-hydraulic traits and climate using both field data and theoretical modelling approaches. Here I summarize the key findings of Chapter 2 to 4.

In Chapter 2, I proposed EEO-based model to understand the relationships between hydraulic and non-hydraulic traits. This model incorporated trait coordination network based on the EEO hypothesis that plants optimally allocate carbon to leaf and stem (optimal v_H) to balance water supply through stem and water demand driven by photosynthesis to minimize carbon cost. The model predicted that plants with high V_{cmax25} have high K_S, as v_H mediated both photosynthesis and hydraulic processes at whole plant level. This hypothesis aligned with field observations, as the v_H model could replicate the trait-trait and trait-climate relationships at a site level along an elevation gradient. Furthermore, the path analysis revealed that more structurally dependent traits such as LMA and WD, constrained the variation in more plastic traits like V_{cmax25}. Huber Value, which was at the centre of this trait network, linked traits of different degrees of plasticity, functions and strategies. The traits coordination network indicated a trade-off between resource acquisition efficiency and water transport capacity. This chapter provided a theoretical framework to explain coordination between hydraulic and photosynthetic traits.

In Chapter 3, I tested the predictability of recently developed photosynthetic traits models based on EEO along elevation. EEO-based models for photosynthetic traits predicted community-level traits variability with elevation and climate in the Gongga region, with no need for site- or regional-scale calibration. The trait predictions related to relationships with different climate inputs concluded that V_{cmax} and χ that are mainly driven by metabolic processes can be adjusted to “keep pace” with changing climate at monthly timescales. In contrast the variations in LMA and N_{area} were explained by climate variations at yearly timescales. The photosynthetic traits models further quantified the importance of different climate variables in trait variations. Temperature and vapour pressure deficit largely controlled the variation in χ, temperature and

irradiance controlled the variations in V_{cmax} and LMA. This chapter serves as the support for integration of photosynthetic traits models into hydraulic trait model with suitable timeframes of climate data.

In Chapter 4, the trait coordination model built in chapter 2 was advanced into a hydraulic trait model incorporating the photosynthetic traits models to understand hydraulic trait variation at a global scale and their response to climate. The model predicted the theoretical sensitivities of v_H to climate variables, which were consistent with observed patterns across sites and species on a global scale. Under low temperature, high irradiance and atmospheric dryness, plants allocated more carbon to stem than leaf (high v_H) and had low hydraulic efficiency. This strategy reduced the risks of freezing-thawing and cavitation by thickening cell walls, but at the cost of water transport capacity, which was significantly reduced under these conditions. Lastly, the hydraulic trait model predicted nearly 60% of the observed global hydraulic trait variations at a site level. This hydraulic trait model based on EEO principles therefore offers a promising way forward to improve both the robustness (with fewer parameters) and realism (considering the adaptation of traits and species turnover) of terrestrial ecosystem models through the prediction of continuous trait variation along environmental gradients.

5.2 Limitations and future directions

The theoretical framework was built to understand trait coordination and trait variations in response to climate with several assumptions and simplifications, which allowed the model to be easily to run and validated. However, these assumptions mean that there are potentially important physiological processes and key traits that are missing in the current framework. This may limit our understanding of trait coordination and model predictive capacity under certain climate conditions. Below I address some of the issues regarding this modelling framework, which were revealed from the work presented in chapter 2 to 4 and which required future investigation.

(1) Trait coordination in tropics

Tropical forests are significant contributors to the global terrestrial carbon sink (Friedlingstein et al., 2023). Climate change, especially drought stress, jeopardizes the ability of tropical forests to absorb carbon and function as a

carbon sink (Maia et al., 2020). Given this, it is pivotal to investigate trait coordination and variation in tropical regions to understand tropical forest responses to future climate change. In this thesis, we only sampled plants in the temperate zone and compiled global hydraulic traits datasets that only included a few sites and species in the tropics, due to limitations with existing data availability. To further understand traits coordination in tropical forests, I conducted fieldwork in tropical rainforests in Hainan province, China during summer 2023. In a team I contributed to measuring hydraulic, photosynthetic and LES traits of dominant species at three sites with contrasting water and nutrient conditions. The bivariate relationships between traits and trait coordination network were examined across and within sites. The trait network across sites showed that leaf nutrients and χ were key to controlling trait coordination, as assessed by weighted coefficients (Figure 5.1). Contrary to the trait coordination observed in the Gongga region, v_H was not related to photosynthetic or LES traits across the three study sites, potentially due to the narrow environmental gradients existing in this area. The preliminary results I have obtained from this trip highlighted the important role of soil nutrients in trait coordination, which was not included in my current modelling framework. This indicated that plants adopted different strategies under different climate and soil conditions. Although these results are only in their initial stages of analysis, this work is likely to be pivotal in understanding how soil nutrients could be an essential part of optimally modelling plant hydraulic trait coordination, especially in tropical rain forest regions. However, it should be noted this fieldwork was only conducted in one tropical region in China and it is likely that many more studies across the tropics with data on plant hydraulic and photosynthetic traits coordinated with climate and soils data are needed to facilitate further improvements in modelling the water and carbon dynamics in the tropics.

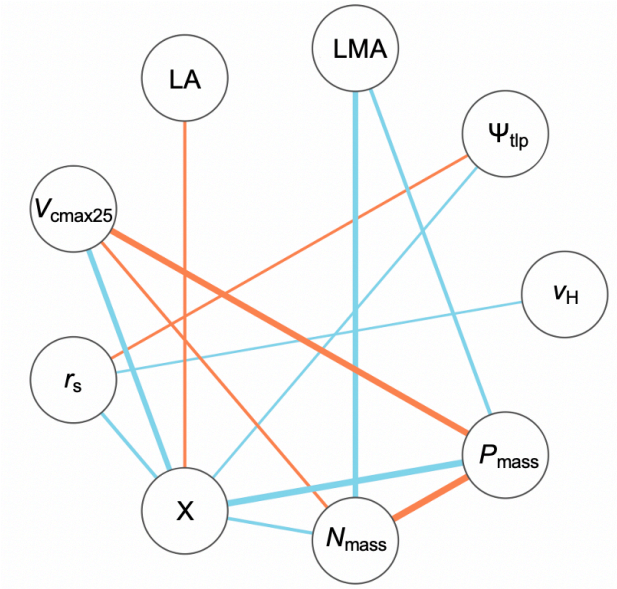

Figure 5.1 The trait coordination network across three sites in tropical rainforests in China. LA is leaf area, LMA is leaf mass per area, Ψ_{tlp} is leaf water potential at turgor loss point, v_H is sapwood to leaf area ratio, P_{mass} is leaf phosphorus per mass, N_{mass} is leaf nitrogen per mass, χ is ratio of leaf internal to ambient CO_2, r_s is branch respiration, V_{cmax25} is maximum capacity of carboxylation at 25 ˚C. The orange and blue lines show positive and negative relationships (p<0.05). respectively. Correlation strength is represented by line thickness.

(2) Interdependence of hydraulic efficiency and v_H

Although the hydraulic trait model no longer required photosynthetic traits inputs, substantial variation in v_H explained by the model resulted from hydraulic efficiency and vice versa. The model created in Chapter 4 currently fails to generate reliable global hydraulic trait map due to the interdependence and paucity of hydraulic traits data. Currently, hydraulic efficiency is estimated using LMA or calibrated with field measurement in DGVMs (Christoffersen et al., 2016; Kennedy et al., 2019; Li et al., 2021), which increases model uncertainty. Thus, the prediction of hydraulic efficiency remains an urgent challenge to tackle in the future. A new hypothesis based on EEO principles needs to be proposed to explain optimal hydraulic efficiency under environmental selection. This might lead to a fully climate-driven v_H model to improve representation of hydraulic traits in DGVMs. The approach used in Wang et al. (2023), which predicts the correlation between LMA and LL, may provide an alternative way to solve this issue by mathematic transformation. Take one climate variable (temperature, T) as an example, LMA_1 can be described as a function of LL_1, T_1

and other climate variables (moisture, irradiance). When other climate variables are kept constant and T_1 changes to T_2, plants have different trait combination – LMA_2 and LL_2. LMA_2 can also be described in the same formation as LMA_1 with climate variables. Combined with the theoretical magnitude of correlation between LMA and LL based on EEO model, the dependency of LMA on LL can be removed by subtracting these two functions and the sensitivity of LMA to temperature can be estimated without consideration of LL. This could narrow the range of trait prediction by removing contribution from trait variation. The scarcity of paired hydraulic traits hinders our capacity to understand the variation of hydraulic efficiency along climate gradient and therefore limits model development. Therefore, more efforts are required to measure hydraulic traits in the field to enhance our capacity to propose a theoretical framework to explain variations in hydraulic traits.

(3) Temporal change of v_H

In this thesis, the model has only been tested at a spatial scale, which involves macro-evolutionary processes, such as species turnover. The equilibrium between maximum water transport through xylem and demand by photosynthesis is assumed to hold true under long-term climate condition around noon as maximum hydraulic efficiency is less plastic in response to short-term climate change. The climate effects on v_H in the current version of hydraulic trait model are derived from photosynthesis processes, which is observed to acclimate to climate at a monthly timescale, implying that this model might be able to simulate seasonal change of v_H. Due to the lack of hydraulic traits data over varying temporal scales, the capacity of this model to predict intra-annual variability of optimal sapwood to leaf area ratio remains untested. The data that does exist on plasticity on these traits from experimental studies is currently very inconclusive concerning both the magnitude and direction of change in these traits in response to climate changes such as drought (Rowland et al., 2023). However, this may be due to the paucity of data availability globally to evaluate plasticity in hydraulic traits. Given this, more efforts should be made to measure hydraulic trait variation across time to understand their plasticity and timescales of acclimation.

When extreme events occur, such as drought and disrupt water equilibrium within a plant, this current model may fail to capture change in v_H or leaf

shedding. Under drought, plants adopt different water use strategies to cope with drought (Bacelar et al., 2012). For example, plants can close stomata early to reduce water loss and maintain leaf water potential (isohydricy), or keep leaf gas exchange and face high risk of embolism (anisohydricy) (Hochberg et al., 2018; Meinzer et al., 2014). This may be related to different combinations and trade-offs of hydraulic traits controlling drought responses, including Ψ_{tlp}, P50 and rooting depth (Martínez-Vilalta and Garcia-Forner, 2017). What's more, plants can release stored water (defined as capacitance) to replenish insufficient water supplies over short timescales and prevent dieback when water transport through xylem is obstructed (Sack and Holbrook, 2006). Leaf and woody capacitance are crucial hydraulic traits that regulate water supply to buffer drought (Salomón et al., 2017), which are likely needed to be incorporated into current framework. Thus, more hydraulic processes need to be considered under EEO framework to improve our understanding of complex hydraulic traits coordination and model performance in response to abrupt drought event.

(4) Functional diversity and trait coordination within a community

Many studies have demonstrated the important role of diversity in ecosystem functioning under climate change, however most DGVMs fail to simulate this. It is well documented that biodiversity has positive effects on ecosystem resilience, stability, and productivity (Brun et al., 2019; Isbell et al., 2015; Wang et al., 2019a). Functional diversity, a key component of diversity, refers to distribution of plant functional traits, which explains mechanisms of biodiversity-resilience relationships (Wang et al., 2024). For example, Anderegg et al. (2018) find that higher hydraulic traits diversity explains most of ecosystem flux change under drought than photosynthetic or LES traits. Plant trait diversity enhances biomass recovery and ecosystem resilience under climate change (Sakschewski et al., 2016). Therefore, functional diversity plays an important role in terrestrial biogeochemical cycle. However, the mechanisms controlling functional diversity variability still remain unknown, both from field observations and our theoretical understanding. Currently there are multiple ways to measure functional diversity (Mammola et al., 2020), which provide varying results (Stewart et al., 2023) and all of these measures are time-consuming to deploy, especially in diverse ecosystems, as they require a high

proportion of species within an ecosystem to be sampled (van der Plas et al., 2017). This leads to few public community- or plot-level traits datasets existing worldwide and hinders our understanding of drivers of functional diversity from empirical analysis. I tried to compile a plot-level trait dataset on a global scale across the tropics (Figure 5.2a), initially using LMA, as it is the most widely measured trait. I searched for plots where all species on the plot had a measured LMA value, but there were very few of these globally and so initially I did comparisons of plots in Brazil and Ghana. The initial analysis showed that the ranges of LMA values were similar across different plots with different temperature and moisture conditions on a regional scale (Ghana or Brazil), despite the changes in site-mean LMA (Figure 5.2b,c). This indicates that changes in functional diversity may be scale dependent. More freely available data on functional diversity is needed to pursue this question further however, as currently there is not enough data to allow model development and calibration. With advanced technologies, recent studies try to derive functional diversity using remote sensing or LiDAR, which facilitates large-scale monitoring and assessment of traits (Helfenstein et al., 2022; Schneider et al., 2017).

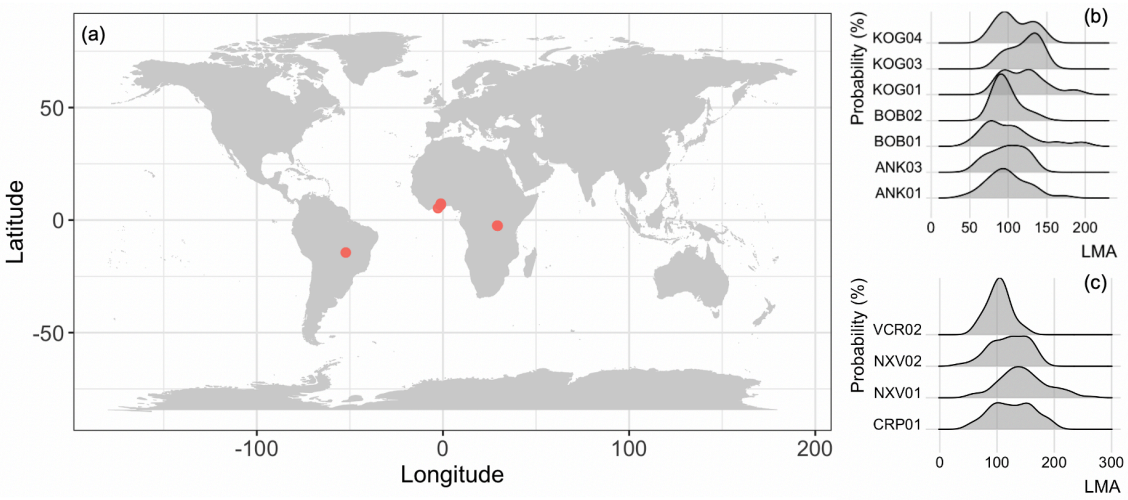

Figure 5.2 The locations of plots I have with available traits and species abundance data (a) and distributions of LMA in Ghana (b) and Brazil (c).

Although the current EEO-based traits models can capture optimal community-mean traits or trait combinations, the models are incapable of predicting functional diversity within community. In the future it may be that the functional diversity acts as a greater control on the ecosystem response to

climate change, than the community mean trait value. Therefore analysing the prior distribution of traits in a species pool and using a joint normal distribution method might give insights to comprehend climate effect on functional diversity based on EEO models (Poggiato et al., 2023). The joint normal distribution modelling describes how two normally distributed traits are correlated along climate gradients, characterized by their community-means, variances, and covariance. This enables predictions on trait variation within a community based on EEO models. For example, our hydraulic trait model predicts the correlation between K_S and v_H with the intercept varying with climate (Equation 4.11). With average values and trait covariances estimated from a global hydraulic trait dataset, I can simulate their standard deviation at each site (see examples in Figure 5.3). The preliminary results showed that this method could predict within-site distributions of v_H. However, there are some uncertainties in the observed trait distributions. The species abundance is not included, as not all species were measured at each site in the hydraulic trait datasets from Chapter 4. Thus, the observed distributions of v_H were not the same as functional diversity. More attempts should be made to measure functional diversity in order to validate our model predictions and investigate its drivers from both empirical and mechanistic approaches.

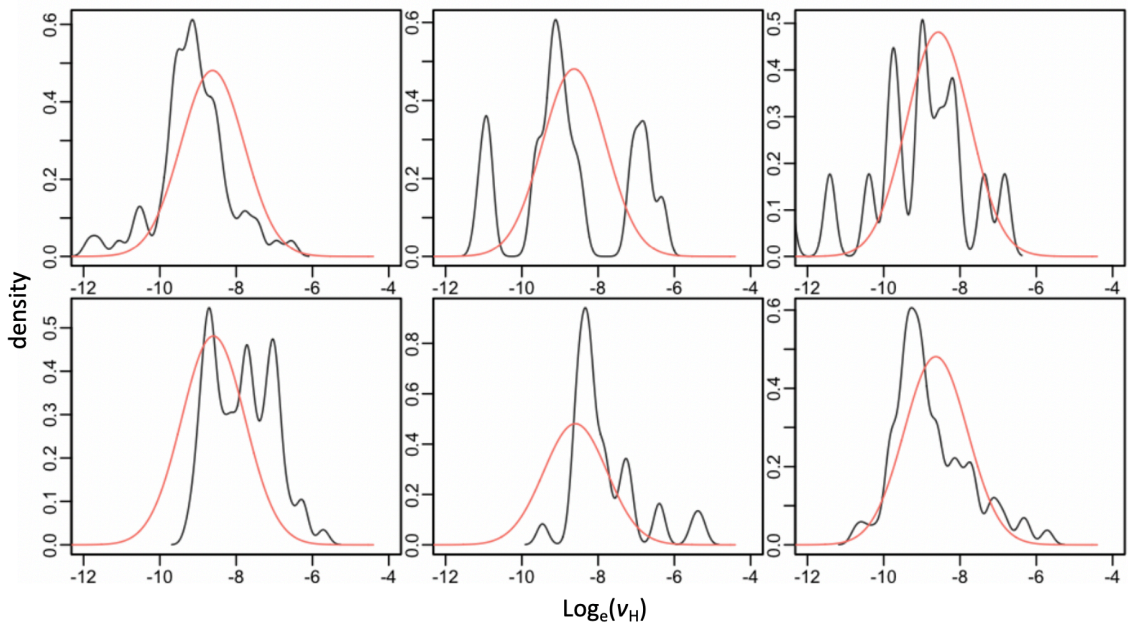

Figure 5.3 The comparisons of v_H distribution at different climate zones in Dataset1. The black and red lines are observed and simulated distributions of v_H.

In conclusion, I have created a new hydraulic model based on EEO principles, which can simulate the standard deviations of variation in v_H and use this to generate effective trait level predictions across sites and climate gradients globally. Future work is however needed to develop and test this model further, this should focus on improving the prediction of trait trade-offs using climate variables. A larger global hydraulic trait dataset, particularly with greater coverage in tropical environments, is urgently needed to facilitate the additional trait changes needed. Furthermore, in the future and with greater data-access for calibration, this modelling method has the potential to be applied to simulate trait distributions, as well as trait means. The capacity to simulate changes in functional diversity, alongside community-mean traits is likely to considerably expand our capacity to understand and predict ecosystem responses to climate change.

Appendices

Appendix 1 – Other publications

First-authored peer-reviewed articles

- Xu H, Wang H, Prentice IC and Harrison SP (2023), Leaf carbon and nitrogen stoichiometric variation along environmental gradients. Biogeosciences, 20: 4511-4525. https://doi.org/10.5194/bg-20-4511-2023

Co-authored peer-reviewed articles

- Wang H, Harrison SP, Li M, Prentice IC, Qiao S, Wang R, Xu H, Mengoli G, Peng Y, Yang Y (2022), The China plant trait database version 2. Scientific Data, 9: 769. https://doi.org/10.1038/s41597-022-01884-4

Appendix 2 – Supplementary material to Chapter 2

Table S2.1 Variance-covariance matrices of traits for deciduous and evergreen species. The values were calculated across all species. All traits were Log_e-transformed except χ, which was logit transformed. Trait abbreviations as follows: wood density (WD), sapwood-specific hydraulic conductivity at 25 ˚C (K_{S25}), leaf water potential at turgor loss point (Ψ_{tlp}), the ratio of sapwood to leaf area (v_H), leaf mass per area (LMA), the ratio of leaf-internal to ambient CO_2 partial pressure (χ), leaf nitrogen content per area (N_{area}) and maximum capacity of carboxylation at 25 ˚C (V_{cmax25}). *P* values are indicated "***" (< 0.001), "**" (< 0.01) and "*" (< 0.05).

Deciduous	v_H	K_{S25}	$-\Psi_{tlp}$	WD	LMA	N_{area}	V_{cmax25}	logit χ
v_H	0.36							
K_{S25}	-0.19***	0.70						
$-\Psi_{tlp}$	0.02*	-0.03**	0.03					
WD	0.03**		0.02***	0.05				
LMA	0.11***	-0.06**	0.02***		0.12			
N_{area}	0.11***		0.02**		0.11***	0.18		
V_{cmax25}						0.09***	0.58	
logit χ			-0.02***		-0.06***	-0.08***		0.26

Evergreen	v_H	K_{S25}	$-\Psi_{tlp}$	WD	LMA	N_{area}	V_{cmax25}	logit χ
v_H	0.43							
K_{S25}	-0.33**	0.76						
$-\Psi_{tlp}$			0.03					
WD				0.05				
LMA	0.14**				0.13			
N_{area}	0.14**				0.07**	0.12		
V_{cmax25}	0.36**						0.79	
logit χ					-0.07*	-0.09*		0.30

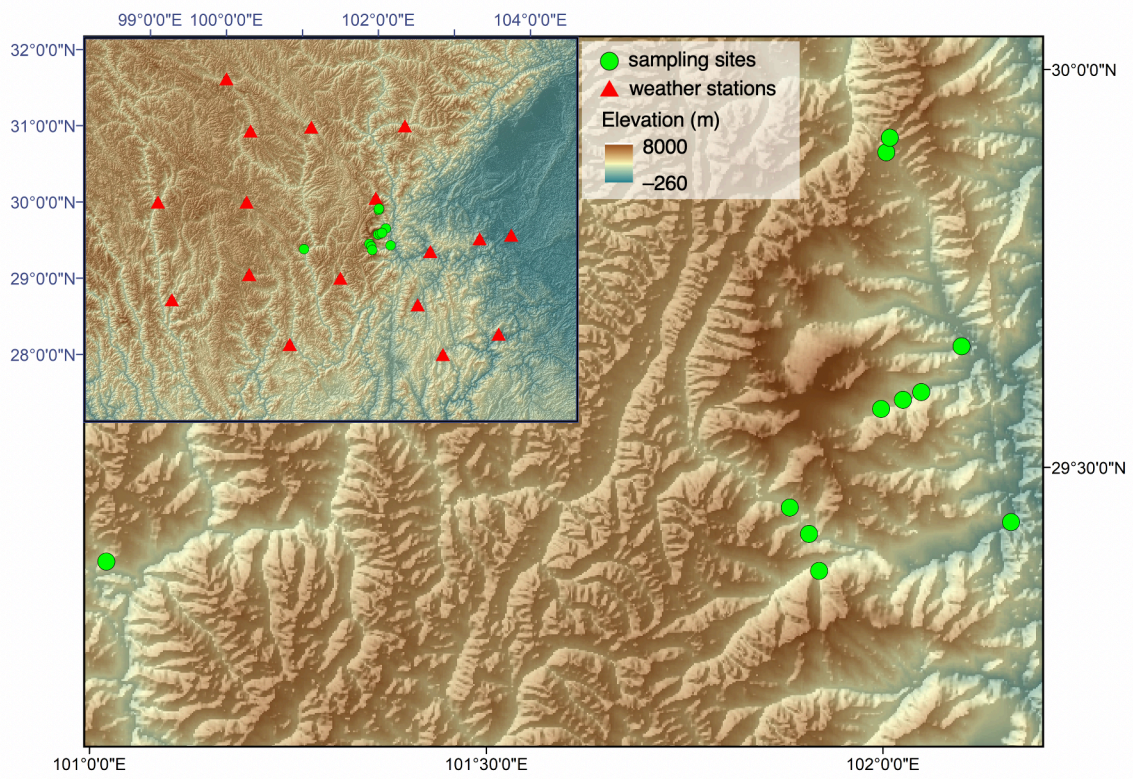

Figure S2.1 Locations of sampling sites and weather stations. The green dots are the sampling sites and red triangles are the weather stations. The latitude and longitude for the outer plot are in black, inset in navy blue. The background colour represents the elevation gradient.

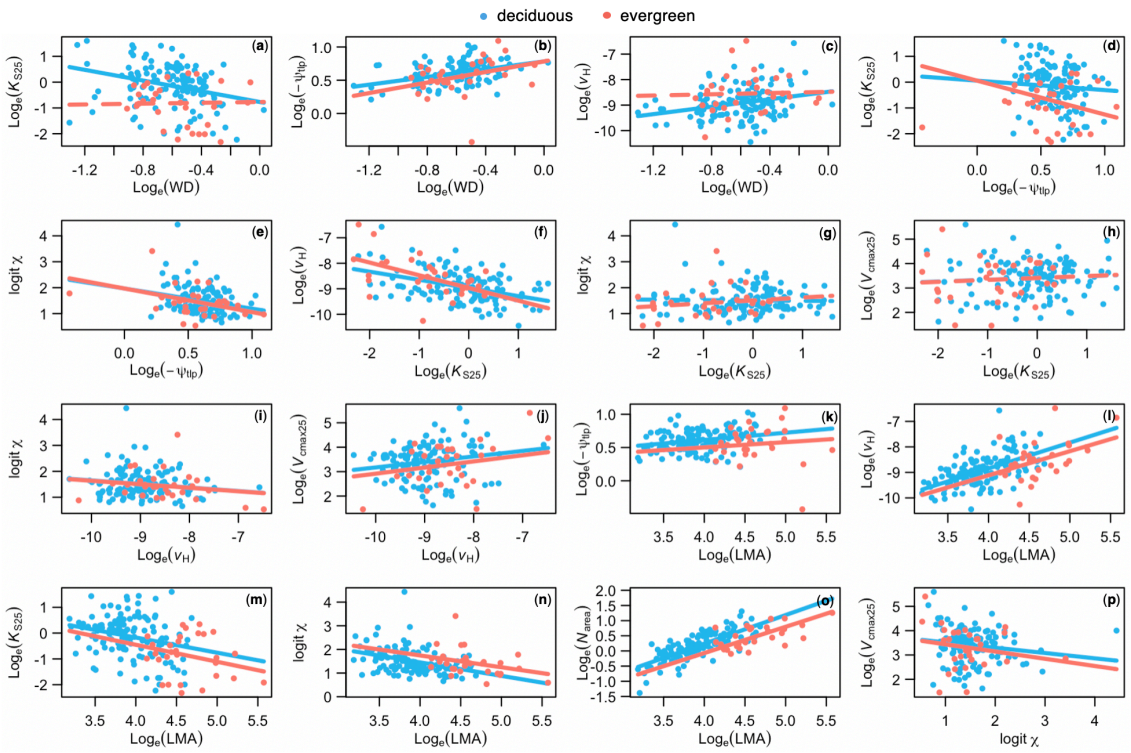

Figure S2.2 Bivariate relationships between traits. All traits were Log_e-transformed except χ, which was logit transformed. Deciduous and evergreen species are shown by blue and red circles, respectively. Solid lines indicate significant relationships ($p < 0.05$), dashed lines nonsignificant relationships. The relationships between wood density (WD) and hydraulic traits are panel (a) to (c). The relationships between leaf water potential at turgor loss point (Ψ_{tlp}) and traits are panel (d) to (e). The relationships between sapwood-specific hydraulic conductivity at 25 ˚C (K_{S25}) and traits are panel (f) to (h). The relationships between the ratio of sapwood to leaf area (v_H) and traits are panel (i) to (j). The relationships between leaf mass per area (LMA) and traits are panel (k) to (o). The relationship between the ratio of leaf-internal to ambient CO_2 partial pressure (χ) and maximum capacity of carboxylation at 25 ˚C (V_{cmax25}) is panel (p). The trait is leaf nitrogen content per area (N_{area}).

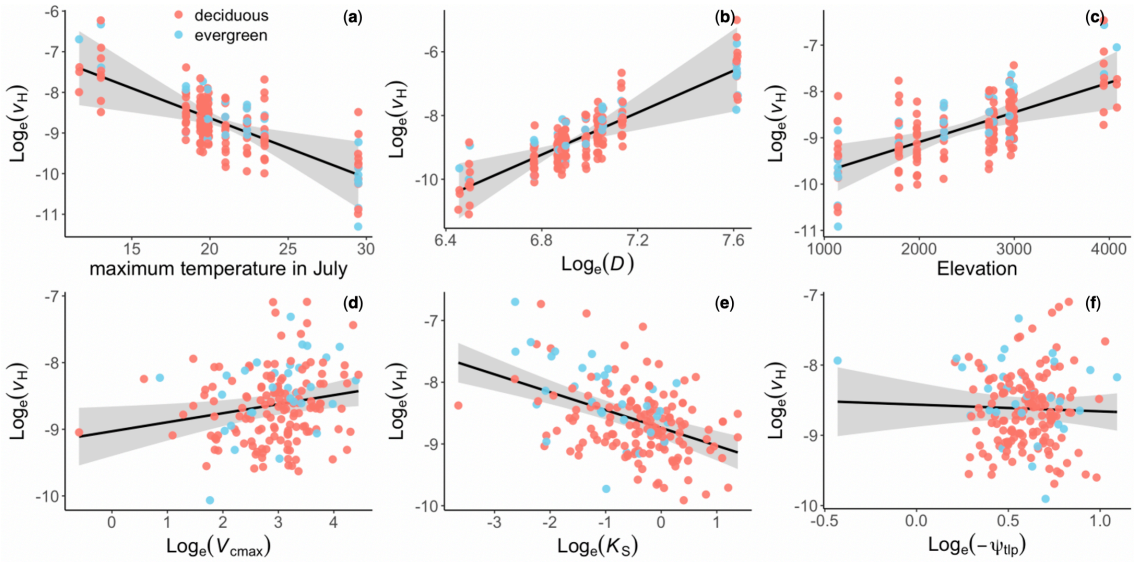

Figure S2.3 Partial residual plots from the regression of Log$_e$-transformed the ratio of sapwood to leaf area (v_H) against different predictors. The traits and climate variables were the second set of predictors shown in Figure 2.3b. The predictors are shown in (a) temperature, (b) vapour pressure deficit (D), (c) elevation, (d) maximum capacity of carboxylation (V_{cmax}), (e) sapwood-specific hydraulic conductivity (K_S), and (f) leaf water potential at turgor loss point (Ψ_{tlp}). Black lines are the fitted across all species, red dots are deciduous species and blue dots are evergreen species. The gray shadings are the 95% confidence intervals around the fitted lines.

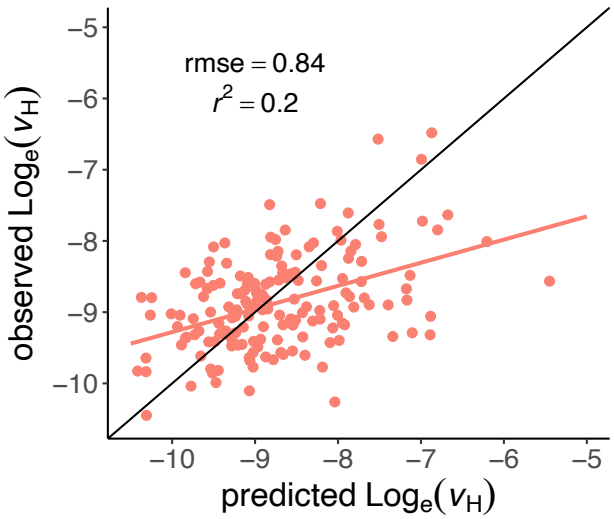

Figure S2.4 Comparison between observed and predicted ratios of sapwood to leaf area (v_H) across species. The black line is 1:1 line and red one is the fitted line across species.

Appendix 3 – Supplementary material to Chapter 3

Table S3.1 Characteristics of the study sites. Climate data: mean temperature during the growing season (T_g), the ratio of growing season length to the number of days in the year (f), mean photosynthetically active radiation (R_0), mean vapor pressure deficit (D_0), mean annual precipitation (MAP), ambient partial pressure of O_2 (P_0), moisture index (α_p) and leaf area index (LAI). The sample size gives the number of species sampled at each site.

Geographic information			Climate information								Vegetation type	Sample size
Elevation (m)	Longitude (°E)	Latitude (°N)	T_g (˚C)	f (day day^{-1})	R_0 (μmol m^{-2} s^{-1})	D_0 (kPa)	MAP (mm)	α_p (mm mm^{-1})	P_0 (Pa)	LAI (m^2 m^{-2})		
1143	102.16	29.43	20.33	1	293	1.18	1046	0.53	18589	3.7	Deciduous broad-leaved forest	27
1650	102.13	29.65	15.89	1	202	0.81	994	0.66	17508	2.6	Deciduous broad-leaved forest	25
1785	102.10	29.65	14.77	1	253	0.74	1292	0.70	17229	2.6	Deciduous broad-leaved forest	21
1976	101.02	29.38	13.14	1	319	0.89	821	0.59	16840	3.6	Deciduous broad-leaved forest	29
2258	102.05	29.59	14.01	1	316	0.72	657	0.72	16279	1.7	Deciduous broad-leaved forest	26
2735	101.91	29.42	13.50	1	330	0.74	1396	0.71	15365	3.0	Deciduous broad-leaved forest	28
2782	102.03	29.59	11.92	1	333	0.62	1500	0.74	15277	3.3	Deciduous broad-leaved forest	36
2950	101.92	29.37	12.57	1	343	0.70	906	0.72	14966	2.6	Deciduous broad-leaved forest	27

2966	101.88	29.45	12.21	1	344	0.69	1113	0.72	14937	1.8	Deciduous broad-leaved forest	29
2993	102.00	29.57	10.73	1	305	0.58	1568	0.75	14888	4.3	Deciduous broad-leaved forest	21
3251	101.99	29.57	8.97	1	330	0.53	1660	0.77	14423	3.2	Evergreen needle-leaved forest	10
3290	101.39	29.55	12.76	1	295	0.81	1145	0.62	14354	3.4	Deciduous broad-leaved forest	20
3500	101.53	29.47	9.78	1	371	0.68	935	0.70	13986	2.1	Deciduous broad-leaved forest	18
3780	101.60	29.45	9.51	1	330	0.66	1108	0.71	13507	1.2	Evergreen needle-leaved forest	17
3794	101.66	29.52	8.61	1	371	0.61	1047	0.73	13483	1.5	Deciduous shrub	15
3943	102.00	29.90	7.03	0.79	341	0.46	1576	0.82	13234	1.5	Deciduous shrub	9
4081	102.01	29.91	6.20	0.74	379	0.46	887	0.84	13007	0.5	Deciduous shrub	17
4361	101.71	29.52	6.14	0.82	383	0.55	1333	0.77	12555	0.7	Evergreen shrub	13

Table S2.2 Species sampled at each site. The list provides information on the plant functional type and the species on which measurements were made.

Elevation	Plant functional type	Species sampled
1143	deciduous broadleaf tree	*Euptelea pleiosperma, Betula utilis, Juglans cathayensis*
	deciduous broadleaf small tree	*Pyracantha fortuneana, Viburnum foetidum var. ceanothoides, Litsea cubeba, Quercus gilliana, Pistacia weinmannifolia*
	evergreen broadleaf tree	*Cunninghamia lanceolata, Cyclobalanopsis glaucoides*
	evergreen broadleaf small tree	*Rhamnus dumetorum, Trachycarpus fortunei, Ilex corallina, Hydrangea xanthoneura*
	deciduous broadleaf shrub	*Debregeasia orientalis, Rubus macilentus, Grewia biloba*
	evergreen broadleaf shrub	*Myrsine semiserrata*
	liana	*Clematis grandidentata*
	forb	*Boehmeria clidemioides var. diffusa, Elatostema cuspidatum, Arisaema erubescens, Begonia henryi, Boenninghausenia albiflora, Lophatherum gracile*
	pteridophyte	*Woodwardia unigemmata*
1650	deciduous broadleaf tree	*Alnus cremastogyne, Quercus serrata var. brevipetiolata, Rhus chinensis, Toxicodendron sylvestre*
	deciduous broadleaf small tree	*Rhamnus tangutica, Morus australis, Alangium chinense*
	evergreen broadleaf tree	*Cyclobalanopsis glaucoides, Ligustrum lucidum*
	evergreen broadleaf small tree	*Lyonia ovalifolia var. lanceolata, Rhododendron augustinii*
	deciduous broadleaf shrub	*Debregeasia orientalis, Neillia affinis, Lespedeza formosa, Rosa glomerata*
	evergreen broadleaf shrub	*Pyracantha fortuneana, Maclura tricuspidata*
	liana	*Clematis smilacifolia var. peltata*
	forb	*Agrimonia pilosa, Arisaema erubescens, Zingiber striolatum, Artemisia argyi, Anaphalis bicolor, Lophatherum gracile*
	pteridophyte	*Pseudocyclosorus esquirolii*
1785	deciduous broadleaf tree	*Alnus ferdinandi-coburgii, Betula utilis, Tetracentron sinense, Salix wallichiana, Rhus chinensis*
	deciduous broadleaf small tree	*Litsea cubeba*
	evergreen broadleaf small tree	*Viburnum oliganthum*
	deciduous broadleaf shrub	*Coriaria nepalensis, Indigofera szechuensis, Elaeagnus umbellata, Rubus mesogaeus, Debregeasia orientalis, Cotoneaster dielsianus, Aster albescens, Pyracantha fortuneana, Lonicera ligustrina, Salix variegata, Hydrangea strigosa, Rubus setchuenensis, Rubus lambertianus, Ficus tikoua*

	evergreen broadleaf shrub	*Viburnum atrocyaneum, Viburnum rhytidophyllum*
	liana	*Stauntonia chinensis, Berchemia floribunda, Galium dahuricum var. lasiocarpum, Paederia foetida, Clematis pogonandra, Fallopia multiflora*
	forb	*Arisaema erubescens, Begonia grandis, Pilea pumila, Artemisia tangutica, Incarvillea arguta*
1976	deciduous broadleaf tree	*Alnus cremastogyne, Juglans cathayensis, Euptelea pleiosperma, Machilus viridis, Toxicodendron vernicifluum*
	deciduous broadleaf small tree	*Elaeagnus bockii, Salix wallichiana, Styrax roseus, Sorbaria arborea, Litsea cubeba, Viburnum betulifolium*
	deciduous broadleaf shrub	*Rubus lambertianus, Rhamnus dumetorum, Hydrangea anomala, Rubus setchuenensis, Neillia affinis, Cotoneaster dielsianus*
	liana	*Viburnum foetidum var. rectangulatum, Clematoclethra scandens subsp. actinidioides*
	forb	*Iris confusa, Zingiber striolatum, Agrimonia pilosa, Artemisia argyi, Boehmeria clidemioides var. diffusa, Oplismenus undulatifolius, Carex henryi, Bambusa multiplex, Arisaema erubescens*
	pteridophyte	*Dryopteris neorosthornii*
2258	deciduous broadleaf tree	*Malus prattii, Euptelea pleiosperma, Sorbus meliosmifolia, Tetracentron sinense*
	deciduous broadleaf small tree	*Corylus ferox, Cornus controversa, Ilex fragilis f. kingii*
	evergreen broadleaf tree	*Lithocarpus cleistocarpus, Machilus viridis*
	evergreen broadleaf small tree	*Rhododendron polylepis, Ilex pernyi, Ilex yunnanensis*
	deciduous broadleaf shrub	*Polygala fallax, Rubus pentagonus, Ribes longiracemosum, Viburnum kansuense*
	evergreen broadleaf shrub	*Viburnum oliganthum*
	liana	*Clematoclethra scandens subsp. actinidioides*
	forb	*Adenocaulon himalaicum, Pternopetalum davidii, Oxalis griffithii, Rubus fockeanus, Calanthe tricarinata, Carex henryi, Fargesia ferax*
	pteridophyte	*Polystichum braunii*
2735	deciduous broadleaf tree	*Sorbus pallescens, Tilia chinensis var. intonsa, Padus buergeriana, Acer laxiflorum, Betula utilis*
	deciduous broadleaf small tree	*Lonicera lanceolata, Malus yunnanensis, Viburnum betulifolium*
	evergreen broadleaf tree	*Rhododendron polylepis, Abies fabri, Larix potaninii var. marcrocarpa, Picea likiangensis, Ilex pernyi*
	deciduous broadleaf shrub	*Rubus pungens var. oldhamii, Smilax stans, Ribes glaciale, Meliosma cuneifolia*
	evergreen broadleaf shrub	*Berberis potaninii*
	liana	*Sabia yunnanensis subsp. Latifolia, Schisandra grandiflora*
	forb	*Artemisia argyi, Thalictrum javanicum, Ophiopogon bodinieri, Rubia schumanniana, Valeriana officinalis, Brachypodium sylvaticum, Arundinaria faberi*

	pteridophyte	*Lepisorus thunbergianus*
2782	deciduous broadleaf tree	*Acer flabellatum, Acer oliverianum, Acer laxiflorum, Betula utilis, Maddenia wilsonii, Ilex macrocarpa*
	needleleaf evergreen tree	*Picea likiangensis, Abies fabri, Tsuga chinensis*
	deciduous broadleaf small tree	*Enkianthus chinensis, Viburnum nervosum, Viburnum cylindricum, Malus prattii, Euonymus semenovii, Litsea chunii, Sorbus rufopilosa, Rubus delavayi, Ribes glaciale, Cerasus trichostoma*
	evergreen broadleaf small tree	*Rhododendron calophytum, Rhododendron polylepis*
	deciduous broadleaf shrub	*Hydrangea robusta*
	evergreen broadleaf shrub	*Ilex yunnanensis*
	liana	*Clematoclethra scandens subsp. actinidioides, Rubia cordifolia, Clematis kweichowensis, Clematis montana*
	forb	*Pilea martini, Oxalis griffithii, Ligularia dentata, Arisaema elephas, Beesia calthifolia, Arundinaria faberi*
2950	deciduous broadleaf tree	*Acer laxiflorum, Betula utilis, Sorbus rufopilosa, Sorbus pallescens, Tilia chinensis var. intonsa*
	deciduous broadleaf small tree	*Cerasus trichostoma, Litsea chunii, Viburnum betulifolium, Cotoneaster bullatus, Dipelta yunnanensis*
	evergreen broadleaf tree	*Tsuga chinensis, Abies fabri, Rhododendron pachytrichum, Larix potaninii var. marcrocarpa*
	evergreen broadleaf small tree	*Rhododendron decorum*
	deciduous broadleaf shrub	*Rubus fockeanus, Lonicera tangutica, Rosa moyesii, Salix cathayana, Buddleja davidii*
	evergreen broadleaf shrub	*Berberis potaninii*
	forb	*Polygonum aviculare, Parasenecio palmatisectus, Artemisia argyi, Gentiana robusta, Arundinaria faberi*
	pteridophyte	*Athyrium niponicum*
2966	deciduous broadleaf tree	*Betula utilis, Padus buergeriana, Sorbus pallescens, Acer laxiflorum, Populus kangdingensis*
	deciduous broadleaf small tree	*Viburnum betulifolium, Sorbus rufopilosa, Litsea chunii, Viburnum nervosum, Cerasus trichostoma, Sorbaria arborea, Cotoneaster bullatus*
	evergreen broadleaf tree	*Abies forrestii, Larix potaninii var. australis*
	deciduous broadleaf shrub	*Berberis tischleri, Rosa moyesii, Lonicera lanceolata, Lonicera tangutica*
	evergreen broadleaf shrub	*Berberis potaninii, Daphne tangutica*
	liana	*Schisandra grandiflora*
	forb	*Impatiens tortisepala, Parasenecio palmatisectus, Parasenecio roborowskii, Ligusticum daucoides, Brachypodium sylvaticum, Heracleum hemsleyanum*
	pteridophyte	*Athyrium niponicum, Lepisorus thunbergianus*
2993	deciduous broadleaf tree	*Betula utilis, Acer kungshanense, Acer laxiflorum, Maddenia wilsonii*
	needleleaf evergreen tree	*Abies fabri*
	deciduous broadleaf small tree	*Sorbus prattii, Viburnum betulifolium, Viburnum nervosum, Philadelphus purpurascens, Cotoneaster bullatus, Rubus pungens var. oldhamii, Cerasus trichostoma, Euonymus frigidus, Padus buergeriana*

	evergreen broadleaf small tree	*Rhododendron decorum, Rhododendron calophytum*
	deciduous broadleaf shrub	*Ribes longiracemosum, Lonicera tangutica, Arundinaria faberi, Ribes glaciale, Rosa omeiensis*
	evergreen broadleaf shrub	*Berberis aemulans*
	liana	*Clematis montana, Smilax stans, Clematoclethra scandens subsp. actinidioides*
	forb	*Streptopus obtusatus, Salvia smithii, Arisaema elephas, Berneuxia thibetica, Galium hoffmeisteri*
3251	evergreen needleleaf tree	*Abies fabri*
	deciduous broadleaf small tree	*Acer stachyophyllum*
	evergreen broadleaf small tree	*Rhododendron calophytum, Rhododendron lutescens, Rhododendron pachytrichum*
	deciduous broadleaf shrub	*Sorbus rufopilosa, Acer flabellatum, Rubus pungens, Lonicera tangutica, Lonicera nigra, Euonymus semenovii, Rosa omeiensis, Philadelphus purpurascens, Ribes glaciale*
	liana	*Clematis montana*
	forb	*Maianthemum henryi, Arisaema elephas, Galium innocuum, Parasenecio deltophyllus, Carex capilliformis*
3290	deciduous broadleaf tree	*Acer pictum subsp. mono, Malus rockii, Populus davidiana, Cerasus pleiocerasus, Sorbus thibetica, Salix wallichiana*
	evergreen needleleaf tree	*Picea likiangensis var. hirtella*
	evergreen broadleaf tree	*Quercus guyavifolia*
	deciduous broadleaf shrub	*Rosa soulieana, Zanthoxylum undulatifolium, Rhamnus maximovicziana, Ribes alpestre, Cotoneaster tenuipes*
	liana	*Berchemia yunnanensis*
	forb	*Chrysanthemum glabriusculum, Thalictrum atriplex, Anemone tomentosa, Salvia brevilabra, Elsholtzia ciliata*
	pteridophyte	*Onychium contiguum*
3500	deciduous broadleaf tree	*Hippophae rhamnoides, Cerasus serrula*
	deciduous broadleaf small tree	*Malus transitoria*
	evergreen needleleaf tree	*Picea brachytyla, Juniperus pingii*
	evergreen broadleaf tree	*Quercus guyavifolia*
	deciduous broadleaf shrub	*Caragana franchetiana, Berberis approximata, Ribes alpestre, Spiraea schneideriana*
	evergreen broadleaf shrub	*Rhododendron intricatum*
	evergreen needleleaf shrub	*Juniperus pingii var. wilsonii*
	forb	*Halenia elliptica, Stellera chamaejasme, Thalictrum cultratum, Polygonatum cirrhifolium, Salvia prattii, Carex cardiolepis*
3780	deciduous broadleaf tree	*Hippophae rhamnoides*
	deciduous needleleaf tree	*Larix potaninii var. marcrocarpa*

	evergreen needleleaf tree	*Picea likiangensis var. hirtella, Pinus yunnanensis*
	evergreen broadleaf small tree	*Quercus guyavifolia, Rhododendron intricatum*
	deciduous broadleaf shrub	*Potentilla fruticosa, Berberis approximata, Caragana erinacea*
	evergreen needleleaf shrub	*Juniperus pingii var. wilsonii*
	liana	*Clematis tangutica*
	forb	*Stellera chamaejasme, Spenceria ramalana, Anaphalis flavescens, Potentilla saundersiana, Anemone tomentosa, Deyeuxia scabrescens*
3794	deciduous broadleaf shrub	*Sibiraea angustata, Salix wuxuhaiensis, Rhododendron intricatum, Caragana erinacea, Lonicera rupicola, Potentilla fruticosa var. arbuscula*
	evergreen broadleaf shrub	*Berberis dictyoneura, Quercus guyavifolia*
	evergreen needleleaf shrub	*Juniperus pingii var. wilsonii*
	forb	*Sibbaldia cuneata, Potentilla anserina, Stellera chamaejasme, Anaphalis aureopunctata, Anemone tomentosa, Carex cardiolepis*
3943	deciduous broadleaf shrub	*Berberis dictyophylla, Salix sclerophylla, Salix spodiophylla, Lonicera ligustrina, Lonicera rupicola var. syringantha, Spiraea schneideriana, Potentilla fruticosa, Sorbus rehderiana, Ribes takare*
	evergreen broadleaf shrub	*Rhododendron phaeochrysum, Rhododendron intricatum*
	forb	*Rheum nobile, Gentiana trichotoma, Polygonum macrophyllum, Sedum chauveaudii, Ligularia duciformis, Angelica sinensis*
4081	deciduous broadleaf shrub	*Sorbus rehderiana, Salix sclerophylla, Potentilla fruticosa, Ribes takare, Spiraea schneideriana, Anaphalis souliei*
	evergreen broadleaf shrub	*Rhododendron intricatum, Rhododendron phaeochrysum, Lonicera ligustrina*
	evergreen needleleaf shrub	*Picea likiangensis*
	forb	*Ligularia pleurocaulis, Polygonum macrophyllum, Gentiana trichotoma, Pyrethrum tatsienense, Potentilla stenophylla var. emergens, Poa attenuata, Carex cardiolepis*
4361	deciduous broadleaf shrub	*Salix flabellaris, Lonicera hispida*
	evergreen broadleaf shrub	*Rhododendron intricatum, Rhododendron telmateium, Rhododendron phaeochrysum*
	forb	*Polygonum macrophyllum, Saussurea przewalskii, Hedysarum vicioides, Gentiana trichotoma, Potentilla stenophylla var. emergens, Trisetum spicatum, Carex cardiolepis*
	pteridophyte	*Polystichum gongboense*

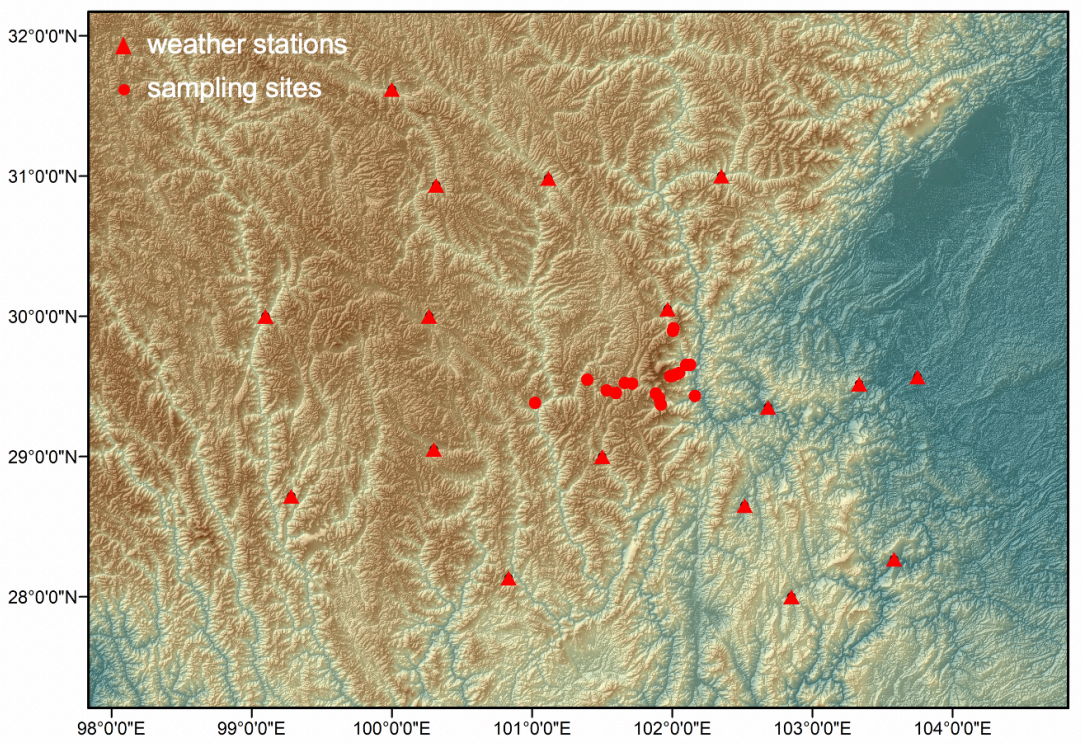

Figure S3.1 The locations of weather stations used to derive estimates of the climate variables at each sampled site. The red triangles are the weather stations and dots are the sampling sites. The background colour represents the elevation gradient which has the same scale in Figure 3.1 in the main text.

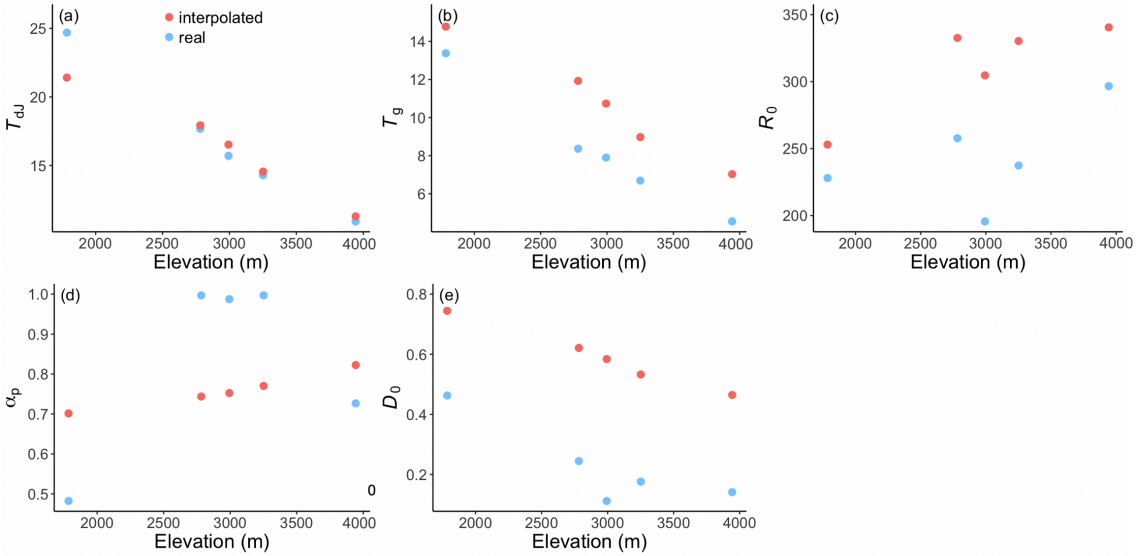

Figure S3.2 The comparisons of interpolated and in-situ climate data at five sites. The red dots are the interpolated climate data and blue dots are the in-situ climate data collected from flux tower or nearby meteorological stations. The bioclimatic variables are daytime temperature in July (T_{dJ}), mean temperature during the growing season, defined as days above a baseline of 0 ˚C (T_g), mean vapor pressure deficit (D_0), mean photosynthetically active radiation (R_0), and a moisture index (α_p) defined as the ratio of annual actual evapotranspiration to annual potential evapotranspiration.

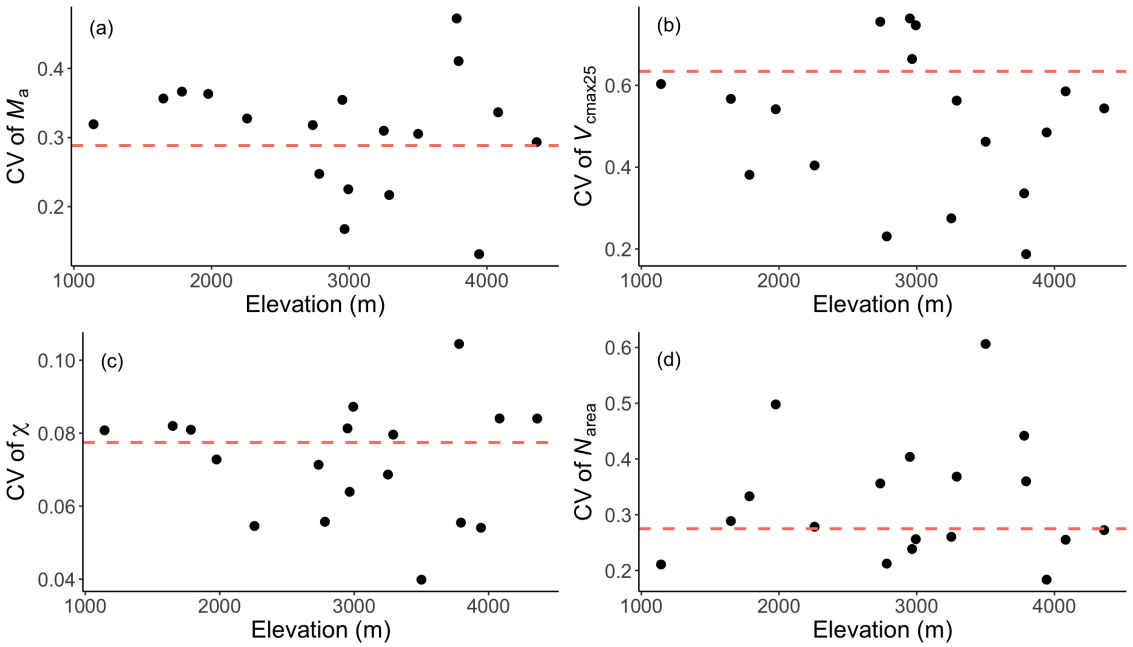

Figure S3.3 The coefficient of variation (CV) of traits at each sampled site. The traits are leaf mass per area (M_a), leaf nitrogen content per unit area (N_{area}); the maximum capacity of carboxylation standardized to 25 ˚C (V_{cmax25}) and the ratio of leaf-internal to ambient CO_2 partial pressure (χ). The red dashed line is the CV of traits across sites.

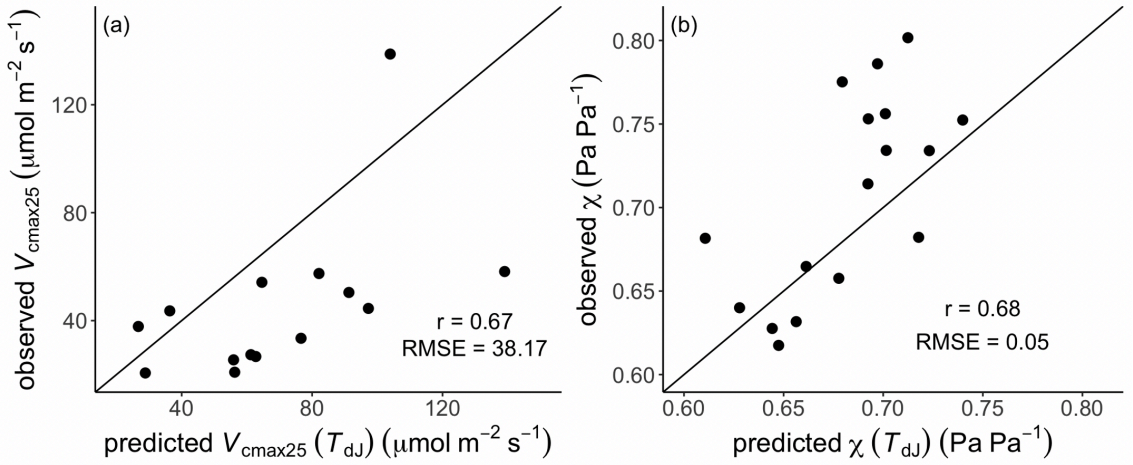

Figure S3.4 Site-mean values of the maximum capacity of carboxylation standardized to 25 ˚C (V_{cmax25}) and the ratio of leaf-internal to ambient CO_2 partial pressure (χ) for evergreen species. Observations are site-mean values of evergreen species. The solid line is the 1:1 line.

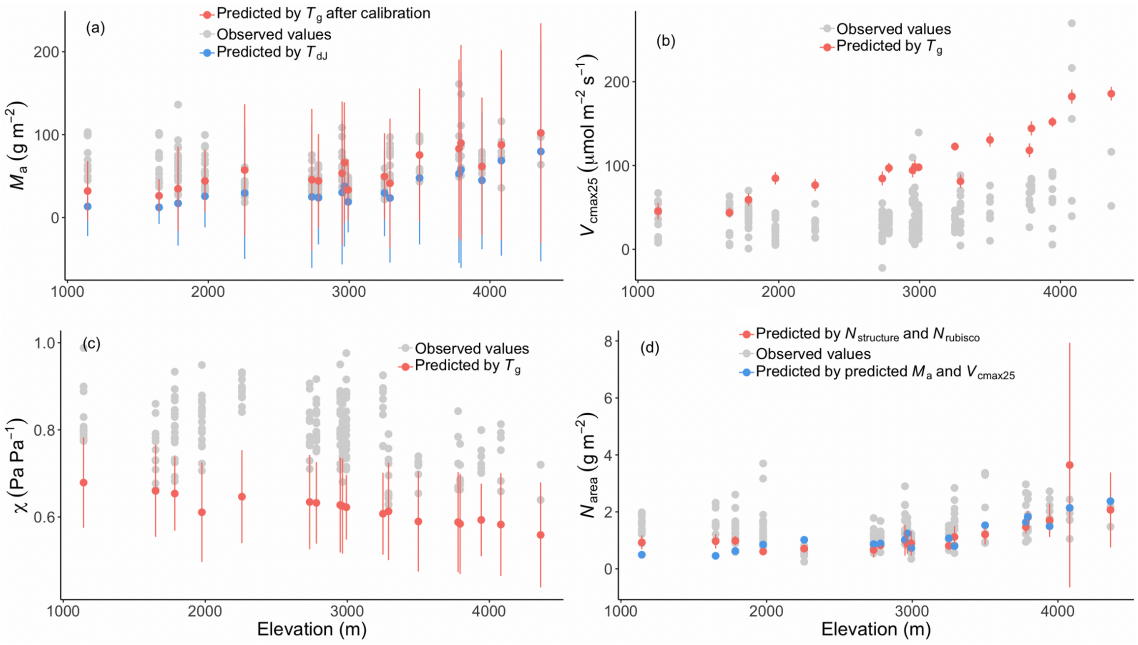

Figure S3.5 The observed and predicted values of traits along the altitudinal gradient. The traits are leaf mass per area (M_a), leaf nitrogen content per unit area (N_{area}); the maximum capacity of carboxylation standardized to 25 ˚C (V_{cmax25}) and the ratio of leaf-internal to ambient CO_2 partial pressure (χ). Observed trait values are shown in grey dots. In panel (a), the red and blue dots show the mean predicted M_a using mean temperature during the growing season (T_g) with regional-calibrated coefficients in Equation 3.15 and using daily temperature in July (T_{dJ}), respectively. In panel (b) and (c), red dots show the mean predicted V_{cmax25} and χ using T_g. In panel (d), predicted N_{area} using $N_{structure}$ and $N_{rubisco}$ following Dong et al. (2017) are shown with red dots, the blue dots show the mean N_{area} predicted from predicted T_g-driven M_a and T_{dJ}-driven V_{cmax25}. Error bars in panel (a) and (c) are the square root of uncertainty caused by parameters, in panel (b) by parameters and observed χ, in panel (d) by parameters and observed M_a and V_{cmax25}.

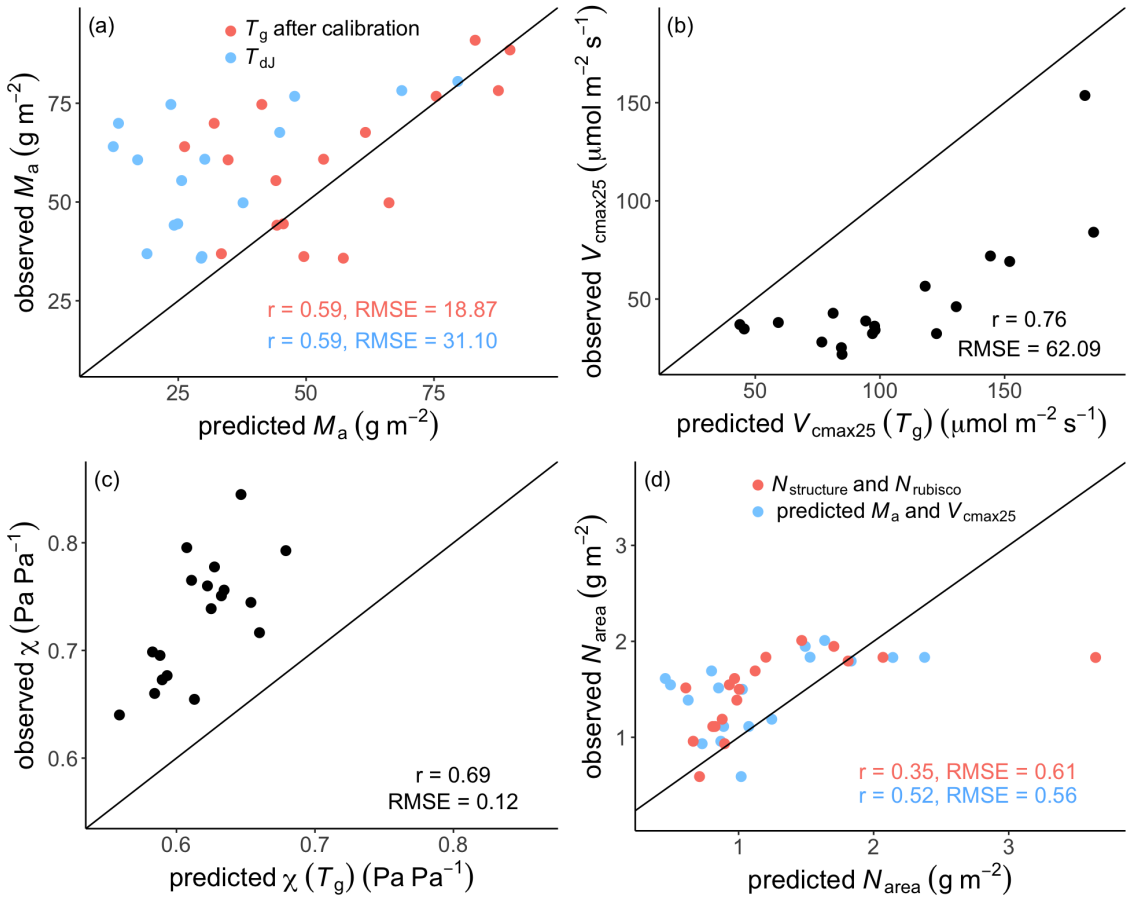

Figure S3.6 Site-mean values of traits for deciduous species. The traits are leaf mass per area (M_a), leaf nitrogen content per unit area (N_{area}); the maximum capacity of carboxylation standardized to 25 ˚C (V_{cmax25}) and the ratio of leaf-internal to ambient CO_2 partial pressure (χ). Observations are site-mean values of deciduous species. In panel (a), the red and blue dots show the mean predicted M_a using mean temperature during the growing season (T_g) with regional-calibrated coefficients in Equation 3.15 and using daily temperature in July (T_{dJ}), respectively. In panel (b) and (c), the red dots show the mean predicted V_{cmax25} and χ using T_g. In panel (d), predicted N_{area} using $N_{structure}$ and $N_{rubisco}$ following Dong et al. (2017) are shown with red dots, the blue dots show the mean N_{area} predicted from predicted T_g-driven M_a and T_{dJ}-driven V_{cmax25}. The solid line is the 1:1 line.

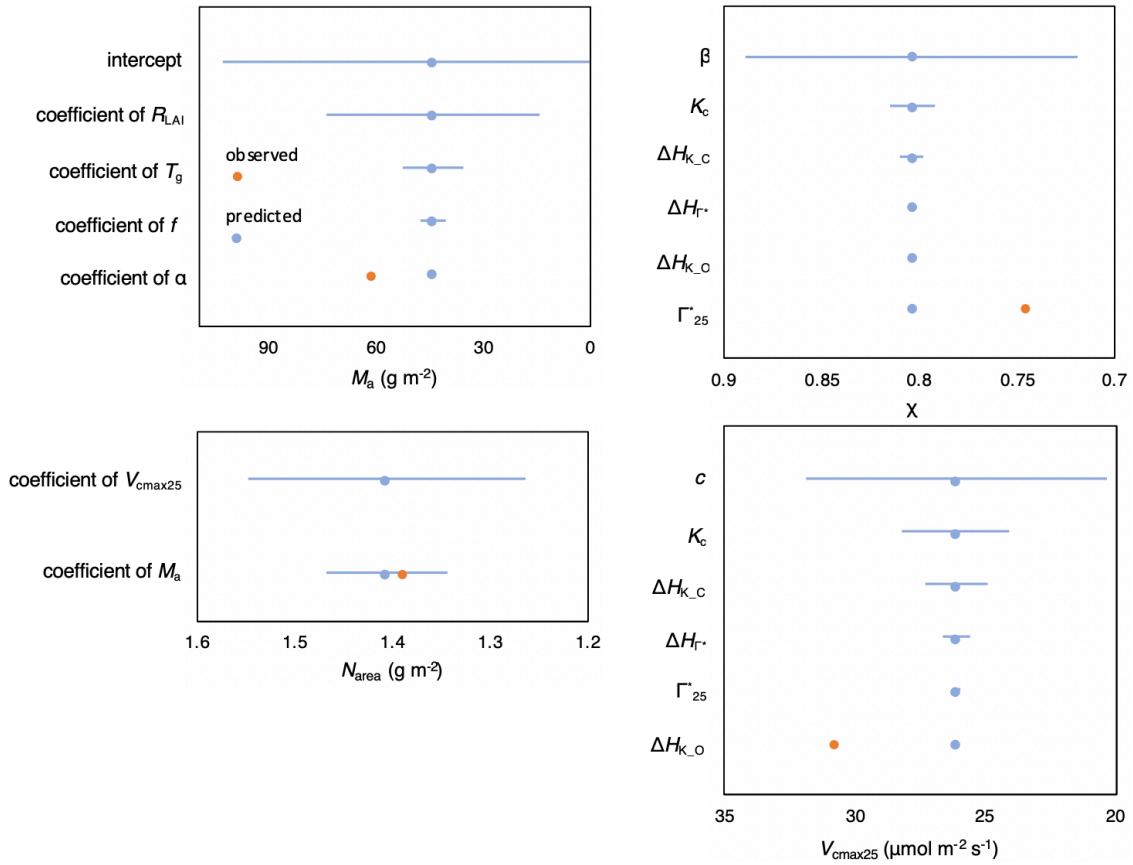

Figure S3.7 The impact of parameter uncertainty on the prediction of traits. Site at 1785 m was selected as a case study. Blue circles are predicted values at 1785 m and orange circles are mean observed values. Error bar is accumulated uncertainty by successive parameters on y-axis from the bottom to the top. M_a is predicted leaf mass per area using T_g, V_{cmax25} is predicted maximum capacity of carboxylation standardized to 25 ˚C using T_{dJ}, χ is predicted ratio of internal to ambient CO_2 partial pressure using T_{dJ}, and N_{area} is predicted leaf mass per area by observed M_a and V_{cmax25} directly. c is the unit cost of maintaining electron transport capacity, K_c (Pa) is Michaelis-Menten coefficient for carboxylation at 25 ˚C, ΔH_{K_C} (J mol^{-1}) is the activation energy of carboxylation, ΔH_{Γ^*} (J mol^{-1}) is the activation energy of Γ^*, Γ^*_{25} (Pa) is photorespiratory compensation point at 25 ˚C, ΔH_{K_O} (J mol^{-1}) is the activation energy of oxygenation. β is the ratio of the unit costs of maintaining carboxylation and transpiration capacities.

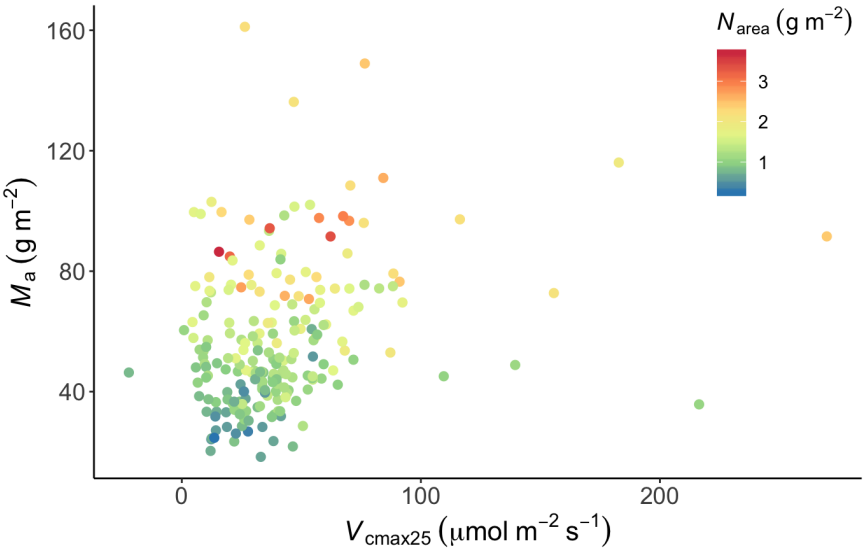

Figure S3.8 The distribution of observed leaf nitrogen content per unit area (N_{area}) values in the space of leaf mass per area (M_a) and the maximum capacity of carboxylation standardized to 25 ˚C (V_{cmax25}). Trait values are indicated by the colour scale.

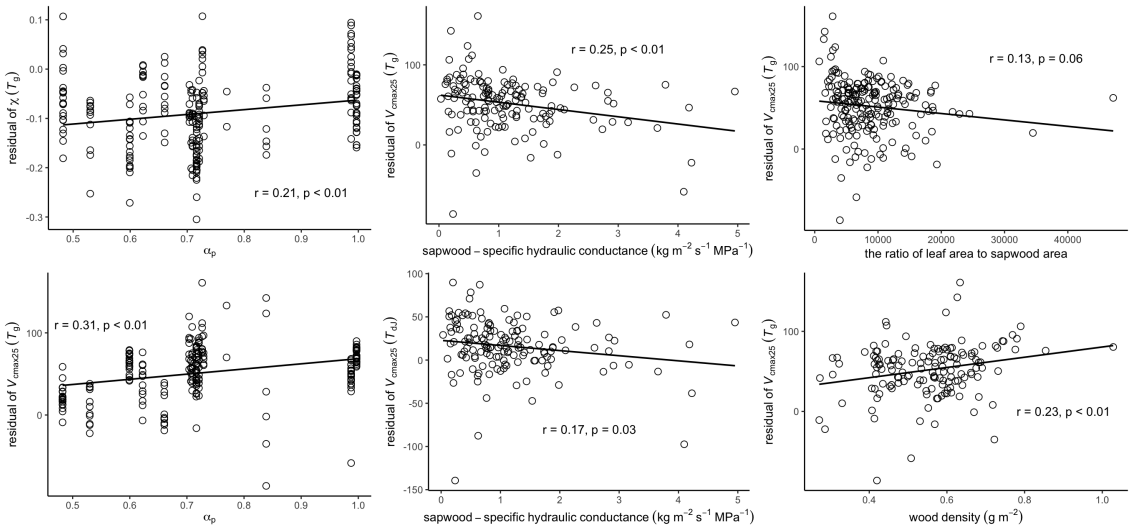

Figure S3.9 The relationships between residual of predictions and hydraulic traits and α_p. Only the significant relationships were represented. T_g means predicted traits using mean temperature during growing season, T_{dJ} means predicted traits using daytime temperature of July. α_p is the ratio of annual actual evapotranspiration to annual potential evapotranspiration.

Appendix 4 – Supplementary material to Chapter 4

Appendix 4.1 Theoretical climate effect on sapwood to leaf area ratio

After replacing photosynthetic traits with climate-driven variables, optimal v_H balancing the hydraulic efficiency in trunks and the water demand from canopy can be expressed by a function of K_S, irradiance, temperature and vapour pressure deficit.

The effect of irradiance (I_{abs}) on v_H comes from V_{cmax}, based on Equation 4.6.

$$\frac{\partial \mathrm{Log_e}(v_\mathrm{H})}{\partial \mathrm{Log_e}(I_\mathrm{abs})} = \frac{\partial \mathrm{Log_e}(V_\mathrm{cmax})}{\partial \mathrm{Log_e}(I_\mathrm{abs})} = 1 \tag{S4.1}$$

Thus, the sensitivity of $\mathrm{Log_e}(v_H)$ to $\mathrm{Log_e}(I_{abs})$ is 1.

Vapour pressure deficit (D) affects v_H through its effects on transpiration and χ, based on Equations 4.6 and 4.7.

$$\frac{\partial \mathrm{Log_e}(v_\mathrm{H})}{\partial \mathrm{Log_e}(D)} = \frac{\partial\left(\mathrm{Log_e}(D)+\mathrm{Log_e}(m_\mathrm{C})-\mathrm{Log_e}(1-\chi)+\mathrm{Log_e}\left(\frac{\chi c_a+K}{\chi c_a+2\Gamma^*}\right)\right)}{\partial \mathrm{Log_e}(D)} \tag{S4.2}$$

$$\frac{\partial\left(\mathrm{Log_e}(m_\mathrm{C})+\mathrm{Log_e}\left(\frac{\chi c_a+K}{\chi c_a+2\Gamma^*}\right)\right)}{\partial \mathrm{Log_e}(D)} = \left(\frac{c_a}{\chi c_a-\Gamma^*}-\frac{c_a}{\chi c_a+2\Gamma^*}\right)\left(\frac{\left(\frac{e^{\frac{\mathrm{Log_e}(D)}{2}}}{2}\right)\xi\left(1-\frac{\Gamma^*}{c_a}\right)}{\left(\xi+\left(e^{Log_e(D)}\right)^{0.5}\right)^2}\right) \tag{S4.3}$$

$$\frac{\partial \mathrm{Log_e}(1-\chi)}{\partial \mathrm{Log_e}(D)} = \left(\frac{1}{1-\chi}\right)\left(\frac{e^{\frac{\mathrm{Log_e}(D)}{2}}}{2}\right)\left(\frac{\xi\left(1-\frac{\Gamma^*}{c_a}\right)}{(\xi+(e^{\mathrm{Log_e}(D)})^{0.5})^2}\right) \tag{S4.4}$$

Thus, at average climate condition (T = 25.5˚C, D = 1.5kPa), the sensitivity of $\mathrm{Log_e}(v_H)$ to $\mathrm{Log_e}(D)$ can be estimated as 0.6.

The temperature effect comes from hydraulic efficiency (K_S) and photosynthetic traits (χ, V_{cmax}), based on Equations 4.6 to 4.9.

Temperature effect on hydraulic efficiency:

$$\frac{\partial \mathrm{Log_e}(v_\mathrm{H})}{\partial\, T} = \frac{\partial\left(-\mathrm{Log_e}(K_\mathrm{S})\right)}{\partial\, T} \tag{S4.5}$$

Here, K_S represents hydraulic efficiency at growth condition, while K_S in dataset was measured in standard room temperature (~25˚C, K_{S25}). Due to temperature effect on water viscosity and permeability of cells, the temperature response of K_S is given by:

$$\mathrm{Log_e}(K_S) = \mathrm{Log_e}\left(K_{S25} Q_{10}^{\frac{T}{10}}\right) \tag{S4.6}$$

We took Q_{10} value as 1.80 from Matzner and Comstock (2001), thus, the temperature response of K_S is –0.06.

Temperature effect on photosynthesis process:

$$\frac{\partial \mathrm{Log_e}(v_H)}{\partial T} = \frac{\partial\left(\mathrm{Log_e}(m_C)+\mathrm{Log_e}(\varphi_0)+\mathrm{Log_e}\left(\frac{\chi c_a+K}{\chi c_a+2\Gamma^*}\right)-\mathrm{Log_e}(1-\chi)\right)}{\partial T} \tag{S4.7}$$

The temperature sensitivity of photosynthetic terms can be divided into following terms:

The temperature sensitivity of K and Γ^* can be achieved (Bernacchi et al., 2001):

$$\frac{\partial K}{\partial T} = \frac{(\Delta H_c(P_o + K_o) - P_o \Delta H_o) K_c}{K_o R T^2} \tag{S4.8}$$

$$\frac{\partial \Gamma^*}{\partial T} = \frac{\Gamma^* \Delta H_{\Gamma^*}}{R T^2} \tag{S4.9}$$

The temperature effect from χ on v_H can be calculated:

$$\frac{\partial \chi}{\partial T} = \frac{\partial \Gamma^*}{\partial T}\left(\frac{1}{c_a}\right)\left(1 - \frac{\xi}{\xi+\sqrt{D}}\right) + \frac{\partial \xi}{\partial T}\left(1 - \frac{\Gamma^*}{c_a}\right)\left(\frac{1}{\xi+\sqrt{D}} - \frac{\xi}{\left(\xi+\sqrt{D}\right)^2}\right) \tag{S4.10}$$

$$\frac{\partial \xi}{\partial T} = \left(\frac{\partial K}{\partial T} + \frac{\partial \Gamma^*}{\partial T}\right)\left(\frac{\beta}{2 * 1.6\xi}\right) - \left(\frac{\beta\left(K+\Gamma^*\right)}{2 * 1.6\xi}\right)\left(\frac{-B}{(C+T)^2}\right) \tag{S4.11}$$

$$\frac{\partial\left(-\mathrm{Log_e}(1-\chi)\right)}{\partial T} = \frac{\partial \Gamma^*}{\partial T}\left(\frac{-1}{1-\chi}\right)\left(\frac{1}{c_a}\right)\left(1 - \frac{\xi}{\xi+\sqrt{D}}\right) + \frac{\partial \xi}{\partial T}\left(1 - \frac{\Gamma^*}{c_a}\right)\left(\frac{1}{\xi+\sqrt{D}} - \frac{\xi}{\left(\xi+\sqrt{D}\right)^2}\right) \tag{S4.12}$$

The temperature effect from m_C and V_{cmax} on v_H is as follows. The intrinsic quantum efficiency of photosynthesis (φ_0) is calculated by temperature-dependence relationship (Bernacchi et al., 2003b). Thus, the sensitivity of φ_0 to temperature is given by:

$$\frac{\partial \operatorname{Log_e}(\varphi_0)}{\partial T} = \frac{0.021 - 0.00068T}{0.352 + 0.021T - 0.00034T^2} \quad \text{(S4.13)}$$

Combining the temperature sensitivities of K and Γ*, the temperature sensitivities of the rest terms are given by:

$$\frac{\partial \operatorname{Log_e}\left(\frac{\chi c_a + K}{\chi c_a + 2\Gamma^*}\right)}{\partial T} = \left(c_a \frac{\partial \chi}{\partial T} + \frac{\partial K}{\partial T}\right)\left(\frac{1}{\chi c_a T + K}\right) - \left(c_a \frac{\partial \chi}{\partial T} + \frac{2\,\partial \Gamma^*}{\partial T}\right)\left(\frac{1}{\chi c_a + 2\Gamma^*}\right) \quad \text{(S4.14)}$$

$$\frac{\partial \operatorname{Log_e}(m_C)}{\partial T} = \left(c_a \frac{\partial \chi}{\partial T} - \frac{\partial \Gamma^*}{\partial T}\right)\left(\frac{1}{\chi c_a - \Gamma^*}\right) - \left(c_a \frac{\partial \chi}{\partial T} + \frac{\partial K}{\partial T}\right)\left(\frac{1}{\chi c_a + K}\right) \quad \text{(S4.15)}$$

In summary, in average climate condition (T = 25.5˚C, *D* = 1.5kPa), the estimated temperature sensitivity of combined photosynthetic terms is 0.03. Therefore, the temperature sensitivities of hydraulic efficiency and photosynthesis process are –0.06 and 0.03 respectively, which yields –0.03 in total.

The relationships between hydraulic traits and climate variables can be expressed by the following equation.

$$\begin{aligned}\operatorname{Log_e}(v_H) = {} & 0.6\operatorname{Log_e}(D_{max}) + \operatorname{Log_e}(I_{abs}) - 0.03T_{max} - \operatorname{Log_e}(K_{S25}) \\ & - \operatorname{Log_e}(\Delta\Psi_{max}) + C\end{aligned} \quad \text{(S4.16)}$$

Here K_{S25} is K_S under 25˚C, *C* is the parameter containing information about photosynthetic traits values under standard climate condition (25˚C) and plant height. In practice, effects of K_S and *h* are not separable, because the tip-to-base widening of xylem elements implies a positive correlation between them that greatly reduces the effect of path length on whole-stem conductance, so that the whole-stem conductance is similar to or only slightly lower than the conductance measured near the branch tip (Christoffersen et al., 2016; Mencuccini et al., 2019b; Olson et al., 2021).

The model predicted that v_H was positively related to vapour pressure deficit and irradiance, negatively to air temperature and CO_2, and its negative correlations with K_S and $\Delta\Psi_{max}$. The sensitivities of maximum vapour pressure deficit (D_{max}) and air temperature (T_{max}), mean irradiance (I_{abs}) during growing season to v_H variation after $\log_e$-transformed were 0.6, 1 and –0.03 theoretically derived from our model, which implied that high v_H should be expected at dry and cold areas with high irradiance.

Appendix 4.2 Supplementary figures

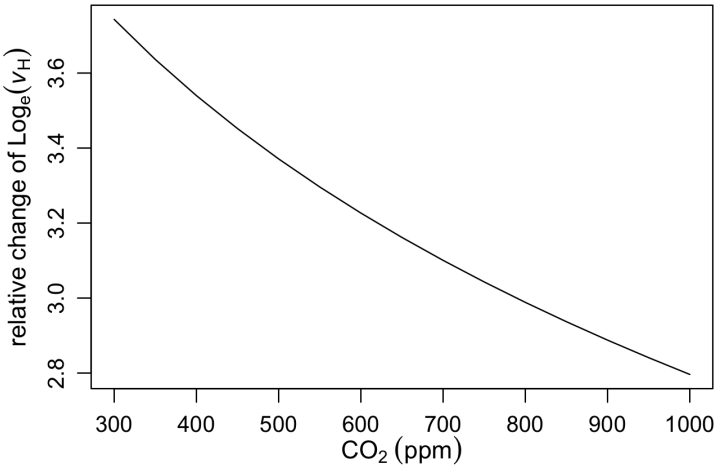

Figure S4.1 The theoretical sensitivity of $\log_e$-transformed ratio of sapwood to leaf area (v_H) to ambient CO_2.

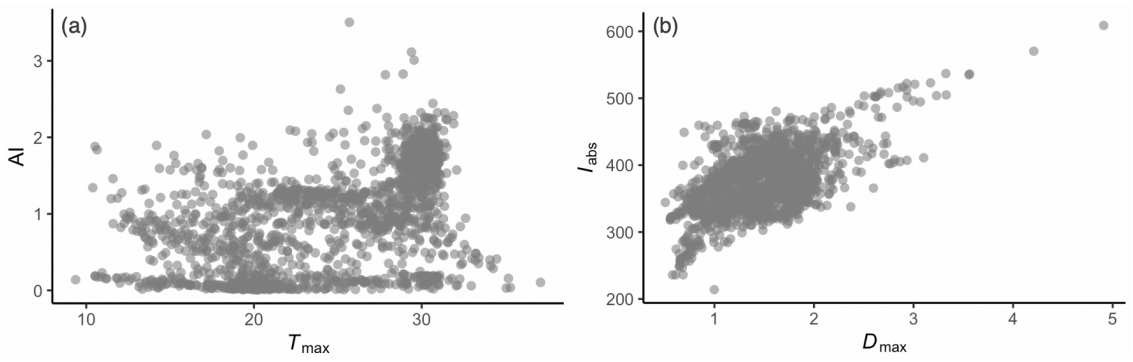

Figure S4.2 Species distribution along climate gradients in Dataset1. AI is aridity index (ratio of precipitation of evapotranspiration), T_{max} is maximum temperature, D_{max} is maximum vapour pressure deficit and mean irradiance (I_{abs}) during growing season.

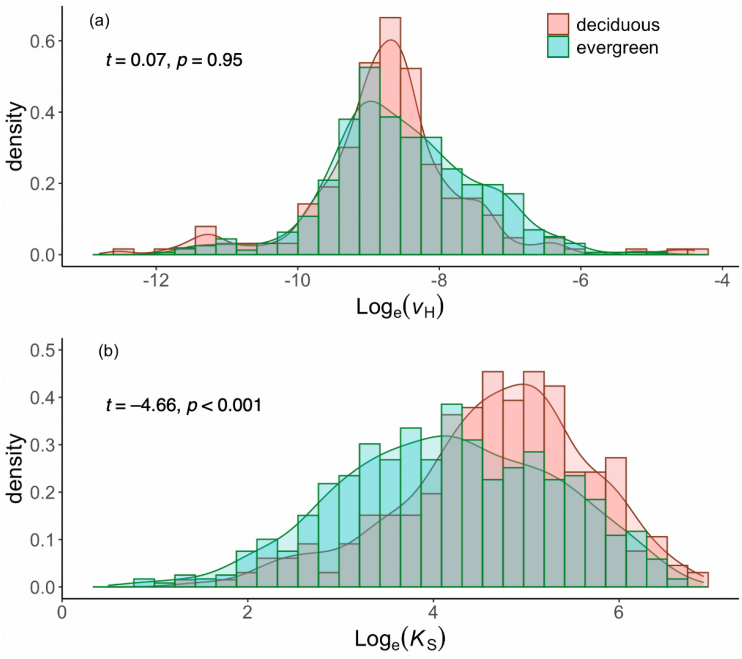

Figure S4.3 The distribution of ratio of sapwood to leaf area (v_H) and hydraulic conductivity (K_S) among deciduous and evergreen species in Dataset1. T-test is carried out to examine the difference of v_H and K_S between leaf phenology.

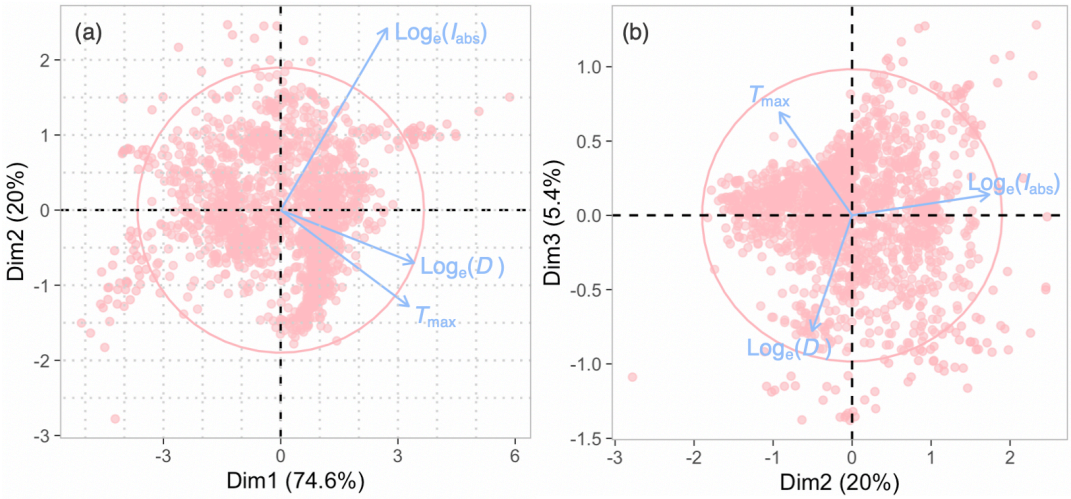

Figure S4.4 Principal components analysis of climate variables including maximum vapour pressure deficit (D_{max}), maximum temperature (T_{max}) and mean irradiance during growing season in Dataset1. (a) PC1 vs PC2, grey dotted lines show the site division according to loadings of PC1 and PC2 axes. (b) PC2 cs PC3. The pink points represent species.

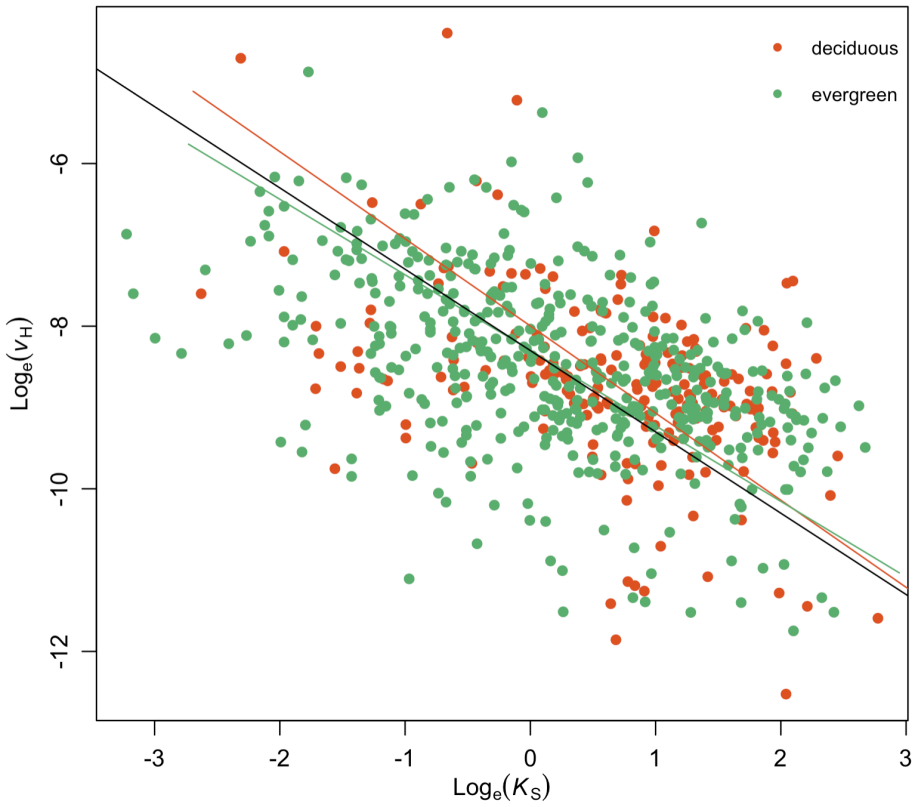

Figure S4.5 The relationships between log$_e$-transformed ratio of sapwood to leaf area (v_H) and hydraulic conductivity (K_S) at species level using Dataset1. The red dots are deciduous species, green dots are evergreen species. The black line is 1:1 line, the red and green lines are fitted using standardised major axis (SMA) regression among deciduous and evergreen species respectively.

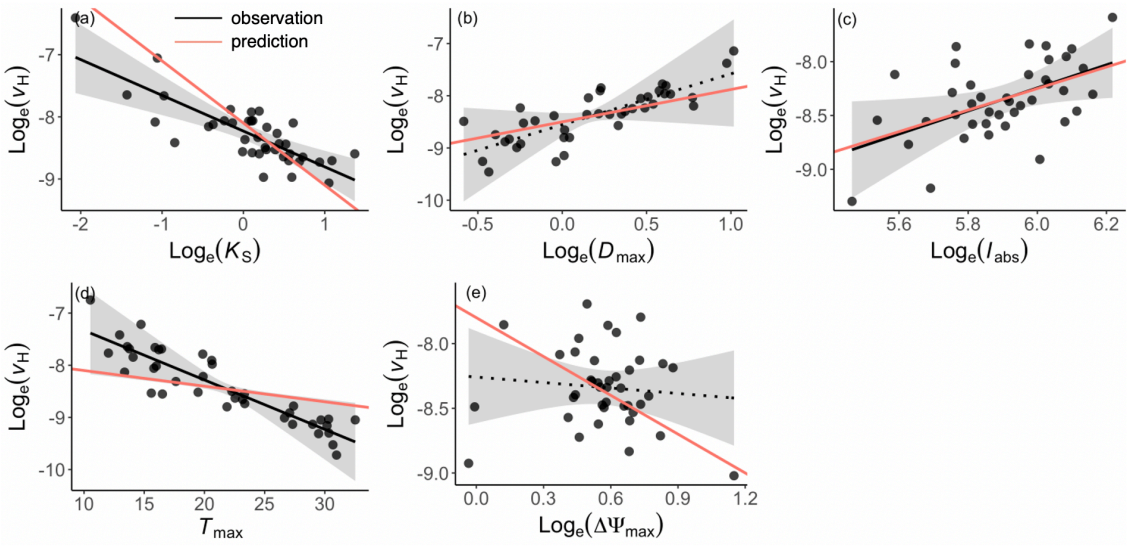

Figure S4.6 Partial residual plots from the multiple linear regression of $\log_e$-transformed the ratio of sapwood to leaf area (v_H) against different predictors at site level using Dataset1. The predictors are shown in (a) sapwood-specific hydraulic conductivity (K_S), (b) maximum vapour pressure deficit (D_{max}), (c) mean irradiance (I_{abs}), (d) maximum temperature (T_{max}) and (e) maximum water potential difference between soil and leaf ($\Delta\Psi_{max}$) during growing season. Black lines are the fitted across all sites and the grey shadings are the 95% confidence intervals around the fitted lines. The black solid lines are significant (p<0.05) and dotted line is insignificant (p>0.05). The red lines are theoretical sensitivities in Equation 4.1.

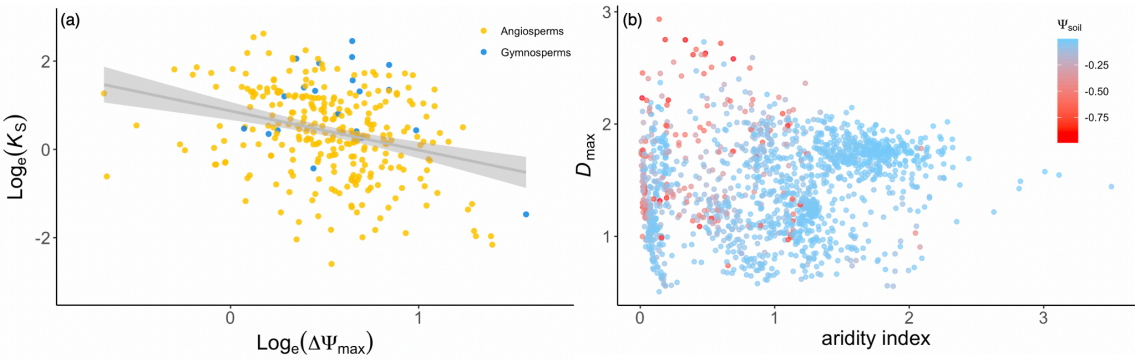

Figure S4.7 (a) The bivariate relationship between Log$_e$-transformed hydraulic conductivity (K_S) and maximum water potential difference between soil and leaf ($\Delta\Psi_{max}$). The yellow dots are angiosperms and blue dots are gymnosperms. The gray line is fitted across all species. (b) The soil water potential (Ψ_{soil}) variation along maximum vapour pressure deficit (D_{max}) and aridity index for each species.

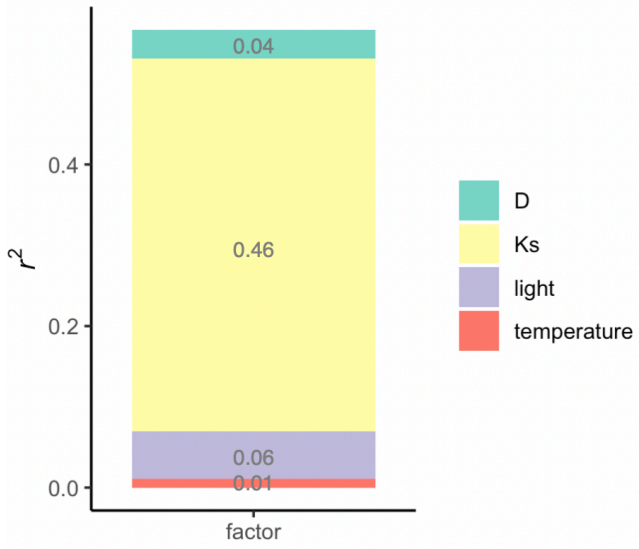

Figure S4.8 The contribution (r^2) of different predictors to the ratio of sapwood to leaf area (v_H) prediction. The green bar is vapour pressure deficit (D), yellow is hydraulic conductivity (K_S), purple is irradiance/light and red is temperature.

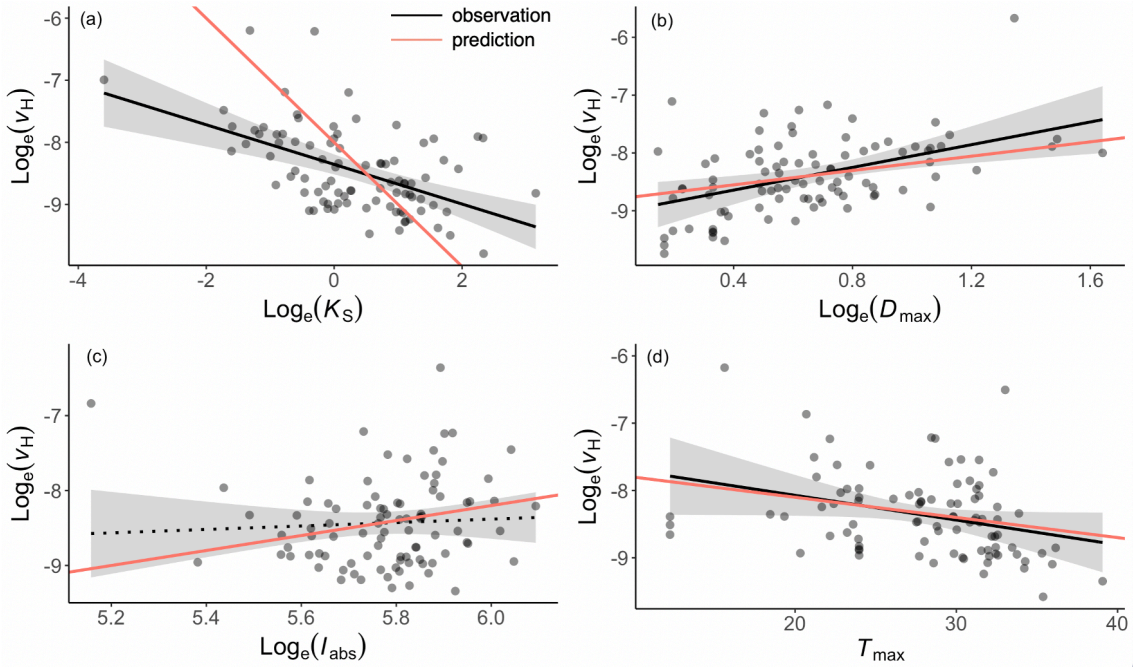

Figure S4.9 Partial residual plots from the multiple linear regression of log$_e$-transformed the ratio of sapwood to leaf area (v_H) against different predictors at site level using Dataset2. The predictors are shown in (a) sapwood-specific hydraulic conductivity (K_S), (b) maximum vapour pressure deficit (D_{max}), (c) mean irradiance (I_{abs}), (d) maximum temperature (T_{max}) during growing season. Black lines are the fitted across all sites and the gray shadings are the 95% confidence intervals around the fitted lines. The black solid lines are significant (p<0.05) and dotted line is insignificant (p>0.05). The red lines are theoretical sensitivities in Equation 4.1.

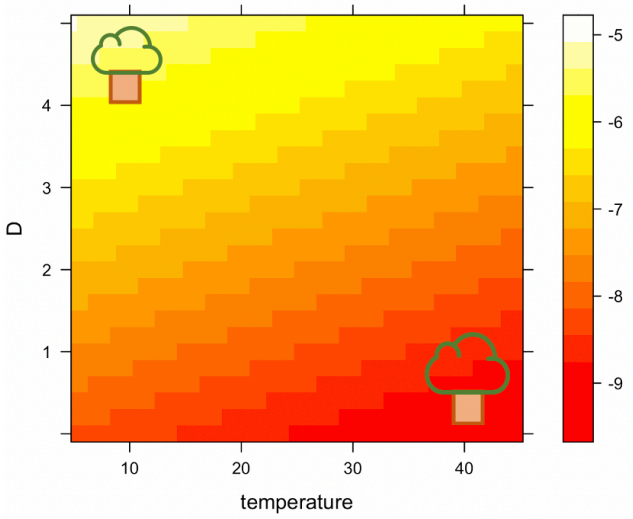

Figure S4.10 Theoretical variation of the ratio of sapwood to leaf area (v_H) along temperature and vapour pressure deficit (D) with other predictors kept as median values.

Bibliography

Allen, C. D., Macalady, A. K., Chenchouni, H., Bachelet, D., McDowell, N., Vennetier, M., Kitzberger, T., Rigling, A., Breshears, D. D., Hogg, E. H., Gonzalez, P., Fensham, R., Zhang, Z., Castro, J., Demidova, N., Lim, J.-H., Allard, G., Running, S. W., Semerci, A., and Cobb, N.: A global overview of drought and heat-induced tree mortality reveals emerging climate change risks for forests, Forest Ecology and Management, 259, 660-684, 10.1016/j.foreco.2009.09.001, 2010.

Álvarez-Cansino, L., Comita, L. S., Jones, F. A., Manzané-Pinzón, E., Browne, L., and Engelbrecht, B. M. J.: Turgor loss point predicts survival responses to experimental and natural drought in tropical tree seedlings, Ecology, 103, e3700, https://doi.org/10.1002/ecy.3700, 2022.

Ambrose, A. R., Sillett, S. C., and Dawson, T. E.: Effects of tree height on branch hydraulics, leaf structure and gas exchange in California redwoods, Plant Cell Environ, 32, 743-757, 10.1111/j.1365-3040.2009.01950.x, 2009.

Anderegg, L. D. L., Loy, X., Markham, I. P., Elmer, C. M., Hovenden, M. J., HilleRisLambers, J., and Mayfield, M. M.: Aridity drives coordinated trait shifts but not decreased trait variance across the geographic range of eight Australian trees, New Phytologist, 229, 1375-1387, 10.1111/nph.16795, 2021.

Anderegg, L. D. L.: Why can't we predict traits from the environment?, New Phytologist, 237, 1998-2004, 10.1111/nph.18586, 2023.

Anderegg, W. R., Klein, T., Bartlett, M., Sack, L., Pellegrini, A. F., Choat, B., and Jansen, S.: Meta-analysis reveals that hydraulic traits explain cross-species patterns of drought-induced tree mortality across the globe, Proceedings of the National Academy of Sciences of the United States of America, 113, 5024-5029, 10.1073/pnas.1525678113, 2016.

Anderegg, W. R. L., Konings, A. G., Trugman, A. T., Yu, K., Bowling, D. R., Gabbitas, R., Karp, D. S., Pacala, S., Sperry, J. S., Sulman, B. N., and Zenes, N.: Hydraulic diversity of forests regulates ecosystem resilience during drought, Nature, 561, 538-541, 10.1038/s41586-018-0539-7, 2018.

Anderegg, W. R. L., Trugman, A. T., Bowling, D. R., Salvucci, G., and Tuttle, S. E.: Plant functional traits and climate influence drought intensification and land–atmosphere feedbacks, Proceedings of the National Academy of Sciences of the United States of America, 116, 14071-14076, 10.1073/pnas.1904747116 %J Proceedings of the National Academy of Sciences, 2019.

Asner, G. P., and Martin, R. E.: Convergent elevation trends in canopy chemical traits of tropical forests, Glob. Change Biol., 22, 2216-2227, 10.1111/gcb.13164, 2016.

Asner, G. P., Martin, R. E., Anderson, C. B., Kryston, K., Vaughn, N., Knapp, D. E., Bentley, L. P., Shenkin, A., Salinas, N., Sinca, F., Tupayachi, R., Quispe Huaypar, K., Montoya Pillco, M., Ccori Alvarez, F. D., Diaz, S., Enquist, B. J., and Malhi, Y.: Scale dependence of canopy trait distributions along a tropical forest elevation gradient, New Phytol., 214, 973-988, 10.1111/nph.14068, 2017.

Ávila-Lovera, E., Garcillán, P. P., Silva-Bejarano, C., and Santiago, L. S.: Functional traits of leaves and photosynthetic stems of species from a sarcocaulescent scrub in the southern Baja California Peninsula, American Journal of Botany, 107, 1-13, 10.1002/ajb2.1546, 2020.

Bacelar, E. L. V. A., Moutinho-Pereira, J. M., Gonçalves, B. M. C., Brito, C. V. Q., Gomes-Laranjo, J., Ferreira, H. M. F., and Correia, C. M.: Water Use Strategies of Plants Under Drought Conditions, in: Plant Responses to Drought Stress: From Morphological to Molecular Features, edited by: Aroca, R., Springer Berlin Heidelberg, Berlin, Heidelberg, 145-170, 2012.

Bartlett, M. K., Scoffoni, C., Ardy, R., Zhang, Y., Sun, S., Cao, K., and Sack, L.: Rapid determination of comparative drought tolerance traits: using an osmometer to predict turgor loss point, Methods in Ecology and Evolution, 3, 880-888, 10.1111/j.2041-210X.2012.00230.x, 2012a.

Bartlett, M. K., Scoffoni, C., and Sack, L.: The determinants of leaf turgor loss point and prediction of drought tolerance of species and biomes: a global meta-analysis, Ecology Letters, 15, 393-405, 10.1111/j.1461-0248.2012.01751.x, 2012b.

Bartlett, M. K., Zhang, Y., Kreidler, N., Sun, S., Ardy, R., Cao, K., and Sack, L.: Global analysis of plasticity in turgor loss point, a key drought tolerance trait, Ecology Letters, 17, 1580-1590, 10.1111/ele.12374, 2014.

Bartlett, M. K., Klein, T., Jansen, S., Choat, B., and Sack, L.: The correlations and sequence of plant stomatal, hydraulic, and wilting responses to drought, Proceedings of the National Academy of Sciences of the United States of America, 113, 13098-13103, 10.1073/pnas.1604088113, 2016.

Bernacchi, C. J., Singsaas, E. L., Pimentel, C., Portis Jr, A. R., and Long, S. P.: Improved temperature response functions for models of Rubisco-limited photosynthesis, Plant, Cell & Environment, 24, 253-259, 10.1111/j.1365-3040.2001.00668.x, 2001.

Bernacchi, C. J., Pimentel, C., and Long, S. P.: In vivo temperature response functions of parameters required to model RuBP-limited photosynthesis, Pl. Cell Env., 26, 1419-1430, 2003a.

Bernacchi, C. J., Pimentel, C., and Long, S. P.: In vivo temperature response functions of parameters required to model RuBP-limited photosynthesis, Plant, Cell & Environment, 26, 1419-1430, 10.1046/j.0016-8025.2003.01050.x, 2003b.

Berzaghi, F., Wright, I. J., Kramer, K., Oddou-Muratorio, S., Bohn, F. J., Reyer, C. P. O., Sabate, S., Sanders, T. G. M., and Hartig, F.: Towards a New Generation of Trait-Flexible Vegetation Models, Trends in Ecology & Evolution, 35, 191-205, 10.1016/j.tree.2019.11.006, 2020.

Bittencourt, P. R. L., Oliveira, R. S., da Costa, A. C. L., Giles, A. L., Coughlin, I., Costa, P. B., Bartholomew, D. C., Ferreira, L. V., Vasconcelos, S. S., Barros, F. V., Junior, J. A. S., Oliveira, A. A. R., Mencuccini, M., Meir, P., and Rowland, L.: Amazonia trees have limited capacity to acclimate plant hydraulic properties in response to long-term drought, Global Change Biology, 26, 3569-3584, 10.1111/gcb.15040, 2020.

Blackman, C. J., Brodribb, T. J., and Jordan, G. J.: Leaf hydraulic vulnerability is related to conduit dimensions and drought resistance across a diverse range of woody angiosperms, New Phytologist, 188, 1113-1123, 10.1111/j.1469-

8137.2010.03439.x, 2010.

Blonder, B., Kapas, R. E., Dalton, R. M., Graae, B. J., Heiling, J. M., Opedal, Ø. H., and Salguero-Gómez, R.: Microenvironment and functional-trait context dependence predict alpine plant community dynamics, Journal of Ecology, 106, 1323-1337, 10.1111/1365-2745.12973, 2018.

Bohm, J.: Capillarität und saftsteigen, Berichte der Deutschen Botanischen Gesellschaft, 11, 203-212, 1893.

Bonan, G. B.: Forests and climate change: forcings, feedbacks, and the climate benefits of forests, Science, 320, 1444-1449, 2008.

Bonan, G. B., and Doney, S. C.: Climate, ecosystems, and planetary futures: The challenge to predict life in Earth system models, Science, 359, eaam8328, 10.1126/science.aam8328, 2018.

Box, E. O.: Plant functional types and climate at the global scale, Journal of Vegetation Science, 7, 309-320, 1996.

Breheny, P., and Burchett, W.: Visualization of regression models using visreg, R package, 1-15, 2013.

Breheny, P., and Burchett, W.: Visualization of regression models using visreg, The R Journal, 9, 56-71, 2017.

Brodribb, T. J., and Feild, T. S.: Stem hydraulic supply is linked to leaf photosynthetic capacity: evidence from New Caledonian and Tasmanian rainforests, Plant, Cell & Environment, 23, 1381–1388, 2000.

Brodribb, T. J., Holbrook, N. M., and Gutiérrez, M. V.: Hydraulic and photosynthetic coordination in seasonally dry tropical forest trees, Plant, Cell & Environment, 25, 1435-1444, 2002.

Brodribb, T. J., Holbrook, N. M., Edwards, E. J., and GutiÉRrez, M. V.: Relations between stomatal closure, leaf turgor and xylem vulnerability in eight tropical dry forest trees, Plant, Cell & Environment, 26, 443-450, 10.1046/j.1365-3040.2003.00975.x, 2003.

Brodribb, T. J., Feild, T. S., and Jordan, G. J.: Leaf maximum photosynthetic rate and venation are linked by hydraulics, Plant Physiology, 144, 1890-1898, 10.1104/pp.107.101352, 2007.

Brodribb, T. J.: Xylem hydraulic physiology: The functional backbone of terrestrial plant productivity, Plant Science, 177, 245-251, 10.1016/j.plantsci.2009.06.001, 2009.

Brun, P., Zimmermann, N. E., Graham, C. H., Lavergne, S., Pellissier, L., Münkemüller, T., and Thuiller, W.: The productivity-biodiversity relationship varies across diversity dimensions, Nature Communications, 10, 5691, 10.1038/s41467-019-13678-1, 2019.

Bucci, S. J., Scholz, F. G., Campanello, P. I., Montti, L., Jimenez-Castillo, M., Rockwell, F. A., Manna, L. L., Guerra, P., Bernal, P. L., Troncoso, O., Enricci, J., Holbrook, M. N., and Goldstein, G.: Hydraulic differences along the water transport system of South American Nothofagus species: do leaves protect the stem functionality?, Tree Physiology, 32, 880-893, 10.1093/treephys/tps054, 2012.

Bugmann, H., Seidl, R., Hartig, F., Bohn, F., Bruna, J., Cailleret, M., Francois, L., Heinke, J., Henrot, A. J., Hickler, T., Hulsmann, L., Huth, A., Jacquemin, I., Kollas, C., Lasch-Born, P., Lexer, M. J., Merganic, J., Merganicova, K., Mette, T., Miranda, B. R., Nadal-Sala, D., Rammer, W., Rammig, A., Reineking, B., Roedig, E., Sabate, S., Steinkamp, J., Suckow, F., Vacchiano, G., Wild, J., Xu, C., and Reyer, C. P. O.: Tree mortality submodels drive simulated long-term forest dynamics: assessing 15 models from the stand to global scale, Ecosphere, 10, e02616, 10.1002/ecs2.2616, 2019.

Butler, E. E., Datta, A., Flores-Moreno, H., Chen, M., Wythers, K. R., Fazayeli, F., Banerjee, A., Atkin, O. K., Kattge, J., Amiaud, B., Blonder, B., Boenisch, G., Bond-Lamberty, B., Brown, K. A., Byun, C., Campetella, G., Cerabolini, B. E. L., Cornelissen, J. H. C., Craine, J. M., Craven, D., de Vries, F. T., Diaz, S., Domingues, T. F., Forey, E., Gonzalez-Melo, A., Gross, N., Han, W., Hattingh, W. N., Hickler, T., Jansen, S., Kramer, K., Kraft, N. J. B., Kurokawa, H., Laughlin, D. C., Meir, P., Minden, V., Niinemets, U., Onoda, Y., Penuelas, J., Read, Q., Sack, L., Schamp, B., Soudzilovskaia, N. A., Spasojevic, M. J., Sosinski, E., Thornton,

P. E., Valladares, F., van Bodegom, P. M., Williams, M., Wirth, C., and Reich, P. B.: Mapping local and global variability in plant trait distributions, Proceedings of the National Academy of Sciences, 114, E10937-E10946, 10.1073/pnas.1708984114, 2017.

Carnicer, J., Coll, M., Ninyerola, M., Pons, X., Sanchez, G., and Penuelas, J.: Widespread crown condition decline, food web disruption, and amplified tree mortality with increased climate change-type drought, Proceedings of the National Academy of Sciences, 108, 1474-1478, 10.1073/pnas.1010070108, 2011.

Cavanagh, A. P., and Kubien, D. S.: Can phenotypic plasticity in Rubisco performance contribute to photosynthetic acclimation?, Photosynth Res, 119, 203-214, 10.1007/s11120-013-9816-3, 2014a.

Cavanagh, A. P., and Kubien, D. S.: Can phenotypic plasticity in Rubisco performance contribute to photosynthetic acclimation?, Photosynthesis Research, 119, 203-214, 2014b.

Cernusak, L. A., Ubierna, N., Winter, K., Holtum, J. A., Marshall, J. D., and Farquhar, G. D.: Environmental and physiological determinants of carbon isotope discrimination in terrestrial plants, New Phytologist, 200, 950-965, 10.1111/nph.12423, 2013.

Chave, J., Coomes, D., Jansen, S., Lewis, S. L., Swenson, N. G., and Zanne, A. E.: Towards a worldwide wood economics spectrum, Ecology Letters, 12, 351-366, 10.1111/j.1461-0248.2009.01285.x, 2009.

Chen, B., and Chen, J. M.: Diurnal, seasonal and interannual variability of carbon isotope discrimination at the canopy level in response to environmental factors in a boreal forest ecosystem, Plant, Cell & Environment, 30, 1223-1239, 10.1111/j.1365-3040.2007.01703.x, 2007.

Chen, J.-L., Reynolds, J. F., Harley, P. C., and Tenhunen, J. D.: Coordination theory of leaf nitrogen distribution in a canopy, Oecologia, 93, 63-69, 1993a.

Chen, J. L., Reynolds, J. F., Harley, P. C., and Tenhunen, J. D.: Coordination

theory of leaf nitrogen distribution in a canopy, Oecologia, 93, 63-69, 1993b.

Chen, J. L., and Reynolds, J. F.: A coordination model of whole-plant carbon allocation in relation to water stress, Ann. Bot., 80, 45-55, 1997.

Choat, B., Sack, L., and Holbrook, N. M.: Diversity of hydraulic traits in nine Cordia species growing in tropical forests with contrasting precipitation, New Phytologist, 175, 686-698, 10.1111/j.1469-8137.2007.02137.x, 2007.

Choat, B., Cobb, A. R., and Jansen, S.: Structure and function of bordered pits: new discoveries and impacts on whole-plant hydraulic function, New Phytologist, 177, 608-626, 10.1111/j.1469-8137.2007.02317.x, 2008.

Choat, B., Brodribb, T. J., Brodersen, C. R., Duursma, R. A., López, R., and Medlyn, B. E.: Triggers of tree mortality under drought, Nature, 558, 531-539, 10.1038/s41586-018-0240-x, 2018.

Christoffersen, B. O., Gloor, M., Fauset, S., Fyllas, N. M., Galbraith, D. R., Baker, T. R., Kruijt, B., Rowland, L., Fisher, R. A., Binks, O. J., Sevanto, S., Xu, C., Jansen, S., Choat, B., Mencuccini, M., McDowell, N. G., and Meir, P.: Linking hydraulic traits to tropical forest function in a size-structured and trait-driven model (TFS v.1-Hydro), Geoscientific Model Development, 9, 4227-4255, 10.5194/gmd-9-4227-2016, 2016.

Clark, D., Mercado, L., Sitch, S., Jones, C., Gedney, N., Best, M., Pryor, M., Rooney, G., Essery, R., and Blyth, E.: The Joint UK Land Environment Simulator (JULES), model description–Part 2: carbon fluxes and vegetation dynamics, Geoscientific Model Development, 4, 701-722, 2011.

Cochard, H., Martin, R., Gross, P., and Bogeat-Triboulot, M. B. a.: Temperature effects on hydraulic conductance and water relations of Quercus robur L, Journal of Experimental Botany, 51, 1255-1259, 10.1093/jxb/51.348.1255, 2000.

Cochard, H., Coll, L., Le Roux, X., and Améglio, T.: Unraveling the Effects of Plant Hydraulics on Stomatal Closure during Water Stress in Walnut, Plant Physiology, 128, 282-290, 10.1104/pp.010400, 2002.

Cook, B. I., Mankin, J. S., and Anchukaitis, K. J.: Climate Change and Drought:

From Past to Future, Current Climate Change Reports, 4, 164-179, 10.1007/s40641-018-0093-2, 2018.

Cornelissen, J. H. C., Lavorel, S., Garnier, E., Díaz, S., Buchmann, N., Gurvich, D. E., Reich, P. B., Ter Steege, H., Morgan, H. D., Van Der Heijden, M. G. A., Pausas, J. G., and Poorter, H.: A handbook of protocols for standardised and easy measurement of plant functional traits worldwide, Australian Journal of Botany, 51, 335-380, 10.1071/BT02124, 2003a.

Cornelissen, J. H. C., Lavorel, S., Garnier, E. S., Buchmann, N., and Gurvich: A handbook of protocols for standardised and easy measurement of plant functional traits worldwide, Aust. J. Bot., 51, 335-380, 2003b.

Cornwell, W. K., Wright, I. J., Turner, J., Maire, V., Barbour, M. M., Cernusak, L. A., Dawson, T., Ellsworth, D., Farquhar, G. D., Griffiths, H., Keitel, C., Knohl, A., Reich, P. B., Williams, D. G., Bhaskar, R., Cornelissen, J. H. C., Richards, A., Schmidt, S., Valladares, F., Körner, C., Schulze, E.-D., Buchmann, N., and Santiago, L. S.: Climate and soils together regulate photosynthetic carbon isotope discrimination within C3 plants worldwide, Glob Ecol Biogeogr, 27, 1056-1067, doi:10.1111/geb.12764, 2018.

Cosme, L. H. M., Schietti, J., Costa, F. R. C., and Oliveira, R. S.: The importance of hydraulic architecture to the distribution patterns of trees in a central Amazonian forest, New Phytologist, 215, 113-125, https://doi.org/10.1111/nph.14508, 2017.

Cui, E., Huang, K., Arain, M. A., Fisher, J. B., Huntzinger, D. N., Ito, A., Luo, Y., Jain, A. K., Mao, J., Michalak, A. M., Niu, S., Parazoo, N. C., Peng, C., Peng, S., Poulter, B., Ricciuto, D. M., Schaefer, K. M., Schwalm, C. R., Shi, X., Tian, H., Wang, W., Wang, J., Wei, Y., Yan, E., Yan, L., Zeng, N., Zhu, Q., and Xia, J.: Vegetation Functional Properties Determine Uncertainty of Simulated Ecosystem Productivity: A Traceability Analysis in the East Asian Monsoon Region, Global Biogeochemical Cycles, 33, 668-689, 10.1029/2018gb005909, 2019.

Davis, T. W., Prentice, I. C., Stocker, B. D., Thomas, R. T., Whitley, R. J., Wang, H., Evans, B. J., Gallego-Sala, A. V., Sykes, M. T., and Cramer, W.: Simple process-led algorithms for simulating habitats (SPLASH v.1.0): robust indices of

radiation, evapotranspiration and plant-available moisture, Geoscientific Model Development, 10, 689-708, 10.5194/gmd-10-689-2017, 2017a.

Davis, T. W., Prentice, I. C., Stocker, B. D., Thomas, R. T., Whitley, R. J., Wang, H., Evans, B. J., Gallegosala, A. V., Sykes, M. T., and Cramer, W.: Simple process-led algorithms for simulating habitats (SPLASH v.1.0): robust indices of radiation, evapotranspiration and plant-available moisture, Geosci. Model Dev., 10, 1-25, 2017b.

De Guzman, M. E., Acosta-Rangel, A., Winter, K., Meinzer, F. C., Bonal, D., and Santiago, L. S.: Hydraulic traits of Neotropical canopy liana and tree species across a broad range of wood density: implications for predicting drought mortality with models, Tree Physiology, 41, 24-34, 10.1093/treephys/tpaa106, 2021.

De Kauwe, M. G., Medlyn, B. E., Zaehle, S., Walker, A. P., Dietze, M. C., Hickler, T., Jain, A. K., Luo, Y., Parton, W. J., Prentice, I. C., Smith, B., Thornton, P. E., Wang, S., Wang, Y. P., Warlind, D., Weng, E., Crous, K. Y., Ellsworth, D. S., Hanson, P. J., Seok Kim, H., Warren, J. M., Oren, R., and Norby, R. J.: Forest water use and water use efficiency at elevated CO2 : a model-data intercomparison at two contrasting temperate forest FACE sites, Global Change Biology, 19, 1759-1779, 10.1111/gcb.12164, 2013.

De Kauwe, M. G., Kala, J., Lin, Y. S., Pitman, A. J., Medlyn, B. E., Duursma, R. A., Abramowitz, G., Wang, Y. P., and Miralles, D. G.: A test of an optimal stomatal conductance scheme within the CABLE land surface model, Geoscientific Model Development, 8, 431-452, 10.5194/gmd-8-431-2015, 2015.

De Kauwe, M. G., Lin, Y. S., Wright, I. J., Medlyn, B. E., Crous, K. Y., Ellsworth, D. S., Maire, V., Prentice, I. C., Atkin, O. K., and Rogers, A.: A test of the 'one-point method' for estimating maximum carboxylation capacity from field-measured, light-saturated photosynthesis, New Phytol., 210, 1130-1144, 2016a.

De Kauwe, M. G., Lin, Y. S., Wright, I. J., Medlyn, B. E., Crous, K. Y., Ellsworth, D. S., Maire, V., Prentice, I. C., Atkin, O. K., Rogers, A., Niinemets, U., Serbin, S. P., Meir, P., Uddling, J., Togashi, H. F., Tarvainen, L., Weerasinghe, L. K., Evans, B. J., Ishida, F. Y., and Domingues, T. F.: A test of the 'one-point method' for

estimating maximum carboxylation capacity from field-measured, light-saturated photosynthesis, New Phytologist, 210, 1130-1144, 10.1111/nph.13815, 2016b.

Deans, R. M., Brodribb, T. J., Busch, F. A., and Farquhar, G. D.: Optimization can provide the fundamental link between leaf photosynthesis, gas exchange and water relations, Nature Plants, 6, 1116-1125, 10.1038/s41477-020-00760-6, 2020.

Deckmyn, G., Evans, S. P., and Randle, T. J.: Refined pipe theory for mechanistic modeling of wood development, Tree Physiology, 26, 703-717, 10.1093/treephys/26.6.703, 2006.

Devos, N., Ingouff, M., Loppes, R., and Matagne, R. F.: Rubisco adaptation to low temperatures: a comparative study in psychrophilic and mesophilic unicellular algae., J. Phycol., 34, 655-660, 2010.

Diaz, S., Kattge, J., Cornelissen, J. H., Wright, I. J., Lavorel, S., Dray, S., Reu, B., Kleyer, M., Wirth, C., Prentice, I. C., Garnier, E., Bonisch, G., Westoby, M., Poorter, H., Reich, P. B., Moles, A. T., Dickie, J., Gillison, A. N., Zanne, A. E., Chave, J., Wright, S. J., Sheremet'ev, S. N., Jactel, H., Baraloto, C., Cerabolini, B., Pierce, S., Shipley, B., Kirkup, D., Casanoves, F., Joswig, J. S., Gunther, A., Falczuk, V., Ruger, N., Mahecha, M. D., and Gorne, L. D.: The global spectrum of plant form and function, Nature, 529, 167-171, 10.1038/nature16489, 2016.

Dixon, H. H., and Joly, J.: On the ascent of sap, Proceedings of the Royal Society of London, 57, 3-5, 1894.

Dong, N., Prentice, I. C., Evans, B. J., Caddy-Retalic, S., Lowe, A. J., and Wright, I. J.: Leaf nitrogen from first principles: field evidence for adaptive variation with climate, Biogeosciences, 14, 1-28, 2017a.

Dong, N., Prentice, I. C., Evans, B. J., Caddy-Retalic, S., Lowe, A. J., and Wright, I. J.: Leaf nitrogen from first principles: field evidence for adaptive variation with climate, Biogeosciences, 14, 481-495, 10.5194/bg-14-481-2017, 2017b.

Dong, N., Prentice, I. C., Wright, I. J., Evans, B. J., Togashi, H. F., Caddy-Retalic, S., McInerney, F. A., Sparrow, B., Leitch, E., and Lowe, A. J.: Components of leaf-trait variation along environmental gradients, New Phytologist, 228, 82-94,

10.1111/nph.16558, 2020.

Dong, N., Prentice, I. C., Wright, I. J., Wang, H., Atkin, O. K., Bloomfield, K. J., Domingues, T. F., Gleason, S. M., Maire, V., Onoda, Y., Poorter, H., and Smith, N. G.: Leaf nitrogen from the perspective of optimal plant function, Journal of Ecology, 110, 2585-2602, 10.1111/1365-2745.13967, 2022.

Dong, N., Dechant, B., Wang, H., Wright, I. J., and Prentice, I. C.: Global leaf-trait mapping based on optimality theory, Global Ecology and Biogeography, 32, 1152-1162, https://doi.org/10.1111/geb.13680, 2023.

Doughty, C. E., Keany, J. M., Wiebe, B. C., Rey-Sanchez, C., Carter, K. R., Middleby, K. B., Cheesman, A. W., Goulden, M. L., da Rocha, H. R., Miller, S. D., Malhi, Y., Fauset, S., Gloor, E., Slot, M., Oliveras Menor, I., Crous, K. Y., Goldsmith, G. R., and Fisher, J. B.: Tropical forests are approaching critical temperature thresholds, Nature, 621, 105-111, 10.1038/s41586-023-06391-z, 2023.

Dusenge, M. E., Duarte, A. G., and Way, D. A.: Plant carbon metabolism and climate change: elevated CO(2) and temperature impacts on photosynthesis, photorespiration and respiration, New Phytologist, 221, 32-49, 10.1111/nph.15283, 2019.

Eller, C. B., Rowland, L., Oliveira, R. S., Bittencourt, P. R. L., Barros, F. V., da Costa, A. C. L., Meir, P., Friend, A. D., Mencuccini, M., Sitch, S., and Cox, P.: Modelling tropical forest responses to drought and El Nino with a stomatal optimization model based on xylem hydraulics, Philos. Trans. R. Soc. B-Biol. Sci., 373, 10.1098/rstb.2017.0315, 2018a.

Eller, C. B., Rowland, L., Oliveira, R. S., Bittencourt, P. R. L., Barros, F. V., da Costa, A. C. L., Meir, P., Friend, A. D., Mencuccini, M., Sitch, S., and Cox, P.: Modelling tropical forest responses to drought and El Nino with a stomatal optimization model based on xylem hydraulics, Philosophical Transactions of The Royal Society B Biological Sciences, 373, 20170315, 10.1098/rstb.2017.0315, 2018b.

Eller, C. B., Rowland, L., Mencuccini, M., Rosas, T., Williams, K., Harper, A.,

Medlyn, B. E., Wagner, Y., Klein, T., Teodoro, G. S., Oliveira, R. S., Matos, I. S., Rosado, B. H. P., Fuchs, K., Wohlfahrt, G., Montagnani, L., Meir, P., Sitch, S., and Cox, P. M.: Stomatal optimization based on xylem hydraulics (SOX) improves land surface model simulation of vegetation responses to climate, New Phytologist, 226, 1622-1637, 10.1111/nph.16419, 2020.

Evans, J. R.: Photosynthesis and nitrogen relationships in leaves of C_3 plants, Oecologia, 78, 9-19, 1989.

Fan, Z. X., Zhang, S. B., Hao, G. Y., Ferry Slik, J. W., and Cao, K. F.: Hydraulic conductivity traits predict growth rates and adult stature of 40 Asian tropical tree species better than wood density, Journal of Ecology, 100, 732-741, 10.1111/j.1365-2745.2011.01939.x, 2012.

Fang, Z., Zhang, W., Brandt, M., Abdi, A. M., and Fensholt, R.: Globally Increasing Atmospheric Aridity Over the 21st Century, Earth's Future, 10, e2022EF003019, 10.1029/2022ef003019, 2022.

Farquhar, G. D., Caemmerer, S. V., and Berry, J. A.: A biochemical model of photosynthetic CO_2 assimilation in leaves of C_3 species, Planta, 149, 78-90, 1980a.

Farquhar, G. D., von Caemmerer, S., and Berry, J. A.: A biochemical model of photosynthetic CO2 assimilation in leaves of C3 species, Planta, 149, 78-90, 10.1007/BF00386231, 1980b.

Farquhar, G. D., Ehleringer, J. R., and Hubick, K. T.: Carbon isotope discrimination and photosynthesis, Annual Review of Plant Biology, 40, 503-537, 1989.

Fatichi, S., Pappas, C., Zscheischler, J., and Leuzinger, S.: Modelling carbon sources and sinks in terrestrial vegetation, New Phytologist, 221, 652-668, 10.1111/nph.15451, 2019.

Fick, A.: Ueber Diffusion, Annalen der Physik, 170, 59-86, https://doi.org/10.1002/andp.18551700105, 1855.

Fick, S. E., and Hijmans, R. J.: WorldClim 2: new 1-km spatial resolution climate

surfaces for global land areas, International Journal of Climatology, 37, 4302-4315, 10.1002/joc.5086, 2017.

Flexas, J., Scoffoni, C., Gago, J., and Sack, L.: Leaf mesophyll conductance and leaf hydraulic conductance: an introduction to their measurement and coordination, Journal of Experimental Botany, 64, 3965-3981, 10.1093/jxb/ert319, 2013.

Fontana, S., Rasmann, S., de Bello, F., Pomati, F., and Moretti, M.: Reconciling trait based perspectives along a trait-integration continuum, Ecology, 102, e03472, 10.1002/ecy.3472, 2021.

Forsythe, W. C., Rykiel, E. J., Stahl, R. S., Wu, H., and Schoolfield, R. M.: A model comparison for daylength as a function of latitude and day of year, Ecol. Model., 80, 87-95, 1995.

Frank, D., Reichstein, M., Bahn, M., Thonicke, K., Frank, D., Mahecha, M. D., Smith, P., van der Velde, M., Vicca, S., Babst, F., Beer, C., Buchmann, N., Canadell, J. G., Ciais, P., Cramer, W., Ibrom, A., Miglietta, F., Poulter, B., Rammig, A., Seneviratne, S. I., Walz, A., Wattenbach, M., Zavala, M. A., and Zscheischler, J.: Effects of climate extremes on the terrestrial carbon cycle: concepts, processes and potential future impacts, Global Change Biology, 21, 2861-2880, https://doi.org/10.1111/gcb.12916, 2015.

Franklin, O., Harrison, S. P., Dewar, R., Farrior, C. E., Brannstrom, A., Dieckmann, U., Pietsch, S., Falster, D., Cramer, W., Loreau, M., Wang, H., Makela, A., Rebel, K. T., Meron, E., Schymanski, S. J., Rovenskaya, E., Stocker, B. D., Zaehle, S., Manzoni, S., van Oijen, M., Wright, I. J., Ciais, P., van Bodegom, P. M., Penuelas, J., Hofhansl, F., Terrer, C., Soudzilovskaia, N. A., Midgley, G., and Prentice, I. C.: Organizing principles for vegetation dynamics, Nature Plants, 6, 444-453, 10.1038/s41477-020-0655-x, 2020.

Franklin, O., Fransson, P., Hofhansl, F., Jansen, S., and Joshi, J.: Optimal balancing of xylem efficiency and safety explains plant vulnerability to drought, Ecology Letters, 26, 1485-1496, 10.1111/ele.14270, 2023.

Friedlingstein, P., O'Sullivan, M., Jones, M. W., Andrew, R. M., Bakker, D. C. E.,

Hauck, J., Landschützer, P., Le Quéré, C., Luijkx, I. T., Peters, G. P., Peters, W., Pongratz, J., Schwingshackl, C., Sitch, S., Canadell, J. G., Ciais, P., Jackson, R. B., Alin, S. R., Anthoni, P., Barbero, L., Bates, N. R., Becker, M., Bellouin, N., Decharme, B., Bopp, L., Brasika, I. B. M., Cadule, P., Chamberlain, M. A., Chandra, N., Chau, T.-T.-T., Chevallier, F., Chini, L. P., Cronin, M., Dou, X., Enyo, K., Evans, W., Falk, S., Feely, R. A., Feng, L., Ford, D. J., Gasser, T., Ghattas, J., Gkritzalis, T., Grassi, G., Gregor, L., Gruber, N., Gürses, Ö., Harris, I., Hefner, M., Heinke, J., Houghton, R. A., Hurtt, G. C., Iida, Y., Ilyina, T., Jacobson, A. R., Jain, A., Jarníková, T., Jersild, A., Jiang, F., Jin, Z., Joos, F., Kato, E., Keeling, R. F., Kennedy, D., Klein Goldewijk, K., Knauer, J., Korsbakken, J. I., Körtzinger, A., Lan, X., Lefèvre, N., Li, H., Liu, J., Liu, Z., Ma, L., Marland, G., Mayot, N., McGuire, P. C., McKinley, G. A., Meyer, G., Morgan, E. J., Munro, D. R., Nakaoka, S.-I., Niwa, Y., O'Brien, K. M., Olsen, A., Omar, A. M., Ono, T., Paulsen, M., Pierrot, D., Pocock, K., Poulter, B., Powis, C. M., Rehder, G., Resplandy, L., Robertson, E., Rödenbeck, C., Rosan, T. M., Schwinger, J., Séférian, R., Smallman, T. L., Smith, S. M., Sospedra-Alfonso, R., Sun, Q., Sutton, A. J., Sweeney, C., Takao, S., Tans, P. P., Tian, H., Tilbrook, B., Tsujino, H., Tubiello, F., van der Werf, G. R., van Ooijen, E., Wanninkhof, R., Watanabe, M., Wimart-Rousseau, C., Yang, D., Yang, X., Yuan, W., Yue, X., Zaehle, S., Zeng, J., and Zheng, B.: Global Carbon Budget 2023, Earth System Science Data, 15, 5301-5369, 10.5194/essd-15-5301-2023, 2023.

Fu, P. L., Jiang, Y. J., Wang, A. Y., Brodribb, T. J., Zhang, J. L., Zhu, S. D., and Cao, K. F.: Stem hydraulic traits and leaf water-stress tolerance are co-ordinated with the leaf phenology of angiosperm trees in an Asian tropical dry karst forest, Annals of Botany, 110, 189-199, 10.1093/aob/mcs092, 2012.

Fu, Y. H., Piao, S., Vitasse, Y., Zhao, H., De Boeck, H. J., Liu, Q., Yang, H., Weber, U., Hänninen, H., and Janssens, I. A.: Increased heat requirement for leaf flushing in temperate woody species over 1980–2012: effects of chilling, precipitation and insolation, Global Change Biology, 21, 2687-2697, https://doi.org/10.1111/gcb.12863, 2015.

Fu, Z., Ciais, P., Prentice, I. C., Gentine, P., Makowski, D., Bastos, A., Luo, X., Green, J. K., Stoy, P. C., Yang, H., and Hajima, T.: Atmospheric dryness reduces photosynthesis along a large range of soil water deficits, Nature Communications,

13, 989, 10.1038/s41467-022-28652-7, 2022.

Gale, J.: Elevation and transpiration: some theoretical considerations with special reference to Mediterranean-type climate, J. Appl. Ecol., 691-702, 1972.

Gleason, S. M., Butler, D. W., and Waryszak, P.: Shifts in leaf and stem hydraulic traits across aridity gradients in Eastern Australia, International Journal of Plant Sciences, 174, 1292-1301, 10.1086/673239, 2013.

Gleason, S. M., Westoby, M., Jansen, S., Choat, B., Hacke, U. G., Pratt, R. B., Bhaskar, R., Brodribb, T. J., Bucci, S. J., Cao, K. F., Cochard, H., Delzon, S., Domec, J. C., Fan, Z. X., Feild, T. S., Jacobsen, A. L., Johnson, D. M., Lens, F., Maherali, H., Martinez-Vilalta, J., Mayr, S., McCulloh, K. A., Mencuccini, M., Mitchell, P. J., Morris, H., Nardini, A., Pittermann, J., Plavcova, L., Schreiber, S. G., Sperry, J. S., Wright, I. J., and Zanne, A. E.: Weak tradeoff between xylem safety and xylem-specific hydraulic efficiency across the world's woody plant species, New Phytologist, 209, 123-136, 10.1111/nph.13646, 2016.

Groemping, U.: Relative Importance for Linear Regression in R: The Package relaimpo, Journal of Statistical Software, 17, 925-933, 2006.

Grossiord, C., Buckley, T. N., Cernusak, L. A., Novick, K. A., Poulter, B., Siegwolf, R. T. W., Sperry, J. S., and McDowell, N. G.: Plant responses to rising vapor pressure deficit, New Phytologist, 226, 1550-1566, 10.1111/nph.16485, 2020.

Grunwald, Y., Yaaran, A., and Moshelion, M.: Illuminating plant water dynamics: the role of light in leaf hydraulic regulation, New Phytologist, 241, 1404-1414, 10.1111/nph.19497, 2024.

Guan, X., Wen, Y., Zhang, Y., Chen, Z., and Cao, K. F.: Stem hydraulic conductivity and embolism resistance of Quercus species are associated with their climatic niche, Tree Physiology, 43, 234-247, 10.1093/treephys/tpac119, 2023.

Guillemot, J., Martin-StPaul, N. K., Bulascoschi, L., Poorter, L., Morin, X., Pinho, B. X., le Maire, G., P, R. L. B., Oliveira, R. S., Bongers, F., Brouwer, R., Pereira, L., Gonzalez Melo, G. A., Boonman, C. C. F., Brown, K. A., Cerabolini, B. E. L.,

Niinemets, U., Onoda, Y., Schneider, J. V., Sheremetiev, S., and Brancalion, P. H. S.: Small and slow is safe: On the drought tolerance of tropical tree species, Global Change Biology, 28, 2622-2638, 10.1111/gcb.16082, 2022.

Gvozdevaite, A., Oliveras, I., Domingues, T. F., Peprah, T., Boakye, M., Afriyie, L., da Silva Peixoto, K., de Farias, J., Almeida de Oliveira, E., Almeida Farias, C. C., Dos Santos Prestes, N. C. C., Neyret, M., Moore, S., Schwantes Marimon, B., Marimon Junior, B. H., Adu-Bredu, S., and Malhi, Y.: Leaf-level photosynthetic capacity dynamics in relation to soil and foliar nutrients along forest-savanna boundaries in Ghana and Brazil, Tree Physiology, 38, 1912-1925, 10.1093/treephys/tpy117, 2018.

Hacke, U. G., and Sperry, J. S.: Functional and ecological xylem anatomy, Perspectives in Plant Ecology, Evolution and Systematics, 4, 97-115, 10.1078/1433-8319-00017, 2001.

Hacke, U. G., Sperry, J. S., Pockman, W. T., Davis, S. D., and McCulloh, K. A.: Trends in wood density and structure are linked to prevention of xylem implosion by negative pressure, Oecologia, 126, 457-461, 10.1007/s004420100628, 2001a.

Hacke, U. G., Stiller, V., Sperry, J. S., Pittermann, J., and McCulloh, K. A.: Cavitation Fatigue. Embolism and Refilling Cycles Can Weaken the Cavitation Resistance of Xylem1, Plant Physiology, 125, 779-786, 10.1104/pp.125.2.779, 2001b.

Hagen, G.: Ueber die Bewegung des Wassers in engen cylindrischen Röhren, Annalen der Physik, 122, 423-442, 1839.

Hammond, W. M., Yu, K., Wilson, L. A., Will, R. E., Anderegg, W. R. L., and Adams, H. D.: Dead or dying? Quantifying the point of no return from hydraulic failure in drought-induced tree mortality, New Phytologist, 223, 1834-1843, 10.1111/nph.15922, 2019.

Hammond, W. M.: A Matter of Life and Death: Alternative Stable States in Trees, From Xylem to Ecosystems, Frontiers in Forests and Global Change, 3, 10.3389/ffgc.2020.560409, 2020.

Harrison, M. T., Edwards, E. J., Farquhar, G. D., Nicotra, A. B., and Evans, J. R.: Nitrogen in cell walls of sclerophyllous leaves accounts for little of the variation in photosynthetic nitrogen-use efficiency, Pl. Cell Env., 32, 259-270, 10.1111/j.1365-3040.2008.01918.x, 2009.

Harrison, S. P., Cramer, W., Franklin, O., Prentice, I. C., Wang, H., Brannstrom, A., de Boer, H., Dieckmann, U., Joshi, J., Keenan, T. F., Lavergne, A., Manzoni, S., Mengoli, G., Morfopoulos, C., Penuelas, J., Pietsch, S., Rebel, K. T., Ryu, Y., Smith, N. G., Stocker, B. D., and Wright, I. J.: Eco-evolutionary optimality as a means to improve vegetation and land-surface models, New Phytologist, 231, 2125-2141, 10.1111/nph.17558, 2021.

Hastie, T. J., and Tibshirani, R. J.: Generalized additive models, CRC press, 1990.

He, M., Dijkstra, F. A., Zhang, K., Li, X., Tan, H., Gao, Y., and Li, G.: Leaf nitrogen and phosphorus of temperate desert plants in response to climate and soil nutrient availability, Scientific Reports, 4, 6932, 10.1038/srep06932, 2014.

He, P., Gleason, S. M., Wright, I. J., Weng, E., Liu, H., Zhu, S., Lu, M., Luo, Q., Li, R., Wu, G., Yan, E., Song, Y., Mi, X., Hao, G., Reich, P. B., Wang, Y., Ellsworth, D. S., and Ye, Q.: Growing-season temperature and precipitation are independent drivers of global variation in xylem hydraulic conductivity, Global Change Biology, 26, 1833-1841, 10.1111/gcb.14929, 2020.

Helfenstein, I. S., Schneider, F. D., Schaepman, M. E., and Morsdorf, F.: Assessing biodiversity from space: Impact of spatial and spectral resolution on trait-based functional diversity, Remote Sensing of Environment, 275, 113024, https://doi.org/10.1016/j.rse.2022.113024, 2022.

Hengl, T., Mendes de Jesus, J., Heuvelink, G. B., Ruiperez Gonzalez, M., Kilibarda, M., Blagotic, A., Shangguan, W., Wright, M. N., Geng, X., Bauer-Marschallinger, B., Guevara, M. A., Vargas, R., MacMillan, R. A., Batjes, N. H., Leenaars, J. G., Ribeiro, E., Wheeler, I., Mantel, S., and Kempen, B.: SoilGrids250m: Global gridded soil information based on machine learning, PLoS One, 12, e0169748, 10.1371/journal.pone.0169748, 2017.

Hickler, T., Prentice, I. C., Smith, B., Sykes, M. T., and Zaehle, S.: Implementing

plant hydraulic architecture within the LPJ Dynamic Global Vegetation Model, Global Ecology and Biogeography, 0, 060811081017001-???, 10.1111/j.1466-822X.2006.00254.x, 2006.

Hirose, T., and Werger, M. J. A.: Maximizing daily canopy photosynthesis with respect to the leaf nitrogen allocation pattern in the canopy, Oecologia, 72, 520-526, 1987.

Hochberg, U., Rockwell, F. E., Holbrook, N. M., and Cochard, H.: Iso/anisohydry: A plant-environment interaction rather than a simple hydraulic trait, Trends in Plant Science, 23, 112-120, 10.1016/j.tplants.2017.11.002, 2018.

Hoeber, S., Leuschner, C., Köhler, L., Arias-Aguilar, D., and Schuldt, B.: The importance of hydraulic conductivity and wood density to growth performance in eight tree species from a tropical semi-dry climate, Forest Ecology and Management, 330, 126-136, 10.1016/j.foreco.2014.06.039, 2014.

Hutchinson, M. F., and Xu, T.: Anusplin version 4.2 user guide, Centre for Resource and Environmental Studies, The Australian National University, Canberra, 54, 2004.

IPCC: Climate Change 2023: Synthesis Report. Contribution of Working Groups I, II and III to the Sixth Assessment Report of the Intergovernmental Panel on Climate Change [Core Writing Team, H. Lee and J. Romero (eds.)]. IPCC, Geneva, Switzerland, pp. 35-115, 2023.

Iqbal, A., Dong, Q., Wang, X., Gui, H., Zhang, H., Zhang, X., and Song, M.: High Nitrogen Enhance Drought Tolerance in Cotton through Antioxidant Enzymatic Activities, Nitrogen Metabolism and Osmotic Adjustment, Plants, 9, 178, 2020.

Isbell, F., Craven, D., Connolly, J., Loreau, M., Schmid, B., Beierkuhnlein, C., Bezemer, T. M., Bonin, C., Bruelheide, H., de Luca, E., Ebeling, A., Griffin, J. N., Guo, Q., Hautier, Y., Hector, A., Jentsch, A., Kreyling, J., Lanta, V., Manning, P., Meyer, S. T., Mori, A. S., Naeem, S., Niklaus, P. A., Polley, H. W., Reich, P. B., Roscher, C., Seabloom, E. W., Smith, M. D., Thakur, M. P., Tilman, D., Tracy, B. F., van der Putten, W. H., van Ruijven, J., Weigelt, A., Weisser, W. W., Wilsey, B., and Eisenhauer, N.: Biodiversity increases the resistance of ecosystem

productivity to climate extremes, Nature, 526, 574-577, 10.1038/nature15374, 2015.

Janssen, T. A. J., Holtta, T., Fleischer, K., Naudts, K., and Dolman, H.: Wood allocation trade-offs between fiber wall, fiber lumen, and axial parenchyma drive drought resistance in neotropical trees, Plant, Cell & Environment, 43, 965-980, 10.1111/pce.13687, 2020.

Jarvis, P. G., and McNaughton, K. G.: Stomatal Control of Transpiration: Scaling Up from Leaf to Region, in: Advances in Ecological Research, edited by: MacFadyen, A., and Ford, E. D., Academic Press, 1-49, 1986.

Jian, Q., Keming, M., and Yuxin, Z.: Leaf-trait relationships of *Quercus liaotungensis* along an altitudinal gradient in Dongling Mountain, Beijing, Ecol. Res., 24, 1243-1250, 10.1007/s11284-009-0608-3, 2009.

Jiang, C., Ryu, Y., Wang, H., and Keenan, T. F.: An optimality-based model explains seasonal variation in C3 plant photosynthetic capacity, Global Change Biology, 26, 6493-6510, 10.1111/gcb.15276, 2020.

Jiménez-Rodríguez, C. D., Sulis, M., and Schymanski, S.: The Role of the Intraspecific Variability of Hydraulic Traits for Modeling the Plant Water Use in Different European Forest Ecosystems, Journal of Advances in Modeling Earth Systems, 16, e2022MS003494, 10.1029/2022ms003494, 2024.

Jin, Y., Hao, G., Hammond, W. M., Yu, K., Liu, X., Ye, Q., Zhou, Z., and Wang, C.: Aridity-dependent sequence of water potentials for stomatal closure and hydraulic dysfunctions in woody plants, Global Change Biology, 29, 2030-2040, 10.1111/gcb.16605, 2023.

Joshi, J., Stocker, B. D., Hofhansl, F., Zhou, S., Dieckmann, U., and Prentice, I. C.: Towards a unified theory of plant photosynthesis and hydraulics, bioRxiv, 2020.2012.2017.423132, 10.1101/2020.12.17.423132, 2020.

Joshi, J., Stocker, B. D., Hofhansl, F., Zhou, S., Dieckmann, U., and Prentice, I. C.: Towards a unified theory of plant photosynthesis and hydraulics, Nature Plants, 8, 1304-1316, 10.1038/s41477-022-01244-5, 2022.

Kattge, J., and Knorr, W.: Temperature acclimation in a biochemical model of photosynthesis: a reanalysis of data from 36 species, Plant, Cell & Environment, 30, 1176-1190, 10.1111/j.1365-3040.2007.01690.x, 2007.

Kelley, D. I., Harrison, S. P., and Prentice, I. C.: Improved simulation of fire–vegetation interactions in the Land surface Processes and eXchanges dynamic global vegetation model (LPX-Mv1), Geoscientific Model Development, 7, 2411-2433, 2014.

Kennedy, D., Swenson, S., Oleson, K. W., Lawrence, D. M., Fisher, R., Lola da Costa, A. C., and Gentine, P.: Implementing Plant Hydraulics in the Community Land Model, Version 5, Journal of Advances in Modeling Earth Systems, 11, 485-513, 10.1029/2018ms001500, 2019.

Kikuzawa, K.: A cost-benefit analysis of leaf habit and leaf longevity of trees and their geographical pattern, The American Naturalist, 138, 1250-1263, 10.1086/285281, 1991.

Kim, J. B., Kerns, B. K., Drapek, R. J., Pitts, G. S., and Halofsky, J. E.: Simulating vegetation response to climate change in the Blue Mountains with MC2 dynamic global vegetation model, Climate Services, 10, 20-32, 10.1016/j.cliser.2018.04.001, 2018.

Knipfer, T., Bambach, N., Hernandez, M. I., Bartlett, M. K., Sinclair, G., Duong, F., Kluepfel, D. A., and McElrone, A. J.: Predicting Stomatal Closure and Turgor Loss in Woody Plants Using Predawn and Midday Water Potential, Plant Physiology, 184, 881-894, 10.1104/pp.20.00500, 2020.

Körner, C., Farquhar, G. D., and Wong, S. C.: Carbon isotope discrimination by plants follows latitudinal and altitudinal trends, Oecologia, 88, 30-40, 1991.

Krinner, G., Viovy, N., de Noblet-Ducoudré, N., Ogée, J., Polcher, J., Friedlingstein, P., Ciais, P., Sitch, S., and Prentice, I. C.: A dynamic global vegetation model for studies of the coupled atmosphere-biosphere system, Global Biogeochemical Cycles, 19, https://doi.org/10.1029/2003GB002199, 2005.

Kucharik, C. J., Foley, J. A., Delire, C., Fisher, V. A., Coe, M. T., Lenters, J. D.,

Young-Molling, C., Ramankutty, N., Norman, J. M., and Gower, S. T.: Testing the performance of a dynamic global ecosystem model: Water balance, carbon balance, and vegetation structure, Global Biogeochemical Cycles, 14, 795-825, 10.1029/1999gb001138, 2000.

Kunert, N., Zailaa, J., Herrmann, V., Muller-Landau, H. C., Wright, S. J., Perez, R., McMahon, S. M., Condit, R. C., Hubbell, S. P., Sack, L., Davies, S. J., and Anderson-Teixeira, K. J.: Leaf turgor loss point shapes local and regional distributions of evergreen but not deciduous tropical trees, New Phytol, 230, 485-496, 10.1111/nph.17187, 2021.

Lambers, H., and Poorter, H.: Inherent variation in growth rate between higher plants: a search for physiological causes and ecological consequences, Adv. Ecol. Res., 23, 187-261, 1992.

Lavergne, A., Sandoval, D., Hare, V. J., Graven, H., and Prentice, I. C.: Impacts of soil water stress on the acclimated stomatal limitation of photosynthesis: Insights from stable carbon isotope data, Global Change Biology, 26, 7158-7172, 10.1111/gcb.15364, 2020a.

Lavergne, A., Voelker, S., Csank, A., Graven, H., de Boer, H. J., Daux, V., Robertson, I., Dorado-Linan, I., Martinez-Sancho, E., Battipaglia, G., Bloomfield, K. J., Still, C. J., Meinzer, F. C., Dawson, T. E., Julio Camarero, J., Clisby, R., Fang, Y., Menzel, A., Keen, R. M., Roden, J. S., and Prentice, I. C.: Historical changes in the stomatal limitation of photosynthesis: empirical support for an optimality principle, New Phytologist, 225, 2484-2497, 10.1111/nph.16314, 2020b.

Lawrence, D. M., Fisher, R. A., Koven, C. D., Oleson, K. W., Swenson, S. C., Bonan, G., Collier, N., Ghimire, B., van Kampenhout, L., Kennedy, D., Kluzek, E., Lawrence, P. J., Li, F., Li, H., Lombardozzi, D., Riley, W. J., Sacks, W. J., Shi, M., Vertenstein, M., Wieder, W. R., Xu, C., Ali, A. A., Badger, A. M., Bisht, G., van den Broeke, M., Brunke, M. A., Burns, S. P., Buzan, J., Clark, M., Craig, A., Dahlin, K., Drewniak, B., Fisher, J. B., Flanner, M., Fox, A. M., Gentine, P., Hoffman, F., Keppel-Aleks, G., Knox, R., Kumar, S., Lenaerts, J., Leung, L. R., Lipscomb, W. H., Lu, Y., Pandey, A., Pelletier, J. D., Perket, J., Randerson, J. T., Ricciuto, D. M., Sanderson, B. M., Slater, A., Subin, Z. M., Tang, J., Thomas, R. Q., Val Martin, M., and Zeng, X.: The Community Land Model Version 5: Description of New

Features, Benchmarking, and Impact of Forcing Uncertainty, Journal of Advances in Modeling Earth Systems, 11, 4245-4287, https://doi.org/10.1029/2018MS001583, 2019.

Le Quéré, C., Andrew, R. M., Friedlingstein, P., Sitch, S., Hauck, J., Pongratz, J., Pickers, P. A., Korsbakken, J. I., Peters, G. P., Canadell, J. G., Arneth, A., Arora, V. K., Barbero, L., Bastos, A., Bopp, L., Chevallier, F., Chini, L. P., Ciais, P., Doney, S. C., Gkritzalis, T., Goll, D. S., Harris, I., Haverd, V., Hoffman, F. M., Hoppema, M., Houghton, R. A., Hurtt, G., Ilyina, T., Jain, A. K., Johannessen, T., Jones, C. D., Kato, E., Keeling, R. F., Goldewijk, K. K., Landschützer, P., Lefèvre, N., Lienert, S., Liu, Z., Lombardozzi, D., Metzl, N., Munro, D. R., Nabel, J. E. M. S., Nakaoka, S.-i., Neill, C., Olsen, A., Ono, T., Patra, P., Peregon, A., Peters, W., Peylin, P., Pfeil, B., Pierrot, D., Poulter, B., Rehder, G., Resplandy, L., Robertson, E., Rocher, M., Rödenbeck, C., Schuster, U., Schwinger, J., Séférian, R., Skjelvan, I., Steinhoff, T., Sutton, A., Tans, P. P., Tian, H., Tilbrook, B., Tubiello, F. N., van der Laan-Luijkx, I. T., van der Werf, G. R., Viovy, N., Walker, A. P., Wiltshire, A. J., Wright, R., Zaehle, S., and Zheng, B.: Global Carbon Budget 2018, Earth System Science Data, 10, 2141-2194, 10.5194/essd-10-2141-2018, 2018.

Legendre, P., and Legendre, L. F.: Numerical ecology, 3rd edn. Amsterdam ed., Elsevier, 2012.

Lehnebach, R., Beyer, R., Letort, V., and Heuret, P.: The pipe model theory half a century on: a review, Annals of Botany, 121, 773-795, 10.1093/aob/mcx194, 2018.

Lehner, F., Coats, S., Stocker, T. F., Pendergrass, A. G., Sanderson, B. M., Raible, C. C., and Smerdon, J. E.: Projected drought risk in 1.5˚C and 2˚C warmer climates, Geophysical Research Letters, 44, 7419-7428, 2017.

Li, L., Yang, Z. L., Matheny, A. M., Zheng, H., Swenson, S. C., Lawrence, D. M., Barlage, M., Yan, B., McDowell, N. G., and Leung, L. R.: Representation of Plant Hydraulics in the Noah-MP Land Surface Model: Model Development and Multiscale Evaluation, Journal of Advances in Modeling Earth Systems, 13, e2020MS002214, 10.1029/2020ms002214, 2021.

Li, W., Pacheco-Labrador, J., Migliavacca, M., Miralles, D., Hoek van Dijke, A.,

Reichstein, M., Forkel, M., Zhang, W., Frankenberg, C., Panwar, A., Zhang, Q., Weber, U., Gentine, P., and Orth, R.: Widespread and complex drought effects on vegetation physiology inferred from space, Nature Communications, 14, 4640, 10.1038/s41467-023-40226-9, 2023.

Liang, X., Zhang, T., Lu, X., Ellsworth, D. S., BassiriRad, H., You, C., Wang, D., He, P., Deng, Q., Liu, H., Mo, J., and Ye, Q.: Global response patterns of plant photosynthesis to nitrogen addition: A meta-analysis, Global Change Biology, 26, 3585-3600, 10.1111/gcb.15071, 2020.

Limousin, J. M., Longepierre, D., Huc, R., and Rambal, S.: Change in hydraulic traits of Mediterranean Quercus ilex subjected to long-term throughfall exclusion, Tree Physiology, 30, 1026-1036, 10.1093/treephys/tpq062, 2010.

Limousin, J. M., Roussel, A., Rodriguez-Calcerrada, J., Torres-Ruiz, J. M., Moreno, M., Garcia de Jalon, L., Ourcival, J. M., Simioni, G., Cochard, H., and Martin-StPaul, N.: Drought acclimation of Quercus ilex leaves improves tolerance to moderate drought but not resistance to severe water stress, Plant, Cell & Environment, 45, 1967-1984, 10.1111/pce.14326, 2022.

Lin, Y.-S., Medlyn, B. E., Duursma, R. A., Prentice, I. C., Wang, H., Baig, S., Eamus, D., de Dios, Victor R., Mitchell, P., Ellsworth, D. S., de Beeck, M. O., Wallin, G., Uddling, J., Tarvainen, L., Linderson, M.-L., Cernusak, L. A., Nippert, J. B., Ocheltree, T. W., Tissue, D. T., Martin-StPaul, N. K., Rogers, A., Warren, J. M., De Angelis, P., Hikosaka, K., Han, Q., Onoda, Y., Gimeno, T. E., Barton, C. V. M., Bennie, J., Bonal, D., Bosc, A., Löw, M., Macinins-Ng, C., Rey, A., Rowland, L., Setterfield, S. A., Tausz-Posch, S., Zaragoza-Castells, J., Broadmeadow, M. S. J., Drake, J. E., Freeman, M., Ghannoum, O., Hutley, Lindsay B., Kelly, J. W., Kikuzawa, K., Kolari, P., Koyama, K., Limousin, J.-M., Meir, P., Lola da Costa, A. C., Mikkelsen, T. N., Salinas, N., Sun, W., and Wingate, L.: Optimal stomatal behaviour around the world, Nature Climate Change, 5, 459-464, 10.1038/nclimate2550, 2015.

Liu, H., Gleason, S. M., Hao, G., Hua, L., He, P., Goldstein, G., and Ye, Q.: Hydraulic traits are coordinated with maximum plant height at the global scale, Science Advances, 5, eaav1332, 2019.

Liu, H., Ye, Q., Gleason, S. M., He, P., and Yin, D.: Weak tradeoff between xylem hydraulic efficiency and safety: climatic seasonality matters, New Phytologist, 229, 1440-1452, 10.1111/nph.16940, 2021.

Liu, H., Ye, Q., Simpson, K. J., Cui, E., and Xia, J.: Can evolutionary history predict plant plastic responses to climate change?, New Phytologist, 235, 1260-1271, 10.1111/nph.18194, 2022.

Lovie, P.: Coefficient of Variation, in: Encyclopedia of Statistics in Behavioral Science, 2005.

Luo, Y., Su, B., Currie, W. S., Dukes, J. S., Finzi, A., Hartwig, U., Hungate, B., McMurtrie, R. E., Oren, R., Parton, W. J., Pataki, D. E., Shaw, R. M., Zak, D. R., and Field, C. B.: Progressive Nitrogen Limitation of Ecosystem Responses to Rising Atmospheric Carbon Dioxide, BioScience, 54, 731-739, 10.1641/0006-3568(2004)054[0731:Pnloer]2.0.Co;2, 2004.

Ma, S., Baldocchi, D. D., Mambelli, S., and Dawson, T. E.: Are temporal variations of leaf traits responsible for seasonal and inter-annual variability in ecosystem CO2exchange?, Functional Ecology, 25, 258-270, 10.1111/j.1365-2435.2010.01779.x, 2010.

Magnani, F., Mencuccini, M., and Grace, J.: Age-related decline in stand productivity: the role of structural acclimation under hydraulic constraints, Plant, Cell & Environment, 23, 251-263, 2000.

Magnani, F., Grace, J., and Borghetti, M.: Adjustment of tree structure in response to the environment under hydraulic constraints, Functional Ecology, 16, 385-393, https://doi.org/10.1046/j.1365-2435.2002.00630.x, 2002.

Maia, V. A., Santos, A. B. M., de Aguiar-Campos, N., de Souza, C. R., de Oliveira, M. C. F., Coelho, P. A., Morel, J. D., da Costa, L. S., Farrapo, C. L., Fagundes, N. C. A., de Paula, G. G. P., Santos, P. F., Gianasi, F. M., da Silva, W. B., de Oliveira, F., Girardelli, D. T., de Carvalho Araújo, F., Vilela, T. A., Pereira, R. T., da Silva, L. C. A., de Oliveira Menino, G. C., Garcia, P. O., Fontes, M. A. L., and dos Santos, R. M.: The carbon sink of tropical seasonal forests in southeastern Brazil can be under threat, Science Advances, 6, eabd4548, doi:10.1126/sciadv.abd4548,

2020.

Maire, V., Martre, P., Kattge, J., Gastal, F., Esser, G., Fontaine, S., and Soussana, J.-F.: The coordination of leaf photosynthesis links C and N fluxes in C3 plant species, PLoS One, 7, e38345, 2012.

Mammola, S., Cardoso, P., and Poisot, T.: Functional diversity metrics using kernel density n-dimensional hypervolumes, Methods in Ecology and Evolution, 00, 1-10, 10.1111/2041-210x.13424, 2020.

Mantova, M., Cochard, H., Burlett, R., Delzon, S., King, A., Rodriguez-Dominguez, C. M., Ahmed, M. A., Trueba, S., and Torres-Ruiz, J. M.: On the path from xylem hydraulic failure to downstream cell death, New Phytologist, 237, 793-806, 10.1111/nph.18578, 2023.

Maréchaux, I., Bartlett, M. K., Sack, L., Baraloto, C., Engel, J., Joetzjer, E., Chave, J., and Kitajima, K.: Drought tolerance as predicted by leaf water potential at turgor loss point varies strongly across species within an Amazonian forest, Functional Ecology, 29, 1268-1277, 10.1111/1365-2435.12452, 2015.

Markesteijn, L., Poorter, L., Paz, H., Sack, L., and Bongers, F.: Ecological differentiation in xylem cavitation resistance is associated with stem and leaf structural traits, Plant, Cell & Environment, 34, 137-148, 10.1111/j.1365-3040.2010.02231.x, 2011.

Martín Belda, D., Anthoni, P., Wårlind, D., Olin, S., Schurgers, G., Tang, J., Smith, B., and Arneth, A.: LPJ-GUESS/LSMv1.0: a next-generation land surface model with high ecological realism, Geoscientific Model Development, 15, 6709-6745, 10.5194/gmd-15-6709-2022, 2022.

Martin-StPaul, N., Delzon, S., and Cochard, H.: Plant resistance to drought depends on timely stomatal closure, Ecology Letters, 20, 1437-1447, 10.1111/ele.12851, 2017.

Martinez-Vilalta, J., Cochard, H., Mencuccini, M., Sterck, F., Herrero, A., Korhonen, J. F., Llorens, P., Nikinmaa, E., Nole, A., Poyatos, R., Ripullone, F., Sass-Klaassen, U., and Zweifel, R.: Hydraulic adjustment of Scots pine across

Europe, New Phytologist, 184, 353-364, 10.1111/j.1469-8137.2009.02954.x, 2009.

Martínez-Vilalta, J., and Garcia-Forner, N.: Water potential regulation, stomatal behaviour and hydraulic transport under drought: deconstructing the iso/anisohydric concept, Plant, Cell & Environment, 40, 962-976, 10.1111/pce.12846, 2017.

Matzner, S., and Comstock, J.: The temperature dependence of shoot hydraulic resistance: implications for stomatal behaviour and hydraulic limitation, Plant, Cell & Environment, 24, 1299-1307, https://doi.org/10.1046/j.0016-8025.2001.00785.x, 2001.

McBranch, N. A., Grossiord, C., Adams, H., Borrego, I., Collins, A. D., Dickman, T., Ryan, M., Sevanto, S., and McDowell, N. G.: Lack of acclimation of leaf area:sapwood area ratios in pinon pine and juniper in response to precipitation reduction and warming, Tree Physiology, 39, 135-142, 10.1093/treephys/tpy066, 2019.

McDowell, N. G., Sapes, G., Pivovaroff, A., Adams, H. D., Allen, C. D., Anderegg, W. R. L., Arend, M., Breshears, D. D., Brodribb, T., Choat, B., Cochard, H., De Cáceres, M., De Kauwe, M. G., Grossiord, C., Hammond, W. M., Hartmann, H., Hoch, G., Kahmen, A., Klein, T., Mackay, D. S., Mantova, M., Martínez-Vilalta, J., Medlyn, B. E., Mencuccini, M., Nardini, A., Oliveira, R. S., Sala, A., Tissue, D. T., Torres-Ruiz, J. M., Trowbridge, A. M., Trugman, A. T., Wiley, E., and Xu, C.: Mechanisms of woody-plant mortality under rising drought, CO2 and vapour pressure deficit, Nature Reviews Earth & Environment, 3, 294-308, 10.1038/s43017-022-00272-1, 2022.

McKown, A. D., Guy, R. D., Azam, M. S., Drewes, E. C., and Quamme, L. K.: Seasonality and phenology alter functional leaf traits, Oecologia, 172, 653-665, 10.1007/s00442-012-2531-5, 2013.

Meinzer, F., Woodruff, D. R., Marias, D. E., Mcculloh, K. A., and Sevanto, S.: Dynamics of leaf water relations components in co-occurring iso- and anisohydric conifer species, Plant, Cell & Environment, 37, 2577-2586, https://doi.org/10.1111/pce.12327, 2014.

Meinzer, F. C., Campanello, P. I., Domec, J.-C., Gatti, M. G., Goldstein, G., Villalobos-Vega, R., and Woodruff, D. R.: Constraints on physiological function associated with branch architecture and wood density in tropical forest trees, Tree Physiology, 28, 1609-1617, 2008.

Meinzer, F. C., McCulloh, K. A., Lachenbruch, B., Woodruff, D. R., and Johnson, D. M.: The blind men and the elephant: the impact of context and scale in evaluating conflicts between plant hydraulic safety and efficiency, Oecologia, 164, 287-296, 10.1007/s00442-010-1734-x, 2010.

Mencuccini, M., Manzoni, S., and Christoffersen, B.: Modelling water fluxes in plants: from tissues to biosphere, New Phytologist, 222, 1207-1222, 10.1111/nph.15681, 2019a.

Mencuccini, M., Rosas, T., Rowland, L., Choat, B., Cornelissen, H., Jansen, S., Kramer, K., Lapenis, A., Manzoni, S., Niinemets, U., Reich, P., Schrodt, F., Soudzilovskaia, N., Wright, I. J., and Martinez-Vilalta, J.: Leaf economics and plant hydraulics drive leaf : wood area ratios, New Phytologist, 224, 1544-1556, 10.1111/nph.15998, 2019b.

Méndez-Alonzo, R., Paz, H., Zuluaga, R. C., Rosell, J. A., and Olson, M. E.: Coordinated evolution of leaf and stem economics in tropical dry forest trees, Ecology, 93, 2397-2406, https://doi.org/10.1890/11-1213.1, 2012.

Meng, T. T., Wang, H., Harrison, S. P., Prentice, I. C., Ni, J., and Wang, G.: Responses of leaf traits to climatic gradients: adaptive variation versus compositional shifts, Biogeosciences, 12, 5339-5352, 10.5194/bg-12-5339-2015, 2015.

Mengoli, G., Agustí-Panareda, A., Boussetta, S., Harrison, S. P., Trotta, C., and Prentice, I. C.: Ecosystem Photosynthesis in Land-Surface Models: A First-Principles Approach Incorporating Acclimation, Journal of Advances in Modeling Earth Systems, 14, e2021MS002767, 10.1029/2021ms002767, 2022.

Moran, E. V., Hartig, F., and Bell, D. M.: Intraspecific trait variation across scales: implications for understanding global change responses, Global Change Biology, 22, 137-150, 10.1111/gcb.13000, 2016.

Nadal, M., Clemente-Moreno, M. J., Perera-Castro, A. V., Roig-Oliver, M., Onoda, Y., Gulias, J., and Flexas, J.: Incorporating pressure-volume traits into the leaf economics spectrum, Ecology Letters, 26, 549-562, 10.1111/ele.14176, 2023.

Nadal-Sala, D., Grote, R., Birami, B., Knüver, T., Rehschuh, R., Schwarz, S., and Ruehr, N. K.: Leaf Shedding and Non-Stomatal Limitations of Photosynthesis Mitigate Hydraulic Conductance Losses in Scots Pine Saplings During Severe Drought Stress, Frontiers in Plant Science, 12, 715127, 10.3389/fpls.2021.715127, 2021.

Niccoli, F., Kabala, J. P., Pacheco-Solana, A., and Battipaglia, G.: Impact of Intra Annual Wood Density Fluctuation on Tree Hydraulic Function: Insights from a Continuous Monitoring Approach, Tree Physiology, 44, tpad145, 10.1093/treephys/tpad145, 2023.

O'Sullivan, M., Friedlingstein, P., Sitch, S., Anthoni, P., Arneth, A., Arora, V. K., Bastrikov, V., Delire, C., Goll, D. S., Jain, A., Kato, E., Kennedy, D., Knauer, J., Lienert, S., Lombardozzi, D., McGuire, P. C., Melton, J. R., Nabel, J., Pongratz, J., Poulter, B., Seferian, R., Tian, H., Vuichard, N., Walker, A. P., Yuan, W., Yue, X., and Zaehle, S.: Process-oriented analysis of dominant sources of uncertainty in the land carbon sink, Nature Communications, 13, 4781, 10.1038/s41467-022-32416-8, 2022.

Oberpriller, J., Herschlein, C., Anthoni, P., Arneth, A., Krause, A., Rammig, A., Lindeskog, M., Olin, S., and Hartig, F.: Climate and parameter sensitivity and induced uncertainties in carbon stock projections for European forests (using LPJ-GUESS 4.0), Geoscientific Model Development, 15, 6495-6519, 10.5194/gmd-15-6495-2022, 2022.

Ocheltree, T. W., Nippert, J. B., and Prasad, P. V.: A safety vs efficiency trade-off identified in the hydraulic pathway of grass leaves is decoupled from photosynthesis, stomatal conductance and precipitation, New Phytologist, 210, 97-107, 10.1111/nph.13781, 2016.

Oksanen, J., Blanchet, F. G., Friendly, M., Kindt, R., Legendre, P., McGlinn, D., Minchin, P. R., O'hara, R., Simpson, G. L., Solymos, P., Stevens, M. H. H., Szoecs, E., and Wagner, H.: vegan: Community Ecology Package. R package version

2.4-4., 2, 1-295, 2017.

Oliveira, R. S., Eller, C. B., Barros, F. V., Hirota, M., Brum, M., and Bittencourt, P.: Linking plant hydraulics and the fast-slow continuum to understand resilience to drought in tropical ecosystems, New Phytologist, 230, 904-923, 10.1111/nph.17266, 2021.

Olson, M. E., Anfodillo, T., Gleason, S. M., and McCulloh, K. A.: Tip-to-base xylem conduit widening as an adaptation: causes, consequences, and empirical priorities, New Phytologist, 229, 1877-1893, 10.1111/nph.16961, 2021.

Onoda, Y., Hikosaka, K., and Hirose, T.: Allocation of nitrogen to cell walls decreases photosynthetic nitrogen-use efficiency, Funct. Ecol., 18, 419-425, 2004.

Ordoñez, J. C., van Bodegom, P. M., Witte, J.-P. M., Wright, I. J., Reich, P. B., and Aerts, R.: A global study of relationships between leaf traits, climate and soil measures of nutrient fertility, Glob. Ecol. Biogeogr., 18, 137-149, 10.1111/j.1466-8238.2008.00441.x, 2009.

Pappas, C., Fatichi, S., and Burlando, P.: Modeling terrestrial carbon and water dynamics across climatic gradients: does plant trait diversity matter?, New Phytologist, 209, 137-151, 10.1111/nph.13590, 2016.

Park Williams, A., Allen, C. D., Macalady, A. K., Griffin, D., Woodhouse, C. A., Meko, D. M., Swetnam, T. W., Rauscher, S. A., Seager, R., Grissino-Mayer, H. D., Dean, J. S., Cook, E. R., Gangodagamage, C., Cai, M., and McDowell, N. G.: Temperature as a potent driver of regional forest drought stress and tree mortality, Nature Climate Change, 3, 292-297, 10.1038/nclimate1693, 2012.

Pavlick, R., Drewry, D. T., Bohn, K., Reu, B., and Kleidon, A.: The Jena Diversity-Dynamic Global Vegetation Model (JeDi-DGVM): a diverse approach to representing terrestrial biogeography and biogeochemistry based on plant functional trade-offs, Biogeosciences, 10, 4137-4177, 10.5194/bg-10-4137-2013, 2013.

Peltoniemi, M. S., Duursma, R. A., and Medlyn, B. E.: Co-optimal distribution of

leaf nitrogen and hydraulic conductance in plant canopies, Tree Physiol., 32, 510-519, 10.1093/treephys/tps023, 2012.

Peng, Y., Bloomfield, K. J., and Prentice, I. C.: A theory of plant function helps to explain leaf-trait and productivity responses to elevation, New Phytologist, 226, 1274-1284, 10.1111/nph.16447, 2020.

Peng, Y., Bloomfield, K. J., Cernusak, L. A., Domingues, T. F., and Colin Prentice, I.: Global climate and nutrient controls of photosynthetic capacity, Communications Biology, 4, 462, 10.1038/s42003-021-01985-7, 2021.

Pfennigwerth, A. A., Bailey, J. K., and Schweitzer, J. A.: Trait variation along elevation gradients in a dominant woody shrub is population-specific and driven by plasticity, Aob Plants, 9, plx027, 10.1093/aobpla/plx027, 2017.

Piao, S., Wang, X., Park, T., Chen, C., Lian, X., He, Y., Bjerke, J. W., Chen, A., Ciais, P., Tømmervik, H., Nemani, R. R., and Myneni, R. B.: Characteristics, drivers and feedbacks of global greening, Nature Reviews Earth & Environment, 1, 14-27, 10.1038/s43017-019-0001-x, 2019.

Pigliucci, M.: Phenotypic integration: studying the ecology and evolution of complex phenotypes, Ecology Letters, 6, 265-272, 10.1046/j.1461-0248.2003.00428.x, 2003.

Pittermann, J., Choat, B., Jansen, S., Stuart, S. A., Lynn, L., and Dawson, T. E.: The relationships between xylem safety and hydraulic efficiency in the Cupressaceae: the evolution of pit membrane form and function, Plant Physiology, 153, 1919-1931, 10.1104/pp.110.158824, 2010.

Pivovaroff, A. L., Sack, L., and Santiago, L. S.: Coordination of stem and leaf hydraulic conductance in southern California shrubs: a test of the hydraulic segmentation hypothesis, New Phytologist, 203, 842-850, 10.1111/nph.12850, 2014.

Pivovaroff, A. L., Cook, V. M. W., and Santiago, L. S.: Stomatal behaviour and stem xylem traits are coordinated for woody plant species under exceptional drought conditions, Plant, Cell & Environment, 41, 2617-2626,

10.1111/pce.13367, 2018.

Pivovaroff, A. L., McDowell, N. G., Rodrigues, T. B., Brodribb, T., Cernusak, L. A., Choat, B., Grossiord, C., Ishida, Y., Jardine, K. J., Laurance, S., Leff, R., Li, W., Liddell, M., Mackay, D. S., Pacheco, H., Peters, J., de, J. S. F. I., Souza, D. C., Wang, W., Zhang, P., and Chambers, J.: Stability of tropical forest tree carbon-water relations in a rainfall exclusion treatment through shifts in effective water uptake depth, Global Change Biology, 27, 6454-6466, 10.1111/gcb.15869, 2021.

Poggiato, G., Gaüzere, P., Martinez-Almoyna, C., Deschamps, G., Renaud, J., Violle, C., Münkemüller, T., and Thuiller, W.: Predicting combinations of community mean traits using joint modelling, Global Ecology and Biogeography, 32, 1409-1422, 10.1111/geb.13706, 2023.

Poorter, H., Niinemets, U., Poorter, L., Wright, I. J., and Villar, R.: Causes and consequences of variation in leaf mass per area (LMA): a meta-analysis, New Phytologist, 182, 565-588, 10.1111/j.1469-8137.2009.02830.x, 2009.

Poorter, L., McDonald, I., Alarcon, A., Fichtler, E., Licona, J. C., Pena-Claros, M., Sterck, F., Villegas, Z., and Sass-Klaassen, U.: The importance of wood traits and hydraulic conductance for the performance and life history strategies of 42 rainforest tree species, New Phytologist, 185, 481-492, 10.1111/j.1469-8137.2009.03092.x, 2010.

Prentice, I. C., Dong, N., Gleason, S. M., Maire, V., and Wright, I. J.: Balancing the costs of carbon gain and water transport: testing a new theoretical framework for plant functional ecology, Ecology Letters, 17, 82-91, 10.1111/ele.12211, 2014a.

Prentice, I. C., Dong, N., Gleason, S. M., Vincent, M., and Wright, I. J.: Balancing the costs of carbon gain and water transport: testing a new theoretical framework for plant functional ecology, Ecol. Lett., 17, 82-91, 2014b.

Prentice, I. C., Liang, X., Medlyn, B. E., and Wang, Y.-P.: Reliable, robust and realistic: the three R's of next-generation land-surface modelling, Atmospheric Chemistry and Physics, 15, 5987-6005, 2015.

Preston, K. A., Cornwell, W. K., and Denoyer, J. L.: Wood density and vessel traits

as distinct correlates of ecological strategy in 51 California coast range angiosperms, New Phytologist, 170, 807-818, 10.1111/j.1469-8137.2006.01712.x, 2006.

Quillet, A., Peng, C., and Garneau, M.: Toward dynamic global vegetation models for simulating vegetation–climate interactions and feedbacks: recent developments, limitations, and future challenges, Environmental Reviews, 18, 333-353, 2010.

Reich, P. B., Walters, M. B., and Ellsworth, D. S.: From tropics to tundra: global convergence in plant functioning, Proceedings of the National Academy of Sciences, 94, 13730-13734, 1997.

Reich, P. B., and Cornelissen, H.: The world-wide 'fast-slow' plant economics spectrum: a traits manifesto, Journal of Ecology, 102, 275-301, 10.1111/1365-2745.12211, 2014.

Reid, D. E., Silins, U., Mendoza, C., and Lieffers, V. J.: A unified nomenclature for quantification and description of water conducting properties of sapwood xylem based on Darcy's law, Tree physiology, 25, 993-1000, 2005.

Richardson, A. D., Keenan, T. F., Migliavacca, M., Ryu, Y., Sonnentag, O., and Toomey, M.: Climate change, phenology, and phenological control of vegetation feedbacks to the climate system, Agricultural and Forest Meteorology, 169, 156-173, https://doi.org/10.1016/j.agrformet.2012.09.012, 2013.

Rodríguez Casal, A., and Pateiro López, B.: Generalizing the convex hull of a sample: the R package alphahull, Journal of Statistical Software, 34, 1-28, 10.18637/jss.v034.i05, 2010.

Rodriguez-Dominguez, C. M., Buckley, T. N., Egea, G., de Cires, A., Hernandez-Santana, V., Martorell, S., and Diaz-Espejo, A.: Most stomatal closure in woody species under moderate drought can be explained by stomatal responses to leaf turgor, Plant, Cell & Environment, 39, 2014-2026, 10.1111/pce.12774, 2016.

Rodriguez-Dominguez, C. M., and Brodribb, T. J.: Declining root water transport drives stomatal closure in olive under moderate water stress, New Phytologist,

225, 126-134, 10.1111/nph.16177, 2020.

Rokka, A., Zhang, L., and Aro, E. M.: Rubisco activase: an enzyme with a temperature-dependent dual function?, Plant J., 25, 463-471, 2010.

Rosas, T., Mencuccini, M., Barba, J., Cochard, H., Saura-Mas, S., and Martinez-Vilalta, J.: Adjustments and coordination of hydraulic, leaf and stem traits along a water availability gradient, New Phytologist, 223, 632-646, 10.1111/nph.15684, 2019.

Rosseel, Y.: Lavaan: An R package for structural equation modeling and more. Version 0.5–12 (BETA), Journal of statistical software, 48, 1-36, 2012.

Rowland, L., da Costa, A. C., Galbraith, D. R., Oliveira, R. S., Binks, O. J., Oliveira, A. A., Pullen, A. M., Doughty, C. E., Metcalfe, D. B., Vasconcelos, S. S., Ferreira, L. V., Malhi, Y., Grace, J., Mencuccini, M., and Meir, P.: Death from drought in tropical forests is triggered by hydraulics not carbon starvation, Nature, 528, 119-122, 10.1038/nature15539, 2015.

Rowland, L., Oliveira, R. S., Bittencourt, P. R. L., Giles, A. L., Coughlin, I., Costa, P. B., Domingues, T., Ferreira, L. V., Vasconcelos, S. S., Junior, J. A. S., Oliveira, A. A. R., da Costa, A. C. L., Meir, P., and Mencuccini, M.: Plant traits controlling growth change in response to a drier climate, New Phytologist, 229, 1363-1374, 10.1111/nph.16972, 2021.

Rowland, L., Ramirez-Valiente, J. A., Hartley, I. P., and Mencuccini, M.: How woody plants adjust above- and below-ground traits in response to sustained drought, New Phytologist, 239, 1173-1189, 10.1111/nph.19000, 2023.

Ruffault, J., Limousin, J. M., Pimont, F., Dupuy, J. L., De Caceres, M., Cochard, H., Mouillot, F., Blackman, C. J., Torres-Ruiz, J. M., Parsons, R. A., Moreno, M., Delzon, S., Jansen, S., Olioso, A., Choat, B., and Martin-StPaul, N.: Plant hydraulic modelling of leaf and canopy fuel moisture content reveals increasing vulnerability of a Mediterranean forest to wildfires under extreme drought, New Phytologist, 237, 1256-1269, 10.1111/nph.18614, 2023.

Sabot, M. E. B., De Kauwe, M. G., Pitman, A. J., Medlyn, B. E., Ellsworth, D. S.,

Martin-StPaul, N. K., Wu, J., Choat, B., Limousin, J. M., Mitchell, P. J., Rogers, A., and Serbin, S. P.: One Stomatal Model to Rule Them All? Toward Improved Representation of Carbon and Water Exchange in Global Models, Journal of Advances in Modeling Earth Systems, 14, e2021MS002761, 10.1029/2021ms002761, 2022.

Sack, L., and Holbrook, N. M.: Leaf hydraulics, Annual Review of Plant Biology, 57, 361-381, 10.1146/, 2006.

Sack, L., Scoffoni, C., John, G. P., Poorter, H., Mason, C. M., Mendez-Alonzo, R., and Donovan, L. A.: How do leaf veins influence the worldwide leaf economic spectrum? Review and synthesis, Journal of Experimental Botany, 64, 4053-4080, 10.1093/jxb/ert316, 2013.

Sakschewski, B., von Bloh, W., Boit, A., Poorter, L., Peña-Claros, M., Heinke, J., Joshi, J., and Thonicke, K.: Resilience of Amazon forests emerges from plant trait diversity, Nature Climate Change, 6, 1032-1036, 10.1038/nclimate3109, 2016.

Salomón, R. L., Limousin, J.-M., Ourcival, J.-M., Rodríguez-Calcerrada, J., and Steppe, K.: Stem hydraulic capacitance decreases with drought stress: implications for modelling tree hydraulics in the Mediterranean oak Quercus ilex, Plant, Cell & Environment, 40, 1379-1391, https://doi.org/10.1111/pce.12928, 2017.

Sanchez-Martinez, P., Martínez-Vilalta, J., Dexter, K. G., Segovia, R. A., Mencuccini, M., and Cleland, E.: Adaptation and coordinated evolution of plant hydraulic traits, Ecology Letters, 23, 1599-1610, 10.1111/ele.13584, 2020.

Santiago, L. S., Goldstein, G., Meinzer, F. C., Fisher, J. B., Machado, K., Woodruff, D., and Jones, T.: Leaf photosynthetic traits scale with hydraulic conductivity and wood density in Panamanian forest canopy trees, Oecologia, 140, 543-550, 10.1007/s00442-004-1624-1, 2004.

Santiago, L. S., De Guzman, M. E., Baraloto, C., Vogenberg, J. E., Brodie, M., Herault, B., Fortunel, C., and Bonal, D.: Coordination and trade-offs among hydraulic safety, efficiency and drought avoidance traits in Amazonian rainforest

canopy tree species, New Phytologist, 218, 1015-1024, 10.1111/nph.15058, 2018.

Sapes, G., Demaree, P., Lekberg, Y., and Sala, A.: Plant carbohydrate depletion impairs water relations and spreads via ectomycorrhizal networks, New Phytologist, 229, 3172-3183, 10.1111/nph.17134, 2021.

Savi, T., Love, V. L., Dal Borgo, A., Martellos, S., and Nardini, A.: Morpho-anatomical and physiological traits in saplings of drought-tolerant Mediterranean woody species, Trees, 31, 1137-1148, 10.1007/s00468-017-1533-7, 2017.

Saxton, K. E., and Rawls, W. J.: Soil Water Characteristic Estimates by Texture and Organic Matter for Hydrologic Solutions, Soil Science Society of America Journal, 70, 1569-1578, 10.2136/sssaj2005.0117, 2006.

Scheiter, S., Langan, L., and Higgins, S. I.: Next-generation dynamic global vegetation models: learning from community ecology, New Phytologist, 198, 957-969, 10.1111/nph.12210, 2013.

Schimel, D., Stephens, B. B., and Fisher, J. B.: Effect of increasing CO2 on the terrestrial carbon cycle, Proceedings of the National Academy of Sciences, 112, 436-441, doi:10.1073/pnas.1407302112, 2015.

Schneider, F. D., Morsdorf, F., Schmid, B., Petchey, O. L., Hueni, A., Schimel, D. S., and Schaepman, M. E.: Mapping functional diversity from remotely sensed morphological and physiological forest traits, Nature Communications, 8, 1441, 10.1038/s41467-017-01530-3, 2017.

Scoffoni, C., Chatelet, D. S., Pasquet-Kok, J., Rawls, M., Donoghue, M. J., Edwards, E. J., and Sack, L.: Hydraulic basis for the evolution of photosynthetic productivity, Nat. Plants, 2, 16072, 10.1038/nplants.2016.72, 2016.

Seddon, A. W., Macias-Fauria, M., Long, P. R., Benz, D., and Willis, K. J.: Sensitivity of global terrestrial ecosystems to climate variability, Nature, 531, 229-232, 10.1038/nature16986, 2016.

Settele, J., Scholes, R., Betts, R. A., Bunn, S., Leadley, P., Nepstad, D., Overpeck, J., Taboada, M. A., Fischlin, A., and Moreno, J. M.: Terrestrial and inland water systems, in: Climate Change 2014 Impacts, Adaptation and Vulnerability: Part A:

Global and Sectoral Aspects, Cambridge University Press, 271-360, 2015.

Shinozaki, K., Yoda, K., Hozumi, K., and Kira, T.: A quantitative analysis of plant form – the pipe model theory. II. Further evidence of the theory and its application in forest ecology, Japanese Journal of Ecology, 14, 133-139, 10.18960/seitai.14.4_133, 1964.

Sitch, S., Smith, B., Prentice, I. C., Arneth, A., Bondeau, A., Cramer, W., Kaplan, J. O., Levis, S., Lucht, W., Sykes, M. T., Thonicke, K., and Venevsky, S.: Evaluation of ecosystem dynamics, plant geography and terrestrial carbon cycling in the LPJ dynamic global vegetation model, Global Change Biology, 9, 161-185, 2003.

Sitch, S., Huntingford, C., Gedney, N., Levy, P. E., Lomas, M., Piao, S. L., Betts, R., Ciais, P., Cox, P., Friedlingstein, P., Jones, C. D., Prentice, I. C., and Woodward, F. I.: Evaluation of the terrestrial carbon cycle, future plant geography and climate-carbon cycle feedbacks using five Dynamic Global Vegetation Models (DGVMs), Global Change Biology, 14, 2015-2039, 10.1111/j.1365-2486.2008.01626.x, 2008.

Smith, N. G., and Dukes, J. S.: Short-term acclimation to warmer temperatures accelerates leaf carbon exchange processes across plant types, Global Change Biology, 13, 4840-4853, 2017a.

Smith, N. G., and Dukes, J. S.: Short-term acclimation to warmer temperatures accelerates leaf carbon exchange processes across plant types, Glob. Change Biol., 23, 4840-4853, 10.1111/gcb.13735, 2017b.

Smith, N. G., Lombardozzi, D., Tawfik, A., Bonan, G., and Dukes, J. S.: Biophysical consequences of photosynthetic temperature acclimation for climate: Temperature acclimation and climate, J. Adv. Model. Earth Syst., 9, 536-547, 2017a.

Smith, N. G., Lombardozzi, D., Tawfik, A., Bonan, G., and Dukes, J. S.: Biophysical consequences of photosynthetic temperature acclimation for climate, Journal of Advances in Modeling Earth Systems, 9, 536-547, 2017b.

Smith, N. G., Keenan, T. F., Colin Prentice, I., Wang, H., Wright, I. J., Niinemets, U., Crous, K. Y., Domingues, T. F., Guerrieri, R., Yoko Ishida, F., Kattge, J., Kruger, E. L., Maire, V., Rogers, A., Serbin, S. P., Tarvainen, L., Togashi, H. F., Townsend, P. A., Wang, M., Weerasinghe, L. K., and Zhou, S. X.: Global photosynthetic capacity is optimized to the environment, Ecol. Lett., 22, 506-517, 10.1111/ele.13210, 2019.

Song, C., Xu, W., Li, S., Liu, H., Chu, C., He, B., Chen, X., Piao, S., Lu, H., Ma, M., and Yuan, W.: Differential tree demography mediated by water stress and functional traits in a moist tropical forest, Functional Ecology, 37, 2927-2939, 10.1111/1365-2435.14424, 2023.

Song, X., and Zeng, X.: Investigation of uncertainties of establishment schemes in dynamic global vegetation models, Advances in Atmospheric Sciences, 31, 85-94, 10.1007/s00376-013-3031-1, 2014.

Sperry, J. S., Donnelly, J. R., and Tyree, M. T.: A method for measuring hydraulic conductivity and embolism in xylem, Plant, Cell & Environment, 11, 35-40, 1988.

Sperry, J. S., Adler, F. R., Campbell, G. S., and Comstock, J. P.: Limitation of plant water use by rhizosphere and xylem conductance: Results from a model, Plant, Cell & Environment, 21, 347-359, 1998.

Sperry, J. S.: Hydraulic constraints on plant gas exchange, Agricultural and Forest Meteorology, 104, 13-23, https://doi.org/10.1016/S0168-1923(00)00144-1, 2000.

Sperry, J. S., Meinzer, F. C., and McCulloh, K. A.: Safety and efficiency conflicts in hydraulic architecture: scaling from tissues to trees, Plant, Cell & Environment, 31, 632-645, 10.1111/j.1365-3040.2007.01765.x, 2008.

Sperry, J. S., and Love, D. M.: What plant hydraulics can tell us about responses to climate-change droughts, New Phytologist, 207, 14-27, 10.1111/nph.13354, 2015.

Sperry, J. S., Wang, Y., Wolfe, B. T., Mackay, D. S., Anderegg, W. R., McDowell, N. G., and Pockman, W. T.: Pragmatic hydraulic theory predicts stomatal responses to climatic water deficits, New Phytologist, 212, 577-589,

10.1111/nph.14059, 2016.

Sperry, J. S., Venturas, M. D., Anderegg, W. R. L., Mencuccini, M., Mackay, D. S., Wang, Y., and Love, D. M.: Predicting stomatal responses to the environment from the optimization of photosynthetic gain and hydraulic cost, Plant, Cell & Environment, 40, 816-830, doi:10.1111/pce.12852, 2017.

Stewart, K., Carmona, C. P., Clements, C., Venditti, C., Tobias, J. A., and González-Suárez, M.: Functional diversity metrics can perform well with highly incomplete data sets, Methods in Ecology and Evolution, 14, 2856-2872, https://doi.org/10.1111/2041-210X.14202, 2023.

Stocker, B. D., Zscheischler, J., Keenan, T. F., Prentice, I. C., Peñuelas, J., and Seneviratne, S. I.: Quantifying soil moisture impacts on light use efficiency across biomes, New Phytologist, 218, 1430-1449, https://doi.org/10.1111/nph.15123, 2018.

Stocker, B. D., Wang, H., Smith, N. G., Harrison, S. P., Keenan, T. F., Sandoval, D., Davis, T., and Prentice, I. C.: P-model v1.0: an optimality-based light use efficiency model for simulating ecosystem gross primary production, Geoscientific Model Development, 13, 1545-1581, 10.5194/gmd-13-1545-2020, 2020.

Stocker, T. F., Qin, D., Plattner, G.-K., Tignor, M., Allen, S. K., Boschung, J., Nauels, A., Xia, Y., Bex, V., and Midgley, P. M.: Climate change 2013: The physical science basis. Cambridge University Press Cambridge, 2013.

Terashima, I., Masuzawa, T., Ohba, H., and Yokoi, Y.: Is photosynthesis suppressed at higher elevations due to low CO_2 pressure?, Ecology, 76, 2663-2668, 1995.

Togashi, H. F., Prentice, I. C., Evans, B. J., Forrester, D. I., Drake, P., Feikema, P., Brooksbank, K., Eamus, D., and Taylor, D.: Morphological and moisture availability controls of the leaf area-to-sapwood area ratio: analysis of measurements on Australian trees, Ecology and Evolution, 5, 1263-1270, 10.1002/ece3.1344, 2015.

Torres-Ruiz, J. M., Cochard, H., Delzon, S., Boivin, T., Burlett, R., Cailleret, M., Corso, D., Delmas, C. E. L., De Caceres, M., Diaz-Espejo, A., Fernández-Conradi, P., Guillemot, J., Lamarque, L. J., Limousin, J.-M., Mantova, M., Mencuccini, M., Morin, X., Pimont, F., De Dios, V. R., Ruffault, J., Trueba, S., and Martin-StPaul, N. K.: Plant hydraulics at the heart of plant, crops and ecosystem functions in the face of climate change, New Phytologist, 241, 984-999, https://doi.org/10.1111/nph.19463, 2024.

Towers, I. R., Vesk, P. A., Wenk, E. H., Gallagher, R. V., Windecker, S. M., Wright, I. J., and Falster, D. S.: Revisiting the role of mean annual precipitation in shaping functional trait distributions at a continental scale, New Phytologist, 241, 1900-1909, 10.1111/nph.19478, 2023.

Tripathy, K. P., Mukherjee, S., Mishra, A. K., Mann, M. E., and Williams, A. P.: Climate change will accelerate the high-end risk of compound drought and heatwave events, Proceedings of the National Academy of Sciences, 120, e2219825120, doi:10.1073/pnas.2219825120, 2023.

Trugman, A. T., Detto, M., Bartlett, M. K., Medvigy, D., Anderegg, W. R. L., Schwalm, C., Schaffer, B., and Pacala, S. W.: Tree carbon allocation explains forest drought-kill and recovery patterns, Ecology Letters, 21, 1552-1560, 10.1111/ele.13136, 2018.

Trugman, A. T., Anderegg, L. D. L., Sperry, J. S., Wang, Y., Venturas, M., and Anderegg, W. R. L.: Leveraging plant hydraulics to yield predictive and dynamic plant leaf allocation in vegetation models with climate change, Global Change Biology, 25, 4008-4021, 10.1111/gcb.14814, 2019a.

Trugman, A. T., Anderegg, L. D. L., Wolfe, B. T., Birami, B., Ruehr, N. K., Detto, M., Bartlett, M. K., and Anderegg, W. R. L.: Climate and plant trait strategies determine tree carbon allocation to leaves and mediate future forest productivity, Global Change Biology, 25, 3395-3405, 10.1111/gcb.14680, 2019b.

Trugman, A. T., Anderegg, L. D. L., Shaw, J. D., and Anderegg, W. R. L.: Trait velocities reveal that mortality has driven widespread coordinated shifts in forest hydraulic trait composition, Proceedings of National Academy of Sciences, 117, 8532-8538, 10.1073/pnas.1917521117, 2020.

Trugman, A. T., Anderegg, L. D. L., Anderegg, W. R. L., Das, A. J., and Stephenson, N. L.: Why is Tree Drought Mortality so Hard to Predict?, Trends in Ecology & Evolution, 36, 520-532, https://doi.org/10.1016/j.tree.2021.02.001, 2021.

Turner, N. C., Schulze, E. D., and Gollan, T.: The responses of stomata and leaf gas exchange to vapour pressure deficits and soil water content, Oecologia, 63, 338-342, 10.1007/BF00390662, 1984.

Tyree, M. T., and Sperry, J. S.: Vulnerability of xylem to cavitation and embolism, Annual Review of Plant Biology, 40, 19-36, 1989.

Tyree, M. T., and Ewers, F. W.: The hydraulic architecture of trees and other woody plants, New Phytologist, 119, 345-360, 1991.

Ubierna, N., and Farquhar, G. D.: Advances in measurements and models of photosynthetic carbon isotope discrimination in C3 plants, Plant, Cell & Environment, 37, 1494-1498, 10.1111/pce.12346, 2014.

Valladares, F., Gianoli, E., and Gomez, J. M.: Ecological limits to plant phenotypic plasticity, New Phytologist, 176, 749-763, 10.1111/j.1469-8137.2007.02275.x, 2007.

van der Plas, F., van Klink, R., Manning, P., Olff, H., and Fischer, M.: Sensitivity of functional diversity metrics to sampling intensity, Methods in Ecology and Evolution, 8, 1072-1080, https://doi.org/10.1111/2041-210X.12728, 2017.

van der Sande, M. T., Poorter, L., Schnitzer, S. A., Engelbrecht, B. M. J., and Markesteijn, L.: The hydraulic efficiency–safety trade-off differs between lianas and trees, Ecology, 100, e02666, 2019.

Venturas, M. D., Sperry, J. S., and Hacke, U. G.: Plant xylem hydraulics: What we understand, current research, and future challenges, Journal of Integrative Plant Biology, 59, 356-389, 10.1111/jipb.12534, 2017.

Venturas, M. D., Sperry, J. S., Love, D. M., Frehner, E. H., Allred, M. G., Wang, Y., and Anderegg, W. R. L.: A stomatal control model based on optimization of carbon gain versus hydraulic risk predicts aspen sapling responses to drought,

New Phytologist, 220, 836-850, 10.1111/nph.15333, 2018.

Venturas, M. D., Todd, H. N., Trugman, A. T., and Anderegg, W. R. L.: Understanding and predicting forest mortality in the western United States using long-term forest inventory data and modeled hydraulic damage, New Phytologist, 10.1111/nph.17043, 2020.

Violle, C., Reich, P. B., Pacala, S. W., Enquist, B. J., and Kattge, J.: The emergence and promise of functional biogeography, Proceedings of the National Academy of Sciences of the United States of America, 111, 13690-13696, 2014.

Vogel, H.: Temperaturabhängigkeitsgesetz der Viskosität von Flüssigkeiten, Physik Z, 22, 645-646, 1921.

von Caemmerer, S., Evans, J. R., Hudson, G. S., and Andrews, T. J.: The kinetics of ribulose-1, 5-bisphosphate carboxylase/oxygenase in vivo inferred from measurements of photosynthesis in leaves of transgenic tobacco, Planta, 195, 88-97, 1994.

Walker, A. P., Beckerman, A. P., Gu, L., Kattge, J., Cernusak, L. A., Domingues, T. F., Scales, J. C., Wohlfahrt, G., Wullschleger, S. D., and Woodward, F. I.: The relationship of leaf photosynthetic traits - Vcmax and Jmax - to leaf nitrogen, leaf phosphorus, and specific leaf area: a meta-analysis and modeling study, Ecology and Evolution, 4, 3218-3235, 10.1002/ece3.1173, 2014.

Wang, H., Prentice, I. C., Davis, T. W., Keenan, T. F., Wright, I. J., and Peng, C.: Photosynthetic responses to altitude: an explanation based on optimality principles, New Phytologist, 213, 976-982, 10.1111/nph.14332, 2017a.

Wang, H., Prentice, I. C., Keenan, T. F., Davis, T. W., Wright, I. J., Cornwell, W. K., Evans, B. J., and Peng, C.: Towards a universal model for carbon dioxide uptake by plants, Nature Plants, 3, 734-741, 10.1038/s41477-017-0006-8, 2017b.

Wang, H., Harrison, S. P., Prentice, I. C., Yang, Y., Bai, F., Togashi, H. F., Wang, M., Zhou, S., and Ni, J.: The China Plant Trait Database: toward a comprehensive regional compilation of functional traits for land plants, Ecology, 99, 500-500, 10.1002/ecy.2091, 2018.

Wang, H., Atkin, O. K., Keenan, T. F., Smith, N. G., Wright, I. J., Bloomfield, K. J., Kattge, J., Reich, P. B., and Prentice, I. C.: Acclimation of leaf respiration consistent with optimal photosynthetic capacity, Global Change Biology, 26, 2573-2583, 10.1111/gcb.14980, 2020a.

Wang, H., Prentice, I. C., Wright, I. J., Warton, D. I., Qiao, S., Xu, X., Zhou, J., Kikuzawa, K., and Stenseth, N. C.: Leaf economics fundamentals explained by optimality principles, Science Advances, 9, eadd5667, doi:10.1126/sciadv.add5667, 2023.

Wang, R., Yu, G., He, N., Wang, Q., Xia, F., Zhao, N., Xu, Z., and Ge, J.: Elevation-related variation in leaf stomatal traits as a function of plant functional type: evidence from Changbai Mountain, China, PLoS One, 9, e115395, 2014.

Wang, S., Zhang, Y., Ju, W., Chen, J. M., Ciais, P., Cescatti, A., Sardans, J., Janssens, I. A., Wu, M., Berry, J. A., Campbell, E., Fernández-Martínez, M., Alkama, R., Sitch, S., Friedlingstein, P., Smith, W. K., Yuan, W., He, W., Lombardozzi, D., Kautz, M., Zhu, D., Lienert, S., Kato, E., Poulter, B., Sanders, T. G. M., Krüger, I., Wang, R., Zeng, N., Tian, H., Vuichard, N., Jain, A. K., Wiltshire, A., Haverd, V., Goll, D. S., and Peñuelas, J.: Recent global decline of CO2 fertilization effects on vegetation photosynthesis, Science, 370, 1295-1300, doi:10.1126/science.abb7772, 2020b.

Wang, S., Hong, P., Adler, P. B., Allan, E., Hautier, Y., Schmid, B., Spaak, J. W., and Feng, Y.: Towards mechanistic integration of the causes and consequences of biodiversity, Trends in Ecology & Evolution, 10.1016/j.tree.2024.02.008, 2024.

Wang, Y., Cadotte, M. W., Chen, Y., Fraser, L. H., Zhang, Y., Huang, F., Luo, S., Shi, N., and Loreau, M.: Global evidence of positive biodiversity effects on spatial ecosystem stability in natural grasslands, Nature Communications, 10, 3207, 10.1038/s41467-019-11191-z, 2019a.

Wang, Y., Sperry, J. S., Venturas, M. D., Trugman, A. T., Love, D. M., and Anderegg, W. R. L.: The stomatal response to rising CO2 concentration and drought is predicted by a hydraulic trait-based optimization model, Tree Physiology, 39, 1416-1427, 10.1093/treephys/tpz038, 2019b.

Waring, R. H., Schroeder, P. E., and Oren, R.: Application of the pipe model theory to predict canopy leaf area, Canadian Journal of Forest Research, 12, 556-560, 10.1139/x82-086, 1982.

Warton, D. I., Duursma, R. A., Falster, D. S., and Taskinen, S.: smatr 3– an R package for estimation and inference about allometric lines, Methods in Ecology and Evolution, 3, 257-259, https://doi.org/10.1111/j.2041-210X.2011.00153.x, 2012.

Way, D. A., Domec, J. C., and Jackson, R. B.: Elevated growth temperatures alter hydraulic characteristics in trembling aspen (Populus tremuloides) seedlings: implications for tree drought tolerance, Plant, Cell & Environment, 36, 103-115, 10.1111/j.1365-3040.2012.02557.x, 2013.

Werger, M. J. A., and Hirose, T.: Leaf nitrogen distribution and whole canopy photosynthetic carbon gain in herbaceous stands, Vegetatio, 97, 11-20, 1991.

Westoby, M., Cornwell, W. K., and Falster, D. S.: An evolutionary attractor model for sapwood cross section in relation to leaf area, Journal of Theoretical Biology, 303, 98-109, 10.1016/j.jtbi.2012.03.008, 2012.

Whitehead, D., Edwards, W. R. N., and Jarvis, P. G.: Conducting sapwood area, foliage area, and permeability in mature trees of Piceasitchensis and Pinuscontorta, Canadian Journal of Forest Research, 14, 940-947, 10.1139/x84-166, 1984.

Whitehead, D.: Regulation of stomatal conductance and transpiration in forest canopies, Tree Physiology, 18, 633-644, 10.1093/treephys/18.8-9.633, 1998.

Wolfe, B. T., Sperry, J. S., and Kursar, T. A.: Does leaf shedding protect stems from cavitation during seasonal droughts? A test of the hydraulic fuse hypothesis, New Phytologist, 212, 1007-1018, https://doi.org/10.1111/nph.14087, 2016.

Wood, S. N.: mgcv: GAMs and generalized ridge regression for R, R news, 1, 20-25, 2001.

Wright, I. J., and Westoby, M.: Leaves at low versus high rainfall: coordination of structure, lifespan and physiology, New Phytol., 155, 403-416, 2002.

Wright, I. J., Reich, P. B., and Westoby, M.: Least-cost input mixtures of water and nitrogen for photosynthesis, The American Naturalist, 161, 98-111, 2003.

Wright, I. J., Reich, P. B., Mark, W., Ackerly, D. D., Zdravko, B., Frans, B., Jeannine, C. B., Terry, C., Cornelissen, J. H. C., and Matthias, D.: The worldwide leaf economics spectrum, Nature, 428, 821, 2004a.

Wright, I. J., Reich, P. B., Westoby, M., Ackerly, D. D., Baruch, Z., Bongers, F. J. J. M., Cavenderbares, J., Chapin, T., Cornelissen, J. H. C., and Diemer, M.: The worldwide leaf economics spectrum, Nature, 428, 821-827, 2004b.

Wright, I. J., Reich, P. B., Cornelissen, J. H. C., Falster, D. S., Groom, P. K., Hikosaka, K., Lee, W., Lusk, C. H., Niinemets, Ü., Oleksyn, J., Osada, N., Poorter, H., Warton, D. I., and Westoby, M.: Modulation of leaf economic traits and trait relationships by climate, Glob. Ecol. Biogeogr., 14, 411-421, 10.1111/j.1466-822x.2005.00172.x, 2005.

Wright, I. J., Dong, N., Maire, V., Prentice, I. C., Westoby, M., Díaz, S., Gallagher, R. V., Jacobs, B. F., Kooyman, R., and Law, E. A.: Global climatic drivers of leaf size, Science, 357, 917-921, 2017.

Wu, J., Feng, Y., Li, L. Z. X., Ciais, P., Piao, S., Chen, A., and Zeng, Z.: Earth greening mitigates hot temperature extremes despite the effect being dampened by rising CO2, One Earth, 7, 100-109, https://doi.org/10.1016/j.oneear.2023.12.003, 2024.

Xie, S., Mo, X., Liu, S., and Hu, S.: Plant Hydraulics Improves Predictions of ET and GPP Responses to Drought, Water Resources Research, 59, 10.1029/2022wr033402, 2023.

Xu, C., McDowell, N. G., Fisher, R. A., Wei, L., Sevanto, S., Christoffersen, B. O., Weng, E., and Middleton, R. S.: Increasing impacts of extreme droughts on vegetation productivity under climate change, Nature Climate Change, 9, 948-953, 10.1038/s41558-019-0630-6, 2019.

Xu, H., Wang, H., Prentice, I. C., Harrison, S. P., Wang, G., and Sun, X.: Predictability of leaf traits with climate and elevation: a case study in Gongga

Mountain, China, Tree Physiol, 10.1093/treephys/tpab003, 2021a.

Xu, H., Wang, H., Prentice, I. C., Harrison, S. P., Wang, G., and Sun, X.: Predictability of leaf traits with climate and elevation: a case study in Gongga Mountain, China, Tree Physiology, 41, 1336–1352, 10.1093/treephys/tpab003, 2021b.

Xu, H., Wang, H., Prentice, I. C., Harrison, S. P., and Wright, I. J.: Coordination of plant hydraulic and photosynthetic traits: confronting optimality theory with field measurements, New Phytologist, 232, 1286-1296, 10.1111/nph.17656, 2021c.

Xu, H., Wang, H., Prentice, I. C., and Harrison, S. P.: Leaf carbon and nitrogen stoichiometric variation along environmental gradients, Biogeosciences, 20, 4511-4525, 10.5194/bg-20-4511-2023, 2023.

Xu, L., and Baldocchi, D. D.: Seasonal trends in photosynthetic parameters and stomatal conductance of blue oak (Quercus douglasii) under prolonged summer drought and high temperature, Tree Physiology, 23, 865-877, 2003.

Xu, X., Medvigy, D., Powers, J. S., Becknell, J. M., and Guan, K.: Diversity in plant hydraulic traits explains seasonal and inter-annual variations of vegetation dynamics in seasonally dry tropical forests, New Phytologist, 212, 80-95, 10.1111/nph.14009, 2016.

Xu, X., Medvigy, D., Joseph Wright, S., Kitajima, K., Wu, J., Albert, L. P., Martins, G. A., Saleska, S. R., and Pacala, S. W.: Variations of leaf longevity in tropical moist forests predicted by a trait-driven carbon optimality model, Ecology letters, 20, 1097-1106, 2017.

Yan, B., and Dickinson, R. E.: Modeling hydraulic redistribution and ecosystem response to droughts over the Amazon basin using Community Land Model 4.0 (CLM4), Journal of Geophysical Research: Biogeosciences, 119, 2130-2143, 10.1002/2014jg002694, 2014.

Yan, Y., Piao, S., Hammond, W. M., Chen, A., Hong, S., Xu, H., Munson, S. M., Myneni, R. B., and Allen, C. D.: Climate-induced tree-mortality pulses are obscured by broad-scale and long-term greening, Nature Ecology & Evolution,

10.1038/s41559-024-02372-1, 2024.

Yan, Z., Sardans, J., Peñuelas, J., Detto, M., Smith, N. G., Wang, H., Guo, L., Hughes, A. C., Guo, Z., Lee, C. K. F., Liu, L., and Wu, J.: Global patterns and drivers of leaf photosynthetic capacity: The relative importance of environmental factors and evolutionary history, Global Ecology and Biogeography, 32, 668-682, 10.1111/geb.13660, 2023.

Yang, D., Zhang, Y. J., Song, J., Niu, C. Y., and Hao, G. Y.: Compound leaves are associated with high hydraulic conductance and photosynthetic capacity: evidence from trees in Northeast China, Tree Physiology, 39, 729-739, 10.1093/treephys/tpy147, 2019a.

Yang, H., Ciais, P., Wang, Y., Huang, Y., Wigneron, J. P., Bastos, A., Chave, J., Chang, J., E. Doughty, C., Fan, L., Goll, D., Joetzjer, E., Li, W., Lucas, R., Quegan, S., Le Toan, T., Yu, K., and Gillespie, T.: Variations of carbon allocation and turnover time across tropical forests, Global Ecology and Biogeography, 30, 1271-1285, 10.1111/geb.13302, 2021.

Yang, Y., Wang, H., Harrison, S. P., Prentice, I. C., Wright, I. J., Peng, C., and Lin, G.: Quantifying leaf-trait covariation and its controls across climates and biomes, New Phytol., 221, 155-168, 10.1111/nph.15422, 2019b.

Yang, Y., Roderick, M. L., Guo, H., Miralles, D. G., Zhang, L., Fatichi, S., Luo, X., Zhang, Y., McVicar, T. R., Tu, Z., Keenan, T. F., Fisher, J. B., Gan, R., Zhang, X., Piao, S., Zhang, B., and Yang, D.: Evapotranspiration on a greening Earth, Nature Reviews Earth & Environment, 4, 626-641, 10.1038/s43017-023-00464-3, 2023.

Yuan, W., Zheng, Y., Piao, S., Ciais, P., Lombardozzi, D., Wang, Y., Ryu, Y., Chen, G., Dong, W., Hu, Z., Jain, A. K., Jiang, C., Kato, E., Li, S., Lienert, S., Liu, S., Nabel, J. E. M. S., Qin, Z., Quine, T., Sitch, S., Smith, W. K., Wang, F., Wu, C., Xiao, Z., and Yang, S.: Increased atmospheric vapor pressure deficit reduces global vegetation growth, Science Advances, 5, eaax1396, 10.1126/sciadv.aax1396, 2019.

Zaehle, S., Sitch, S., Smith, B., and Hatterman, F.: Effects of parameter uncertainties on the modeling of terrestrial biosphere dynamics, Global

Biogeochemical Cycles, 19, 10.1029/2004gb002395, 2005.

Zanne, A. E., Westoby, M., Falster, D. S., Ackerly, D. D., Loarie, S. R., Arnold, S. E., and Coomes, D. A.: Angiosperm wood structure: Global patterns in vessel anatomy and their relation to wood density and potential conductivity, American Journal of Botany, 97, 207-215, 10.3732/ajb.0900178, 2010.

Zhang, J., Liu, B., Liu, S., Feng, Z., and Jiang, K.: plantlist: Looking Up the Status of Plant Scientific Names based on The Plant List Database, 2019.

Zhang, Q. W., Zhu, S. D., Jansen, S., Cao, K. F., and McCulloh, K.: Topography strongly affects drought stress and xylem embolism resistance in woody plants from a karst forest in Southwest China, Functional Ecology, 35, 566-577, 10.1111/1365-2435.13731, 2020.

Zhu, L. W., and Zhao, P.: Climate-driven sapwood-specific hydraulic conductivity and the Huber value but not leaf-specific hydraulic conductivity on a global scale, Science of Total Environment, 857, 159334, 10.1016/j.scitotenv.2022.159334, 2022.

Zhu, S. D., Chen, Y. J., Ye, Q., He, P. C., Liu, H., Li, R. H., Fu, P. L., Jiang, G. F., and Cao, K. F.: Leaf turgor loss point is correlated with drought tolerance and leaf carbon economics traits, Tree Physiology, 38, 658-663, 10.1093/treephys/tpy013, 2018.

Zhu, Z., Piao, S., Myneni, R. B., Huang, M., Zeng, Z., Canadell, J. G., Ciais, P., Sitch, S., Friedlingstein, P., Arneth, A., Cao, C., Cheng, L., Kato, E., Koven, C., Li, Y., Lian, X., Liu, Y., Liu, R., Mao, J., Pan, Y., Peng, S., Peñuelas, J., Poulter, B., Pugh, T. A. M., Stocker, B. D., Viovy, N., Wang, X., Wang, Y., Xiao, Z., Yang, H., Zaehle, S., and Zeng, N.: Greening of the Earth and its drivers, Nature Climate Change, 6, 791-795, 10.1038/nclimate3004, 2016.

Zhu, Z., Wang, H., Harrison, S. P., Prentice, I. C., Qiao, S., and Tan, S.: Optimality principles explaining divergent responses of alpine vegetation to environmental change, Global Change Biology, 29, 126-142, 10.1111/gcb.16459, 2023.

Ziemińska, K., Butler, D. W., Gleason, S. M., Wright, I. J., and Westoby, M.: Fibre

wall and lumen fractions drive wood density variation across 24 Australian angiosperms, AoB PLANTS, 5, plt046, 10.1093/aobpla/plt046, 2013.